SOME STUDIES

ON

MIXED MOLECULAR COMPLEXES

Zainal A. Ahmad,
University of Kent,
Canterbury.

Doctor of Philosophy Thesis
Chemistry
April 1981.

This Thesis is Dedicated to

My Mother, Father, Sister,

Grandmother, Wife and Son.

Acknowledgements

It is a pleasure to thank all those to whom the Author is indebted for their generous help during the work reported here, and in the preparation of this thesis.

- Dr. J. D. Wright for continued guidance, encouragement, patience, and friendship. His family is specially thanked for being a good host and being attentive during the birth of the Author's son;
- Dr. J. D. Wright for data collection and computing in the crystal structure determination;
- Dr. A. V. Chadwick for the use of vapour phase chromatography and differential scanning calorimetry apparatus;
- Members of the University Technical staff, in particular Messrs. P. R. J. Smith, L. V. Bush, S. Gilbert, R. Oliver, W. T. Povey, K. P. Scroggins, D. A. Pugh, R. A. Roots, A. J. Fassam and Mrs. M. Williamson and Miss L. S. Smith;
- Professor G. R. Martin for the provision of research facilities in his department;
- Mr. A. K. Jumat for valuable assistance in drawing many of the diagrams;
- Di Mayes who typed this thesis so expertly;
- Mr. B. Meadows who sacrificed his time willingly to assist in computing
- The Malaysian Government for the grant and "Universiti Sains Malaysia" for an A.S.T.S. Fellowship Award;
- and finally numerous others all of whom have helped to make my stay here and my work so enjoyable and rewarding.

* * * * * *

Abstract

Mixed donor π-π^* molecular complexes $(donor_1)_x(donor_2)_{1-x}$/TCNQ with donors anthracene, chrysene, dibenzofuran, dibenzothiophen, perylene, phenanthrene, phenazine and pyrene, have been prepared, and analysed by spectroscopic and chromatographic methods. Formation of a continuous series of isostructural crystalline mixed complexes with $0<x<1$ requires similar parent complex solubilities, formation constants and crystal structure, and similar donor shapes and sizes. Where these requirements are not met, mixed complexes of limited composition range may be formed having either a completely new lattice structure or that of one of the parents.

The crystal structure of dibenzothiophen/TCNQ has been determined. The donor acceptor relative orientation and separation are consistent with weak charge transfer interactions. Interstack donor-donor and acceptor-acceptor overlap is poor. Dibenzofuran/TCNQ has a similar structure, with possible donor disorder.

Diffuse reflectance spectral data on relative intensities of charge transfer transitions in different complexes show the same trends as predictions from SCF-MO-CI calculations. These trends have been qualitatively interpreted in terms of donor and acceptor orbital symmetries and relative orientations. Comparison with relative intensities of such transitions in mixed complexes has been used to deduce whether or not donor-acceptor orientations are similar in mixed and parent complexes.

Regular variations in single crystal semiconductivity as a function of mixed complex composition are obscured by the influence of physical defects. Such defects also alter the magnitude of photoconduction, by acting as recombination centres (e.g. in anthracene/pyromellitic dianhydride) or sites for dissociation of charge transfer excited state to charge carriers (e.g. in dibenzothiophen/dibenzofuran/TCNQ). Photoconduction studies on mixed complexes have shown that the action spectrum of a mixed complex will only correspond to the appropriately weighted sum of the action spectra of the parent complexes if the density and distribution of defects, degree of interstack donor-donor and acceptor-acceptor π orbital overlap and relative orientations of donors and acceptor are similar in parent and mixed complexes.

* * * * * *

Contents

		Page
CHAPTER 1 :	INTRODUCTION	1
CHAPTER 2 :	MATERIALS, PREPARATION AND COMPOSITIONAL ANALYSIS OF MIXED MOLECULAR COMPLEXES	7
2.1	Choice of Materials	7
2.2	Purification	9
2.3	Growth of Crystals of the Complexes	15
2.4	Experimental Conditions for Growing Crystals	16
2.5	Analysis of Mixed Molecular Complexes	21
2.6	Spectroscopic Analysis	21
2.7	Results	33
2.8	Chromatographic Analysis - Method and Results	33
2.9	Discussion	56
CHAPTER 3 :	STRUCTURAL STUDIES OF MIXED MOLECULAR COMPLEXES ..	61
3.1	Introduction	61
3.2	The Forces Involved in a Molecular Crystal	62
3.3	Charge Transfer Interaction	63
3.4	Attractive Forces	65
3.5	Repulsive Forces	67
3.6	Factors that Determine the Crystal Structure of π-π^* Molecular Complexes	67
3.7	The Crystal Structure of Dibenzothiophen/TCNQ	72
3.8	Results and Discussion	77
3.9	The Melting Point Against Composition Plot	92
3.10	X-Ray Powder Diffraction - Apparatus and Experimental	96
3.11	Results	98
3.12	Conclusions	109

Contents (Cont'd.)

		Page
CHAPTER 4 :	CHARGE TRANSFER SPECTROSCOPY	112
4.1	Introduction	112
4.2	The Theory of Diffuse Reflectance Spectroscopy . ..	113
	4.2.1 Derivation of the Kubelka-Munk Function . ..	113
	4.2.2 The Dilution Method	116
4.3	Experimental	117
	4.3.1 Preparation of Samples	117
	4.3.2 Measurement of Spectra	118
4.4	Results	119
4.5	Discussion	156
	4.5.1 Spectra of Parent Complexes	156
	4.5.2 Spectra of Mixed Complexes	164
	4.5.2.1 (Dibenzothiophen)(Dibenzofuran)(TCNQ)	164
	4.5.2.2 (Anthracene)(Dibenzothiophen)(TCNQ)..	168
	4.5.2.3 (Anthracene)(Chrysene)(TCNQ)	169
	4.5.2.4 (Pyrene)(Perylene)(TCNQ)	170
4.6	Conclusions	170
CHAPTER 5 :	SEMICONDUCTIVITY	172
5.1	Introduction	172
5.2	Mobility	174
5.3	Activation Energy	178
5.4	Interpretation of Activation Energy Data	180
5.5	Trapping	184
5.6	The Apparatus..	185
5.7	Experimental	197
5.8	Results	198
5.9	Discussion	220
5.10	Conclusions	234

Contents (Cont'd.)

		Page
CHAPTER 6 :	PHOTOCONDUCTIVITY	237
6.1	Introduction	237
6.2	Steady State Photoconductivity..	238
6.3	Photoconductivity and Charge Transfer Spectra .	243
6.4	Photoconductivity and Crystal Structure	247
6.5	Apparatus	249
6.6	Experimental	251
6.7	Results	252
6.8	Discussion	275
6.9	Conclusions	295
CHAPTER 7 :	CONCLUSIONS	299
APPENDIX I -	X-RAY CRYSTALLOGRAPHY	305
A.1.1	Dibenzothiophen/TCNQ Structure Determination	305
APPENDIX II-	BASIC PROGRAM	324
REFERENCES	.. ..	326

* * * * * *

Chapter 1

Introduction

The study of molecular complexes began in 1858, when Fritzsche reported the isolation of benzene, naphthalene and anthracene picrates. However, it was not until much later that Mulliken (1950), following work by Weiss (1942) and Brackmann (1949), formulated the charge transfer resonance model to describe the interactions between the two components of a molecular complex and to account for the characteristic charge transfer spectra of molecular complexes. The development and applications of this model have been fully discussed in Mulliken and Person's (1969) book, and relevant features are discussed in later chapters of this thesis. Molecular complexes may be arranged into several classes according to the nature of the orbitals involved in the charge transfer interactions. Electron donation may be from lone pairs of electrons or from σ or π bonding orbitals, while electron acceptors may receive electrons into vacant non-bonding orbitals or into antibonding σ^* or π^* orbitals. The studies reported in this thesis involve π-π^* molecular complexes.

The development of Mulliken's theory catalysed investigations of many physical properties of molecular complexes. The crystal structures of a large number of molecular complexes have been determined, and these are discussed in several reviews (Prout & Wright, 1968; Herbstein, 1971; Prout & Kamenar, 1973). The relative orientations of donor and acceptor in crystalline π-π^* molecular complexes have been shown by Mayoh and Prout (1972) to be close to those maximising charge transfer interactions in many cases. These structural studies have been used in the interpretation of the crystal spectra of molecular complexes (e.g. Kuroda,

Kunii, Hiroma and Akamatu, 1967). Charge transfer spectra and formation constants of many molecular complexes in solution have been studied, and the results are discussed in several texts (Mulliken & Person, 1969; Briegleb, 1961; Foster, 1969,1973).

The understanding of the significance of charge transfer processes in molecular complexes provided by Mulliken's theory also led to the idea that the energy required to produce separated positive and negative charge carriers in crystalline molecular complexes might be related to the energy of the charge transfer transitions visible in their absorption spectra. Studies by Eley, Inokuchi and Willis (1959) and Kuroda, Kobayashi, Kinoshita and Takemoto (1962) and other subsequent studies indicated that this idea was correct. Later investigations of semiconductivity of tetracyanoquinodimethane (TCNQ) (Hurditch, Vincent & Wright, 1972) and molecular complexes of this and other electron acceptors (Vincent & Wright, 1974) showed that the seebeck coefficients and semiconduction activation energies for these molecular complexes could also possibly be explained in terms of extrinsic effects, with charge carrier generation from Na^+ $Acceptor^-$ impurities. This interpretation was supported by Pethig and Soni (1975), who interpreted conductivity measurements under conditions of high electric field on perylene complexes of chloranil and dichlorodicyano-p-benzoquinone (DDQ) in terms of a mechanism involving electrons hopping between localised states associated with such impurities. However, Munnoch and Wright (1976), using electron spin resonance to determine the concentrations of $Acceptor^-$ impurity species, showed that, for carefully purified complexes these concentrations were too low to account for the observed magnitude of conduction unless large values of charge carrier mobility, inconsistent with typical results of drift mobility measurements (e.g. Karl & Ziegler, 1975) were assumed. The original interpretation of semiconduction in π-π^* molecular complexes being related to intrinsic

charge transfer processes therefore still seems tenable.

The relationship between the charge transfer excited state and the conduction state in molecular complexes is also clear from studies of photoconduction in π-π^* complexes. Akamatu and Kuroda (1963) showed a correlation between the photoconduction action spectra and the charge transfer absorption spectra in these complexes. This was confirmed by later work in this laboratory (Vincent & Wright, 1974) which also revealed a relationship between the size of the photocurrent and the crystal structure of the complexes, discussed later in Chapter 6 of this thesis.

Almost all of these various studies of molecular complex have been carried out on systems composed of a single donor and acceptor. However, it is possible to prepare mixed molecular complexes of the type $(\text{donor}_1)_x(\text{donor}_2)_{1-x}\text{acceptor}_{1.0}$ or $\text{donor}_{1.0}(\text{acceptor}_1)_x(\text{acceptor}_2)_{1-x}$. Many crystalline mixed molecular complexes may have been isolated accidentally from preparations involving impure donor or acceptor materials. For example, commercial phenanthrene may contain up to 5% of anthracene, and the 1,2,4,5 tetracyano benzene (TCNB) complex of this impure phenanthrene forms orange crystals, whereas the complex formed for carefully chromatographed phenanthrene is yellow (Wright, 1963). More recently there have been several reports of investigations of mixed complexes prepared deliberately. Powder x-ray diffraction and phase diagram studies show that mixed complexes fall into two distinct classes. If the donor or acceptor site in the crystal can accommodate a different donor or acceptor with a minimum of disturbance to the overall lattice structure, the crystal structures of the mixed and parent complexes are all very similar, and the relative orientation of donor and acceptor is independent of composition. The mixed complexes of the donors bis(8-hydroxyquinolinato) Cu(II) and Pd(II) with chloranil are of this type,

and their electrical conductivity has been studied by Prout, Williams & Wright (1966). Another example is anthracene/phenanthrene/tetracyanobenzene, whose structures and single crystal spectra have been reported by Wright, Ohta and Kuroda (1976). In the second class, the lattice structures of the two parent complexes are different and the mixed complex crystals form several distinct structural phases dependent on composition. Anthracene/phenanthrene/1,3,5 trinitrobenzene (Lower, 1969) and anthracene/phenanthrene/picric acid (Koizumi & Matsunaga, 1974) are examples of this class.

Mixed molecular complexes are materials which could provide critical tests of various current interpretations of the physical properties of molecular complexes. This thesis is an account of investigations of the preparation, analysis and structural, spectroscopic and electrical properties of mixed molecular complexes. The principal objectives of the work were as follows:

1. To determine the requirements for formation of crystalline mixed molecular complexes by attempting preparation and analysis of several series of mixed complexes. The results of these studies are reported in Chapter 2.
2. To investigate structural properties of the solid mixed complexes. Lattice packing, charge transfer overlap and dipole-dipole or dipole-induced dipole interactions may all influence crystal structures of π-π^* molecular complexes, and knowledge of the structures adopted by mixed complexes could help to disentangle the relative influences of these various factors in determining the actual structure adopted by a given complex. Chapter 3 describes

structural studies including x-ray powder diffraction and differential scanning calorimetry data on the systems studied, as well as a full structure determination for one of the parent complexes from single crystal x-ray diffraction data.

3. To investigate changes in the relative intensities of the charge transfer transitions characteristic of the two parent complexes as composition is varied in the mixed complex. These experiments were aimed at obtaining reliable experimental data on the relative intensities of charge transfer transitions in different solid complexes, and on the effect of changes in relative orientations of donor and acceptor on these intensities. There is currently relatively little data of this type, which will provide a critical test of current theoretical treatments of charge transfer spectra of π-π^* molecular complexes (e.g. Ohta, Kuroda & Kunii, 1970) as well as being of use as an aid to interpreting photoconduction data in the mixed complexes. Ideally such data should be obtained from measurements on single crystals, with polarised light. Since no instrument suitable for such measurements was available, a secondary objective was to examine the potential of diffuse reflectance spectroscopy for this purpose, by comparison of single crystal and diffuse reflectance spectra for anthracene/phenanthrene/tetracyanobenzene complexes. These

studies are described in Chapter 4.

4. To investigate semiconductivity and photoconductivity as a function of composition in the mixed complexes. Current interpretations of semiconductivity and photoconductivity in molecular complexes predict that controlled modification of these properties may be possible using appropriate mixed complexes. Since mixed complex formation may also alter the defect concentrations in the crystals, this work also included a brief study of the influence of crystal growth technique on electrical properties of one single molecular complex, anthracene/pyromellitic dianhydride (PMDA). Crystals of this complex grown by sublimation and from solution are expected to have different defect concentrations, and comparison of their properties could clarify the role of defects as compared to composition changes in mixed complexes. The results of these studies are reported in Chapter 5 and 6.

Previous work and theory related to each of these objectives is discussed in the appropriate chapters, and a summary of the overall conclusions of this work is given in Chapter 7.

* * * * * *

Chapter 2

Materials, Preparation and Compositional Analysis of Mixed Complexes

2.1 Choice of Materials

Mixed molecular complexes may be of two types - mixed donor (e.g. $(donor_1)_x(donor_2)_{1-x}$/acceptor) or mixed acceptor (e.g. donor/$(acceptor_1)_x(acceptor_2)_{1-x}$) . For the studies reported in this thesis, complexes of the mixed donor type were selected, primarily because a wider range of different π-electron donor molecules is available (e.g. with varying ionisation potential, polarisability, shape and size).than is the case for π-electron acceptors. 7,7,8,8-tetracyanoquinodimethane (TCNQ) was chosen as a fixed electron acceptor because its molecular complexes are stable and easily prepared (Vincent, 1972; Munnoch, 1974) and grown as single crystals (many of whose structures have been determined (Tickle & Prout, 1973; Williams & Wallwork, 1968; Goldberg & Shmueli, 1973; Colton and Henn, 1970; Kobayashi, 1973; Munnoch & Wright, 1974)),and because their electrical conductivity properties have been widely studied. The donor molecules used (both homo- and hetero-cyclic aromatic compounds) are listed in Table 2.1.

The following criteria were applied in choosing the systems for study in this work:

1. The component molecules should be easily obtainable and readily purified.
2. The parent complexes should have the same donor:acceptor ratio, preferably 1:1.
3. Both parent complexes and the mixed complexes should form crystals easily. Conductivity measurements on single

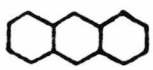

ANTHRACENE
I.P.=7.39eV

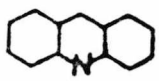

ACRIDINE
I.P.=7.85eV

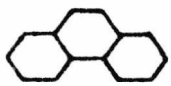

PHENANTHRENE
I.P.=8.03eV

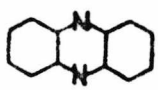

PHENAZINE
I.P.=8.0eV

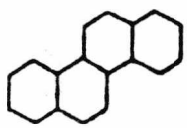

CHRYSENE
I.P.=7.75eV

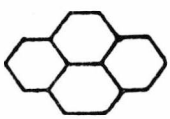

PYRENE
I.P.=7.47eV

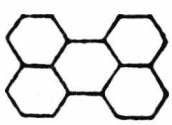

PERYLENE
I.P.=7.15eV

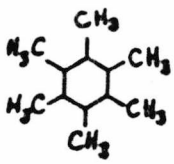

HEXAMETHYLBENZENE
I.P.=7.8eV

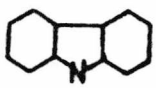

CARBAZOLE
I.P.=7.8eV

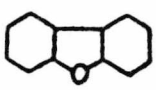

DIBENZOFURAN
I.P.=8.18eV

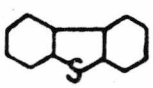

DIBENZOTHIOPHEN
I.P.=8.10eV

TABLE 2.1 MOLECULAR STRUCTURES OF AROMATIC DONOR MOLECULES

crystals are more readily interpreted than those on, for example, compressed pellets.

4. If possible, the crystals should be obtainable by more than one method (e.g. from solution and from sublimation) for comparison of effects due to different defect concentrations.
5. For spectrophotometric analysis of the composition of the mixed complexes, each component should preferably exhibit strong characteristic ultraviolet absorption at a wavelength where the other components do not absorb strongly.
6. Preferably, the crystal structures of the parent complexes should be known.
7. Semiconductivity and photoconductivity properties of the parent complexes should ideally be known.

Further materials criteria and constraints specific to particular aspects of the work reported in this thesis (semiconductivity, photoconductivity, spectroscopy and structural or composition studies) are discussed later in the appropriate chapters.

2.2 Purification

Donor Molecules

A) Continuous Chromatography (Fig. 2.1)

A column was made by pouring aluminium oxide (100/250 mesh) into a condenser containing boiled toluene. Toluene was then allowed to pass through the column into a three-necked 250 ml. flask which was heated in order to return toluene to the top of the column and so complete the

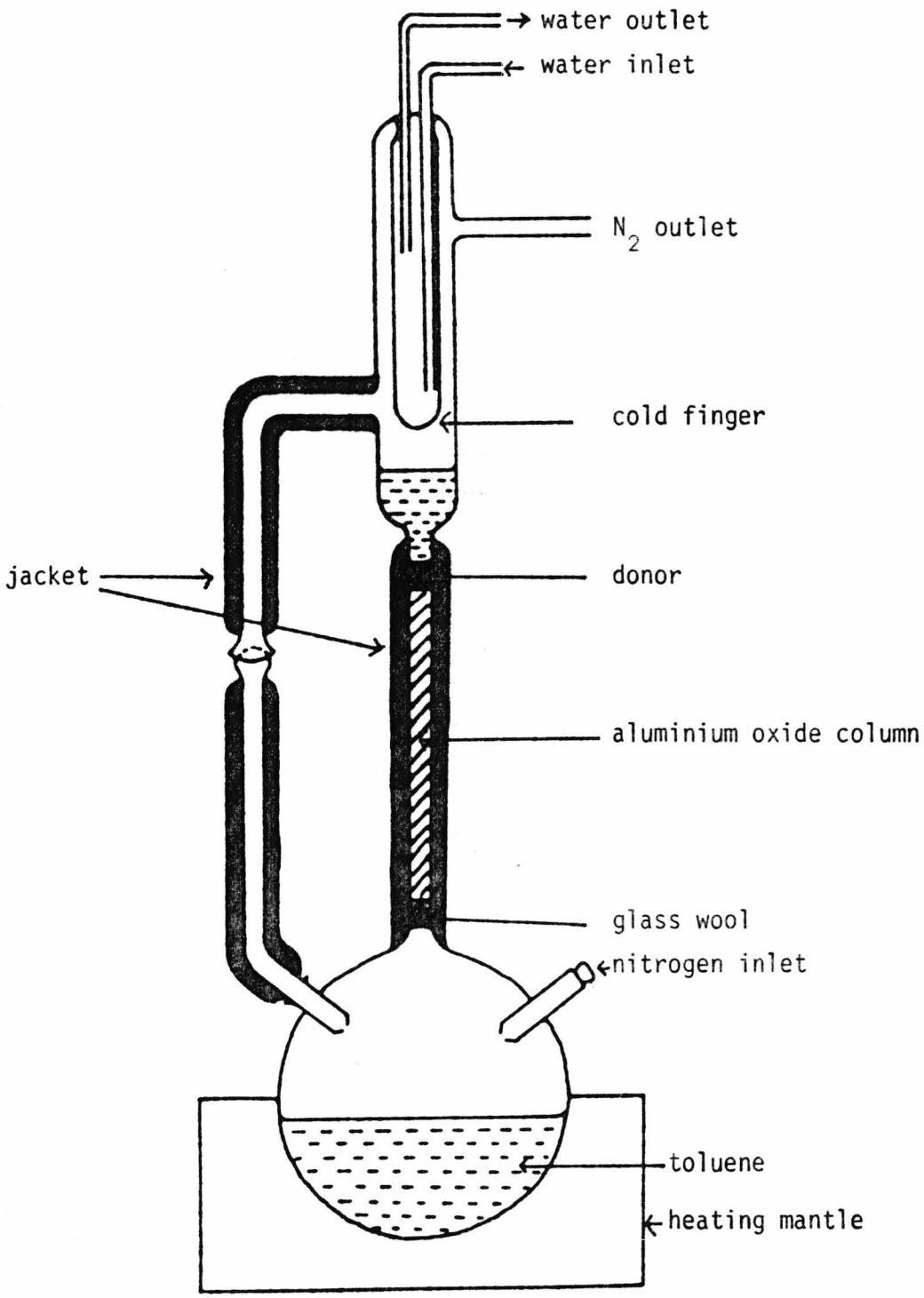

FIGURE 2.1 DIAGRAM FOR CONTINUOUS CHROMATOGRAPHY

cycle. The heating rate was adjusted until a steady state was achieved in which the column neither overflowed nor ran dry. At this stage a steady stream of nitrogen was admitted to the apparatus.

The cold finger was removed and approximately 10 g. of the donor added to the top of the column. The cold finger was reconnected and the donor washed through the column by toluene. Five minutes after the donor had been washed from the top of the column, the heater was turned off and the solution allowed to cool, when the purified donor crystallized out. The crystals were filtered, dried and bottled.

B) Zone Refining

The purified donors were packed in a 7 mm. diameter glass tube ready for zone refining. The tube was sealed at one end and packed with a donor and evacuated. A pressure of 10 cm. of helium was applied. The donor was then melted with gentle heat. The tube was then carefully sealed at the correct length. This was then placed in a zone refiner and adjustments were made to the temperature of the hot zones to produce molten bands about 0.5 cm. in height at each heating coil. The motor was then started to raise the tube slowly through the heaters and return it almost instantly when it reached the top. The process was allowed to continue until 100 passes of molten zones along the tube had been achieved (approximately two days).

TCNQ

TCNQ was obtained from Aldrich and purified by recrystallisation twice from distilled acetonitrile followed by sublimation in a stream of oxygen-free nitrogen at 250°C .

Sublimation was done in a sublimation furnace. The layout of the furnace

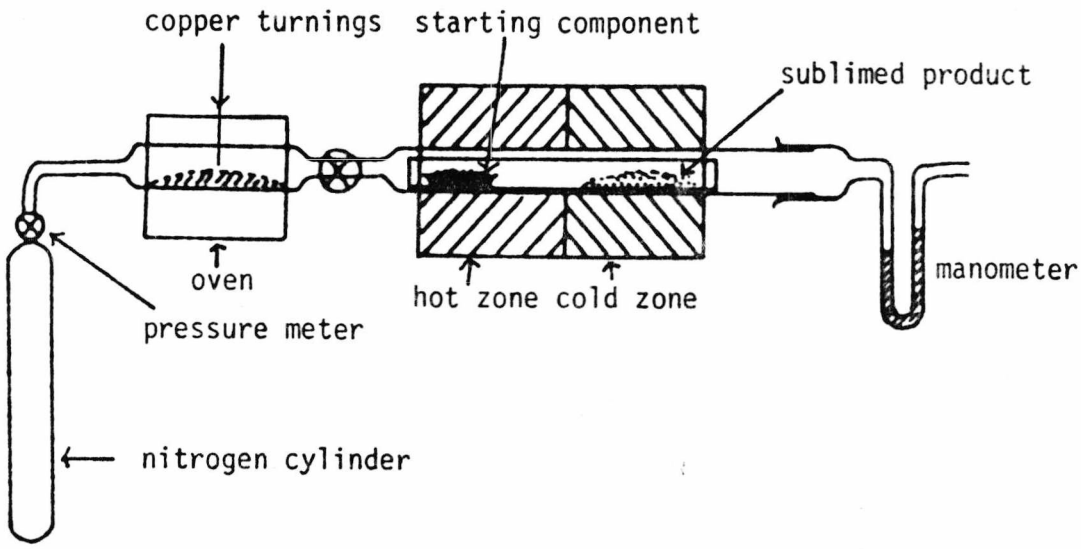

FIG. 2.2 SUBLIMATION FURNACE

is given in Fig. 2.2. The glass tube was treated with

(i) concentrated HNO_3: Concentrated H_2SO_4; 1:1 (to clean the surface);

(ii) distilled water (to remove the acid);

(iii) TCNQ solution (to remove surface Na^+ which would react with $TCNQ \rightarrow TCNQ^-$); and

(iv) acetone (to remove surplus TCNQ and dry).

The tube was properly dried. Then TCNQ was placed in the tube and the furnace. Nitrogen was allowed to flow to get rid of the O_2. After 1 h , the hot and cold zone were adjusted to 250^0C and 150^0C respectively and the sublimation was allowed to proceed for 2 h . The slower the sublimation process the better the result. The sublimation was repeated to get purer TCNQ (Hurditch, Vincent & Wright, 1972).

Table 2.2 summarises the purification methods used for all chemicals in this work. For some of the donors continuous chromatography was not feasible, owing to their polar nature. In these cases, repeated recrystallisation, from the solvents, indicated in the table was used.

PMDA as supplied was found to have a melting point of $270\text{-}273^0C$ as opposed to the literature value of 286^0C. Prolonged heating (overnight) of the powdered material in a salt bath at 230^0C under vacuum yielded material of the correct melting point, and it was concluded that the commerical product contained significant amounts of the parent acid formed from adsorption of water vapour. The powdered material was suspected not to be PMDA because of its failure to form intense red crystals of anthracene-PMDA from solution and sublimation growth. The treated product easily formed anthracene complex both from solution and sublimation growth.

Compound	Source	Purification	M.Pt. (°C)
Pyrene	BDH	b	149-151
Perylene		as supplied purified	277-279
Dibenzofuran	Aldrich	a	81-83
Dibenzothiophen	Aldrich	a	97-100
Phenazine		as supplied purified	174-177
Anthracene	Fisons	a	214-216
Chrysene		b	255-256
Carbazole	Fisons	none	247-248
Acridine	Aldrich	none	107-110
HMB	Kodak	b	162-164
TCNQ	Aldrich	c	287-289
PMDA	BDH	230°C in vacuo overnight	286
			B.P.
Chloroform A.R.	Fisons	d	60-62
Acetonitrile A.R.	Fisons	d	80.5-82.5
Methyl Ethyl Ketone	Fisons	d	79-80.5
Dioxan A.R.	Fisons	none	100-102

a) Twice chromatographed

b) Chromatographed, zone refined

c) Recrystallized, sublimed

d) Distilled

TABLE 2.2 METHODS OF PURIFICATION

2.3 Growth of Crystals of the Complexes

There are four main methods of crystal growth.

1) From the melt.

2) From the vapour-sublimation.

3) From solution.

4) Gel growth.

Many molecular complexes decompose below the melting point. Thus crystal growth from the melt is impracticable. Moreover, molecular complexes tend to sublime below the melting point frequently yielding separate crystals of the individual donor and acceptor. Under controlled conditions to be described later, a few complexes may be successfully sublimed without dissociation. Gel growth is a new technique which will probably permit the growth of larger crystals than solution growth, but lack of experience eliminated this method for use in this work. A major problem is to obtain a suitable gel with organic solvents.

Most molecular complexes are prepared from solution growth. Care should be taken to ensure that starting materials are pure and the solvents used are dry.

There are two methods for growing crystals from solution. Both methods must fulfil the condition that the solution must be supersaturated in order for the crystals to form.

1) The Cooling Method - saturation is approached through controlled lowering of temperature until crystals form because of the decreasing solubility of solute as the temperature is lowered.

2) Evaporation Method - saturation is approached by the evaporation of the solvent making the solution more concentrated until crystals begin to

form. This method very much depends on the volatility of the solvents and the concentration of the starting solution. Sometimes, it may take as long as a month for crystals to form.

Solvents for growing crystals must have the following properties:

(i) They must be chemically inert to components and complexes.

(ii) Their viscosity should be low enough to enable random motion of dissolved solutes to come into contact with already formed crystal surfaces.

(iii) The solubility of the complex should be lower than that of the components to prevent crystallization of the components.

(iv) The complex should be easily formed in the solvent concerned i.e. having a large formation constant.

(v) The solvents should preferably be volatile for the evaporation method.

(vi) The temperature coefficient of solubility of the complex should be large in solvents for use with the cooling method.

(vii) The solvents must be dried and free from dust and dirt, which would provide an excess of sites for nucleation of crystal growth.

2.4 Experimental Conditions for Growing Crystals (Table 2.3)

Most crystals of molecular complexes are grown from solution, rather than by sublimation or from the melt, due to decomposition as discussed

earlier. For growth from solution, the components should be present in the proportion of their molar weights and solubilities with respect to a particular solvent used. For most donor/acceptor complexes, there should be an excess of donor, although there still exists an element of uncertainty in getting good, well formed and homogeneous crystals. Growing crystals is more an art than a science. Optimum conditions were normally determined by trial and error.

In mixed complexes of three components ($Donor_1$ $Donor_2$ and Acceptor) excess of any component is not normally desirable, though occasionally an excess must be used in order to obtain suitable crystals.

The methods used for growing crystals were:

For Donor-Acceptor Complexes

1) A known quantity of acceptor and an excess of donor were dissolved in a large volume of solvent and filtered into a clean conical flask, to be left to evaporate at room temperature. The volume and weights needed were determined on a trial and error basis.
2) The pure components were ground together and zone-refined. The zone-refined product was finely powdered and sublimed, using a small temperature gradient between hot and cold zones. This method is obviously applicable only to components that do not decompose at the melt temperature.

For $(Donor_1)_x(Donor_2)_{1-x}Acceptor_{1.0}$

3) For the series $(Donor_1)_x(Donor_2)_{1-x}Acceptor_{1.0}$, the calculated compositions were dissolved in a solvent and filtered into a clean conical flask then left to evaporate at room temperature.

Complex	Methods of Preparation		Ratios of Donor:Acceptor	Description and Comments
Pyrene/TCNQ	1	Chloroform	1:1	Very fine crystals mostly contaminated. Clustered with platelets. Dark in colour.
	1	Chloroform	4:1	Better crystals but still not satisfactory. Clustered with platelets. Dark in colour.
Perylene/TCNQ	1	Chloroform	1:1	Easily formed. Good crystals. Both plates and needles. Dark green crystals.
$Pyrene_x/Perylene_{1-x}/TCNQ_{1.0}$	3	Chloroform	1:1	Good xtals for each of starting composition $0 \leqslant x \leqslant 1$. Dark brown to dark green (analysed. Solid composition given later).
Dibenzofuran/TCNQ	1	Acetonitrile	1:1	Good crystals. Reddish in colour. Mostly twinned, and have grooves on surface.
Dibenzothiophen/TCNQ	1	Acetonitrile	1:1	Medium-sized crystals. Clustered with plates. Components sometimes contaminate the complex.Dark crystals.
$Dibenzofuran_x/Dibenzothiophen_{1-x}/TCNQ_{1.0}$	3	Acetonitrile	1:1	Good medium-sized crystals for each of starting compositions $0 < x < 1$. Dark to reddish variation through the series (analysed. Solid compositions given later).

TABLE 2.3 PREPARATION OF COMPLEXES

TABLE 2.3 PREPARATION OF COMPLEXES (Cont'd.)

Complex	Methods of Preparation	Solvents	Ratios of Donor:Acceptor	Description and Comments
Phenazine/TCNQ	1	Acetonitrile	1:1	Good crystals. Reddish brown in colour.
$Phenazine_x$/ $Dibenzofuran_{1-x}$/ TCNQ	3	Acetonitrile	1:1	Good large-sized crystals. Only few. Components do sometimes separate out. Good sized xtals throughout the series ($0 \leq x \leq 1$). Analysed. Solid composition given later.
	4	Acetonitrile	Excess Donor	Good crystals formed. Analysed. Solid composition given later.
Anthracene/TCNQ	1	Chloroform	4:1	Dark black crystals contaminated with white platelets.
Chrysene/TCNQ	1	Chloroform	4:1	Dark brown needle crystals.contaminated with white platelets.
$Anthracene_x$/ $Chrysene_{1-x}$/ $TCNQ_{1.0}$	3	Chloroform	1:1	Good crystals throughout the starting series $0 \leq x \leq 1$. Dark black needles or plates. Analysed. Solid composition, given later.
Anthracene/PMDA	1	Ethyl Methyl Ketone	Excess PMDA 2:1	Good intense red complex. No contamination.
Anthracene/PMDA	2	-	1:1	Fine crystals. Not very good. Well contaminated with components. Intense red needle crystals analysed to give anthracene:PMDA ≃ 1:1 ratio.

TABLE 2.3 PREPARATION OF COMPLEXES (Cont'd.)

Complex	Methods of Preparation	Solvents	Ratios of Donor:Acceptor	Description and Comments
Carbazole/TCNQ	2	Acetonitrile	1:1	Black needle shaped crystals. Medium-sized.
$Carbazole_x$/ $Dibenzofuran_{1-x}$/ $TCNQ_{1.0}$	3	Acetonitrile	1:1	Black needle shaped crystals. Not very good. Contaminated with components. Not analysed.
$Anthracene_x$/ $Carbazole_{1-x}$/ $TCNQ_{1.0}$	3	Acetonitrile	1:1	Dark black crystals. Fine. Contaminated. Not analysed.
$Acridine_x$/ $Carbazole_{1-x}$/ $TCNQ_{1.0}$	3	Acetonitrile	1:1	Very fine crystals. Not suitable for conductivity. Dark black crystals. Not analysed.
$Hexamethylbenzene_x$/ $Perylene_{1-x}$/ $TCNQ_{1.0}$	3	Chloroform	1:1	Good dark black crystals. Slight contamination by components. Not possible to analyse.
	3	Chloroform	3:1	Good dark black crystals. More contamination. Not possible to analyse.
$Anthracene_x$/ $Dibenzothiophen_{1-x}$/ $TCNQ_{1.0}$	3	Acetonitrile	1:1	Good medium-sized crystals. Able to get crystals throughout the starting composition $0<x\leq1$. Analysed data given later. Black crystals.

4) If method (3) did not give crystals of the required composition, slight excess of donor (or donors) was tried.

2.5 Analysis of Mixed Molecular Complexes

Introduction

Elemental analysis is not a good method for determining the composition of the solid mixed molecular complexes involved in this work, since the percentages of carbon, hydrogen and nitrogen in the different donor molecules are frequently quite similar. Dibenzothiophen (one example is given as comparison) which has a sulfur atom can be analysed using this method but again the small percentage of sulfur in the complex leads to large errors in compositional analysis. Thus, the accuracy of microanalytical techniques is usually insufficient to determine the ratio of the two different donors to the desired accuracy. Since the compositions of the solid complexes frequently differ from the ratios of the two donors used in the solutions from which the crystals are grown, accurate analysis of the composition of the solid materials is important. Two methods of analysis have been used in this work - spectroscopic analysis, using characteristic ultraviolet absorption bands of the individual components, and vapour phase chromatographic analysis. For some mixed complexes, both methods can be used, and where possible this has been done to provide a check on the reliability of the results. In other cases, only one of the methods is suitable.

2.6 Spectroscopic Analysis

The assumptions made are:

1) The donor:acceptor complex has a 1:1 stoichiometry.

2) The extinction coefficient (ε) of each component is not changed by adding other components.

The precautions taken during the analysis are:

1) The cells used throughout the experiment are the same.
2) The pipettes and flasks are cleaned and dried before and after use.
3) The solutions are freshly prepared.
4) Temperature of experiment (room temperature) as far as possible is kept constant. In practice, the temperature is found to have only a secondary effect, unless varied over an unusually wide range. The concentration will vary slightly with change in temperature, because of volume change.
5) Solvent is not changed within one complex series. The effect of changing the solvent on the absorption of a given solute cannot be predicted in any general way.
6) Solvent does not absorb in the range used.
7) Complex is completely dissolved.
8) As far as possible, too high or too low an absorbance is avoided.
9) Checks are made to ensure peak positions do not shift in solutions of complexes compared to solutions of components.
10) Slit width and resolution: ideally the use of monochromatic light is essential. The spectrophotometer works with a finite band width. Care must be taken to

ensure that the width of the absorption bands is considerably greater than the wavelength interval included by the image of the exit slit to enable correct reading of molar absorptivity (the product of absorptivity and molecular weight of the substance). The slit width is kept to a minimum. If measurements are done on the peak and the slit width accepts wavelengths on either side of the peak, the absorbance will be less than the true value.

11) The wavelength should be chosen in a region where the absorbance does not vary rapidly with change in wavelength. Measurement of absorption is often done at the wavelength of maximum absorption, since at this wavelength the variation in absorbance with wavelength will be smaller than on the steep sides of the peak of maximum absorption, so that errors in wavelength setting and from the bandwidth are less significant.

12) The ε values are determined for each component at all wavelengths used, and the validity of Beer's Law under the conditions of the experiment are checked.

The ε data used in the experiment are given in Table 2.4 and are compared with ε values previously determined.

Procedure for Processing Spectroscopic Analytical Data

This is for three component complexes, $(\text{Donor}_1)_x(\text{Donor}_2)_{1-x}(\text{Acceptor})$, where at λ_1 only the acceptor absorbs and the other two donors do not. At λ_2, only acceptor and one donor absorbs.

Components	Solvents	(λnm)[(ε)](logε) This Experiment	(λnm)(logε) Previous Experiments	Ref.
		$Anthracene_x/Dibenzothiophen_{1-x}/TCNQ$		
TCNQ	Dioxan A.R.	(340)[(9.54±.61)×10³](3.98)		
		(358)[(1.94±.05)×10⁴](4.29)		
		(378)[(3.63±.05)×10⁴](4.56)		
		(403)[(5.28±.10)×10⁴](4.72)		
			Anthracene in Chloroform	
Anthracene	Dioxan A.R.	(340)[(5.78±.12)×10³](3.76)	(342) (3.70)	a
		(358)[(8.83±.16)×10³](3.95)	(359) (3.84)	
		(378)[(8.03±.08)×10³](3.90)	(379) (3.82)	
		$Anthracene_x/Chrysene_{1-x}/TCNQ$	Anthracene in Chloroform	
			(342) (3.5)	b
TCNQ	Chloroform (Distilled)	(342)[(7.80±.27)×10³](3.89)	(358) (3.88)	
		(359)[(1.98±.14)×10⁴](4.30)	(376) (3.84)	

TABLE 2.4 THE EXTINCTION COEFFICIENTS OF COMPONENTS

TABLE 2.4 THE EXTINCTION COEFFICIENTS OF COMPONENTS (Cont'd.)

Components	Solvents	(λnm) (ε) (logε) This Experiment	(λnm)(logε) Previous Experiments	Ref.
		$Anthracene_x/Chrysene_{1-x}/TCNQ$		
TCNQ	Chloroform (Distilled)	(379)[(4.26±.21)×10^4](4.63)		
		(403)[(6.90±.10)×10^4](4.84)		
			Anthracene in Ethanol	
			(341) (3.7)	c
Anthracene	Chloroform (Distilled)	(342)[(5.24±.10)×10^3](3.72)	(357) (4.0)	
		(359)[(7.66±.36)×10^3](3.88)	(375) (3.9)	
		(379)[(6.86±.11)×10^3](3.84)		
		$Dibenzothiophen_x/Dibenzofuran_{1-x}/TCNQ$	Dibenzothiophen in Ethanol	
TCNQ	Dioxan A.R.	(312)[(1.895±.005)×10^3](3.28)]	(317) (3.28)	d
		(324)[(3.92±.06)×10^3](3.59)	(328) (3.39)	
		(404)[(5.45±.04)×10^4](4.74)		

TABLE 2.4 THE EXTINCTION COEFFICIENTS OF COMPONENTS (Cont'd.)

Components	Solvents	(λnm) (ε) (logε) This Experiment	(λnm)(logε) Previous Experiments	Ref.
		$Dibenzothiophen_x/Dibenzofuran_{1-x}$/TCNQ	Dibenzothiophen in Ethanol	
Dibenzothiophen	Dioxan A.R.	(312)[(2.48±.01)×10^3](3.39)		
		(324)[(3.14±.11)×10^3](3.50)		
			(310 (3.5)	e
			(320) (3.5)	
		$Pyrene_x/Perylene_{1-x}$/TCNQ	Pyrene in Dioxan	
TCNQ	Dioxan A.R.	(319)[(3.30±.18)×10^3](3.52)		
		(398)[(5.45±.15)×10^4](4.74)	(321) (4.2)	f
		(407.5)[(5.17±.04)×10^4](4.71)		
		(435)[(4.9±.41)×10^3](3.69)	Pyrene in Dioxan	
			(320) (4.4)	g
Pyrene	Dioxan A.R.	(319)[(3.392±.064)×10^4](4.53)		
			Perylene in Chloroform	
Perylene	Dioxan A.R.	(319)[(6.47±.57)×10^2](2.81)	(417) (4.41)	h
		(398)[(1.516±.450)×10^4](4.18)	(440.3) (4.55)	

TABLE 2.4 THE EXTINCTION COEFFICIENTS OF COMPONENTS (Cont'd.)

Components	Solvents	(λnm) (ε) (logε) This Experiment	(λnm)(logε) Previous Experiments	Ref.
		$Pyrene_x/Perylene_{1-x}/TCNQ$		
	Dioxan A.R.	(407.5)[(2.81±.04)×10^4](4.45)		
		(435)[(3.817±.060)×10^4](4.58)		
			Perylene in Ethanol	
			(407) (4.45)	h
			(435.1) (4.57)	
		$Phenazine_x/Dibenzofuran_{1-x}/TCNQ$		
TCNQ	Dioxan A.R.	(363)[(2.317±.049)×10^4](4.36)		
		(404)[(5.201±.10)×10^4](4.19)		
			Phenazine in Ethanol	
			(360) (4.2)	i
Phenazine	Dioxan A.R.	(363)[(1.549±.020)×10^4](4.19)	Phenazine in Ethanol	
			(362.5) (4.51)	j

[a]MacKenzie, Rodgman and Wright, 1952; [b]Hazlett, Hannan Jr. and Wells, 1950; [c]Martynoff, 1957; [d]Werner, 1948; [e]Sawicki and Ray, 1952; [f]Zander and Franke, 1961; [g]Pichat, Pesteil and Clement, 1953; [h]Schnurmann, Maddams and Barlow, 1953; [i]Badger, Pearce and Pettit, 1951; [j]Birkofer, 1952.

Ideally the spectrum can be drawn as Fig. 2.3.

$$(\text{Absorbance})_{\lambda_1} = (\varepsilon_{\text{acceptor}})_{\lambda_1} C_{\text{acceptor}}$$

Therefore

$$C_{\text{acceptor}} = \frac{(\text{absorbance})_{\lambda_1}}{(\varepsilon_{\text{acceptor}})_{\lambda_1}}$$

Hence:

$$(\text{absorbance})_{\lambda_2} = (\varepsilon_{\text{acceptor}})_{\lambda_2} C_{\text{acceptor}} + (\varepsilon_{\text{donor}_1})_{\lambda_2} C_{\text{donor}_1}$$

Therefore

$$C_{\text{donor}_1} = \frac{(\text{absorbance})_{\lambda_2} - (\varepsilon_{\text{acceptor}})_{\lambda_2} C_{\text{acceptor}}}{(\varepsilon_{\text{donor}_1})_{\lambda_2}}$$

$$x = \frac{C_{\text{donor}_1}}{C_{\text{acceptor}}}$$ if the complex has 1:1 donor:acceptor ratio.

Therefore, the composition of the complex is $(\text{donor}_1)_x(\text{donor}_2)_{1-x}\text{acceptor}$.

To ensure the composition is representative, checks are made at various wavelengths and the weights of each component totalled and compared with the starting weight. If the error is outside the experimental limit, then the experiment is repeated and thorough checking is done on various parameters that determine the composition.

The other case is where there is no particular wavelength at which only the acceptor absorbs as in the previous treatment. When there is also an absorption by a donor where the acceptor absorbs then two equations have to be used to solve two unknowns. (The only complex for which this occurred was $\text{Pyrene}_x/\text{Perylene}_{1-x}/\text{TCNQ}$.) The type of absorption spectrum is given as in Fig. 2.4.

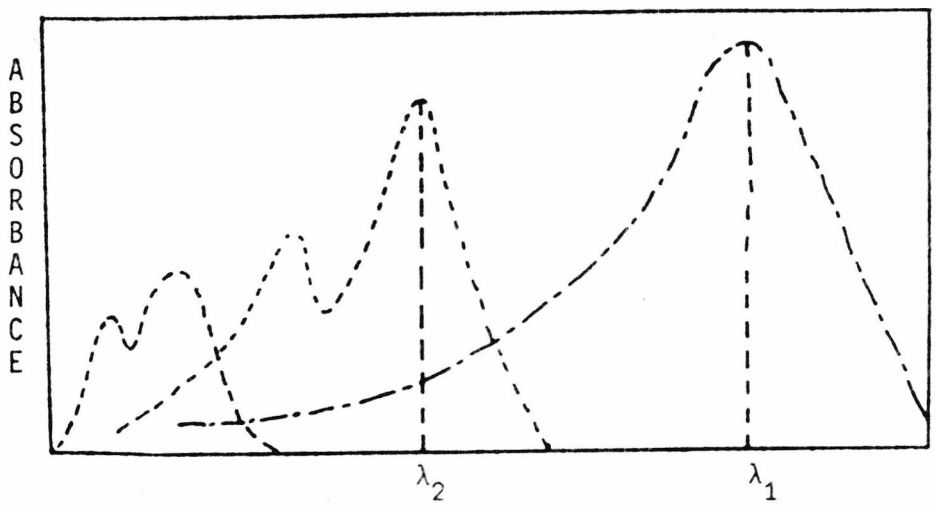

FIG. 2.3: THE COMPONENTS' SPECTRA

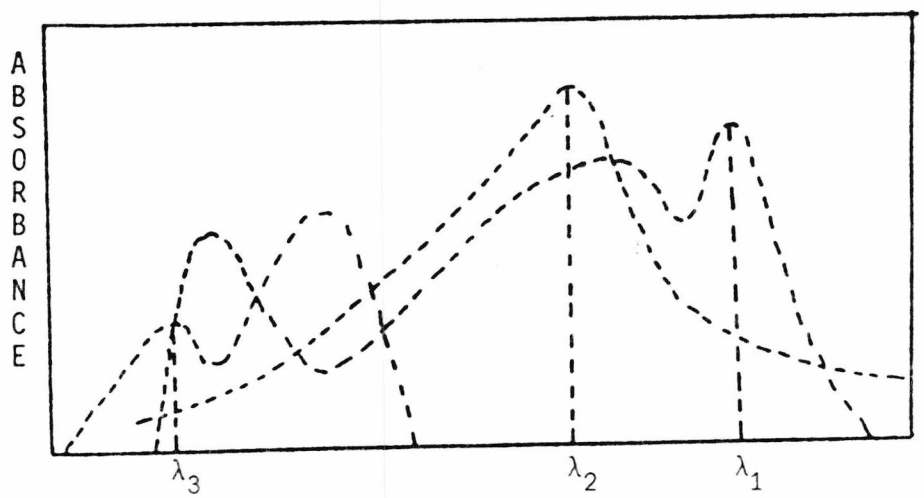

FIG. 2.4: THE COMPONENTS' SPECTRA

I. From absorbance values at λ_1 and λ_2 ,

$$(\text{absorbance})_{\lambda_1} = (\varepsilon_{\text{donor}_1})_{\lambda_1} C_{\text{donor}_1} + (\varepsilon_{\text{acceptor}})_{\lambda_1} C_{\text{acceptor}} \quad (1)$$

$$(\text{absorbance})_{\lambda_2} = (\varepsilon_{\text{donor}_1})_{\lambda_2} C_{\text{donor}_1} + (\varepsilon_{\text{acceptor}})_{\lambda_2} C_{\text{acceptor}} \quad (2)$$

Knowing $(\text{absorbance})_{\lambda_1}$, $(\text{absorbance})_{\lambda_2}$, $(\varepsilon_{\text{donor}_1})_{\lambda_1}$, $(\varepsilon_{\text{acceptor}})_{\lambda_1}$, $(\varepsilon_{\text{donor}_1})_{\lambda_2}$, $(\varepsilon_{\text{acceptor}})_{\lambda_2}$

Multiplying (1) by $\dfrac{(\varepsilon_{\text{donor}_1})_{\lambda_2}}{(\varepsilon_{\text{donor}_1})_{\lambda_1}}$ and subtracting the result from (2) ,

C_{acceptor} is determined.

Using (1), C_{donor_1} is determined.

II. From $(\text{absorbance})_{\lambda_3}$ where λ_3 is a peak for donor_2 and where the degree of overlap is relatively small then using known values of $(\varepsilon_{\text{donor}_1})_{\lambda_3}$, $(\varepsilon_{\text{donor}_2})_{\lambda_3}$, $(\varepsilon_{\text{acceptor}})_{\lambda_3}$, C_{donor_1} and C_{acceptor} , and substituting in equation (3),

$$(\text{absorbance})_{\lambda_3} = (\varepsilon_{\text{donor}_2})_{\lambda_3} C_{\text{donor}_2} + (\varepsilon_{\text{donor}_1})_{\lambda_3} C_{\text{donor}_1} + (\varepsilon_{\text{acceptor}})_{\lambda_3} C_{\text{acceptor}} \quad (3)$$

III. This step and IV were used to analyse $\text{Pyrene}_x/\text{Perylene}_{1-x}/\text{TCNQ}$ Equation (3) gives a good value for C_{pyrene} (equivalent to molarity of Pyrene/TCNQ if a 1:1 complex). Assuming this to be true, the weight of Pyrene/TCNQ in the original sample for analysis can be calculated. This is subtracted from the total weight of sample used, to give the weight of Perylene/TCNQ hence molarity of Perylene/TCNQ.

IV. Using the molarities calculated in III and the known ε at 435, 407.5, 398 and 319 nm , the absorbances at the wavelengths used can be calculated and compared with the observed values as a check on accuracy.

Error Analysis

The calculations of errors are derived from the Beer's Law plot. The best line is used for calculations of ε and composition. The worst lines are drawn for the error limits. Examples of calculations will be given taking the analysis of Phenazine$_x$/dibenzofuran$_{1-x}$/TCNQ as the case. e.g. Fig. 2.5 shows the Beer's Law plot for the determination of ε of TCNQ.

0.0067 g of TCNQ is dissolved in a volumetric flask (50 ml.)

Therefore

$$\text{Mole}/\ell. = \frac{0.0067}{204.2} \times \frac{1000}{50}$$

This solution is diluted 16 times.

Therefore

$$\text{The concentration of TCNQ solution} = \frac{0.0067 \times 1000}{204.2 \times 50 \times 16}$$

$$= 4.1 \times 10^{-5} \text{ Mole}/\ell.$$

This solution is used to determine the Beer's Law plot. The standard procedure for analysis (Section 2.6) is followed.

Calculations: (e.g. Fig. 2.5)

Concentration of TCNQ = 4.1×10^{-5} Mole/ℓ.

The absorbance for this solution at 363 nm = .95

Therefore

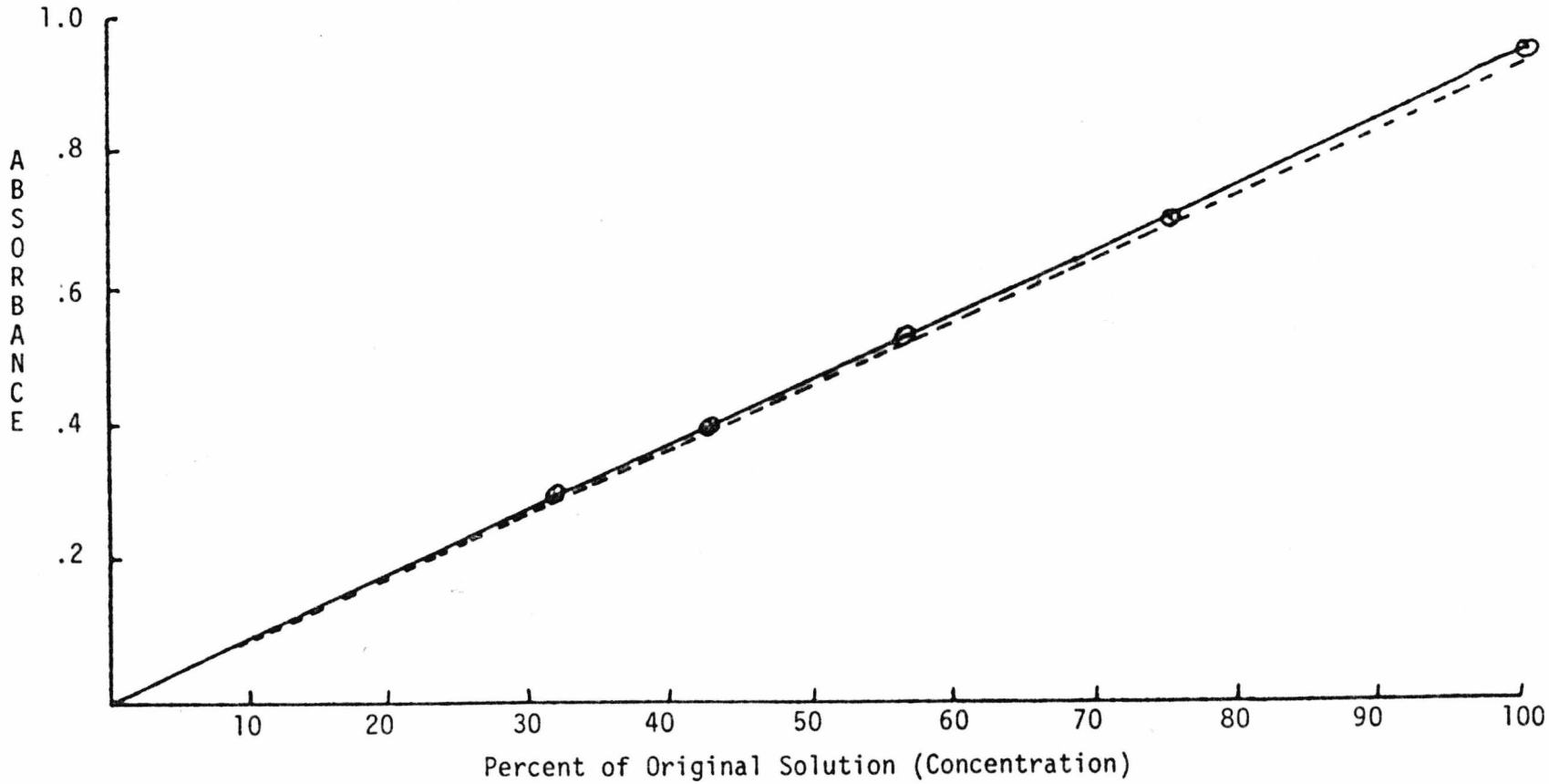

FIG. 2.5 THE DETERMINATION OF ε TCNQ AT 363 nm

$$\varepsilon = \frac{A}{C} = \frac{.95}{4.1 \times 10^{-5}} = 2.317 \times 10^{4}$$

Error: The worst absorbance = .93

Therefore

$$\varepsilon = \frac{A}{C} = 2.268$$

Therefore

ε of TCNQ at 363 nm = $2.317 \pm .049$

$2.32 \pm .05$.

The same procedure was carried out for all the analyses. The results and errors are tabulated in Section 2.7.

2.7 Results

(See Tables 2.5 to 2.9 as follows.)

2.8 Chromatographic Analysis

Analysis of Anthracene$_x$/Chrysene$_{1-x}$/TCNQ$_{1.0}$ by Vapour Phase Chromatography

- Column 4' × $\frac{1}{8}$" standard column
- Packing materials: 2.5% BMBT (N,N'-Bis(p-methoxyl benzylindene)-α,α'bi-p-toluidine on 10 g. chromosorb W.

Packing the Column

Chloroform was heated and then 2.5% by weight BMBT was added. Then 10 g. of chromosorb W was added and mixed thoroughly together in hot $CHCl_3$ solution. The mixture was evaporated and oven-baked at 80°C

Starting Composition		Solid Composition (Anthracene Mole Fraction)	CHECKS 358 nm	378 nm	Weight
$A_{.156}/DBT_{.844}/TCNQ$	i)	.01	-	-	-
	ii)	.01	-	-	-
$A_{.368}/DBT_{.632}/TCNQ$	i)	.27 ± .07	0.5%	0.04%	0.9%
	ii)	.23 ± .03	0.16%	0.18%	4.6%
$A_{.422}/DBT_{.578}/TCNQ$	i)	.27 ± .03	2.8%	1.9%	7.0%
	ii)	.25 ± .04	2.9%	5.4%	2.36%
$A_{.515}/DBT_{.485}/TCNQ$	i)	.45 ± .04	0.58%	0.6%	4.8%
$A_{.567}/DBT_{.433}/TCNQ$	i)	.34 ± .06	2.5%	2.3%	6.6%
	ii)	.39 ± .03	3.2%	3.3%	1.8%
$A_{.776}/DBT_{.224}/TCNQ$	i)	.55 ± .05	2.3%	2.8%	10.0%
	ii)	.50 ± .04	1.96%	2.8%	9.0%

A = Anthracene
DBT = Dibenzothiophen

TABLE 2.5 RESULTS OF COMPOSITIONAL ANALYSIS OF $\underline{\text{ANTHRACENE}_x/\text{DIBENZOTHIOPHEN}_{1-x}/\text{TCNQ}}$

Starting Composition	Solid Composition (Anthracene Mole Fraction)	CHECKS 359 nm	379 nm	Weight
$A_{.16}/C_{.84}$/TCNQ	i) 0.084 ii) 0.08 } 0.082 ± .002	4.9% 3.6%	0.5% 0.3%	1.4% 1.2%
$A_{.19}/C_{.81}$/TCNQ	0.10 ± .05	2.9%	1.8%	4.4%
$A_{.27}/C_{.73}$/TCNQ	0.16 ± .02	3.8%	1.1%	0.36%
$A_{.626}/C_{.374}$/TCNQ	0.14 ± .04	1.3%	1.9%	8.0%
$A_{.628}/C_{.372}$/TCNQ	0.10 0.15 } 0.12 ± .02 0.11	3.9% 6.6% 5.7%	1.4% 0.34% 0.4%	0.67% 7.3% 0.9%
$A_{.74}/C_{.26}$/TCNQ	0.22 ± .03	0.7%	1.6%	10.0%
$A_{.813}/C_{.187}$/TCNQ	0.099 ± .021	1.3%	1.89%	4.1%
$A_{.985}/C_{.015}$/TCNQ	0.164 ± .049	1.7%	0.8%	7.5%

A = Anthracene
C = Chrysene

TABLE 2.6 RESULTS OF COMPOSITIONAL ANALYSIS OF $ANTRHACENE_x/CHRYSENE_{1-x}$/TCNQ

Starting Composition	Solid Composition Mole Fraction of DBT	Weight Check
$DBT_{.153}/DBF_{.847}/TCNQ$	.28 ± .02	5.4%
	.30 ± .02	5.2%
$DBT_{.157}/DBF_{.843}/TCNQ$	.21 ± .02	0.4%
	.19 ± .02	0.4%
$DBT_{.164}/DBF_{.836}/TCNQ$	.414 ± .01	7.0%
	.404 ± .01	7.0%
$DBT_{.261}/DBF_{.739}/TCNQ$ (1)	.387 ± .01	1.8%
	.38 ± .01	1.8%
$DBT_{.261}/DBF_{.739}/TCNQ$ (2)	.363 ± .01	2.2%
	.358 ± .01	2.2%
$DBT_{.43}/DBF_{.57}/TCNQ$	.51 ± .01	0.2%
	.51 ± .01	0.2%
$DBT_{.5}/DBF_{.5}/TCNQ$ (1)	.535 ± .01	2.0%
	.539 ± .01	2.0%
$DBT_{.5}/DBF_{.5}/TCNQ$ (2)	.49 ± .03	1.28%
	.52 ± .03	4.8%
$DBT_{.56}/DBF_{.44}/TCNQ$	.70 ± .02	3.4%
	.68 ± .02	3.4%
$DBT_{.649}/DBF_{.351}/TCNQ$	.73 ± .02	0.4%
	.73 ± .01	2.4%
	.74 ± .02	2.4%

TABLE 2.7 RESULTS OF COMPOSITIONAL ANALYSIS OF $DIBENZOTHIOPHEN_x/DIBENZOFURAN_{1-x}/TCNQ$

TABLE 2.7 RESULTS OF COMPOSITIONAL ANALYSIS OF DIBENZOTHIOPHEN$_x$/DIBENZOFURAN$_{1-x}$/TCNQ (Cont'd.)

Starting Composition	Solid Composition Mole Fraction of DBT	Weight Check
$DBT_{.792}/DBF_{.208}$/TCNQ	.77 ± .03	0.6%
	.74 ± .03	0.6%

DBT = Dibenzothiophen

DBF = Dibenzofuran

Starting Composition	Solid Composition (Py mole fraction)	CHECKS (nm) 319	398	407.5	435
$Py_{.4}/Pe_{.6}/TCNQ$	.39 ± .04	23%	20%	13%	8.2%
$Py_{.6}/Pe_{.4}/TCNQ$	.54 ± .05	1.8%	15%	6%	15%
	.54 ± .01	0.9%	15%	6.5%	3%
	.49 ± .03	2.6%	6%	4.2%	5.9%
$Py_{.7}/Pe_{.3}/TCNQ$	.40 ± .09	1%	6%	0.5%	10%
	.42 ± .07	1%	2.8%	0.9%	2.2%
$Py_{.8}/Pe_{.2}/TCNQ$	.51 ± .02	0.7%	3.4%	3.7%	1%

Py = Pyrene
Pe = Perylene

TABLE 2.8 RESULTS OF COMPOSITIONAL ANALYSIS OF $PYRENE_x/PERYLENE_{1-x}/TCNQ$

Starting Composition (Excess Donor)	Solid Composition (Mole Fraction Phenazine)	Weight Check
Phenazine 3.74×10^{-4} Mole Dibenzofuran $.65\times10^{-4}$ Mole TCNQ 3.546×10^{-4} Mole } grown in 25 ml. acetonitrile (distilled)	.89 ± .01	4.3%
	.85 ± .02	3.2%
Phenazine 4.979×10^{-4} Mole Dibenzofuran $.743\times10^{-4}$ Mole TCNQ 3.576×10^{-4} Mole } grown in 25 ml. acetonitrile (distilled)	.90 ± .02	4.7%
	.84 ± .04	3.8%

TABLE 2.9 RESULTS OF COMPOSITIONAL ANALYSIS† OF PHENAZINE$_x$/DIBENZOFURAN$_{1-x}$/TCNQ

†Analysis is done on individual large single crystals to avoid the possibility of including contaminants with smaller crystals

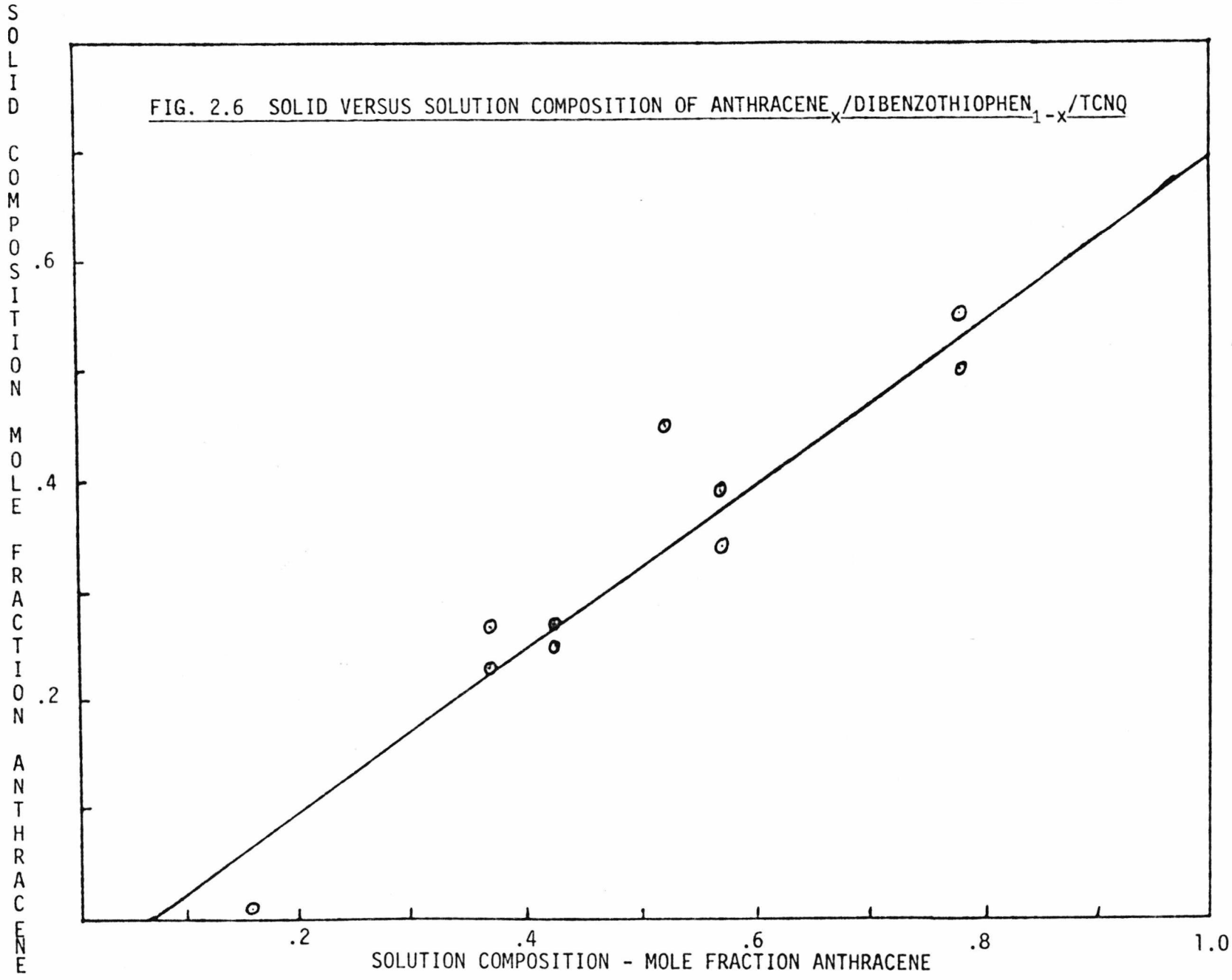
FIG. 2.6 SOLID VERSUS SOLUTION COMPOSITION OF ANTHRACENE$_x$/DIBENZOTHIOPHEN$_{1-x}$/TCNQ
SOLID COMPOSITION MOLE FRACTION ANTHRACENE
.6
.4
.2
.2
.4
.6
.8
1.0
SOLUTION COMPOSITION - MOLE FRACTION ANTHRACENE

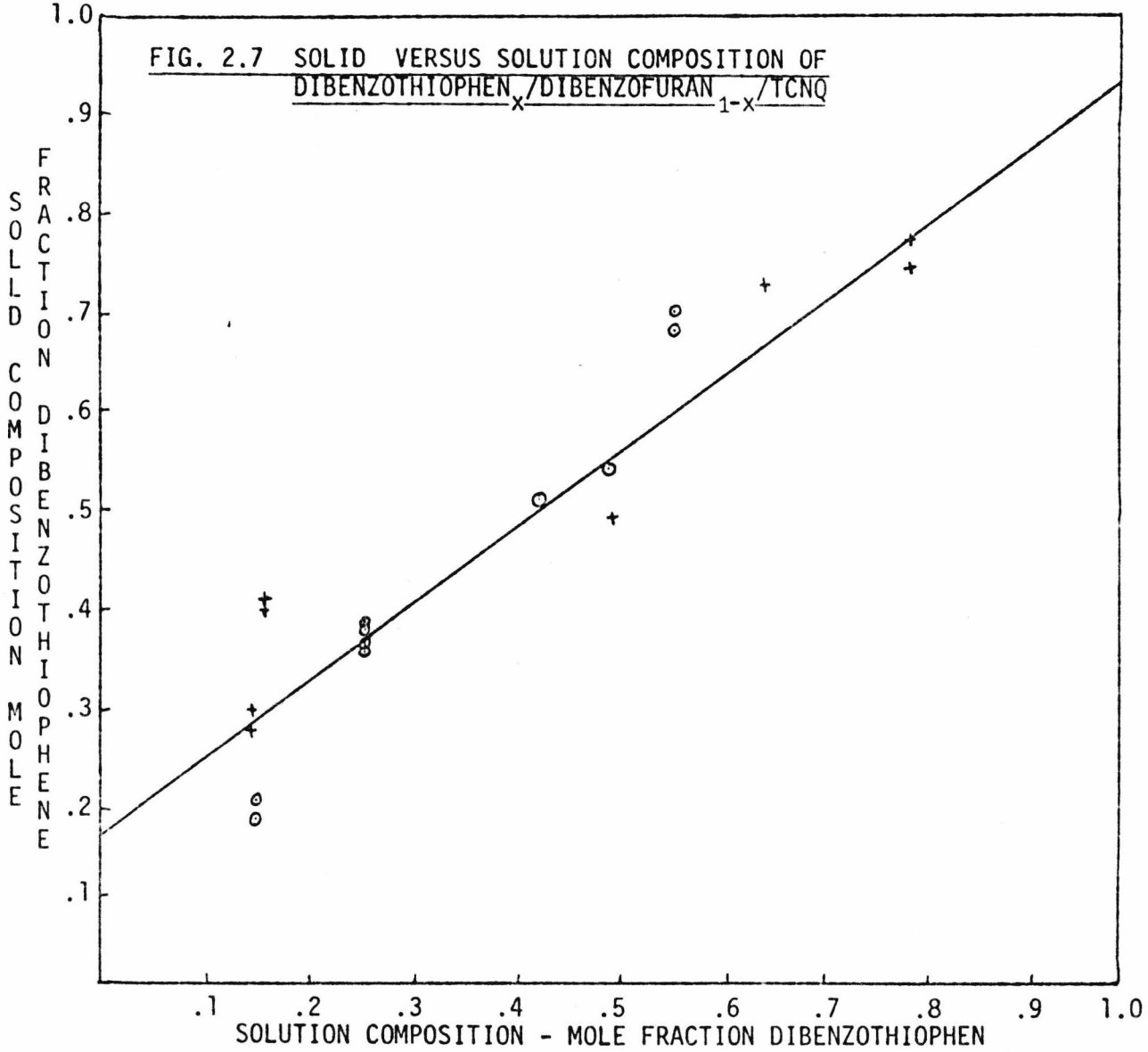
FIG. 2.7 SOLID VERSUS SOLUTION COMPOSITION OF DIBENZOTHIOPHEN$_x$/DIBENZOFURAN$_{1-x}$/TCNQ
SOLLD COMPOSITION MOLE FRACTION DIBENZOTHIOPHENE
1.0
.9
.8
.7
.6
.5
.4
.3
.2
.1
.1 .2 .3 .4 .5 .6 .7 .8 .9 1.0
SOLUTION COMPOSITION - MOLE FRACTION DIBENZOTHIOPHEN

until it was dry. A standard glass tube in the form of a length of coil 4 ft. and an internal diameter of $\frac{1}{8}$" was used to make the packing column. The packing material BMBT on chromosorb W was introduced into the glass coil and was then sucked with a water pump to enable good packing. The column was introduced into the apparatus. The layout of the apparatus is shown in Fig. 2.8. The settings below were found suitable for this analysis:

H_2 pressure = 20 psi

N_2 pressure = 10 psi

Temperature = 185°C

It was found that anthracene peaks overlapped with the solvent front. Chrysene gave a separated peak away from the solvent front and anthracene peak. No peak was observable for TCNQ. The chrysene peak was used to determine the composition. The retention time for chrysene was 36 mins. The peaks observed were symmetrical and the attenuator settings were found suitable at 5×10^2 for all the standard and unknown solutions (to be analysed).

For the analysis of $Pyrene_x/Perylene_{1-x}$/TCNQ the column was packed using chromosorb W and SE 30. The settings were:

H_2 pressure = 20 psi

N_2 pressure = 15 psi

Temperature = 160°C.

Results of Vapour Phase Chromatography

Using solutions of chrysene alone gave symmetrical peaks whose height was a linear function of chrysene concentration. (Table 2.11 and Fig. 2.9). However, for the complex solutions the peaks were no longer symmetrical and integrated peak areas were therefore obtained by cutting the area of

1: Gas Supply 2: Pressure Meter (Continuously Indicating)

3: Injection Point 4: Column

5: Oven 6: Detector Cell

7: Recorder 8: Outlet Flow

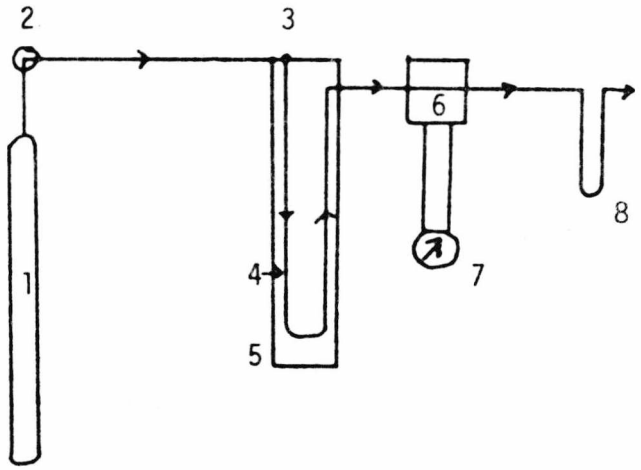

FIG. 2.8 APPARATUS FOR VAPOUR PHASE CHROMATOGRAPHY-SCHEMATIC

chart paper enclosed by the peak and weighing it. The weight was found to be proportional to the area under the curve (Table 2.10) and the uniformity of the chart paper was good. The standard curve of peak area as a function of concentration also gave a straight line (Fig. 2.10). This standard curve was used in analysis of the composition of $Anthracene_x$/ $Chrysene_{1-x}$/$TCNQ_{1.0}$.

Concentration of Chrysene STD. Solution	Expt. No.	Weight of Paper Under Curve (Grams)
2.05 mg./10 ml. $CHCl_3$	1	0.03917
	2	0.04286
3.67 mg./10 ml. $CHCl_3$	3	0.07342
	4	0.06872
	5	0.07088
4.61 mg./10 ml. $CHCl_3$	6	0.08091
	7	0.08511
4.63 mg./10 ml. $CHCl_3$	8	0.09556
	9	0.08020
	10	0.10760
6.84 mg./10 ml. $CHCl_3$	11	0.13120
	12	0.14230

TABLE 2.10

Concentration of Chrysene STD. Solution	Expt. No.	Height in Cm.
2.0 mg./10 ml	13	4.3
	14	4.3
3.67 mg./10 ml.	15	7.6
	16	8.1
	17	7.8
4.61 mg./10 ml.	18	9.3
	19	9.3
6.84 mg./10 ml.	20	13.7
	21	14.3
	22	13.9

TABLE 2.11

FIG. 2.9 CONCENTRATION OF CHRYSENE STANDARD SOLUTION AGAINST HEIGHT OF CHRYSENE PEAK

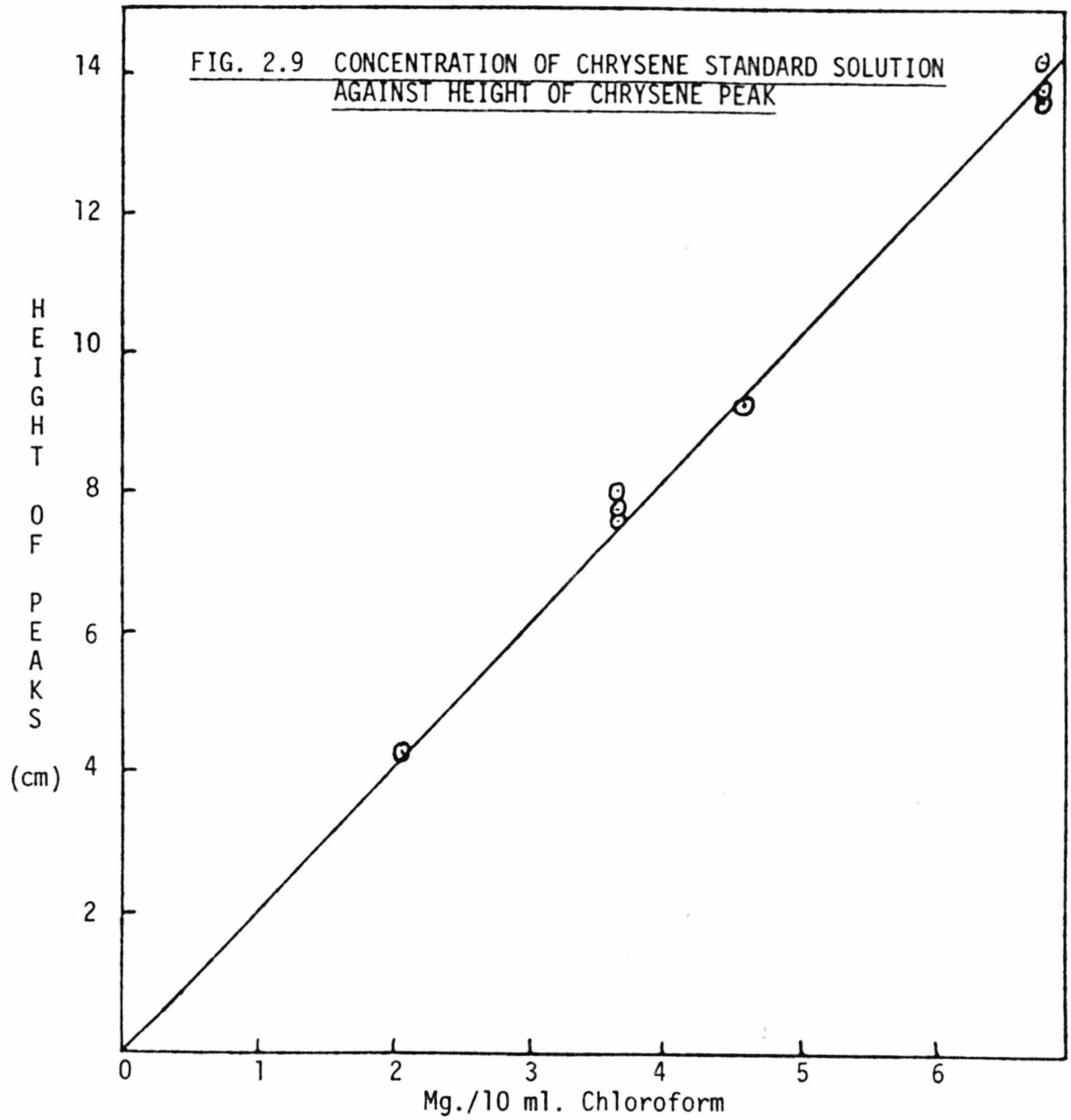

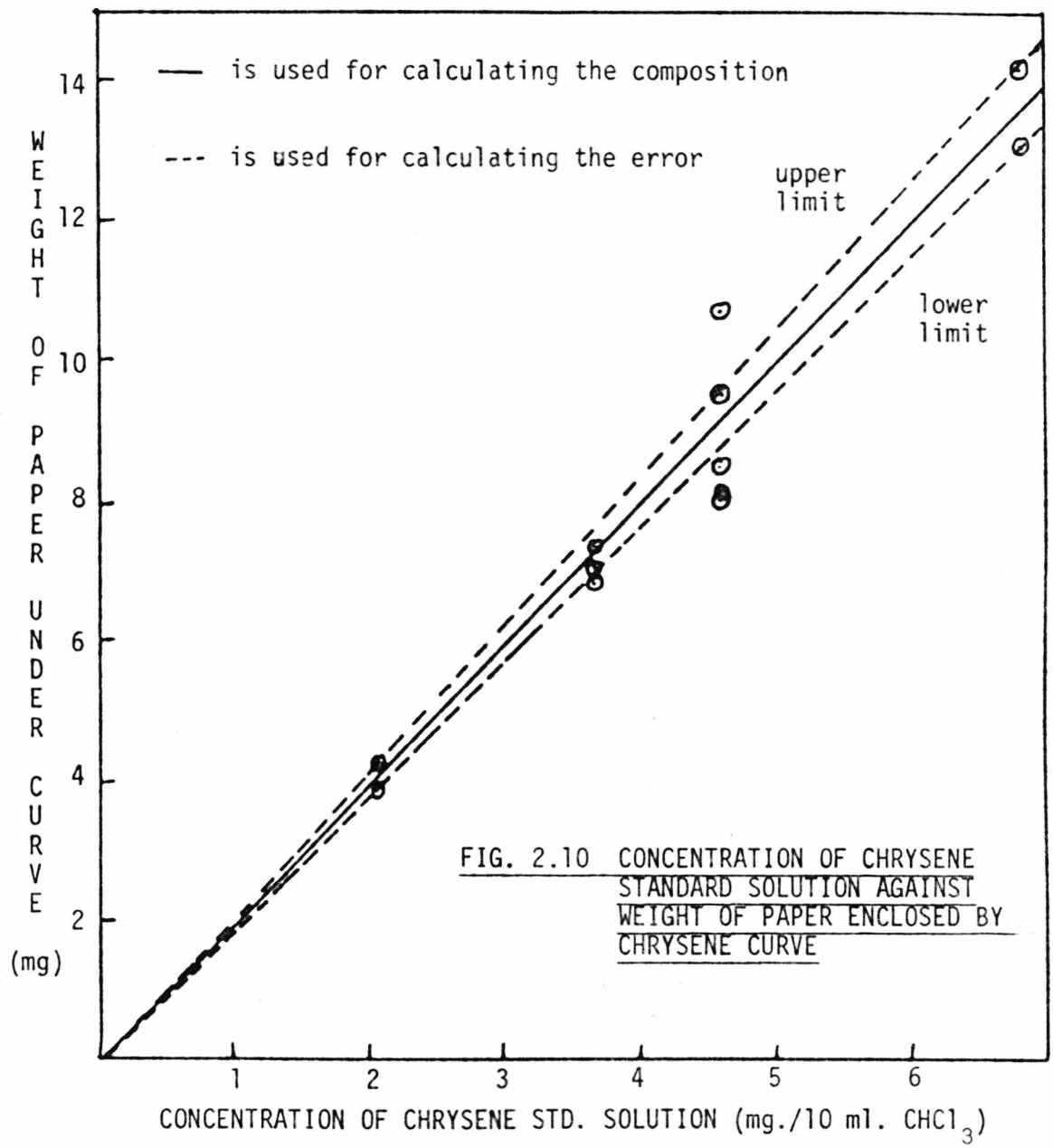

FIG. 2.10 CONCENTRATION OF CHRYSENE STANDARD SOLUTION AGAINST WEIGHT OF PAPER ENCLOSED BY CHRYSENE CURVE

Starting Composition	Concentration of Complexes	Expt. No.	Weight of Paper Under Curve (Grams)	
$A_{.628}/C_{.372}/TCNQ_{1.0}$	0.00378 g./10 ml.	23	0.03554	0.035±0.0005
		24	0.03536	
		25	0.02966	
$A_{.74}/C_{.26}/TCNQ_{1.0}$	0.00387 g./10 ml.	26	0.03817	0.038±0.001
		27	0.03881	
		28	0.03630	
		29	0.03867	
$A_x/C_{1-x}/TCNQ_{1.0}$ (B)	0.00389 g./10 ml.	30	0.03436	0.035±0.001
		31	0.03588	
$A_{.16}/C_{.84}/TCNQ_{1.0}$	0.00382 g./10 ml.	32	0.03753	0.036±0.001
		33	0.03654	
		34	0.03580	
		35	0.03523	
		36	0.03317	
$A_{.19}/C_{.81}/TCNQ_{1.0}$	0.00586 g./10 ml.	37	0.05299	av=0.053±0.001
		38	0.05108	
		39	0.05493	

TABLE 2.12

Starting Composition	V.P.C. Results (A Mole fraction)	Optical Results (A Mole fraction)
$A_{.628}/C_{.372}/TCNQ$	0.08 ± .05	0.12 ± .02
$A_{.74}/C_{.26}/TCNQ$	0.03 ± 0.3	0.22 ± .03
$A_{.626}/C_{.374}/TCNQ_{1.0}$(B)	0.10 ± .04	0.14 ± .04
$A_{.16}/C_{.84}/TCNQ_{1.0}$	0.07 ± .04	0.082 ± .002
$A_{.19}/C_{.81}/TCNQ_{1.0}$	0.09 ± .06	0.10 ± 0.05

TABLE 2.13

Concentration of Pyrene Std. Soln.	Expt. No.	Peak Heights in cm.
1) 0.73 mg./10 ml. $CHCl_3$	1	1.85
	2	1.8
	3	1.9
2) 1.25 mg./10 ml. $CHCl_3$	4	3.4
	5	3.5
	6	3.5
3) 2.84 mg./10 ml. $CHCl_3$	7	7.35
	8	7.3
	9	6.7
	10	6.7
	11	7.0
4) 4.32 mg./10 ml. $CHCl_3$	12	10.6
	13	11.3
	14	11.3

TABLE 2.14 ANALYSIS OF $PYRENE_x/PERYLENE_{1-x}/TCNQ_{1.0}$.

No peaks were observed for either Perylene or TCNQ.

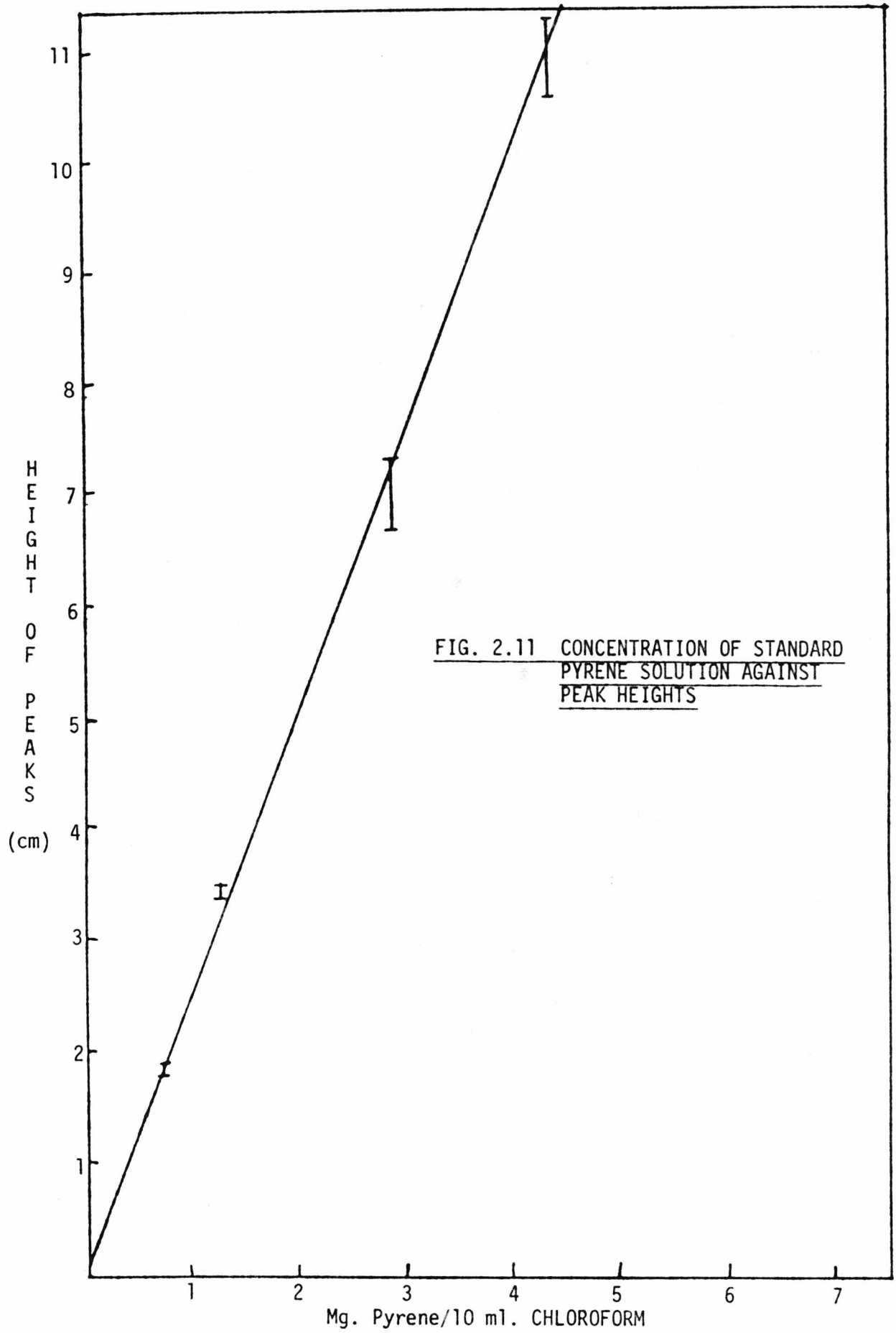

FIG. 2.11 CONCENTRATION OF STANDARD PYRENE SOLUTION AGAINST PEAK HEIGHTS

Concentration of Pyrene Std. Soln. mg./10 ml. $CHCl_3$		Expt. No.	Weight of Area Under Peaks (grams)
1)	1.01	1	0.00489
		2	0.00535
		3	0.00557
2)	1.34	4	0.01000
		5	0.01019
		6	0.01043
3)	2.36	7	0.01786
		8	0.01828
		9	0.01824
4)	4.27	10	0.03131
		11	0.03166
		12	0.03072

TABLE 2.15

The uniformity of chart is also checked. A square inch of the paper is cut and weighted. The results are in Table 2.16 below. The average weight of ten equal square inch of paper is 0.02634 gm.

1) 0.02648 2) 0.02689 3) 0.02662 4) 0.02615

5) 0.02700 6) 0.02683 7) 0.02615 8) 0.02591

9) 0.02605 10) 0.02529

Average = (0.0263±0.00043) gm.

TABLE 2.16

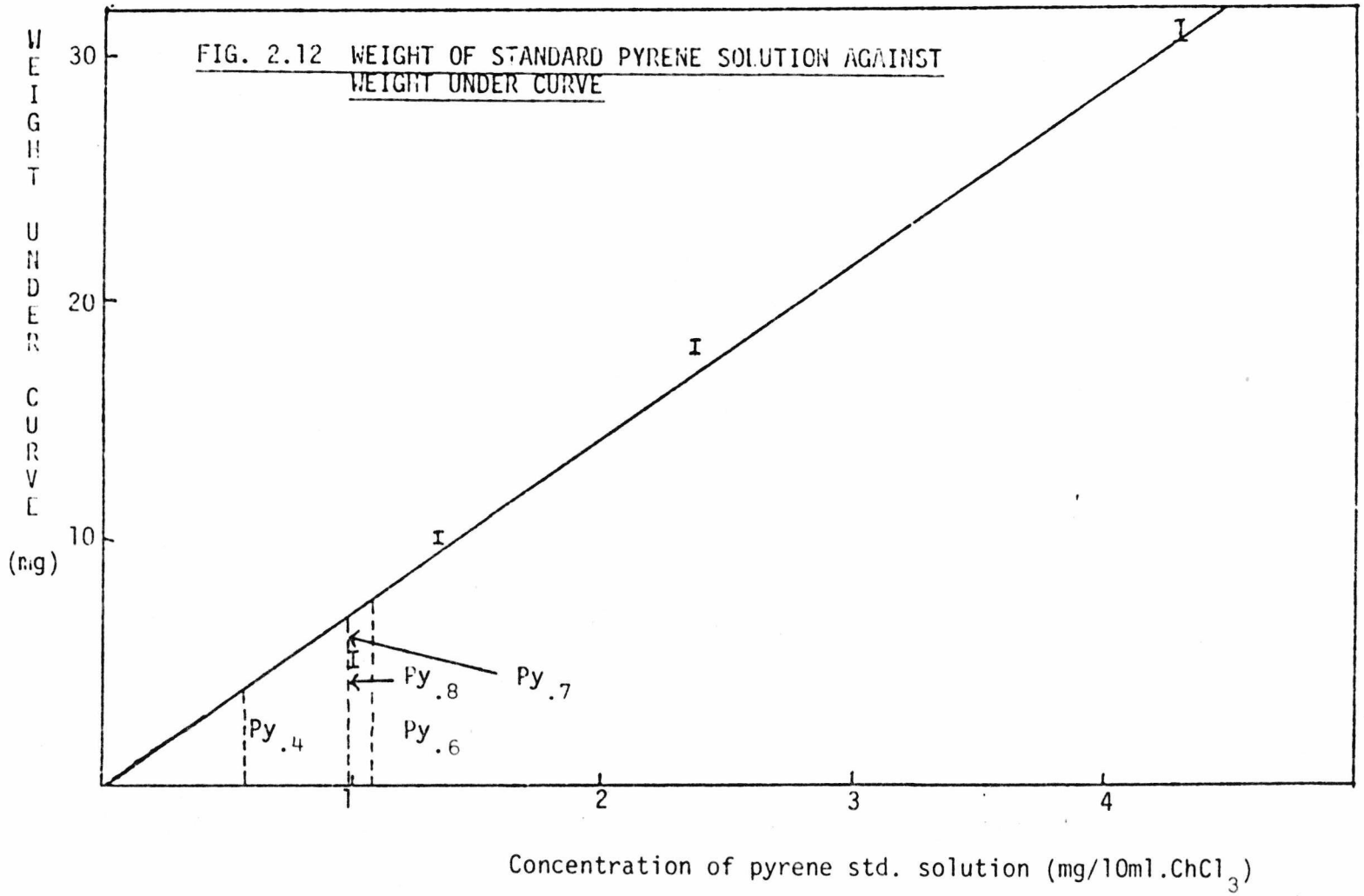
FIG. 2.12 WEIGHT OF STANDARD PYRENE SOLUTION AGAINST WEIGHT UNDER CURVE
WEIGHT UNDER CURVE (mg)
30
20
10
1
2
3
4
Py .4
Py .6
Py .8
Py .7
Concentration of pyrene std. solution (mg/10ml.ChCl3)

Volume of Injection (µl.)	Expt. No.	Peak Heights (cm.)
25	15	9.4
	16	8.6
	17	8.2
	18	8.7
20	19	6.55
	20	7.5
	21	6.7
	22	6.9
15	23	5.5
	24	5.5
	25	6.0
10	26	3.8
	27	3.3
	28	4.0
5	29	2.0
	30	1.9
	31	2.1

TABLE 2.17 SHOWS THE LINEARITY OF PEAK REPRODUCTION WITH RESPECT TO VOLUME OF INJECTION. A SOLUTION OF PYRENE 0.00408 g./10 ml. WAS USED

FIG. 2.13 VOLUME OF STANDARD PYRENE INJECTED AGAINST PEAK HEIGHT

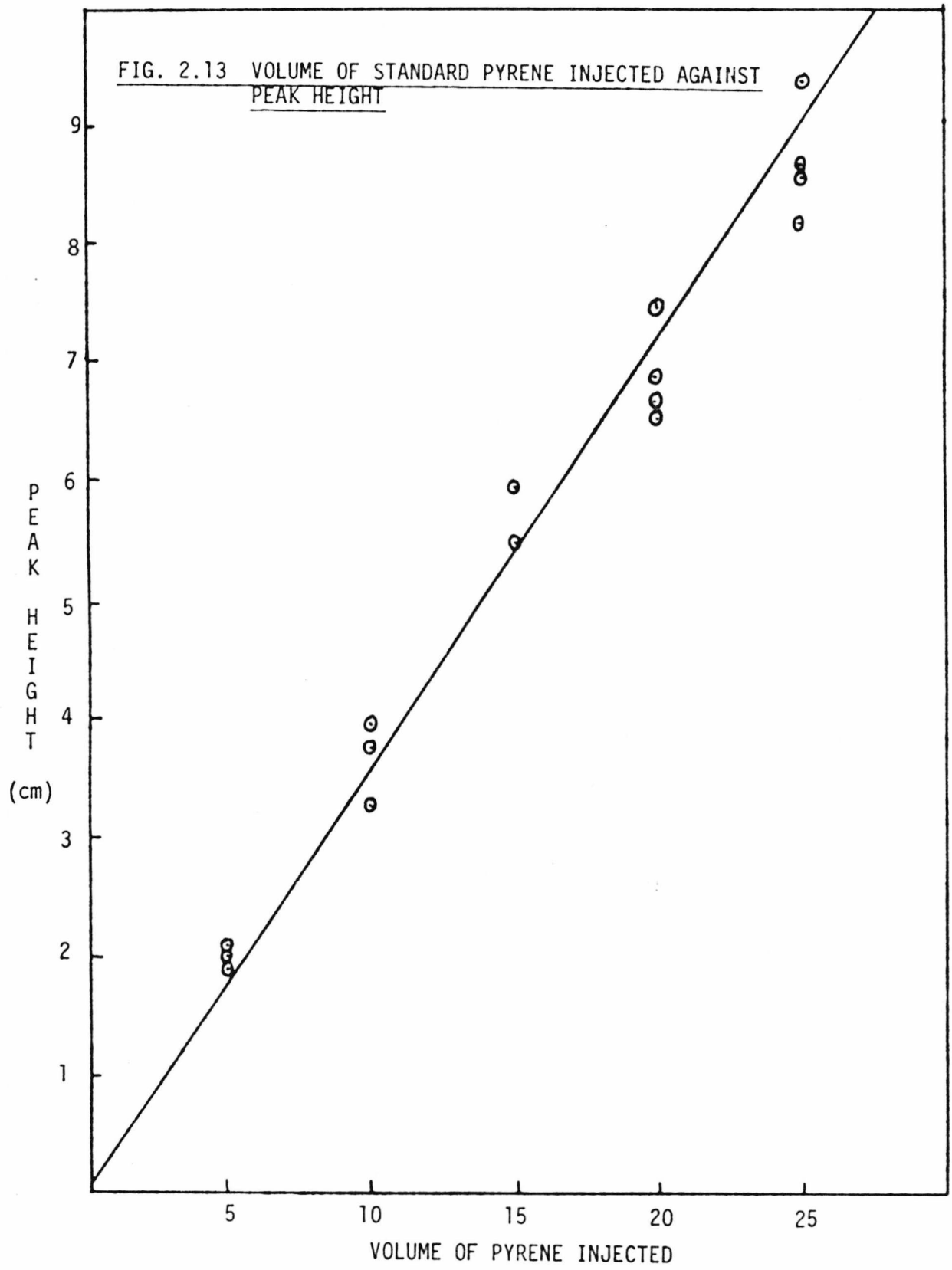

Starting Composition Concentration of Solution	Expt. No.	Weight under Peak (gm.)	Average
1) $Py_{.2}/Pe_{.8}/TCNQ_{1.0}$ 0.00336 g./10 ml.	32	No Detectable Peak	
2) $Py_{.3}/Pe_{.7}/TCNQ_{1.0}$ 0.00412 g./10 ml.	33	No Detectable Peak	
3) $Py_{.4}/Pe_{.6}/TCNQ_{1.0}$ 0.00288 g./10 ml.	34	0.00386	0.00408
	35	0.00410	
	36	0.00400	
	37	0.00435	
4) $Py_{.6}/Pe_{.4}/TCNQ_{1.0}$ 0.00434 g./10 ml.	38	0.00732	0.00768
	39	0.00795	
	40	0.00817	
	41	0.00740	
	42	0.00757	
5) $Py_{.7}/Pe_{.3}/TCNQ_{1.0}$ 0.00474 g./10 ml.	43	0.00780	0.00695
	44	0.00722	
	45	0.00705	
	46	0.00610	
	47	0.00658	
6) $Py_{.8}/Pe_{.2}/TCNQ_{1.0}$ 0.00370 g./10 ml.	48	0.00749	0.0695
	49	0.00726	
	50	0.00640	
	51	0.00665	

TABLE 2.18 COMPLEX ANALYSIS

Starting Composition	V.P.C. Results (Pyrene Mole fraction)	Optical Results (Pyrene Mole fraction)
$Py_{.4}/Pe_{.6}/TCNQ$	.433 ± .029	.39 ± .04
$Py_{.6}/Pe_{.4}/TCNQ$	.53 ± .05	.54 ± .05 .54 ± .01 .49 ± .03
$Py_{.7}/Pe_{.3}/TCNQ$	.44 ± .03	.40 ± .09 .42 ± .07
$Py_{.8}/Pe_{.2}/TCNQ$	.56 ± .04	.51 ± .02

TABLE 2.19 COMPARISON BETWEEN OPTICAL AND V.P.C. RESULTS

Elemental Analysis of $Dibenzothiophen_{.649}/Dibenzofuran_{.351}/TCNQ$

N = 14.59% , C = 74.95% , H = 3.25% ,

S = (6.28-6.32)%

Calculation:

$$\text{Using } 6.28\% \rightarrow \frac{(32.06)(x)(100)}{(184.26)(x)+(168.2)(1-x)+204} = 6.28$$

$$x = .753$$

$$\text{using } 6.32\% \rightarrow x = .758$$

therefore analysed composition is

$Dibenzothiophen_{.756}/Dibenzofuron_{.244}/TCNQ$

cf. spectroscopic analysis (Table 2.7) → x = 0.73 ± .02

0.73 ± .01

0.74 ± .02

2.9 Discussion

The results of vapour phase chromatography and optical analysis are compared for Anthracene$_x$/Chrysene$_{1-x}$/TCNQ and Pyrene$_x$/Perylene$_{1-x}$/TCNQ (Table 2.13 and 2.19). These two independent methods suggested that the two mixed complexes above only formed a fixed donor:donor ratio. The slight variations in the results are only experimental errors. No sign is observed of the formation of 3:1 Perylene/TCNQ as reported recently. (Ishii, 1980). Anthracene$_{.74}$/Chrysene$_{.26}$/TCNQ gave different optical and chromatographic results. This is because this complex is contaminated with component molecules. This analysis was done intentionally to provide a test of sensitivity to changes in donor concentration. The reproducibility of the compositional analysis suggested that the complexes are homogeneous throughout the system. The formation of a fixed ratio is attributed to the difference in lattice structure, molecular shape and size. Table 2.20 lists the lattice type and unit cell dimensions of the parent complexes, for comparison. (See next page.)

Anthracene$_x$/Dibenzothiophen$_{1-x}$/TCNQ and Dibenzothiophen$_x$/Dibenzofuran$_{1-x}$/TCNQ form complete series of mixed molecular complexes (Table 2.5 and 2.7). Anthracene/TCNQ and Dibenzothiophen/TCNQ although having different crystal structure are able to form a mixed complex. This indicated that lattice structure compatibility is not an overriding factor although having the same lattice structure does help. This is further supported by the results of analysis of Phenazine$_x$/Dibenzofuran$_{1-x}$/TCNQ . Both the parent complexes have the same lattice structure and unit cell dimensions; both the donors have almost the same molecular size and shape but the mixed complex formed is of fixed ratio of donors only. This could only be explained in terms of differences in solubilities and formation constants.

Complex	Lattice Type	Cell Dimensions a	b	c	α	β	γ	Reference
Pyrene/TCNQ	Monoclinic	7.14	14.73	10.01			102.5	a
Perylene/TCNQ	Monoclinic	7.32	14.55	10.88			90.4	b
Anthracene/TCNQ	Monoclinic	11.476	12.947	7.004			105.4	c
Chrysene/TCNQ	Triclinic	7.255	7.995	9.210	99.8	89.7	92.7	d
Phenazine/TCNQ	Triclinic	8.437	7.253	8.571	105.61	71.41	101.6	e
Dibenzothiophen/TCNQ	Triclinic	16.29	8.91	6.83	98.4	98.6	100.1	This work
Dibenzofuran/TCNQ	Triclinic	8.0098	8.9971	6.78	97.74	100.68	99.58	This work
Anthracene/TCNB	Monoclinic	9.505	12.748	7.417		92.45		f
Phenanthrene/TCNB	Monoclinic	9.413	13.104	7.260		93.06		g

[a]Prout, Tickle and Wright, 1973; [b]Tickle and Prout, 1973; [c]Williams and Wallwork, 1968;
[d]Munnoch and Wright, 1974; [e]Goldberg and Shmueli, 1973; [f]Tsuchiya, Marumo and Saito, 1972;
[g]Wright, Ohta and Kuroda, 1976

TABLE 2.20 LATTICE TYPE AND UNIT CELL DIMENSIONS OF COMPLEX

The effects of these factors are reflected in the plots of solid compositions against solution compositions (Fig. 2.6 and 2.7). Dibenzothiophen is more favoured than either anthracene or dibenzofuran. Unfortunately, no formation constant data are available for comparison. (The limited solubilities of both donors and acceptors make determination of these formation constants by conventional methods (Mulliken & Person, 1969) difficult and inaccurate.)

It can be suggested that the formation of a complete series of mixed molecular complexes seems to require:

1) Similar solubility and formation constant

2) Similar molecular shape and size

3) Similar crystal lattice structure

in that order. However, in this work it was found that criteria (1) and (2) must be fulfilled.

Wright, Ohta and Kuroda (1976) prepared a series of crystalline mixed complex of $Anthracene_{1-x}/Phenanthrene_{x}$/1,2,4,5 tetracyanobenzene whose parent complex have similar molecular shape and size and also the same crystal lattice structure. Miller and Epstein prepared a series of $(N\text{-methylphenazinium})_{x}(Phenazine)_{1-x}TCNQ$ by substituting neutral phenazine for nontotally symmetric N-methylphenazinium cation. They consider that the removal of the cation would destroy the lattice stability; however, substitution of the N-methylphenazinium cation by a neutral molecule of comparable size, shape and polarisability should stabilize the structure.

Other mixed complexes were prepared in the work (Table 2.3) but they were unable to be analysed for either they are contaminated or no reliable method is available.

Many of the problems encountered in preparation of mixed complexes occur because of the need to use solution growth techniques. If two donors

have very different solubilities or formation constants for complexing with the acceptor, it is unlikely that changing the solvent can totally overcome both problems. Equally, in such cases the vapour growth method is unlikely to be significantly better, as differences in solubility will frequently be reflected in differences in volatility. Melt growth of mixed complexes has been used by Koizumi and Matsunaga (1974) for phenanthrene/anthracene/picric acid, but the method is of limited applicability as mentioned in Section 2.3. Even in cases where varying ratios of two donors could be melted together with an equimolar quantity of acceptor and cooled to form a solid without decomposition, it would be necessary to examine the solid carefully to ensure the product was in fact a mixed complex rather than a mixture of microcrystalline regions of different compositions. The reproducibility of analytical results on different samples of a given mixed complex grown from solution would be unlikely if the samples were simply mixtures of crystals of the two parent complexes, and this conclusion is supported by the results of electrical measurements on single crystals of the mixed complexes reported elsewhere in this thesis.

For the systems studied here, there is no simple method of determining whether the two donors in a mixed complex are arranged randomly amongst the donor sites in the lattice or are either ordered (e.g. in $D_1AD_2AD_1AD_2A$ ... regions) or clustered (e.g. ... $(D_1AD_1AD_1A)_n(D_2AD_2AD_2A)_m$...) However, studies of ESR hyperfine structure in the mixed complexes of bis(8 hydroxyquinolinato)Pd^{II} or Cu^{II} with chloranil (Prout, Williams & Wright, 1966) suggest that where the shapes and sizes of the two donor molecules are similar the arrangement is random. (Any clustering would have resulted in dipolar broadening of the Cu^{II} hyperfine structure even at low doping levels, whereas in fact the onset of broadening coincided with doping levels such that each Cu complex donor site would have at least one

nearest neighbour Cu complex amongst the surrounding donor sites.) Thus, for complexes forming complete mixed series over the whole range $0<x<1$ the assumption of random donor site occupancy is justified. The situation in systems with a strong tendency to one composition irrespective of the donor ratio in the starting solution used for crystal growth (e.g. Pyrene/Perylene/TCNQ) will be discussed later in the Chapter on crystal structures.

* * * * * *

Chapter 3

Structural Studies of Mixed Molecular Complexes

3.1 Introduction

Many properties of crystalline mixed molecular complexes are influenced by crystal structure. The formation of a continuous series of mixed complexes $(\text{Donor 1})_x(\text{Donor 2})_{1-x}\text{Acceptor}$, with $0<x<1$, implies that the lattice structure (or structures) of the mixed complex can accommodate either donor with roughly equal facility. In other cases such as pyrene/perylene/TCNQ and anthracene/chrysene/TCNQ (Chapter 2) the formation of only limited composition ranges of mixed complexes suggests either the formation of specific new phases with structure different from those of either parent complex, or that the parent complex structures are such as to permit only limited replacement of the donor by a guest donor. Information on the crystal structures of the mixed and parent complexes is therefore useful in rationalising the results of Chapter 2 on the preparation of mixed complexes. The intensities of charge transfer transitions in crystalline molecular complexes also depend on the relative orientation and separation of donor and acceptor (Chapter 4), so that structural information is essential to the interpretation of spectroscopic data. Furthermore, as will be shown in Chapter 5 and 6, discussion of the electrical conductivity properties of mixed molecular complexes also involves the use of structural data for the crystalline complexes.

Although the overlap and orientation principle (Mulliken, 1956) provides one basis for predicting the relative orientation of the electron donor and acceptor molecules, there are cases where the observed

and predicted overlap do not agree. As has been pointed out by Mayoh and Prout (1972) several different types of intermolecular interactions occur in molecular complexes. These interactions are discussed in the next section of this chapter. In general, the orientation which maximises any one of these interactions will not necessarily maximise the others, and in some cases it is not even straightforward to determine the orientation maximising just one of the interactions. For example, although the symmetries of the highest occupied donor orbital and lowest vacant acceptor orbital are of some relevance to the discussion of charge transfer interactions, Mayoh and Prout (1972) have shown that only calculations taking into account charge transfer interactions between all occupied donor orbitals and all vacant acceptor orbitals are reliable in predicting which orientation maximises total charge transfer interaction. Hence it is very difficult to predict the structures of π-π^* molecular complexes, and information from x-ray diffraction is essential for correlation of structure with other physical properties of these materials.

The crystal structures of most of the parent complexes of the mixed complex series studied in the present work have been determined. To complete the information on parent complex structures, the crystal structure of the dibenzothiophen/TCNQ complex has been determined and is reported in this chapter. X-ray powder diffraction provides a means of identifying the structures of mixed complexes quickly by comparison with the powder diffraction patterns of the parent complexes, and these studies are also reported in this chapter together with investigations of melting points and differential scanning calorimetric studies.

3.2 The Forces Involved in a Molecular Crystal

In molecular crystals the molecules are held together by intermolecular

forces which are weak compared to the forces that are holding together atoms of the molecule. These intermolecular attractive forces are of the Van der Waals type. In cases where an electron donor and an electron acceptor are involved, charge transfer interaction takes place. Short range intermolecular repulsions also play an important role in determining optimum lattice packing.

3.3 Charge Transfer Interaction

A charge transfer interaction will occur when an electron donor interacts with an electron acceptor forming a stable complex exhibiting characteristic charge transfer bands.

Mulliken (1952) described a 1:1 donor:acceptor complex in the ground state N in terms of the wavefunction ψ_N :

$$\psi_N = a\psi_0(D,A) + b\psi_1(D^+-A^-) \qquad (1)$$

which is normalised to

$$\int \psi_N\psi_N^* dv = a^2 + b^2 + 2abS_{01} = 1$$

(where $S_{01}=\int\psi_0\psi_1 dv$ (2)

with integration carried over all space, is the overlap integral between function ψ_0 and ψ_1) . S_{01} is small if the complex is loose and therefore $a^2+b^2\approx 1$.

b^2 is the fraction of an electron transferred from the donor to the acceptor in the ground state. In loose complexes between closed-shell donors and acceptors $b^2<<a^2$.

Charge-transfer state is given by

$$\psi_v = -b^*\psi_0 (D,A) + a^*\psi_1(D^+-A^-) \qquad (3)$$

b^* and a^* are determined by quantum theory requirement that the excited state wave function be orthogonal to the ground state function:

$$\int \psi_v \psi_N dv = 0$$

which is normalised

$$\int \psi_v^2 dv = a^{*2} + b^{*2} - 2a^* b^* S_{01} = 1 \qquad (4)$$

For loose molecular complexes, the ground state is mostly no bond ($a^2 >> b^2$) and the excited states is mostly dative ($a^{*2} >> b^{*2}$), hence excitation of an electron from ψ_N to ψ_v is essentially an electron transfer from D to A.

Complexes are classified as strong or weak depending on whether their energy of formation and formation constants are large or small respectively. Examples of weak ($\pi.\pi$) and strong ($n.\nu$) complexes are tabulated below in Table 3.1.

TABLE 3.1 COMMON TYPES OF DONORS AND ACCEPTORS

Donor Type	Example	Dative Electron from	Acceptor Type	Example	Dative Electron goes to
n	:NR	Non bonding lone pair	ν	BCl_3	Vacant orbital
$b\pi$	benzene	Bonding π orbital	$a\pi$	TCNE	Antibonding π orbital
			$a\sigma$	I_2, $HQ^{\dagger}$	Antibonding σ orbital

"Dative electron" refers to the electron transferred from Donor to Acceptor

†Molecules such as phenol, water, and other molecules that give hydrogen bonding.

3.4 Attractive Forces

There are four types of attractive forces:

1) Dipole-dipole interaction
2) Dipole-induced-dipole interaction
3) Induced dipole-induced dipole interaction
4) Quadrupolar and higher order interaction.

1. Dipole-Dipole Interaction

The energy of dipole-dipole interaction depends on the magnitude of the dipoles, their separation and their relative orientations.

This energy is given by Keesom (1912) as:

$$E = \frac{-\mu_1 \mu_2}{R^3} \left[2\cos\theta_1 \cos\theta_2 - \sin\theta_1 \sin\theta_2 \cos(\phi_1 - \phi_2)\right]$$

where θ_1, ϕ_1 and θ_2, ϕ_2 specifying polar co-ordinates with orientations respectively. μ_1 and μ_2 are dipole moments and R=distance between the centres of the two dipoles.

If all orientations are equally probable then, the average E over all orientations is zero. However, by using Boltzman statistics, we get: (Lennard-Jones, 1931):

$$E = -\frac{2}{3} \frac{\mu_1^2 \mu_2^2}{R^6} \cdot \frac{1}{kT} \qquad \frac{\mu_1 \mu_2}{R^3} << kT$$

This equation is correct for a solution. In solid, the approach distance is small hence:

$$E = \frac{-2\mu_1 \mu_2}{R^3} \qquad \frac{\mu_1 \mu_2}{R^3} >> kT \quad .$$

Hence in solution the energy of interaction depends on $\frac{1}{R^6}$ while in solid it depends on $\frac{1}{R^3}$.

2. Dipole-Induced Dipole Interaction

Consider a dipole of μ_1: This will produce an electric field of $F = \frac{\mu_1}{R^3}$ at a distance R.

This dipole can induce a dipole μ_2 in a molecule of polarisability α where

$$\mu_2 = \alpha F = \frac{\alpha\mu_1}{R^3}$$

hence the total interaction energy $= -2\left(\frac{\mu_1}{R^3}\right).\left(\frac{\mu_1\alpha}{R^3}\right) = -2\frac{\alpha\mu_1^2}{R^6}$

This interaction is commonly called the Debye induction effect. It varies as $\frac{1}{R^6}$. This type of interaction will only be orientation dependent when the polarisability of the molecule on which the induced dipole is sited is different in different molecular directions.

3. Induced Dipole-Induced Dipole Interaction

The theory of dispersion forces was first developed by London (1937), as follows. Consider two symmetrical molecules, and let one electron on each be displaced by a small amount to produce two dipoles. The interaction energy of the two symmetrical molecules may then be obtained as the sum of the energy required to deform the electron clouds of the two molecules (related to the polarisability) and the attractive force between the two resulting dipoles. Quantum mechanics, however, requires, via the uncertainty principle, that the displaced electrons are moving rather than fixed in a precise position, so that the two dipoles are really oscillators. London calculated the frequency of these oscillators and hence derived the net interaction energy as

$$-\frac{3}{4}\frac{h\nu_0\alpha^2}{R^6}$$

where α is the molecular polarisability and ν_0 is a frequency which may be calculated from the variation of molar refraction with wavelength (hence the

name "dispersion force").

4. Quadrupolar and Higher Order Interaction

The interaction is between a quadrupole with dipoles on adjacent molecules or with adjacent quadrupoles. Lippert, Hanna and Trotter (1969) showed that their interactions are significant. The dipole-quadrupole interactions are proportional to $\frac{1}{R^8}$ and quadrupole-quadrupole interactions are proportional to $\frac{1}{R^{10}}$. Hence they are extremely short range. These interactions are not very orientation sensitive because of the symmetry of the charge distribution in a quadrupole.

3.5 Repulsive Forces

The repulsive forces are electrostatic in nature. When two molecules are brought nearer together, the electron clouds repel one another. Hence, the molecules are kept apart and at the same time the charge clouds are distorted. This distortion is related to their polarisability. As the distance between the molecules becomes smaller, the distortion of electron clouds becomes difficult, hence this results in increasing repulsive force. Repulsive forces tend to be very short range and typically of the form R^{-n} with $n \simeq 12$ or ae^{-bR}, and are important in determining lattice packing.

3.6 Factors that Determine the Crystal Structure of π-π^* Molecular Complexes

Most of the crystal structures of the parent complexes used in this work have been determined. These complexes show characteristic packing

of stacks of alternate donor and acceptor molecules. There are three main stacking arrangements (Prout & Wright, 1968) as shown in Fig. 3.1 . These types of stacking are not surprising because they not only give efficient lattice packing but also favour charge transfer as well as van der Waals interactions. Mayoh and Prout (1972) have done a theoretical study on the influence of charge transfer resonance stabilization of the ground state on the relative orientation of the donor and acceptor, comparing the orientations which theoretically maximise charge transfer interactions with the observed orientations. In most cases the observed orientations are close to those maximising the charge transfer interaction. In cases where the complexes contain metal atoms or show hydrogen bonding, the observed orientation may be far from that maximising charge transfer. Since charge transfer stabilization energy is not as large as London dispersion, dipole-dipole, dipole-induced dipole and hydrogen bonding interactions, the donor acceptor orientation will only significantly be determined by charge transfer stabilization if the above stronger interactions are absent.

Quantum mechanical calculations by Kuroda, Amano, Ikemoto and Akamatu (1967) for naphthalene/TCNE and pyrene/TCNE , including all possible charge transfer configurations, suggested that charge transfer plays an important role in determining the relative positions of the molecular centres but a lesser role in determining the relative orientation of the donor and acceptor.

Goldberg (1975) calculated the donor-acceptor intermolecular overlap integrals for interactions of the three highest occupied MO's of the donor molecules with the LUMO of TCNQ . Fig. 3.2 shows the variation in value of the overlap integral S_{ij} , where i symbolises a high occupied MO of the donor and j the LUMO of TCNQ , with rotation of the donor above the acceptor for four molecules. From the calculation,

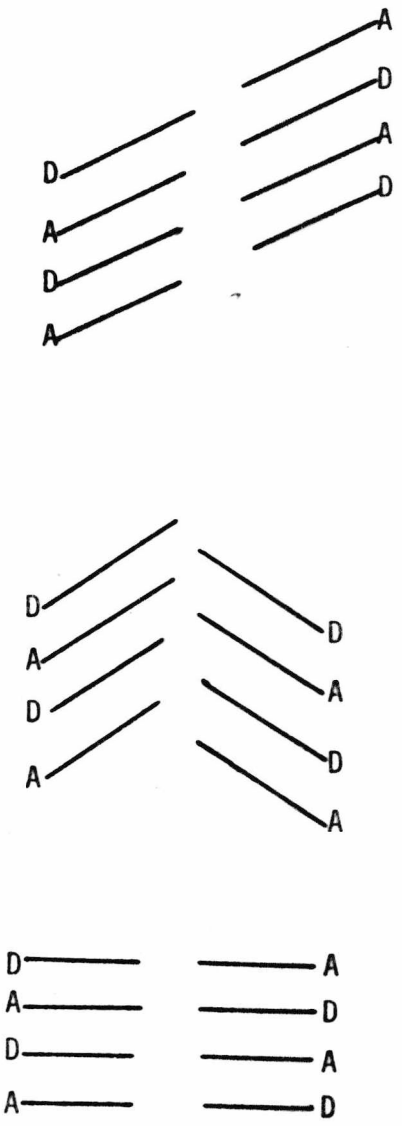

Fig. 3.1 THE THREE MAIN PACKING ARRANGEMENTS OF π-π^* MOLECULAR COMPLEXES

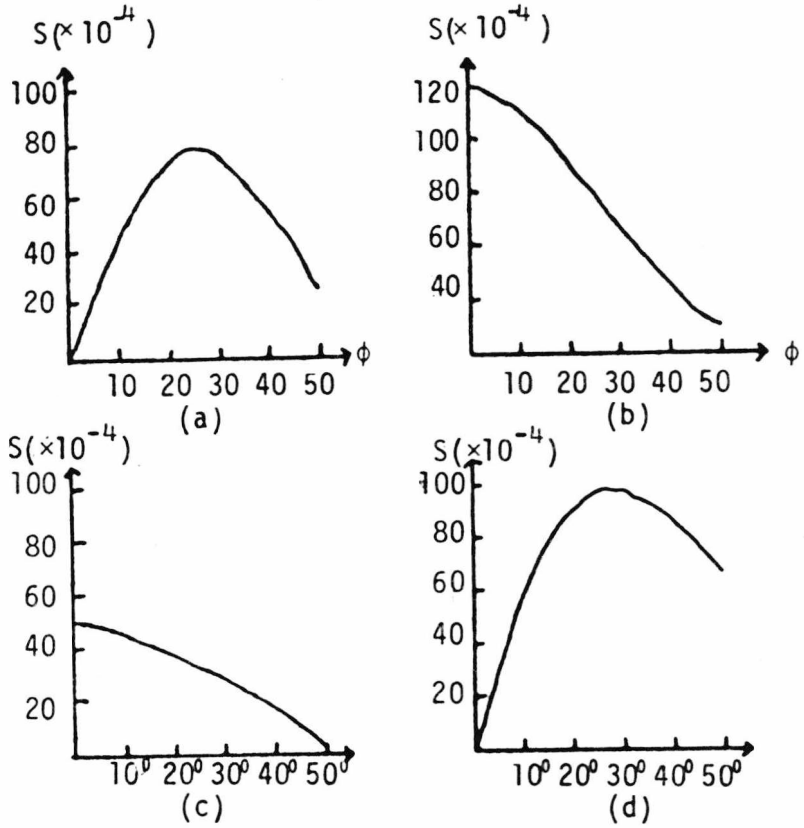

FIG. 3.2 INTERMOLECULAR OVERLAP INTEGRAL S AS A FUNCTION OF ROTATION OF THE DONOR ABOVE A FIXED ACCEPTOR BY AN ANGLE ϕ .
The results correspond to overlap between the HOMO of the donor and the LUMO of the acceptor in the TCNQ complexes with
a) PHT b) TMPD c) DPDO d) Phenazine.
In (a), (b) and (d) molecular centres of unlike molecules are superimposed, while in (c) the centre of DPDO is displaced by 1.0 Å along the axis of lowest inertia of TCNQ . $\phi=0^0$ correspond to parallel axial systems of the constituents.

PHT = 1,10-phenanthroline
TMPD= N,N,N',N' tetramethyl-p-phenylenediamine
DPDO= Dibenzo-p-dioxin

the conclusion is that though charge transfer interaction is much weaker than the repulsion and dispersion forces, it is a determining factor on the mode of donor acceptor overlap. However, most of the best electron donors are those that tend to be highly polarisable, and the best acceptors contain highly polar electron withdrawing substituents. This will result in the likelihood that dipole-induced dipole and dispersion forces are also of significance in determining the donor acceptor overlap.

Dewar and Thompson (1966) have made a systematical comparison of the equilibrium constants for a series of TCNE complexes of polycyclic aromatic hydrocarbons and concluded that the charge transfer interaction is not a major factor determining the intermolecular binding in these complexes in solution. However, conclusions based on interactions in solution need not necessarily apply equally to solids, as solvent effects may obscure charge transfer interactions in solution.

The other controlling factor in the crystal structure is the molecular shape. Small molecules find it easier to orientate themselves in the lattice site as compared to bulky molecules. For long molecules like chrysene and TCNQ the repulsion between molecules in adjacent stacks will prevent rotation about an axis perpendicular to the plane of the molecules. This implies that closer approach is achieved only when the molecules align parallel to one another.

Orientational disorder is found in about 40% of the crystalline π-molecular compounds (Herbstein, 1971) studied and this makes a significant contribution to the positive ΔS_f^0 (standard entropies of formation) found for many molecular compounds and thus has an important stabilizing role.

The conclusion, therefore, is that the charge transfer is an important stabilizing force in donor-acceptor orientation. However it is not

the only factor as dipole-induced dipole interactions have been observed to be present in many molecular complexes. Hence there is no one set of forces or factors that determines the crystal structure of π-π^* molecular complexes.

3.7 The Crystal Structure of Dibenzothiophen/TCNQ

Structure Solution

The structure was solved by Patterson and Fourier method. A Fourier series based on $F^2_{hk\ell}$ instead of $F_{hk\ell}$ produces a vector diagram in three-dimensions, in which lines from the origin to the peaks correspond to lengths and directions of vectors between pairs of atoms in the lattice, and peak intensities are proportional to the products of the scattering powers of the atom concerned.

Dibenzothiophen/TCNQ has a triclinic unit cell with space group $P\bar{1}$, containing two molecules of the complex. Each molecule is thus located at a general position possessing no crystallographically required symmetry. However, the TCNQ molecule clearly has a centre of symmetry, even though this is not required crystallographically. Hence the interatomic vectors between two TCNQ molecules related by the crystallographic centre of symmetry at the cell origin include one very large vector (12C-C+4N-N vectors superimposed) at (2x,2y,2z) where x,y and z are the co-ordinates of the centre of the TCNQ molecule, as shown in Fig. 3.3 below. This large vector permits location of the centroid of the TCNQ molecule, while the plane and orientation of the molecule are revealed by the coplanar set of vectors between atoms in an individual TCNQ molecule.

As observed from the overlap diagram of Fig. 3.8, the peak intensities arising from atoms of TCNQ are not affected by scattering of the atoms of dibenzothiophen. The ends of dibenzothiophen molecule are

FIG. 3.3

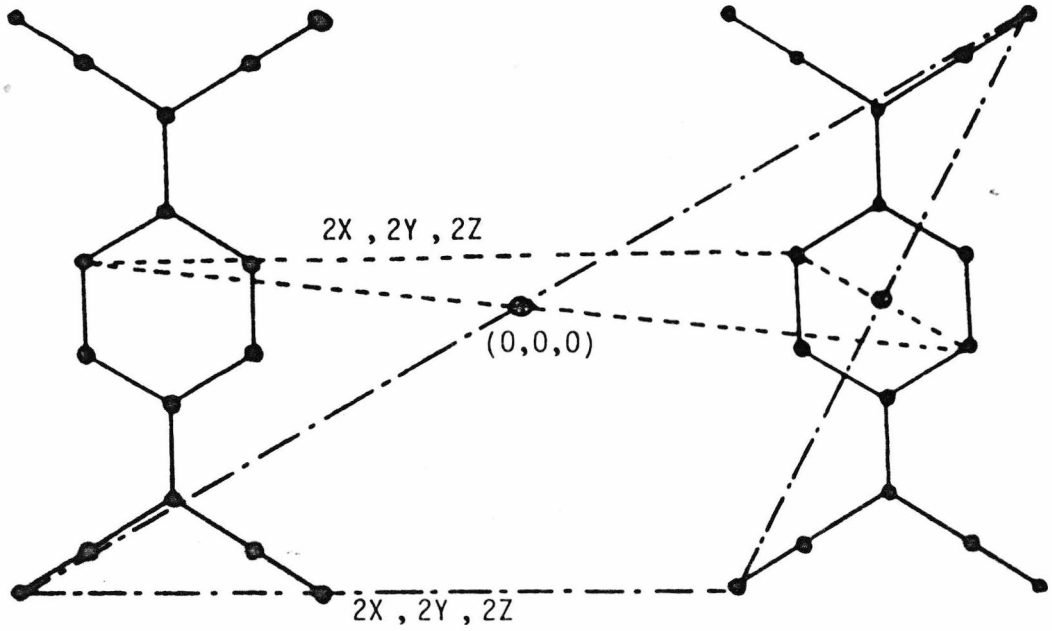

Crystallographic centre of symmetry

Molecular centre of symmetry

slightly twisted and avoid superposition of peaks of atoms of both dibenzothiophen and TCNQ . Even though dibenzothiophen contains a heavy atom, sulfur, the contribution arising from sulfur is no more than that of the superposition of peaks of various C-C and C-N vectors of TCNQ. Thus, the co-ordinates of atoms of TCNQ are derived without much interference from scattering of atoms of dibenzothiophen.

The atomic co-ordinates of TCNQ are derived as follows: the implication diagram (Fig. 3.4) showing the positions and relative magnitudes of intramolecular Patterson peaks for a single TCNQ molecule is first worked out and the relative peak intensities are calculated. Examples of calculations of the relative magnitude of peak intensities are given in Table 3.2.

The procedure of Table 3.2 is repeated for all the points from the implication diagram. The set of peaks around the origin of the actual sharpened three-dimensional Patterson map is then compared with the idealised set from the implication diagram, to obtain a consistent set of co-ordinates for a hypothetical TCNQ molecule in the correct orientation but centred at the crystallographic origin. This procedure was applied, and yielded a satisfactory set of atomic co-ordinates. A large peak at (0.520,0.011,0.048) was identified as the 16-fold interatomic (2x,2y,2z) vector, from which the position of the TCNQ centroid was obtained. This value was added to each of the original TCNQ atom co-ordinates to obtain a TCNQ molecule translated to its correct position in the lattice. An F_0 synthesis with phases calculated for these TCNQ atomic co-ordinates revealed the dibenzothiophen molecule.

Further details of the structure determination together with lists of structure factors and thermal parameters are given in Appendix I.

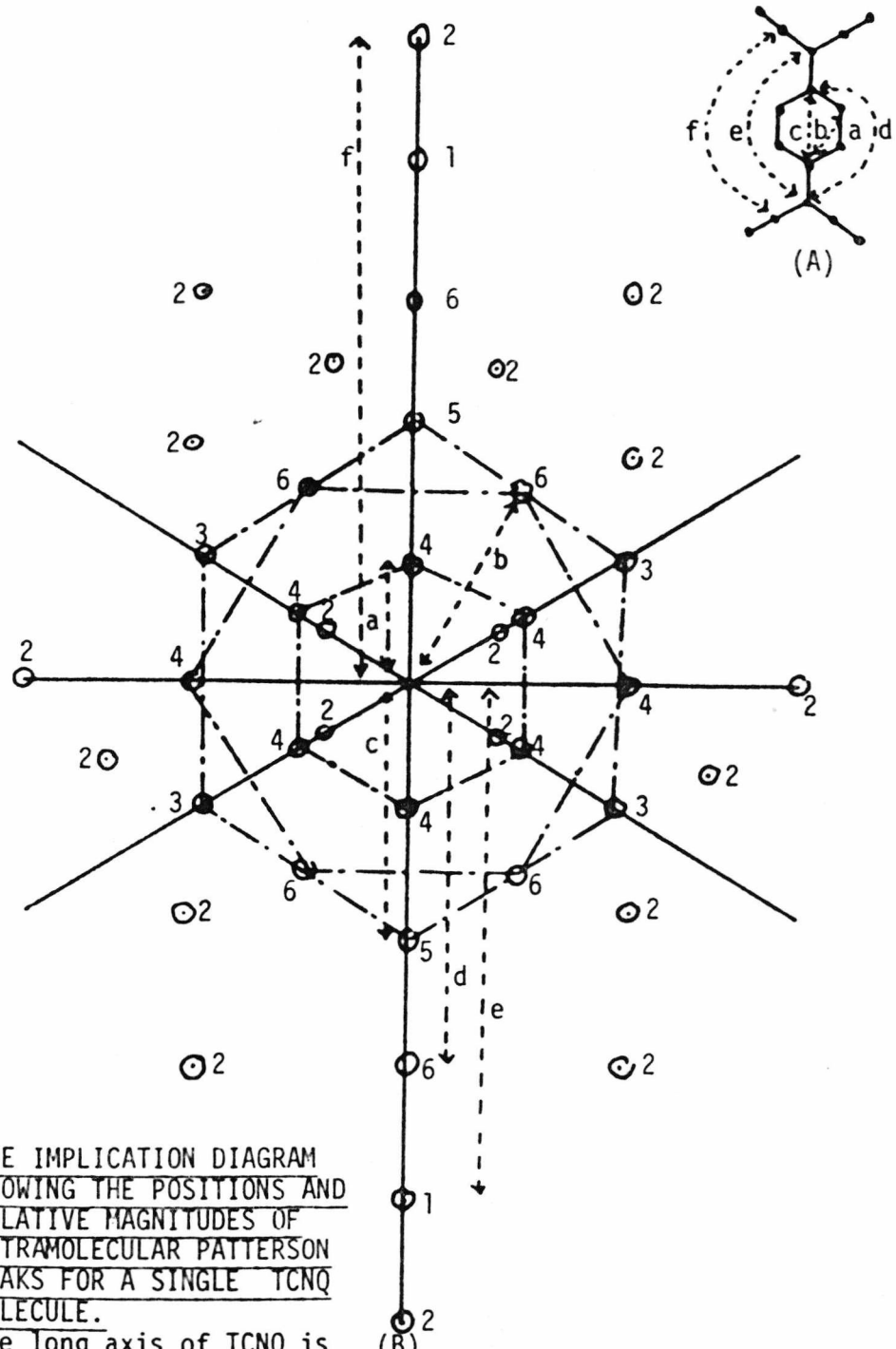

FIG. 3.4 THE IMPLICATION DIAGRAM SHOWING THE POSITIONS AND RELATIVE MAGNITUDES OF INTRAMOLECULAR PATTERSON PEAKS FOR A SINGLE TCNQ MOLECULE.
The long axis of TCNQ is shown in (A). The positions and directions of peaks are derived from (A) and the relative magnitude of peak intensities are given in (B) indicated by numbers.

Vectors (See Fig. 3.4 for Symbols)		Relative Magnitude of Peak Intensities
Large 16-fold intermolecular vectors		12 × 36 = 422
12C-C and 4N-N		4 × 49 = 196
		618
Intramolecular Patterson Peaks		
Vectors are taken along long axis of TCNQ		
a	4C-C	4 × 36 = 144
c	5C-C	5 × 36 = 180
d	6C-C	6 × 36 = 216
e	1C-C	1 × 36 = 36
f	2N-N	2 × 49 = 98

TABLE 3.2 EXAMPLES OF CALCULATIONS OF RELATIVE PEAK INTENSITIES

3.8 Results and Discussion

The final atomic co-ordinates of dibenzothiophen/TCNQ are given in Table 3.3, and bond distances and angles are given in Tables 3.4, 3.5. The labelling schemes of atoms, bonds and angles used in Tables 3.3, 3.4, 3.5, 3.6, 3.7, 3.8 are as shown in either Fig. 3.5 or 3.9. Tables 3.4 and 3.5 compare the dimensions of dibenzothiophen (Schaffrin & Trotter, 1970) and TCNQ (Long, Sparks & Trueblood, 1965) molecules. There are no significant differences between chemically equivalent bond lengths or angles in the two molecules or between these parameters and those reported for dibenzothiophen and TCNQ . In Tables 3.6 and 3.7, some of the TCNQ molecule bond lengths and angles are compared with those determined previously. In addition (Table 3.8) Some of the TCNQ molecules bond lengths are compared with those calculated from MO theory (Lowitz, 1967) and those determined for $TCNQ^-$ (Sundareson & Wallwork, 1972; Goldstein, Seff & Trueblood, 1968). There are two purposes for this comparison. Firstly, distortions due to packing considerations or charge transfer interactions could be identified by comparison with other structures. Secondly, this comparison gives a good indication of which variations are significant and which are simply due to the statistical uncertainty involved in x-ray crystallography. From all the above comparisons, it can be concluded that all the results fall within ± 2 standard deviations. Hence the agreement is good. The degree of scatter due to the uncertainty in x-ray crystallography is shown by the two independent determinations of pyrene/TCNQ. The two sets of figures for acenaphthene/TCNQ correspond to two TCNQ molecules in the unit cell, and therefore reflect the degree of internal consistency of the results.

The structure is shown in Fig. 3.8 projected onto the least squares best plane through the dibenzothiophen molecule at x,y,z . The crystal

	X	Y	Z
C(1)	3230(3)	6327(6)	822(8)
C(2)	3431(3)	4805(6)	570(9)
C(3)	2801(4)	3510(6)	67(9)
C(4)	1933(4)	3659(6)	-206(8)
C(5)	1736(4)	5180(7)	57(9)
C(6)	2354(4)	6453(6)	545(9)
C(7)	3867(4)	7608(6)	1349(9)
(C8)	1288(4)	2347(7)	-738(9)
C(9)	3706(4)	9160(7)	1623(10)
C(10)	4750(4)	7523(7)	1619(10)
C(11)	1464(4)	823(7)	-1046(10)
C(12)	417(4)	2457(7)	-1005(9)
N(1)	3609(4)	10415(6)	1888(11)
N(2)	5447(4)	7476(6)	1863(10)
N(3)	1598(4)	-377(6)	-1316(10)
N(4)	-279(4)	2546(7)	-1199(10)
C(13)	4024(5)	8267(8)	6548(11)
C(14)	3184(5)	8218(7)	6243(10)
C(15)	2640(4)	6750(7)	5714(9)
C(16)	2963(4)	5385(7)	5532(9)
C(17)	3838(4)	5484(8)	5857(9)
C(18)	4363(4)	6950(9)	6375(11)
C(19)	859(5)	1719(11)	3883(11)
C(20)	758(4)	3205(10)	4182(11)
C(21)	1498(4)	4366(8)	4754(9)
C(22)	2300(4)	3999(7)	4964(9)
C(23)	2381(4)	2475(9)	4655(10)
C(24)	1648(5)	1324(9)	4098(11)
S(1)	1538(1)	6370(2)	5241(3)
H(1)	4034	4688	755
H(2)	2947	2463	-105
H(3)	1133	5291	-125
H(4)	2207	7488	740
H(5)	4416	9289	6910

TABLE 3.3 FINAL ATOMIC CO-ORDINATES ($\times 10^4$) , WITH STANDARD DEVIATIONS IN PARENTHESES

TABLE 3.3 FINAL ATOMIC CO-ORDINATES ($\times 10^4$), WITH STANDARD DEVIATIONS IN PARENTHESES (Cont'd.)

	X	Y	Z
H(6)	2962	9187	6396
H(7)	4083	4539	5714
H(8)	4988	7048	6640
H(9)	346	883	3499
H(10)	184	3457	3996
H(11)	2947	2190	4830
H(12)	1691	217	3850

is built up of stacks along $\underline{c}$ of alternating donor and acceptor molecules characteristic of π-π^* electron-donor acceptor complexes. The dibenzothiophen molecule as a whole is close to planar (maximum deviation 0.017 Å). However, better planes (within 0.006 Å) can be fitted to the three individual rings of the molecule, and the angles between the normals to the 5 membered ring and the six membered rings are 0.4 and 0.7°, similar to those found in the structure of pure dibenzothiophen. Similarly, the maximum deviation from the least squares best plane through the whole TCNQ molecule is 0.034 Å, but the central ring is very accurately planar (within 0.002 Å) and planes through the two $-C(CN)_2$ groups (±0.007 Å) make angles of 0.4 and 1.5° with the central ring plane. These small twists of the ends of the molecule may arise from lattice packing effects due to the slight asymmetry in the environment of the TCNQ molecule. The normal to the least squares best plane through the whole dibenzothiophen molecule is only 1.9° away from the $\underline{c}$ axis, and the best planes through the donor and acceptor molecules are only 0.7° away from parallel.

In $P\bar{1}$ with two molecules per cell in general positions, the orientation and separation of TCNQ molecules above and below a given

BOND DISTANCES (Å)	This Work	Literature	ANGLES (Deg.)	This Work	Literature
C(1) - C(2)	1.443(7)	1.446(4)	C(2) - C(1) - C(6)	118.7(5)	118.3(2)
C(2) - C(3)	1.367(8)	1.346(4)	C(1) - C(2) - C(3)	120.5(5)	121.0(2)
C(3) - C(4)	1.432(8)	1.450(4)	C(2) - C(3) - C(4)	119.9(5)	120.7(2)
C(4) - C(5)	1.439(8)	1.446(4)	C(3) - C(4) - C(5)	119.3(5)	118.3(2)
C(5) - C(6)	1.343(8)	1.346(4)	C(4) - C(5) - C(6)	120.8(5)	121.0(2)
C(6) - C(1)	1.440(8)	1.450(4)	C(5) - C(6) - C(1)	120.6(5)	120.7(2)
C(1) - C(7)	1.365(8)	1.374(4)	C(6) - C(1) - C(7)	121.4(5)	120.7(2)
C(4) - C(8)	1.391(8)	1.374(4)	C(2) - C(1) - C(7)	119.8(5)	121.0(2)
C(7) - C(9)	1.443(8)	1.440(4)	C(3) - C(4) - C(8)	120.3(5)	120.7(2)
C(7) - C(10)	1.442(8)	1.441(4)	C(5) - C(4) - C(8)	120.4(5)	121.0(2)
C(8) - C(11)	1.429(8)	1.440(4)	C(1) - C(7) - C(9)	122.4(5)	121.8(2)
C(8) - C(12)	1.427(8)	1.441(4)	C(1) - C(7) - C(10)	122.9(5)	122.0(2)
C(9) - N(1)	1.149(7)	1.139(3)	C(4) - C(8) - C(11)	121.7(5)	121.8(2)
C(10)-N(2)	1.133(7)	1.141(3)	C(4) - C(8) - C(12)	121.6(5)	122.0(2)
C(11)-N(3)	1.124(7)	1.139(3)	C(9) - C(7) - C(10)	114.7(5)	116.1(2)
C(12)-N(4)	1.143(8)	1.141(3)	C(11)-C(8) - C(12)	116.7(5)	116.1(2)
			C(7) - C(9) - N(1)	177.3(7)	179.6(2)
			C(7) - C(10)-N(2)	178.8(7)	179.4(2)
			C(8) - C(11)-N(3)	179.0(8)	179.6(2)
			C(8) - C(12)-N(4)	179.3(7)	179.4(2)

TABLE 3.4 COMPARISON OF BOND DISTANCES (Å) AND ANGLES (DEG.) IN TCNQ WITH E.S.D.'s IN PARENTHESES

BOND	DISTANCES This Work	Literature	ANGLES (Deg.)	This Work	Literature
C(13)-C(14)	1.346(10)	1.371(11)	C(14)-C(13)-C(18)	122.7(6)	122.0(7)
(C13)-C(18)	1.381(10)	1.380(11)	C(13)-C(14)-C(15)	117.7(6)	118.1(7)
C(14)-C(15)	1.409 (9)	1.387(11)	C(14)-C(15)-C(16)	121.1(8)	121.5(7)
C(15)-C(16)	1.406 (8)	1.409(11)	C(14)-C(15)- S(1)	126.8(5)	126.7(7)
C(15)- S(1)	1.741 (6)	1.746 (8)	C(16)-C(15)- S(1)	112.1(5)	111.8(7)
C(16)-C(17)	1.396 (8)	1.393(11)	C(15)-C(16)-C(17)	119.4(6)	118.1(7)
C(16)-C(22)	1.452 (8)	1.441(11)	C(15)-C(16)-C(22)	112.5(5)	112.4(7)
C(17)-C(18)	1.395 (9)	1.379(11)	C(17)-C(16)-C(22)	128.0(6)	129.4(7)
C(19)-C(20)	1.353(11)	1.396(11)	C(16)-C(17)-C(18)	118.4(6)	120.4(7)
C(19)-C(24)	1.386(11)	1.390(11)	C(17)-C(18)-C(13)	120.6(6)	119.8(7)
C(20)-C(21)	1.408 (9)	1.384(11)	C(20)-C(19)-C(24)	122.6(7)	121.1(7)
C(21)-C(22)	1.395 (8)	1.408(11)	C(19)-C(20)-C(21)	117.0(7)	117.4(7)
C(21)-S(1)	1.756 (7)	1.734 (8)	C(20)-C(21)-C(22)	121.4(7)	121.6(7)
C(22)-C(23)	1.377 (9)	1.391(11)	C(20)-C(21)- S(1)	125.9(5)	125.6(6)
C(23)-C(24)	1.395 (9)	1.361(11)	C(22)-C(21)- S(1)	112.7(5)	112.8(6)
			C(15)- S(1)-C(21)	91.2(6)	91.5(4)
			C(21)-C(22)-C(23)	120.1(6)	119.2(7)
			C(21)-C(22)-C(16)	111.4(6)	111.4(7)
			C(16)-C(22)-C(23)	128.5(6)	129.3(7)
			C(22)-C(23)-C(24)	118.5(7)	119.5(7)
			C(23)-C(24)-C(29)	120.3(7)	121.1(7)

TABLE 3.5 COMPARISON OF BOND DISTANCES (Å) AND ANGLES (DEG.) IN DIBENZOTHIOPHEN WITH E.S.D.'s IN PARENTHESES

Variable Donor	Ref.	a	b	c	d	e	f	g	h
HMB	a	1.358	1.462	1.391	1.445	1.152			
Anthracene	b	1.35	1.46	1.37	1.42	1.13			
Cu Ox	c	1.365	1.43	1.377	1.437	1.141	1.448	1.439	1.142
Pyrene	d	1.33	1.45	1.35	1.43	1.14	1.45	1.43	1.14
Pyrene	d	1.33	1.46	1.34	1.47	1.10	1.47	1.47	1.11
Perylene	e	1.348	1.449	1.365	1.426	1.150	1.439	1.434	1.138
Acenaphthene 1	f	1.333	1.447	1.372	1.435	1.142	1.450	1.430	1.144
Acenaphthene 2	f	1.340	1.444	1.371	1.431	1.149	1.444	1.436	1.138
Di Methyl Di Hydro Phenazine	g	1.351	1.442	1.382	1.424	1.147	1.419	1.442	1.132
Di Benzo P Dioxin	h	1.344	1.436	1.361	1.434	1.135	1.424	1.431	1.131
Phenazine	i	1.340	1.430	1.364	1.420	1.140	1.442	1.454	1.149
Chrysene	j	1.343	1.433	1.386	1.431	1.138	1.434	1.425	1.140
TCNQ	k	1.346	1.446	1.374	1.441	1.141	1.450	1.440	1.139
N Methyl Phenothiazine	l	1.349	1.446	1.379	1.422	1.151			
Carbazole	m	1.33	1.38	1.40	1.39	1.16			
Dibenzothiophen†	n	1.355	1.436	1.378	1.436	1.137	1.441	1.435	1.138
Mean		1.345	1.444	1.371	1.433	1.140	1.441	1.439	1.137
Standard Deviation		0.010	0.010	0.014	0.013	0.013	0.013	0.009	0.010

†The mean between opposite bonds

TABLE 3.6

Donor \ Variable	Ref.	α	β	γ	δ	θ	φ	χ	ω
HMB	a	121.3	117.3	122.6	179.1	-	-	-	114.7
Anthracene	b	120.0	120.0	122.5	179.0	120.0	120.0	-	115.0
Cu Ox	c	120.2	118.8	122.5	181.5	119.9	121.3	183.6	115.4
Pyrene	d	120.9	117.6	121.5	178.5	121.7	120.6	178.4	115.9
Pyrene	d	120.8	118.4	123.4	179.0	120.8	120.8	179.3	115.0
Perylene	e	120.9	117.4	121.3	179.2	120.5	122.1	179.6	116.5
Acenaphthene 1	f	121.1	117.9	122.3	179.5	121.0	121.0	178.8	115.4
Acenaphthene 2	f	121.2	118.0	121.8	179.2	120.5	121.5	178.9	116.0
Di Methyl Di Hydro Phenazine	g	120.3	118.3	121.6	177.7	120.9	120.8	178.3	113.6
Di Benzo P Dioxin	h	119.8	117.9	123.8	177.8	121.3	120.8	179.4	113.6
Phenazine	i	121.4	117.6	122.2	179.1	120.7	121.8	179.9	115.3
Chrysene	j	121.1	118.6	121.8	179.1	120.8	120.8	177.8	115.7
TCNQ	k	121.0	118.3	122.0	179.4	121.0	120.7	179.6	116.1
N Methyl Pheno-thiazine	l	119.9	120.1	122.6	177.7	119.9	-	-	114.8
Carbazole	m	119.0	-	125.0	175.0	120.0	-	-	-
Dibenzothiophen†	n	120.7	119.0	122.3	179.1	120.1	120.9	178.2	115.7
Mean		120.7	118.2	122.3	178.8	120.9	121.0	179.3	115.2
Standard Deviation		0.5	0.7	0.5	0.6	0.6	0.5	0.8	0.8

†The mean between opposite angles

[a]Colton and Henn (1970); [b]Williams and Wallwork (1968); [c]Williams and Wallwork (1967) [d]Prout, Tickle and Wright (1973); [e]Tickle and Prout (1973a); [f]Tickle and Prout (1973b); [g]Goldberg and Shmueli (1973a); [h]Goldberg and Shmueli (1973b); [i]Goldberg and Shmueli (1973c); [j]Munnoch and Wright (1974); [k]Long, Sparks and Trueblood (1965); [l]Kobayashi (1973a); [m]Kobayashi (1973b); [n]This work

TABLE 3.7

FIG. 3.5

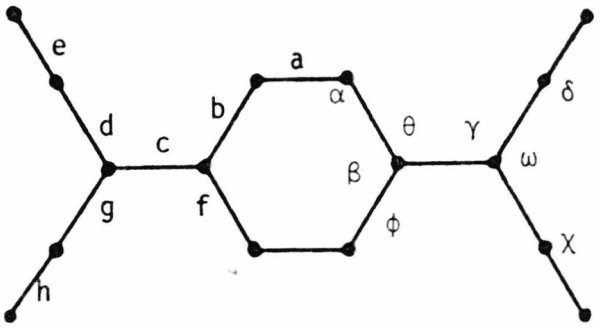

	Reference	a	b	c
TCNQ	a	1.346	1.448	1.374
Calculated $^{1}_{2}$	b	1.360 1.356	1.449 1.453	1.377 1.371
TCNQ	This work†	1.355	1.436	1.378
$TCNQ^{-}$	c	1.341	1.434	1.388
$TCNQ^{-}$	d	1.355	1.426	1.411

†Mean values between opposite bonds.

[a]Long, Sparks and Trueblood, 1965; [b]Lowitz, 1967; [c]Sundaresan and Wallwork, 1972; [d]Goldstein, Seff and Trueblood, 1968

TABLE 3.8

dibenzothiophen molecule need not be the same. In this case the mean interplanar spacings are nearly equal (3.40 and 3.43 A) and the relative orientations of donor and acceptor are almost the same (symmetrical in one case and slightly displaced along the long axis of the molecules in the other). The longer spacing corresponds to the displaced orientation, and may reflect poorer charge transfer overlap in this orientation, although the effect is very small and could equally be ascribed to differences in intermolecular repulsive forces in the two slightly different orientations. These mean separations of donor and acceptor planes are the longest reported for TCNQ complexes having triclinic lattices, and fit the previously noted correlation between D-A separation and donor ionization potential (Munnoch & Wright, 1974), consistent with only weak charge transfer interaction (the ionization potential of dibenzothiophen is 8.14 ev (Mukherjee, 1969)). The correlation is given in Fig. 3.6. Two roughly linear relationships are observed when the complexes are divided into monoclinic and triclinic types. The differences between interplanar spacings in complexes with different lattice types are larger than those due to orbital energy differences, and thus in general the correlation of interplanar spacing and orbital energy may be obscured by the more important lattice packing effects.

The relative orientation of donor and acceptor is very similar to that observed in the carbazole/TCNQ complex (Kobayashi, 1973) but different from that observed in the O-phenanthroline/TCNQ complex (Goldberg & Shmueli, 1977) in which the long axis of the TCNQ molecule is rotated approximately 22° with respect to that of the donor. Semiempirical calculations (Goldberg, 1975) suggest that the latter orientation is close to the one most favourable to charge transfer interactions (Section 3.6). Although

FIG. 3.6

1. Perylene/TCNQ
2. Anthracene/TCNQ
3. Pyrene/TCNQ
4. Hexamethylbenzene/TCNQ
5. Bis(8-hydroxyquinolato)Copper (II)/TCNQ
6. Acenaphthene/TCNQ
7. Chrysene/TCNQ
8. Phenazine/TCNQ
9. Dibenzothiophen/TCNQ

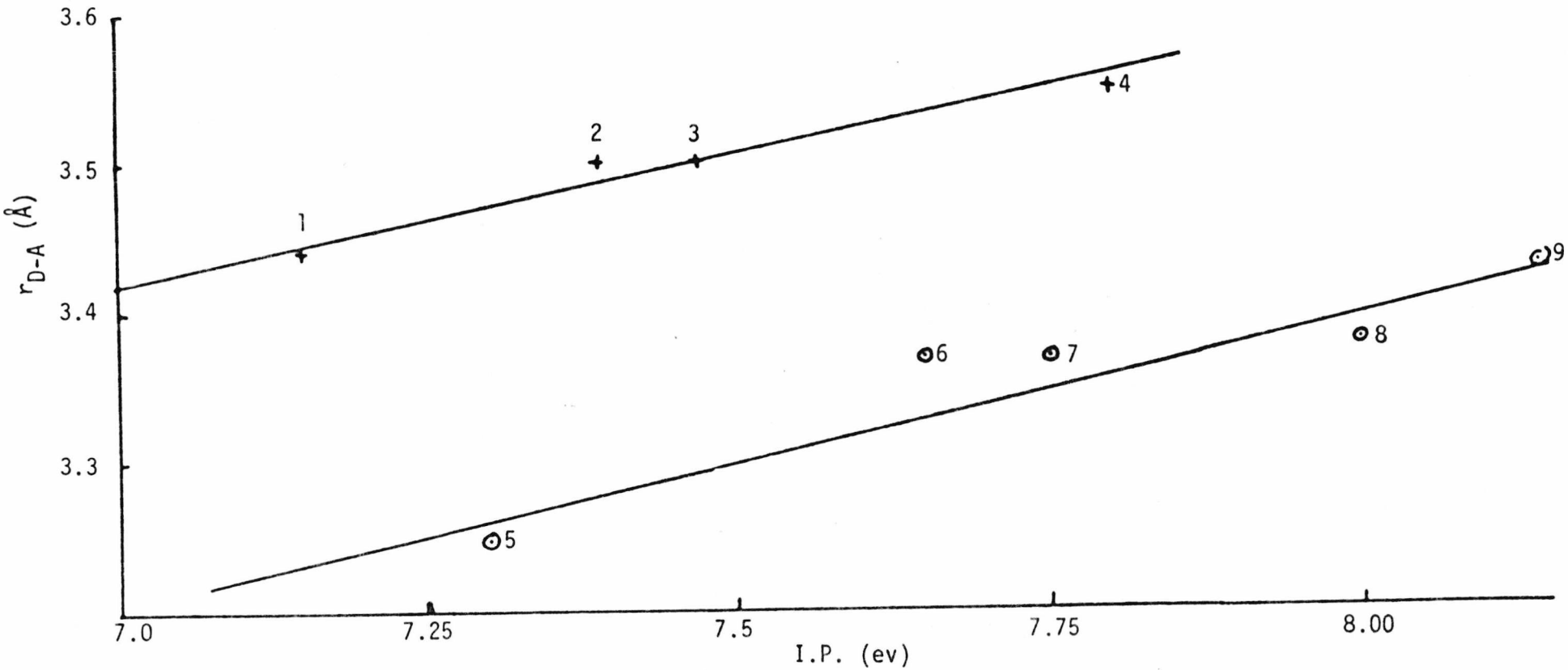

no similar calculations have been carried out for dibenzothiophen/TCNQ, the symmetries of the seven occupied orbitals of the donor only permit significant overlap between the second and sixth highest occupied orbitals and the lowest vacant orbitals of TCNQ in the observed orientation. The fact that this orientation places the polar quinoid double bonds of TCNQ over the centres of polarisable rings of the donor molecules, together with favourable lattice packing, is thus more likely than charge transfer interactions to be the orientation-determining factor in this complex. This type of arrangement has been shown to be common (Prout & Wallwork, 1966) in many one component molecular crystals and in molecular compounds such as perylene/fluoranil and quinhydrone and its analogues (Fig. 3.7). Pyrene/chloranil also shows fairly well-defined parallel orientation of aromatic rings and C=O group consistent with the above arrangement. Gaultier, Hauw and Breton-Lacombe (1969), have drawn attention to this type of overlap in one component crystals; whose examples are also given in Fig. 3.7.

All the peripheral atoms of the TCNQ molecule are in contact with N or H atoms of neighbouring TCNQ molecules. These N...H contacts range from 2.70-2.77 Å , close to the sum of the van der Waals radii of N and H (2.70 Å). In contrast, only two of the peripheral atoms of dibenzothiophen are in van der Waals contact with atoms of neighbouring molecules (S(1)...H(10) at (-x,1-y,1-z) , 2.96 Å c.f. van der Waals radius sum = 3.05 Å ; and H(7)...N(2) at (1-x,1-y,1-z), 2.74 Å) , and this lack of close contacts accounts for the larger in-plane motion of dibenzothiophen compared to TCNQ , apparent from the thermal ellipsoid plots of Fig. 3.9. Many other molecular complexes show larger in-plane motion of the donor than of the acceptor (Fyfe, 1973), suggesting that lattice

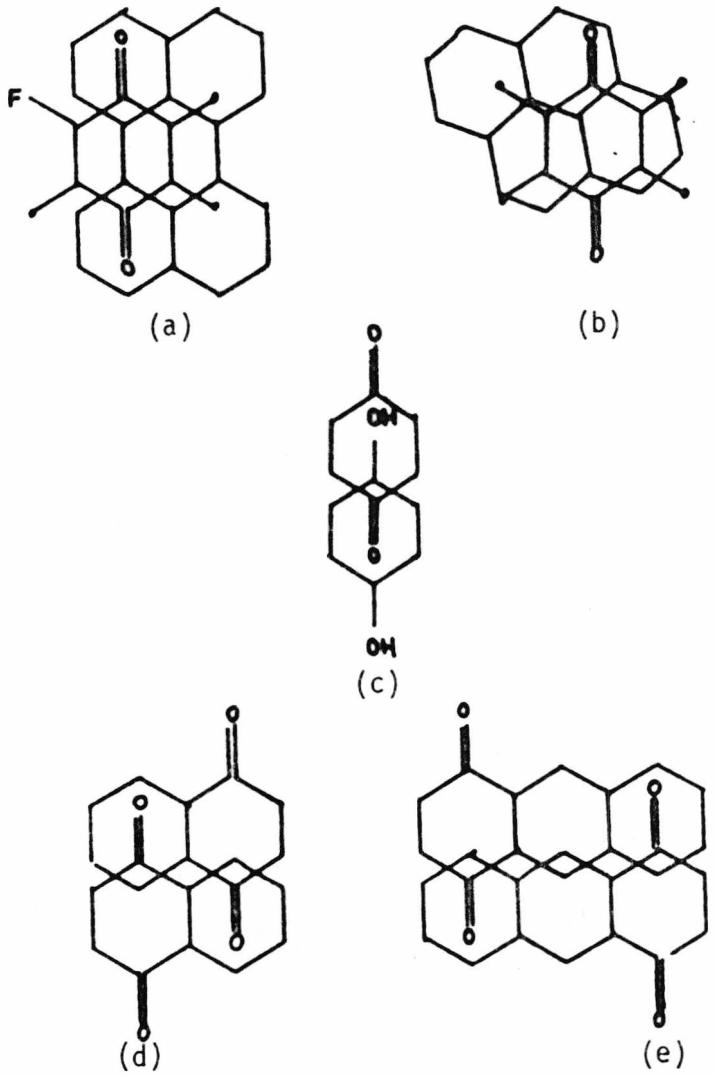

FIG. 3.7 OVERLAP DIAGRAMS

(a) perylene/fluoranil
(b) pyrene-chloranil
(c) quinhydrone
(d) naphthoquinone
(e) 1,4-anthraquinone

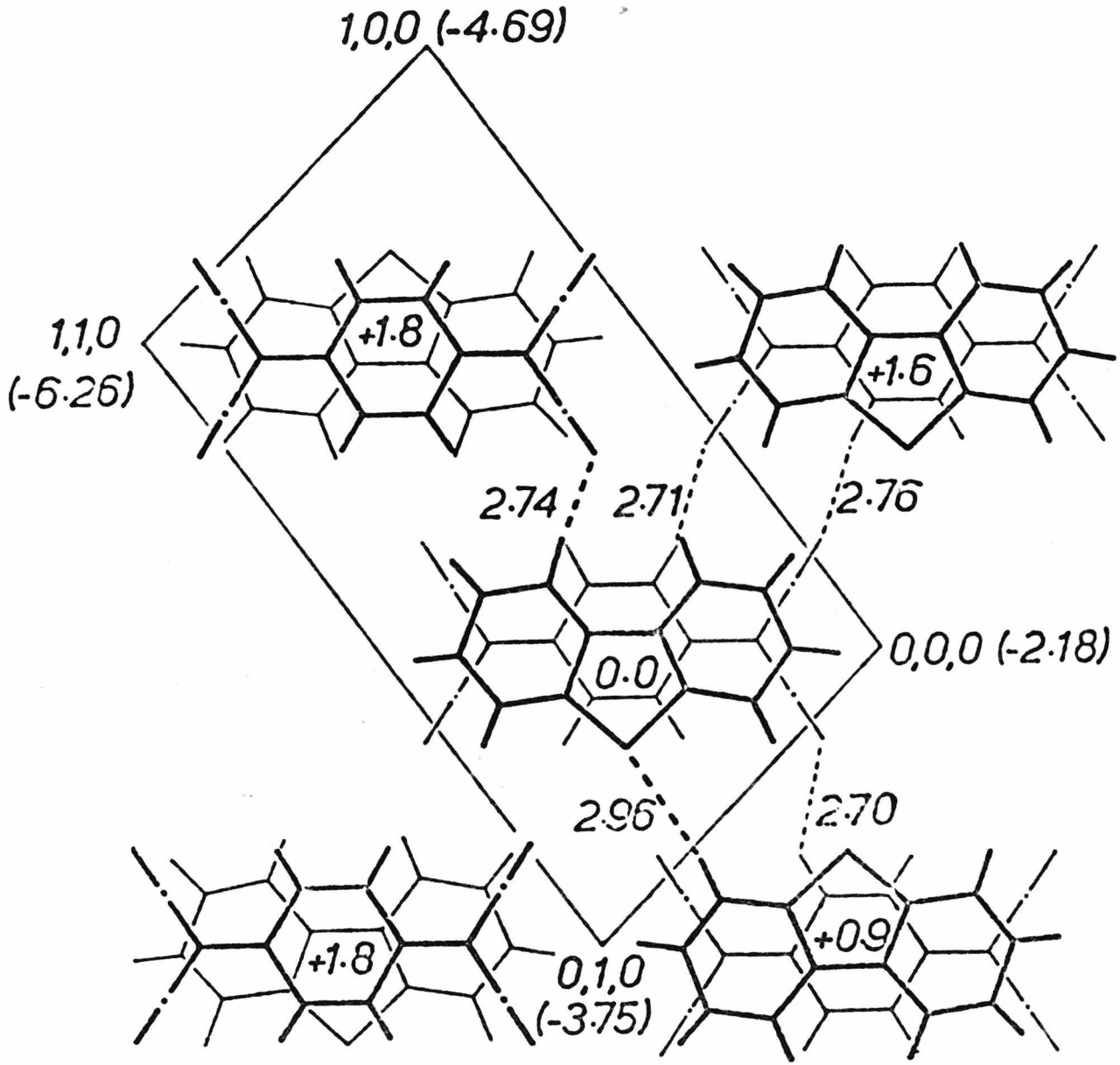

FIG. 3.8

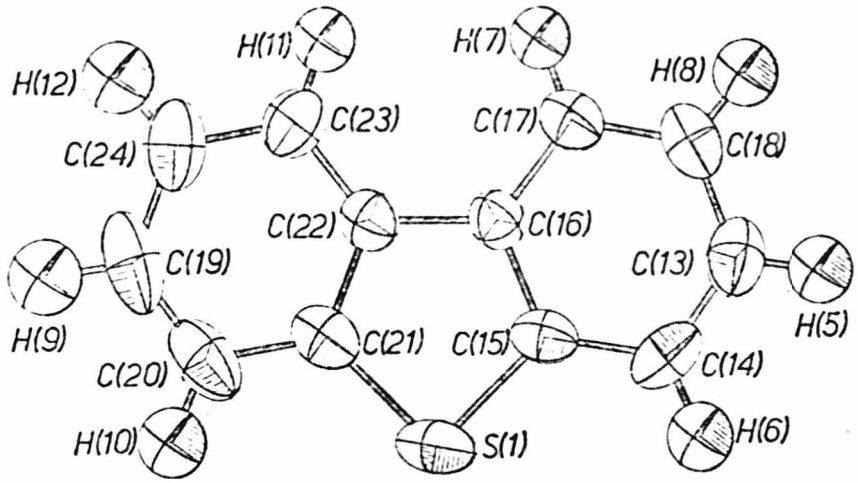
H(11)
H(7)
H(12)
H(8)
C(23)
C(17)
C(24)
C(18)
C(22)
C(16)
C(19)
C(13)
H(5)
H(9)
C(21)
C(15)
C(14)
C(20)
H(6)
H(10)
S(1)

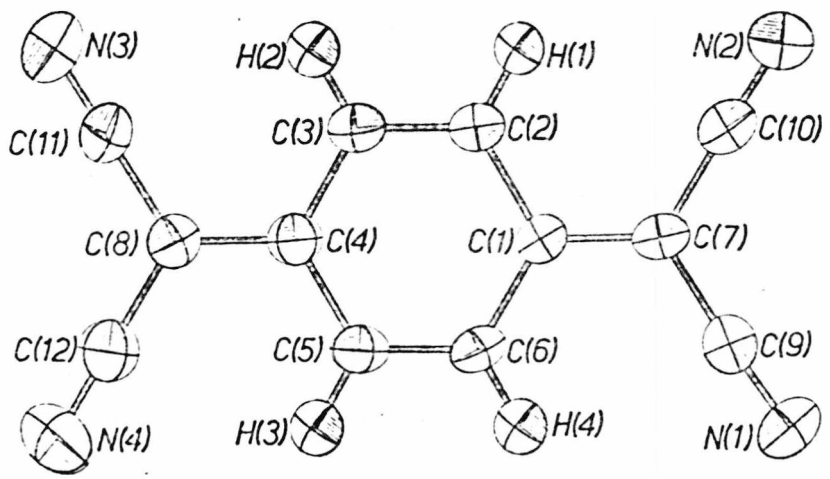
N(3)
H(2)
H(1)
N(2)
C(11)
C(3)
C(2)
C(10)
C(8)
C(4)
C(1)
C(7)
C(12)
C(5)
C(6)
C(9)
N(4)
H(3)
H(4)
N(1)

FIG. 3.9

FIGURE CAPTIONS

FIG. 3.8 Projection of the structure on the plane of the dibenzothiophen molecule at x,y,z . The figures inside the more heavily drawn molecules and at the corners of the projected cell denote heights in Å above and below the plane of this dibenzothiophen molecule. The transformation matrix from the fractional atomic co-ordinates of the triclinic unit cell (with respect to the centroid of the dibenzothiophen molecule at 0.2461, 0.4962, 0.5234) to the orthogonal (Å) best-plane co-ordinates X,Y and Z (with Z perpendicular to the molecular plane) is:

$$\begin{pmatrix} -9.1343 & -6.0314 & -0.1951 \\ 13.2845 & -6.3676 & -0.1107 \\ -2.5034 & -1.5699 & 6.8353 \end{pmatrix}$$

FIG. 3.9 Thermal ellipsoids for dibenzothio phen and TCNQ , at the 50% probability level, projected onto the molecular planes (Johnson, 1965).

packing may often be determined by interactions between electron rich and electrondeficient regions of neighbouring acceptor molecules as well as by the desire to attain a relative orientation of donor and acceptor within the stacks which optimises or nearly optimises charge transfer interactions. Apart from the above mentioned S(1)...H(10) contact, there are no intermolecular contacts shorter than the sum of the van der Waals radii of the atoms involved. However, two-fold rotation of the dibenzothiophen molecule about its long axis would lead to an abnormally short contact (2.76 A) between S(1) and N(2) at (1-x,1-y,1-z) (c.f. sum of van der Waals radii of N and S=3.35 A). This accounts for the absence of disorder at the donor site and the fact that the spacegroup is $P\bar{1}$ with the two asymmetric donor molecules related by a centre of symmetry, rather than P1 with one molecule of the complex in a cell with the a axis halved. In contrast, a dibenzofuran molecule may be fitted in either orientation at the dibenzothiophen site without leading to abnormally short N...O contacts. Hence the observed halving of the a axis in the dibenzofuran/TCNQ complex (Appendix I) corresponds to either an ordered structure in P1 with every dibenzofuran molecule in the same orientation, or a disordered $P\bar{1}$ structure in which each donor site is occupied by a disordered pair of molecules with 50% site occupancy for each of the two possible orientations.

3.9 The Melting Point Against Composition PLOT

Melting points of some of the pure and mixed complexes prepared in this work have been determined using a conventional melting point apparatus and in some cases from differential scanning calorimetry. Where complete series of mixed complexes are formed the melting points against compositions plots are presented by graphs (Figs. 3.11 and 3.12). For pyrene/perylene/TCNQ (only 50:50 composition) the results are tabulated

in Table 3.9. The data shown in Table 3.9 were obtained by means of a conventional method of melting-point measurement with visual observation using a rapid heating condition to minimize thermal decomposition. The data plotted in Figs. 3.11 and 3.12 were obtained by using a differential scanning calorimetry method.

The instrument used was a Perkin Elmer Model DSC-1B in which the operation is based on the temperature control of two similar sample holders in the sample holder assembly. The description of the instrument, operation and set-up procedure are given in the relevant Perkin-Elmer instruction manuals.

A weight of approximately 1-40 mg of sample was usually used. The sample was sealed in the sample pan (made of aluminium). The other pan was empty and was used as a reference.

The settings were adjusted by trial and error. The following settings were used in this work:

Heating rate = 8^{0}/min.

Range = × 16

Chart Speed = was varied to suit conditions.

The melting points were indicated by sharp breaks on the curves recorded by the chart recorder (Fig. 3.10).

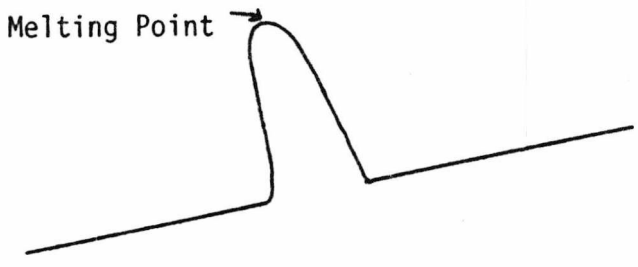

Fig. 3.10 THE CHART RECORDER OUTPUT FOR MELTING POINT DETERMINATION

In each of the three systems studied, the melting points of the pure and mixed complexes span a range of less than $16^{0}C$, and this together with the difficulties in obtaining precise melting points because of the onset

FIG. 3.11 THE PLOT OF MELTING POINT AGAINST COMPOSITION OF ANTHRACENE$_x$/DIBENZOTHIOPHEN$_{1-x}$/TCNQ

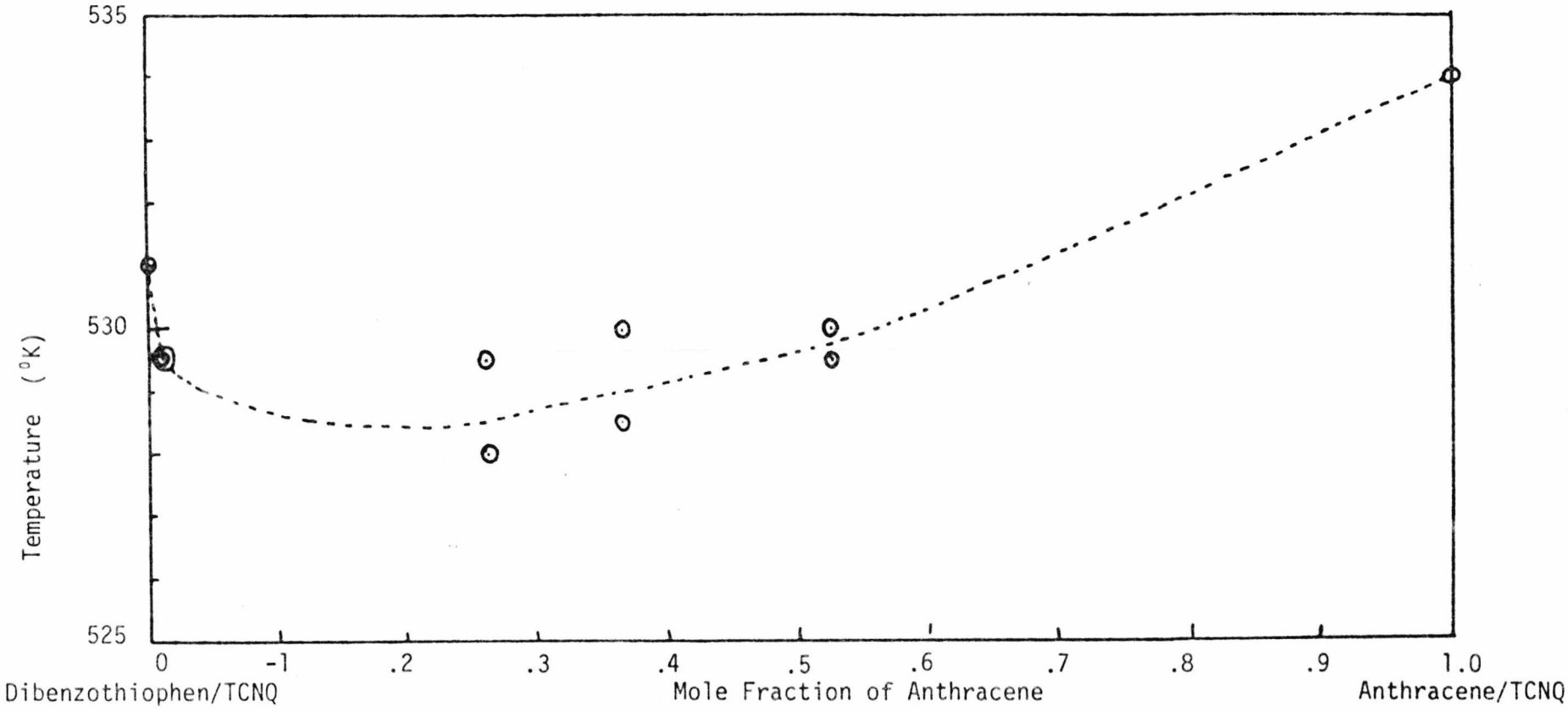

FIG. 3.12 THE PLOT OF MELTING POINT AGAINST COMPOSITION OF $DBT_x/DBF_{1-x}/TCNQ$

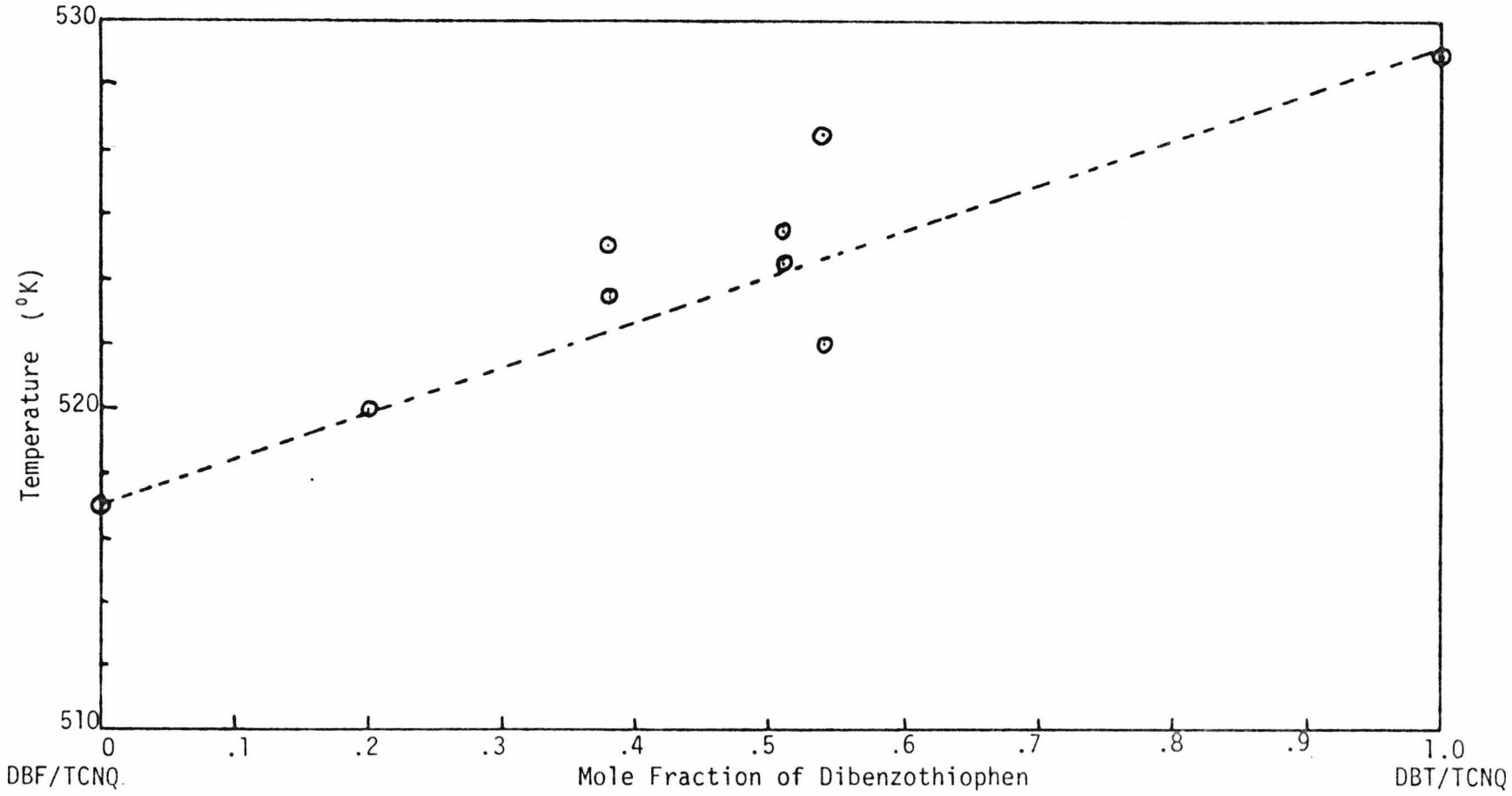

of decomposition, suggests that for these systems melting point data are not useful in determining structural changes which may occur across each series. Furthermore, the scanning calorimetry data showed no significant features apart from the onset of melting. There are thus no phase changes detectable by scanning calorimetry for any of these systems between room temperature and the melting point.

Complex	Melting Points (°C)
Perylene/TCNQ	i) 264 ii) 263
Pyrene/TCNQ	i) 250 ii) 249
$Py_{.51}/Pe_{.49}$/TCNQ	i) 248-250 ii) 248-250
$Py_{.41}/Pe_{.59}$/TCNQ	i) 250 ii) 248

TABLE 3.9 MELTING POINTS OF PARENT AND MIXED COMPLEXES OF PYRENE$_x$/PERYLENE$_{1-x}$/TCNQ

3.10 X-Ray Powder Diffraction

Apparatus

The apparatus used was a Guinier-De Wolff camera. The focussing principle applied in this camera is the well-known Guinier type focussing. The bent crystal (M in Fig. 3.13) reflects K_α radiation from the target F into a sharp focal line at S .

Experimental

A few milligrams of the complex under test, ground to a fine powder,

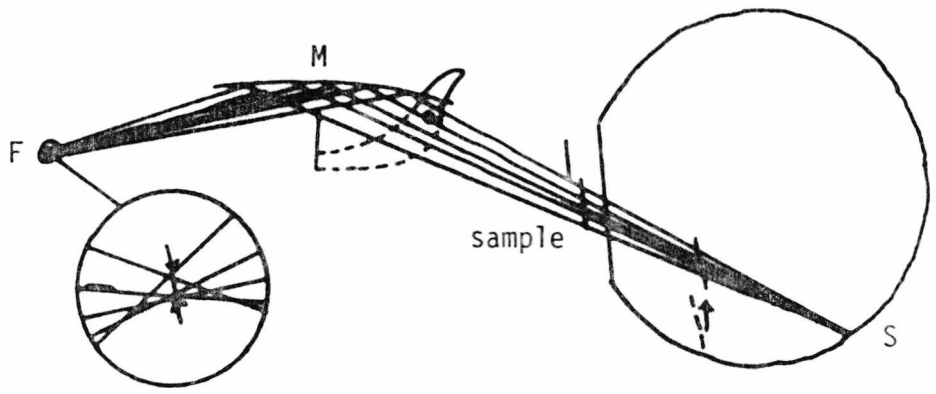

FIG. 3.13 THE GUINIER TYPE FOCUSSING

was mixed to a thick paste with silicone grease. A thin layer of this paste was applied to one of the windows of the metal sample frame, supported on a sellotape film applied to one side of the frame. Four different samples could be studied in one frame. The frame was fitted carefully into the specimen compartment of the camera, and the exposure was 4 h. with Cu K_α radiation, 50 kV , 18 mA .

3.11 Results

The resulting diffraction patterns on the films (Fig. 3.14) were measured and are presented as tables of d spacings with relative intensities given by the symbols s,m and w for strong, medium and weak respectively. Silicone grease which is used as a binding material does not produce lines but gives a diffuse band of background scattering. The films were initially scanned using a recording microdensitometer, but it was found that this technique only revealed the strongest lines. Many more lines could be identified by visual observation, and the line positions in Table 3.10-3.13 were measured directly from the films (Fig. 3.14) using the special ruler calibrated directly in d spacing, supplied with the camera. The calibration was checked by comparing the d spacings observed for dibenzothiophen/TCNQ with the precise d spacings for the most intense peaks in the single crystal diffraction data obtained earlier. The agreement was sufficiently good to permit indexing of the powder lines by comparison with the single crystal data. However, the purpose of these studies was to establish whether the mixed complexes had structures related to those of either parent complex or whether they formed new structures. For this purpose precise line position and indexing of the photographs are not necessary. Comparison of the powder diffraction patterns summarised in Tables 3.10-3.13 leads to the following conclusions:

A	B	C	D	E	F	G
8.63m	8.60m	8.58m	8.58m	8.55m	8.55m	8.52m
7.60m	7.75m	7.75m	7.75m	7.80m	7.95m	7.94m
6.40s	6.45s	6.48s	6.48s	6.50s	6.50s	6.50s
						5.8 w
						5.4 w
5.22w	5.22w	5.26w	5.24w	5.26w	5.26	5.28w
4.80w	4.81w	4.81w		4.81w	4.84w	4.86w
4.68w	4.70w	4.72w	4.69w	4.70w	4.71w	4.70w
						4.56w
4.32w	4.34w	4.34w	4.32w	4.32w	4.31w	4.29w
4.11w	4.14w	4.14w	4.12w	4.14w	4.15w	4.12w
				3.90w	3.92w	3.94w
3.67m	3.69m	3.70m	3.70m	3.70m	3.74w	3.73w
					3.70m	3.69w
						3.63w
3.49w	3.49m	3.50w	3.50m	3.50m	3.50m	3.49w
3.41w	3.42w	3.42w	3.41w	3.41w	3.41w	3.40w
				3.36w	3.37w	3.37w

A=DBF/TCNQ ; B=$DBT_{.20}/DBF_{.80}$/TCNQ ; C=$DBT_{.29}/DBF_{.71}$/TCNQ ; D=$DBT_{.41}/DBF_{.59}$/TCNQ
E=$DBT_{.51}/DBF_{.49}$/TCNQ ; F=$DBT_{.76}/DBF_{.24}$ TCNQ ; G=DBT/TCNQ

TABLE 3.10

TABLE 3.10 (Cont'd.)

A	B	C	D	E	F	G
3.22-3.26s	3.24-3.27s	3.25-3.28s	3.25-3.27s	3.26-3.30s	3.28-3.30s	3.30s
						3.29s
3.20w	3.21w	3.22w	3.21w	3.23w	3.21w	3.21w
					3.17w	3.16w
2.96w	2.96w	2.97w	2.96w	2.96w	3.07w	3.06w
					2.97w	2.94w
2.895w	2.90w	2.90w		2.91w	2.93w	
2.85w	2.86w	2.88w	2.87w			
2.79w	2.82w	2.83w	2.82w	2.82w	2.82w	2.81w
2.62w	2.64w	2.64w			2.65w	
2.56w	2.59w	2.56w	2.55m	2.54m	2.55m	2.55m
		2.53w				
				2.35w	2.36w	2.36w
2.17w				2.17w	2.16w	2.16w
1.68m	1.68m	1.69m	1.68m	1.70m	1.70m	1.70m
1.66w					1.68w	1.68w
1.65w						

Py/TCNQ	$Py_{.51}/Pe_{.49}/TCNQ$	$Py_{.41}/Pe_{.59}/TCNQ$	Pe/TCNQ
10.80m			
	10.0 s	9.9s	
9.6m	9.5-9.7m	9.5-9.7m	
			8.5-8.75
8.25s	8.2s	8.2m	
7.2s	7.2s	7.2s	7.2-7.3s
	6.2m	6.2m	6.0s
	5.73m	5.73m	
5.68s			
	5.6w	5.6w	
			5.58s
	5.48s	5.48-5.52s	
5.42m	5.43w	5.42w	5.4s
5.0m	5.00w	4.98w	5.1m
4.92m			
	4.85s	4.84m	
	4.78w	4.75m	
4.54m			4.6m
			4.4w
			4.35w
4.28w			
4.12w	4.10s	4.08-4.10s	4.15s
4.06s			
3.84m			
	3.8m	3.8m	
3.76s	3.77m	3.77m	3.77w
	3.72w	3.71w	3.71w
3.64w	3.62m	3.62m	3.62-3.63s
3.60w			
3.5s	3.52-3.56s	3.52-3.56s	3.5m
3.44s	3.42-3.45w	3.42w	3.43m
3.37s	3.36m	3.35w	3.35s
3.3s	3.3w		
3.26s	3.25-3.27s	3.25-3.27s	3.24-3.25s

TABLE 3.11

TABLE 3.11 (Cont'd.)

Py/TCNQ	$Py_{.51}/Pe_{.49}$ (TCNQ	$Py_{.41}/Pe_{.59}$/TCNQ	Pe/TCNQ
			3.22m
	3.18w	3.20w	
		3.18m	
		3.16m	
3.14w	3.14m	3.14w	
3.08m	3.10w	3.10w	3.1-3.12s
3.03	3.04-3.06s	3.02-3.06s	
2.98w			2.95
2.90w			
2.82-2.84w			2.81
2.77w	2.775m	2.775m	2.77w
	2.76w	2.76w	
			2.68w
2.67w	2.65w	2.65w	2.65w
	2.6w	2.6w	
2.53w	2.54w	2.54w	2.55w
2.51w			2.53w
2.45m	2.45m	2.45m	
2.42m			2.4-2.42m
	2.39w	2.38w	
2.37m	2.36w	2.35w	2.35w
	2.34w		
2.30m			
		2.25w	
2.18w	2.18w		2.17w
	2.16w		
	2.13w		
	2.04w		1.97-1.98m
	1.872w		1.86w
1.75w	1.75-1.76w		1.74m
1.74w	1.72w	1.725w	
1.675w			1.68w
	1.642		
	1.628w	1.628w	1.61w

A/TCNQ	$A_{.10}$/C/TCNQ	$A_{.099}$/C/TCNQ	C/TCNQ
	9.1m	9.0m	9.0m
8.4m	7.9m	7.9m	7.9m
	6.55s	6.5s	6.55s
6.4s			
5.53w	5.52m	5.48m	5.5m
4.95w	4.95w	4.95w	4.95w
	4.77w	4.75w	4.75w
4.55w	4.55m	4.55m	4.55m
	4.28w	4.27w	4.27w
4.2w			
4.12w	4.12w	4.12w	4.13w
	3.83m	3.83w	3.82w
3.8w	3.68m	3.67m	3.68m
	3.6m	3.61m	3.6m
3.53w	3.525m	3.52m	3.52m
	3.47w	3.48w	3.48w
3.37s	3.35s	3.35-3.36s	3.34-3.36s
3.22w	3.3w	3.29w	3.3w
	3.27w	3.26w	3.27w
	3.21-3.23s	3.21-3.23s	3.21-3.23s
	3.17w	3.17w	3.17w
	3.10w	3.11w	3.10w
	3.07m	3.07m	3.07m
3.01w	3.03w	2.79w	3.02w
2.98w			
2.79w	2.79w	2.75w	2.785w
	2.75w	2.72w	2.75w
	2.73w	2.62w	2.72w
	2.63w	2.6w	2.62w
	2.6w	2.18m	2.6w
	2.18m	2.135w	2.18m
	2.14w	2.05w	2.14w
2.11w	2.05w	2.03w	2.05w
	2.03w		2.03w
	2.01w		2.01w
	1.99w	1.99w	

TABLE 3.12

TABLE 3.12 (Cont'd.)

A(TCNQ	$A_{.10}$/C/TCNQ	$A_{.099}$/C/TCNQ	C/TCNQ
	1.805w	1.805w	
1.74w	1.74w		
1.701w	1.695w	1.695w	1.659w
1.68w	1.605w	1.605w	1.605w

DBT/TCNQ	$A_{.01}/DBT_{.99}/TCNQ$	$A_{.26}/DBT_{.74}/TCNQ$	$A_{.37}/DBT_{.63}/TCNQ$	$A_{.53}/DBT_{.47}/TCNQ$	A/TCNQ
8.52m	8.5m				
		8.25-8.3s	8.3-8.4s	8.4m	8.4m
7.94m	7.9m				
6.5s	6.49s	6.49s	6.5s	6.5s	6.4s
5.8w					
5.4w	5.35w	5.38m	5.45w	5.5w	5.53w
5.28w					
4.86w	4.85w	4.87w	4.9w	4.9w	4.95w
4.7w	4.68m	4.7m	4.73m	4.73w	
4.56w					4.55w
3.29w	4.27				
					4.2w
4.12w	4.12w	4.12w	4.15w	4.15w	4.12w
3.94w	3.95w				
		3.82w	3.85w	3.85w	3.8w
3.73w	3.75				
3.69m	3.70w				
3.63w					
3.49w	3.48w	3.48w	3.5w	3.5w	3.53w
3.4w					
3.37w	3.38w	3.77m	3.38m	3.35s	3.37s

TABLE 3.13

TABLE 3.13 (Cont'd.)

DBT/TCNQ	$A_{.01}/DBT_{.99}/TCNQ$	$A_{.26}/DBT_{.74}/TCNQ$	$A_{.37}/DBT_{.63}/TCNQ$	$A_{.53}/DBT_{.47}/TCNQ$	A/TCNQ
3.30s	3.31w	3.3s	3.31-3.35s		
3.285s	3.28-3.5s				
3.21w	3.24w	3.22w	3.24w	3.25w	3.22w
3.16w	3.16w	3.16w	3.17w	3.18w	
3.06w	3.02				
2.94w	2.97w	2.98w	2.98w	3.00w	3.01w
					2.98w
2.81w	2.79w				2.79w
		2.7w	2.7w	2.7w	
2.6w	2.61w	2.63w	2.63w		
2.55m	2.53w	2.48w	2.48w		
2.36w					
2.155w					
					2.11w
1.698m	1.7	1.703w	1.71w	1.71w	1.74w
					1.72w
					1.68w

Labelling for Fig. 3.14

A = Dibenzothiophen/TCNQ

B = Dibenzothiophen$_{.29}$/Dibenzofuran$_{.71}$/TCNQ

C = Dibenzothiophen$_{.20}$/Dibenzofuran$_{.80}$/TCNQ

D = Dibenzofuran/TCNQ

E = Dibenzothiophen/TCNQ

F = Dibenzothiophen$_{.76}$/Dibenzofuran$_{.24}$/TCNQ

G = Dibenzothiophen$_{.51}$/Dibenzofuran$_{.49}$/TCNQ

H = Dibenzothiophen$_{.41}$/Dibenzofuran$_{.59}$/TCNQ

I = Perylene/TCNQ

J = Pyrene$_{.41}$/Perylene$_{.59}$/TCNQ

K = Pyrene$_{.51}$/Perylene$_{.49}$/TCNQ

L = Pyrene/TCNQ

M = Chrysene/TCNQ

N = Anthracene$_{.099}$/Chrysene$_{.901}$/TCNQ

O = Anthracene$_{.10}$/Chrysene$_{.90}$/TCNQ

P = Anthracene/TCNQ

Q = Anthracene$_{.53}$/Dibenzothiophen$_{.47}$/TCNQ

R = Anthracene$_{.37}$/Dibenzothiophen$_{.63}$/TCNQ

S = Anthracene$_{.26}$/Dibenzothiophen$_{.74}$/TCNQ

T = Anthracene$_{.01}$/Dibenzothiophen$_{.99}$/TCNQ

U = empty frame(lines due to stray scattering)

V = just silicone grease, which is used for binding powder together

W = Pyrene$_{0.0}$/Perylene$_{1.0}$/TCNQ (in fact probably Pe/TCNQ)

X = empty frame.

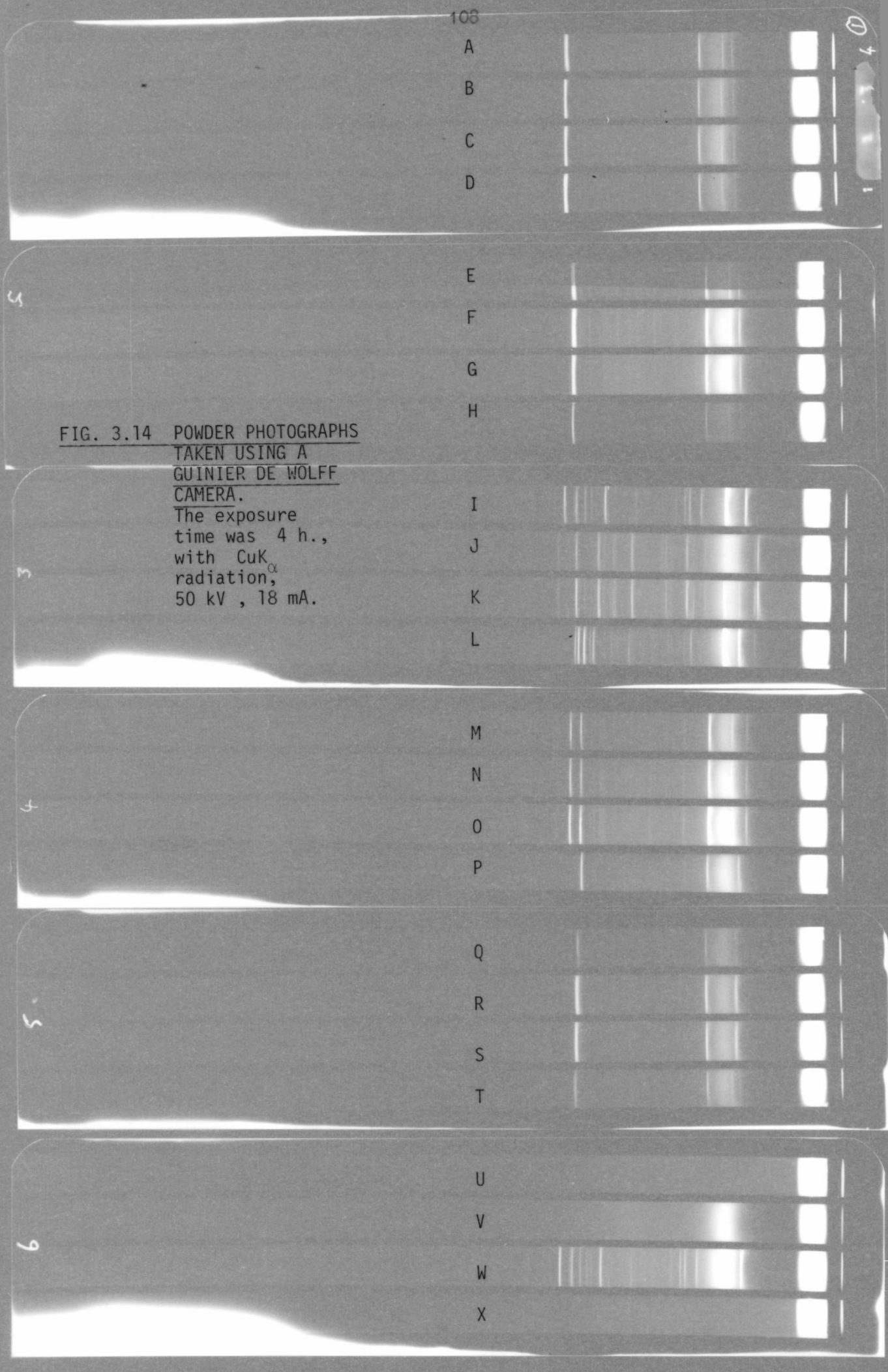

FIG. 3.14 POWDER PHOTOGRAPHS TAKEN USING A GUINIER DE WOLFF CAMERA. The exposure time was 4 h., with CuK_{α} radiation, 50 kV , 18 mA.

3.12 Conclusions

i) Mixed complex of dibenzothiophen/dibenzofuran/TCNQ and the two parent complexes form a series of very similar structure. As mentioned earlier in this chapter, single crystal diffraction studies showed similar triclinic cells for both parent complexes, with the a axis halved in the dibenzofuran complex and minor differences in the other dimensions. The powder diffraction patterns of the mixed complexes are almost identical to those of the parent complexes. (Table 3.10.) This similarity of structure arises because of the similarity of size and shape of dibenzofuran and dibenzothiophen, and this continuous isostructural series is analogous to the anthracene/phenanthrene/tetracyanobenzene system (Wright, Ohta & Kuroda, 1976).

ii) The mixed complexes $(Pyrene)_x(Perylene)_{1-x}TCNQ$, in which x is always close to 0.5 (Chapter 2) all have the same structure, but this structure is different from those of either of the parent complexes (Table 3.11). The difference in molecular shapes of pyrene and perylene is evidently sufficient to prohibit incorporation of either of these donors into the lattice of the TCNQ complex of the other, although the existence of a new phase for $x \simeq 0.5$ suggests the possibility of an ordered structure for the new phase of this composition. Single

crystal diffraction studies, which have not been carried out in this work, would be required to establish the full structure of this new phase, but spectroscopic (Chapter 4) and photoconductivity (Chapter 6) studies provide some information on likely changes in the relative orientations of donor and acceptor in the new phase.

iii) The anthracene/Chrysene/TCNQ complexes, which could only be prepared with relatively small fractions of anthracene incorporated, all have the chrysene/TCNQ lattice and not that of anthracene/TCNQ (Table 3.12) This is expected from the small degree of incorporation of anthracene, and is also consistent with the relative sizes of the two donors. The smaller donor, anthracene, should more readily fit onto a lattice site capable of accommodating the larger donor chrysene, rather than vice-versa.

iv) The anthracene/dibenzothiophen/TCNQ mixed complexes give powder diffraction photographs which require careful examination in order to determine which of the parent complex lattices is adopted, since although the parent complex lattices are different their powder diffraction patterns contain many lines in common. This is clear from Table 3.13, which also shows that the lines with largest d spacing do permit a clear distinction to be made. All the mixed complexes except that with only 1% anthracene show a single line in the range 8.25-8.4 Å , as found for anthracene/TCNQ,

and not the two lines at 8.52 Å and 7.94 Å found for dibenzothiophen/TCNQ. The mixed complexes therefore adopt the anthracene/TCNQ lattice, except for very low anthracene contents when the dibenzothiophen/TCNQ lattice persists. The actual powder diffraction photographs also showed some broadening of the lines for the mixed complexes, which may indicate disorder of dibenzothiophen at the anthracene site.

All the photographs showed a background of diffuse scattering from the silicone grease used to bind the powder together in the frame. This explanation of the diffuse background was confirmed by taking an exposure using a sample frame with one window empty and the other window covered with only silicone grease. The empty frame did not show the diffuse scattering produced by the frame containing the grease, and the scattering from the grease occurred in the same place as the diffuse background for all the other samples.

The relevance of the structural information described in this chapter to spectroscopic and electrical conductivity properties will be discussed in Chapters 4,5 and 6.

* * * * * *

Chapter 4

Charge Transfer Spectroscopy

4.1 Introduction

The solution spectra of molecular complexes consist of bands characteristic of internal transitions of the free donor and acceptor molecules as well as new broad intense bands due to intermolecular charge transfer (Benesi & Hildebrand, 1948,1949; Mulliken, 1950,1952). The observations of the charge transfer peaks led Mulliken (1952) to propose that the new absorption bands are due to the transfer of an electron from donor to acceptor as indicated by:

$$\psi_{complex}(DA) \xrightarrow{h\nu_{CT}} \psi_{complex}\ (D^{+}A^{-})$$

The detailed treatment of charge transfer model was previously discussed in Chapter 3 in connection with the forces involved in a molecular crystal.

Mulliken's proposed electron transfer mechanism (Mulliken, 1952; Foster, 1969; Mulliken & Person, 1969) was in fact confirmed by the observation of solid state charge transfer bands in π-π^* molecular complexes polarised perpendicular to the molecular planes and parallel to the stack axis (Nakamoto, 1952).

In π-π^* electron donor acceptor molecular complexes, which have relatively weak overlapping of donors and acceptors, the charge transfer spectra of the complexes as solids and in solution are usually the same, although they may differ in the extinction coefficient arising from different intensities of transition as well as different degrees of complexing.

Since crystalline complexes are involved in the present work, studies of solid state spectra are desirable. In this work, diffuse

reflectance spectroscopy using powdered samples has been used to determine the charge transfer spectra of the complexes. Though information on the transition direction is lost in this technique, information can be derived from this method concerning the positions and shapes of charge transfer absorption bands and the relative extinction coefficients of the charge transfer transitions of different complexes, and hence possibly also on the likely relative donor and acceptor orientations.

4.2 The Theory of Diffuse Reflectance Spectroscopy

This field was pioneered by three main researchers namely: Kubelka, Munk and Kortum. A detailed treatment of reflectance spectrocopy is given in Kortum's book (Kortum, 1969).

4.2.1 Derivation of the Kubelka-Munk Function (Kortum, 1969)

Consider a plane parallel layer of thickness (d) , capable of both scattering and absorbing radiation (Fig. 4.1), and irradiated in the x-direction with a diffuse, monochromatic radiation flux, $I_{(x=d)}$. The flux of back scattered light is designated J .

Let the extension of the layer in the yz plane be large compared to d so that edge effects can be ignored. As a thin layer (dx) is irradiated in all directions due to scattering, the average path length for the direction θ will be $\frac{dx}{\cos\theta}$.

If the angular distribution of flux is $\frac{\partial I}{\partial \theta}$, then the relative intensity in the θ direction is $\frac{1}{I_0} \frac{\partial I}{\partial \theta} d\theta$, where I_0 is the total flux falling in the hemisphere.

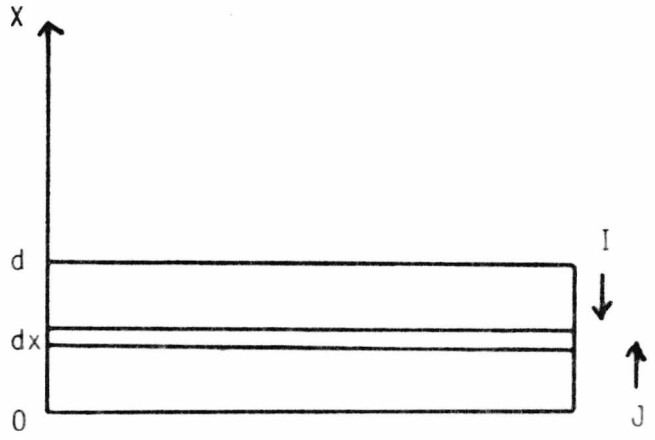

FIG. 4.1

Then the mean path length is equal to $\int_0^{2\pi} \theta d\theta$ i.e. integrating over all values of θ from 0 to $\pi/2$ and this equals $2dx$ for completely diffuse irradiation of the layer dx .

The change in radiation in the layer dx is given by:

$$-dI = -kI\,2dx - sI2dx + sJ2dx \tag{1}$$

and

$$dJ = -kJ2dx - sJ2dx + sI2dx \tag{2}$$

This is made up of three components, absorbed radiation, radiation lost by scattering and radiation scattered from the other direction.

Let $2k=K$ and $2s=S$.

Then (1) and (2) becomes

$$-\frac{dI}{dx} = -(K+S)I+SJ \tag{3}$$

$$+\frac{dJ}{dx} = -(K+S)J + SI \tag{4}$$

they can be rewritten in the form

$$-\frac{dI}{Sdx} = -aI+J \tag{5}$$

and

$$\frac{dJ}{Sdx} = -aJ+I \tag{6}$$

where

$$a = \frac{S+K}{S} = 1 + \frac{K}{S}$$

by dividing (5) by I, and (6) by J and adding the two we have an equation of the form

$$\frac{dr}{Sdx} = r^2 - 2ar + 1 \quad \text{where} \quad r \equiv \frac{J}{I}$$

or

$$\int \frac{dr}{r^2-2ar+1} = S \int dx \quad .$$

By integrating and putting the boundaries

$$x = 0 : (J/I)_{x=0} = R_g = \text{reflectance of the background}$$

$$x = d : (J/I)_{x=0} = R = \text{reflectance of sample}$$

we get:

$$\ln \frac{(R-a-\sqrt{a^2-1})(R_g-a+\sqrt{a^2-1})}{(R_g-a-\sqrt{a^2-1})(R-a+\sqrt{a^2-1})} = 2Sd\sqrt{a^2-1} \qquad (7)$$

For a thick sample, let d tend to infinity then Rg , the background reflection will go to zero and equation (7) becomes

$$(-a-\sqrt{a^2-1})(R_\infty-a+\sqrt{a^2-1} = 0 \qquad (8)$$

$$R_\infty = \frac{1}{a+\sqrt{a^2-1}} = a-\sqrt{a^2-1}$$

$$= 1 + \frac{K}{S} - \sqrt{\frac{K^2}{S^2} + 2\frac{K}{S}} = \frac{S}{S+K+\sqrt{K(K+2S}} \qquad (9)$$

where R_∞ is the diffuse reflectance.

Resolving (9) for $\frac{K}{S}$, we get

$$\frac{K}{S} = \frac{(1-R_\infty)^2}{2R_\infty} = F(R_\infty) \qquad (10)$$

Equation (10) is called the "Kubelka-Munk Function". The same result could have been reached by assuming the layer was continuous.

4.2.2 The Dilution Method

This method is used to eliminate the regular part of the remitted radiation, which will tend to make the Kubelka-Munk Function not valid. Kubelka-Munk Functionas previously derived used the assumption that the light is remitted only from diffuse reflections (scattering). The dilution is done by mixing with an inactive, non-absorbing standard such as MgO , KBr , NaCl etc. The standard should be present in large excess.

By using the same pure standard throughout the experiment the regular part of the remitted radiation is eliminated. The method employed in this work is given in the experimental section.

The advantages of the dilution method are:

1) Most of the complexes studied have intense absorption bands. By this method, the absorption can be brought in the range where the absorption is measured with less error.
2) The scattering coefficient S is determined by the scattering coefficients of the diluent.
3) When measuring relative to pure diluting agent, any deviations from the isotropic scattering distribution can be eliminated so that the measurements are independent of the type of measuring arrangements.

4.3 Experimental

4.3.1 Preparation of Samples

Following the practice of other workers studying charge-transfer complexes potassium bromide (KBr) was used as diluent (Wright, 1965; Vincent, 1972). Potassium bromide is easily obtainable in spectroscopic grade of purity and is convenient to use.

A standard procedure was adopted. A weighed amount of complex was put into an agate mortar with 1 g. of KBr and ground by hand for exactly 5 min.. The sample was packed into a sample holder and compressed to a uniform surface by pressing a clean flat metal surface on the sample. The packing pressure was as far as possible kept constant.

4.3.2 Measurement of Spectra

An SP 540 diffuse reflectance attachment for the unicam SP 500 series 2 ultraviolet visible spectrometer was used. KBr ground for the same time as the samples was used as a standard. The spectra were determined by varying the wavelength in intervals of 10 nm. or 20 nm. and observing the % reflectance. The range covered was from 400 nm. to 1000 nm..

The % reflectance values obtained in this way are relative to the KBr standard, which itself is not 100% reflecting. The Kubelka-Munk function requires reflectivity data (=% reflectance/100) relative to a perfectly reflecting standard. In practice, such a standard is difficult, if not impossible to obtain. Kortum (1969) shows that freshly prepared MgO has a nearly constant reflectivity of 0.98 over the wavelength range of the present work. The following procedure was therefore adopted to obtain correct reflectivity values.

1) Reflectivity values (R_D) at the wavelength concerned were measured for the ground KBr standard against an MgO reference.

2) If the reflectivity of (sample+diluent) relative to pure diluent is R_S, then the absolute reflectivity of (sample+diluent), R, is given by $R=0.98\ R_D R_S$ assuming the MgO is 98% reflecting

$$F(R) = \frac{(1-R)^2}{2R}$$

and

$$F(R_D) = \frac{(1-R_D)^2}{2R_D}$$

so that $\frac{K}{S}$ (sample) $= F(R) - F(R_D)$.

The BASIC program listed in Appendix II was used to calculate the $\frac{K}{S}$ values in this way, and the spectra were plotted as $(\frac{K}{S})$ as a function of wavelength, either by hand or using computerised graph plotting.

4.4 Results

Plots of $\frac{K}{S}$ as a function of wavelength for the parent complexes are given in Figs. 4.3-4.14. Although the scattering coefficients (S) are not known, the standard grinding conditions used should lead to similar scattering coefficients for all samples. Also, Körtum (1969) shows that for particles of the size obtained under similar grinding conditions, the scattering should be essentially wavelength-independent. Thus, provided that the samples are all packed equally uniformly and smoothly in the sample holder, the shapes of these plots should follow accurately the shapes of the true absorption spectra of the solid complexes, while the magnitude of $\frac{K}{S}$ at any wavelength should depend on the amount of the complex uniformly spread over the surface of a given weight of KBr powder. Several experimental checks were made as follows to confirm the validity of these points.

1) The reproducibility of packing of the sample in the sample holder was checked by measuring the spectrum for a sample of dibenzofuran/TCNQ on KBr , emptying and repacking the sample holder with the same material, and re-measuring the spectrum. The result (Fig. 4.9) shows that the two spectra obtained are identical within the accuracy of measurement, so that reproducible sample packing may be assumed.

2) For each complex several samples containing different weights of the complex in a given weight of KBr were prepared and their spectra measured. The resulting curves were scaled to a common value at one wavelength (usually that of the first charge transfer band maximum) and plotted on the same graph. In all cases the agreement between the scaled spectra was good at wavelengths longer than about 450 nm., with significant deviations only at shorter wavelengths. These deviations may be due to small variations in particle size from sample to sample, leading to differences in scattering coefficients at shorter wavelengths.

3) For each complex, plots of $\frac{K}{S}$ at the wavelength of the first CT band maximum as a function of weight of the complex in 1 g. of KBr were found to be reasonable straight lines through the origin. Since the spectrum shapes are similar for different sample concentrations as shown above, it may be concluded that the scattering coefficients are little affected by changes in the concentration of the complex in KBr . Thus, the slopes of plots of $\frac{K}{S}$ against concentration should be proportional to the extinction coefficients of the solid complexes, i.e. these plots are essentially Beer-Lambert plots (Figs. 4.15-4.20). Comparison of the slopes of these plots for different complexes

therefore gives information on the relative intensities of charge transfer transitions in the different solid complexes studied.

Plots of $\frac{K}{S}$ as a function of wavelength for the mixed complexes studied are given in Figs. 4.21,4.28,4.33-4.37. Measurements were first made on the anthracene/phenanthrene/tetracyanobenzene system for comparison with the single crystal data of Wright, Ohta and Kuroda (1976). In this system, the phenanthrene complex does not absorb at all at the wavelength of the first CT band maximum of the anthracene complex, and the relative orientations of donor and acceptor are identical in the two parent and the mixed complexes. In Fig. 4.21 the reflectance spectra of the mixed complexes of this system are shown with $\frac{K}{S}$ values scaled to a common value of 1.0 at the wavelength of the first charge transfer band maximum of the anthracene complex. Subtraction of the pure anthracene/TCNQ spectrum scaled in the same way from each of these curves yields difference spectra (Figs. 4.22-4.26) which are all similar shape and correspond to the spectrum of the pure phenanthrene/TCNB complex (Fig. 4.5). This graphical decomposition technique provides values of the relative intensities of anthracene/TCNB and phenanthrene/TCNB first charge transfer bands in the mixed complexes as a function of composition. If it is assumed that the intensities of the two charge transfer bands of a mixed complex $(\text{anthracene})_x(\text{phenanthrene})_{1-x}\text{TCNB}$ are simply proportional to the probabilities of finding anthracene/TCNB and phenanthrene/TCNB pairs in the crystal, the following relation is expected for the intensity ratio:

$$\frac{I_2}{I_1} = \frac{I_{\text{phen}/\text{TCNB}}}{I_{\text{anth}/\text{TCNB}}} \cdot \frac{1-x}{x}$$

where I_2/I_1 is the observed intensity ratio and $I_{phen}/TCNB$ and $I_{anth}/TCNB$ are the corresponding extinction coefficients for the first charge transfer bands of the pure complexes. Fig. 4.27 is a plot of I_2/I_1 vs. $(1-x)/x$, with gradient 0.21 equal to $I_{phen}/TCNB/I_{anth}/TCNB$. The ratio of the slopes of the Beer-Lambert plots for the two pure complexes (Figs. 4.15 & 4.16), 0.38, gives an independent value of I_2/I_1. These values are in fair agreement with the value of 0.3 obtained from graphical decomposition of polarised crystal spectra of the mixed complexes (Wright, Ohta & Kuroda, 1976). These measurements therefore show that diffuse reflectance spectra can provide useful information on the relative intensities of charge transfer bands in pure and mixed molecular complexes, although the difference between I_2/I_1 obtained from mixed complex spectra and from the ratio of the Beer-Lambert plot slopes of the pure complexes suggests that due caution should be used in interpreting the data and in comparisons with theoretical results.

FIG. 4.2 THE PERCENT REFLECTANCE OF KBr AGAINST MgO STANDARD

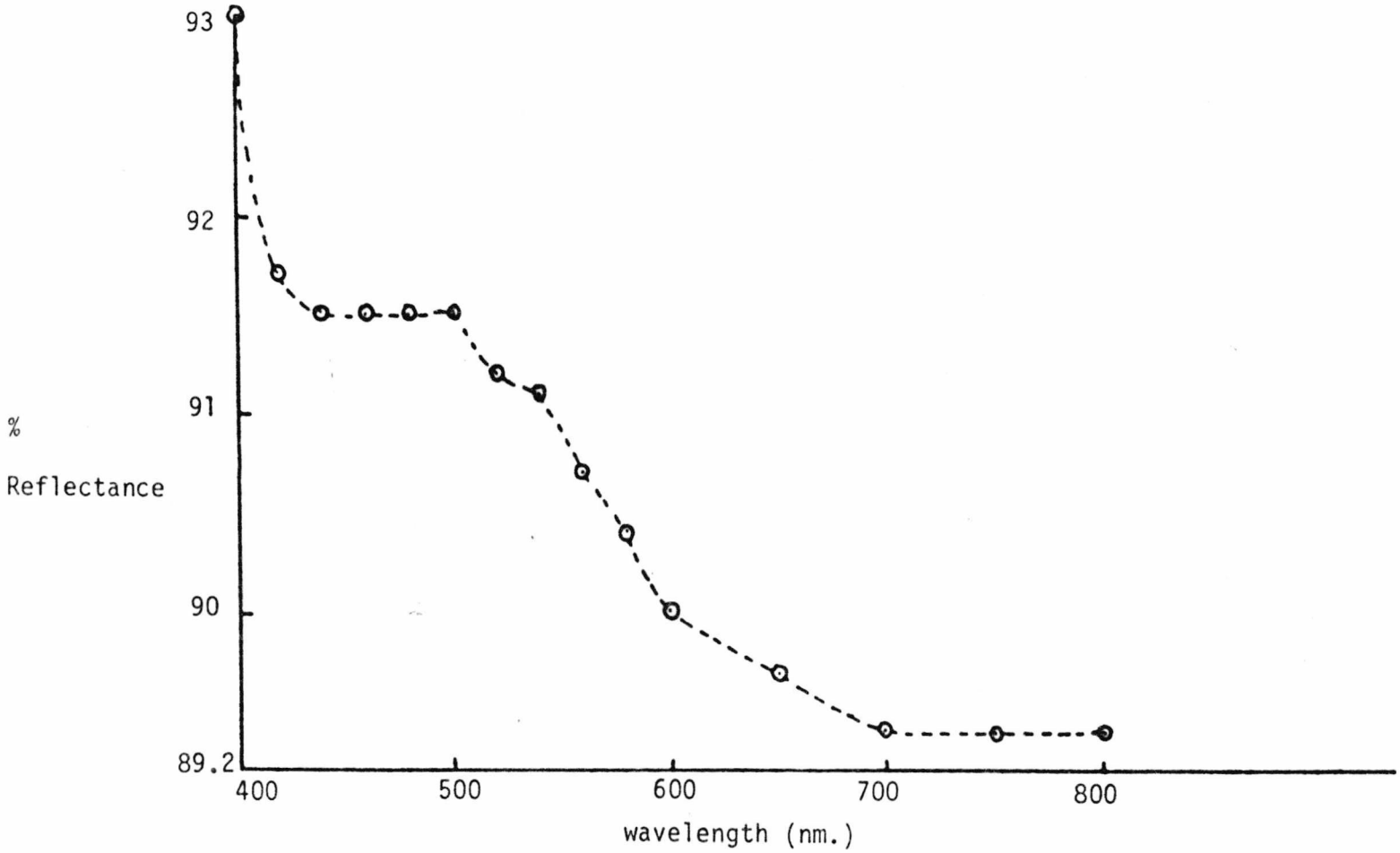

FIG. 4.3 SUPERIMPOSED SPECTRA OF ANTHRACENE/TCNB

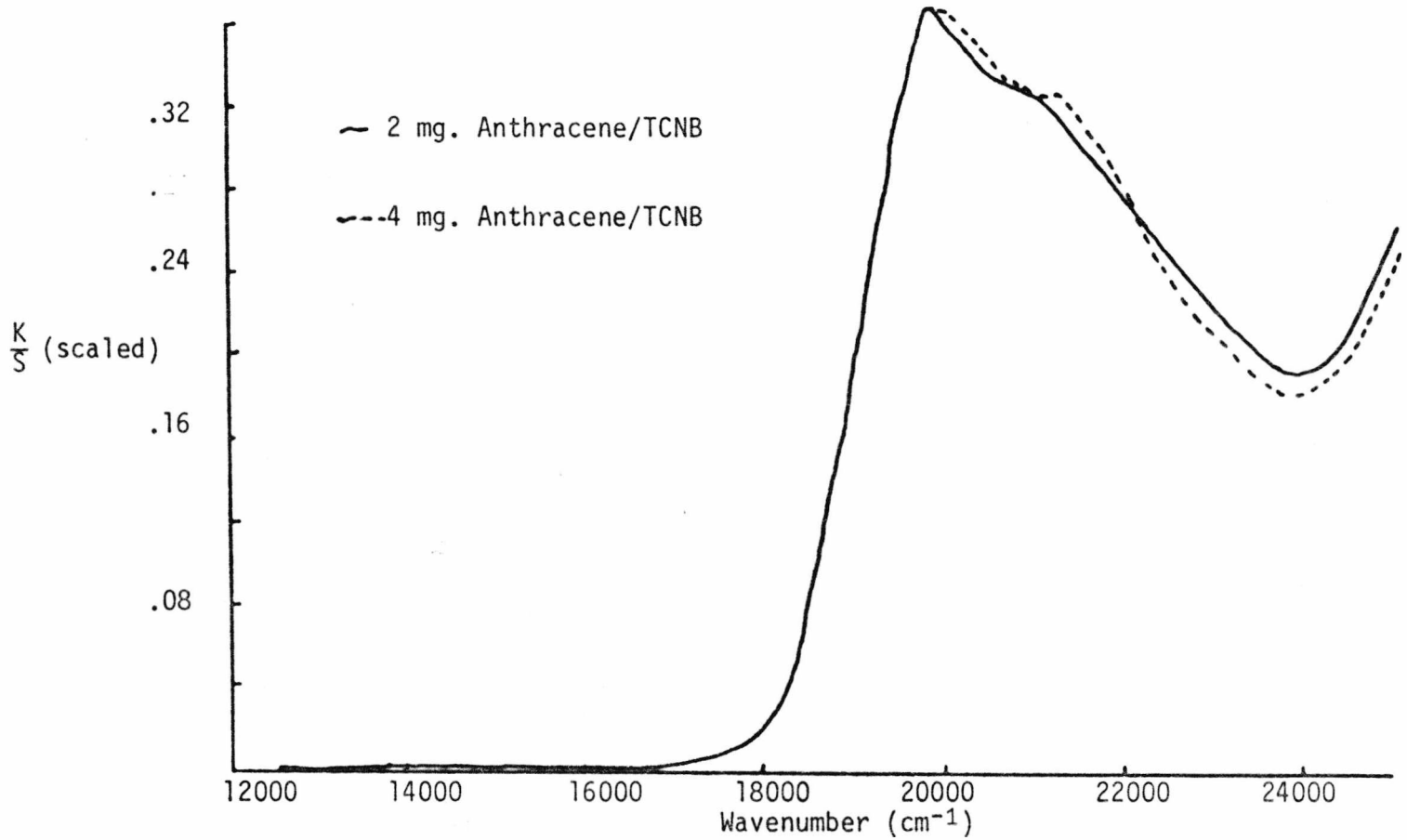

FIG. 4.4 SUPERIMPOSED SPECTRA OF ANTHRACENE/TCNB

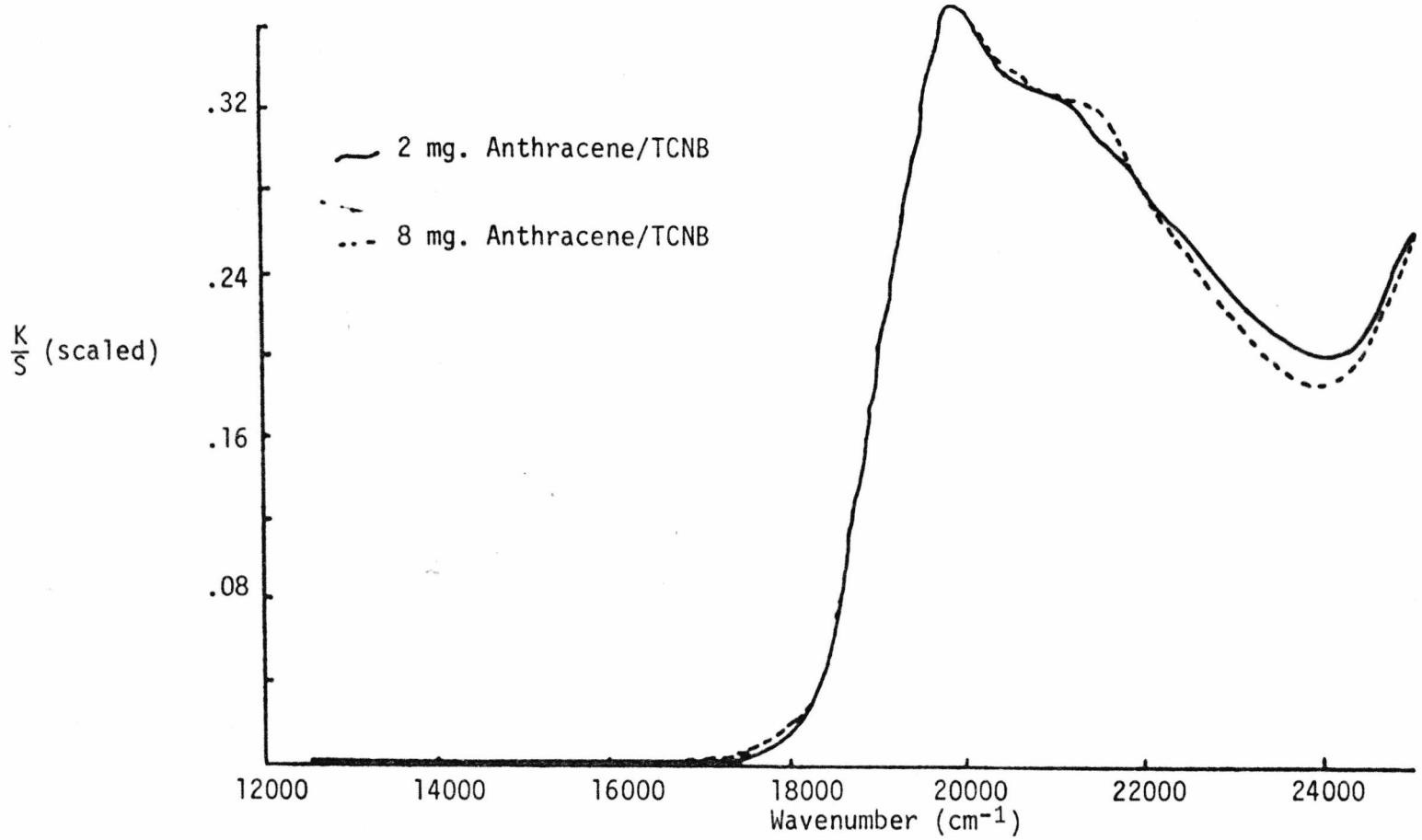

FIG. 4.5 SUPERIMPOSED SPECTRA OF PHENANTHRENE/TCNB

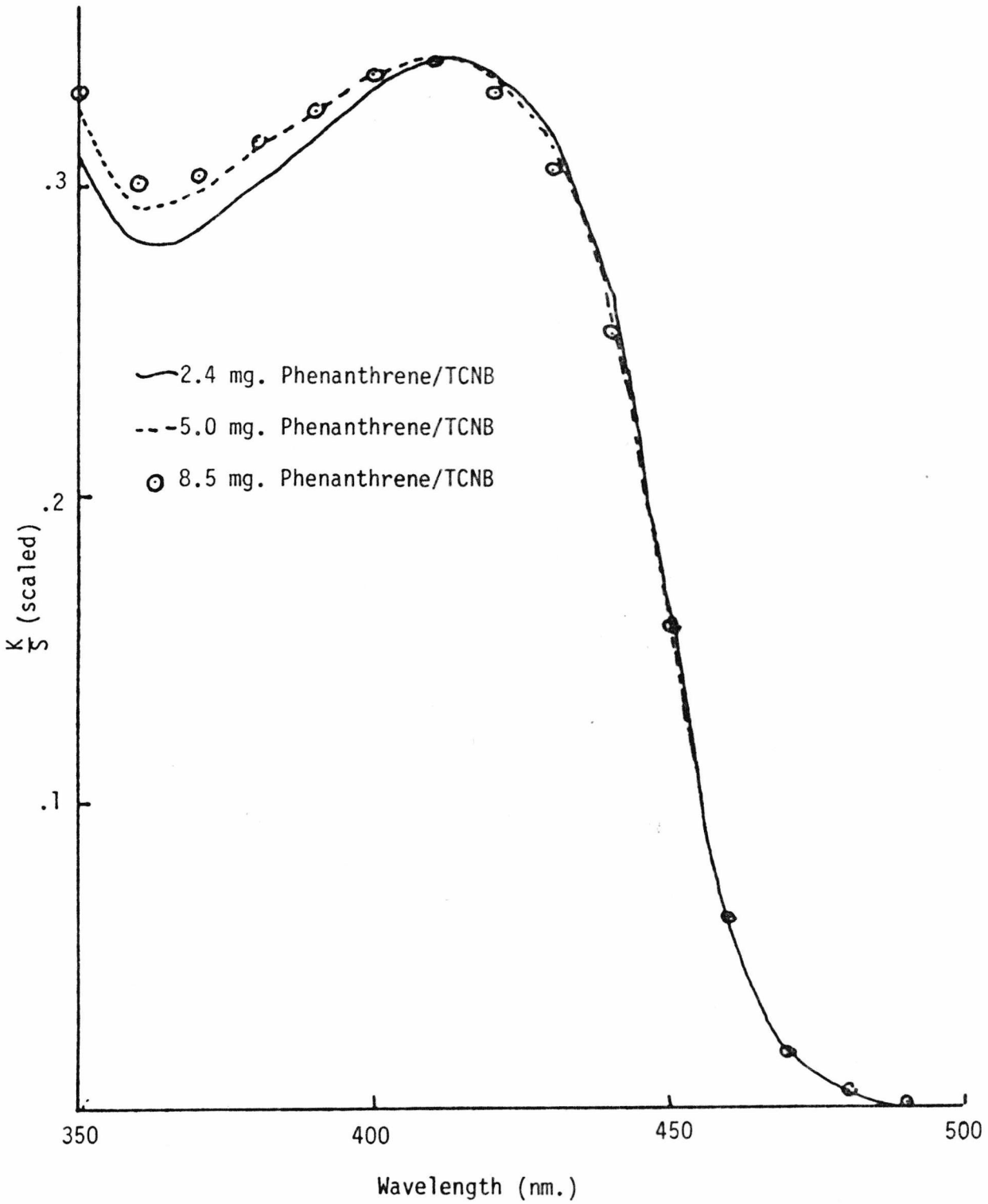

FIG. 4.6 THE REFLECTANCE SPECTRUM OF DIBENZOTHIOPHEN/TCNQ

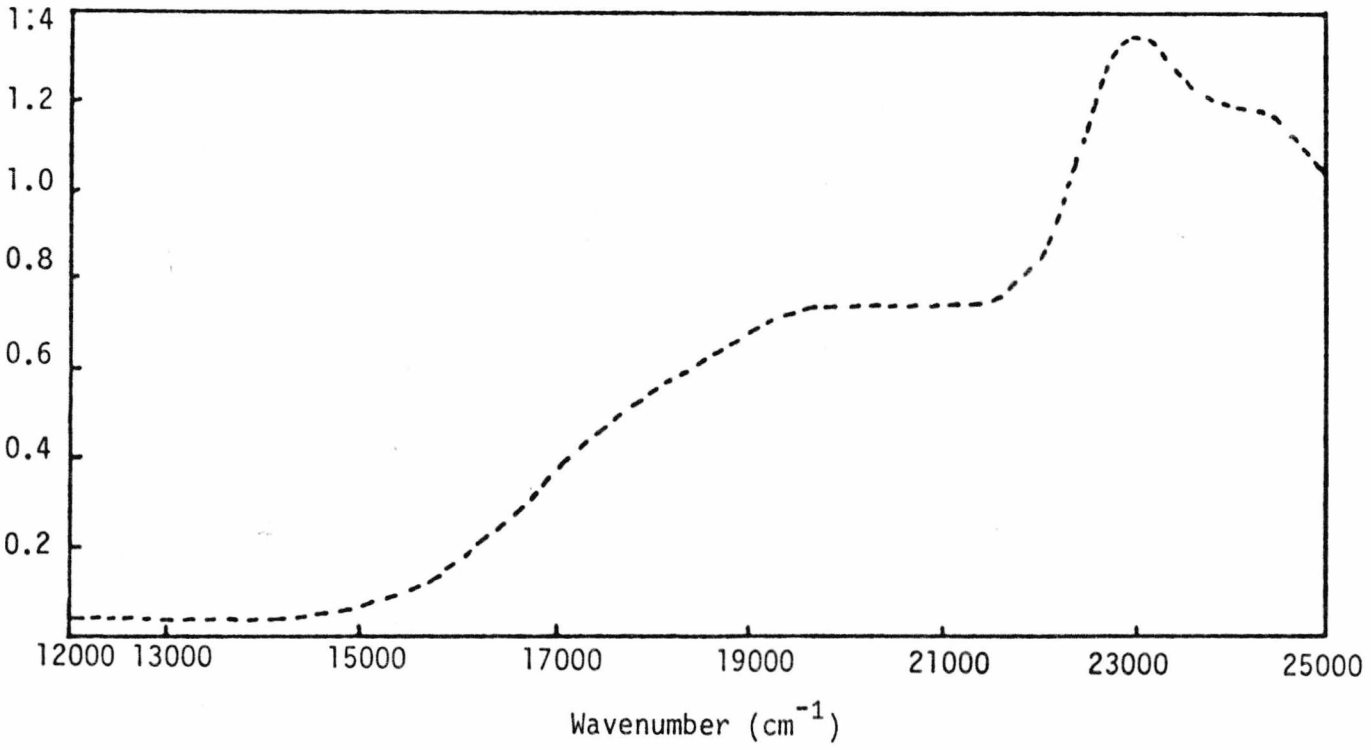

FIG. 4.7 THE REFLECTANCE SPECTRUM OF DIBENZOTHIOPHEN/TCNQ

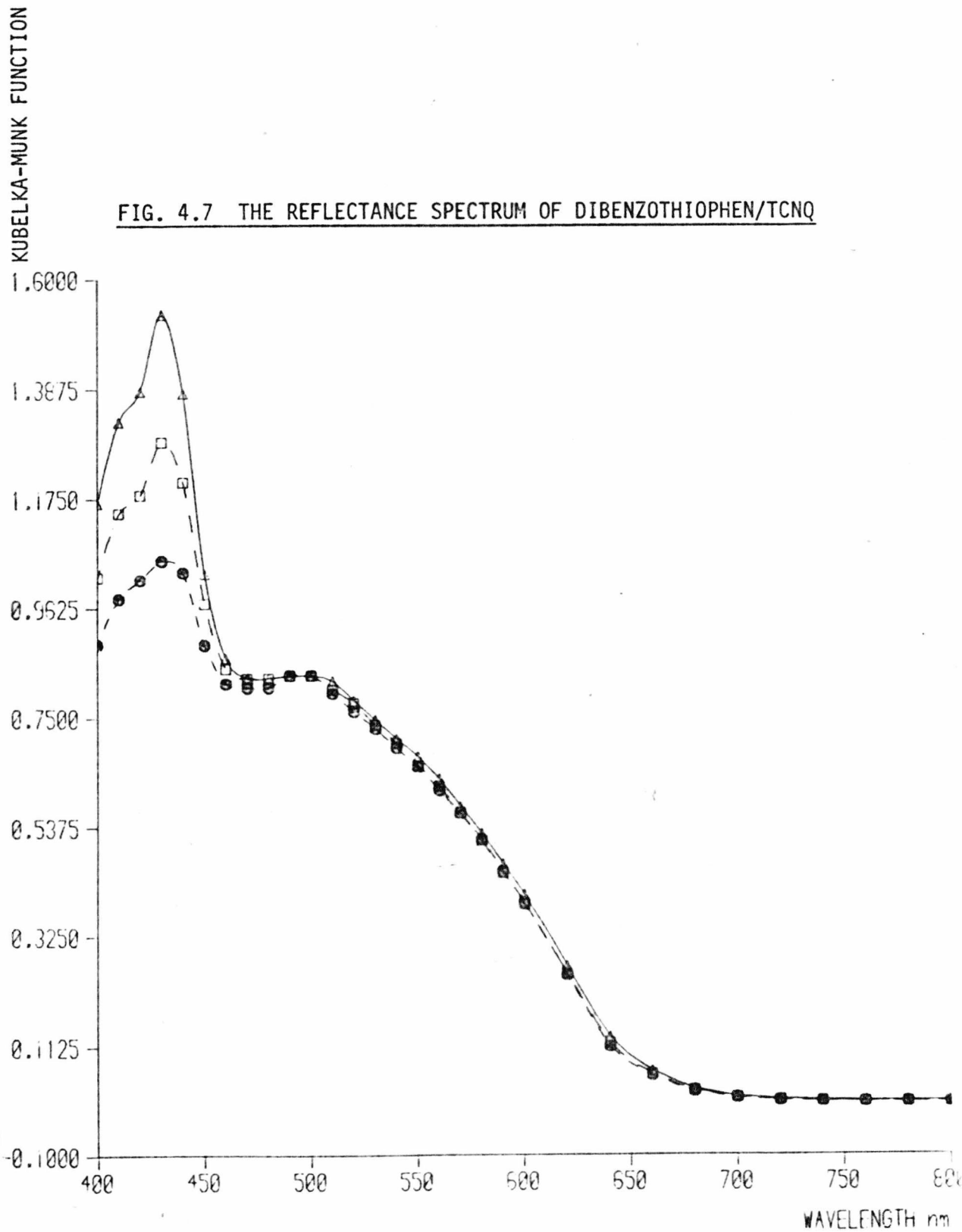

FIG. 4.8 THE REFLECTANCE SPECTRUM OF DIBENZOFURAN/TCNQ

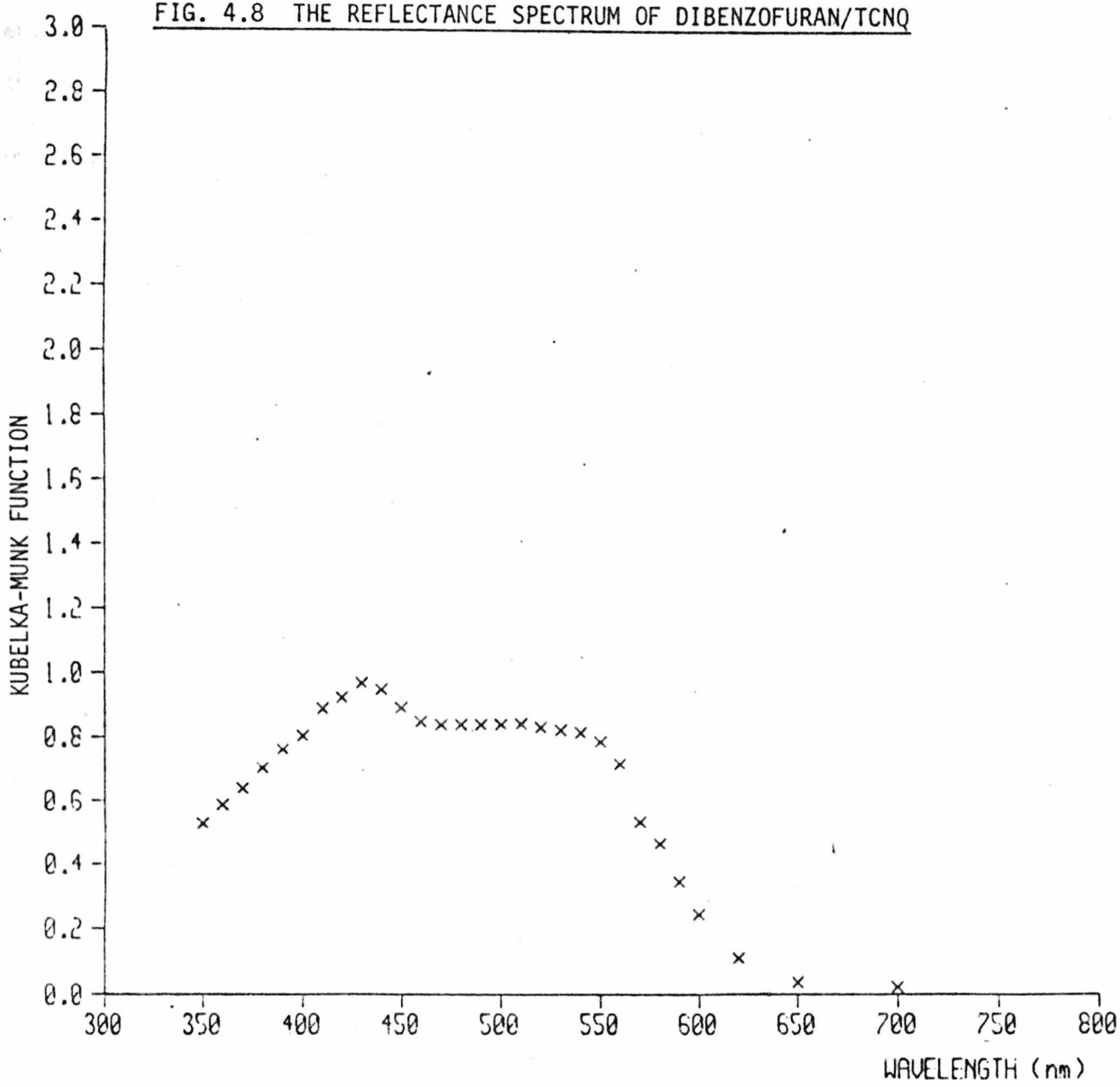

FIG. 4.9 THE REFLECTANCE SPECTRUM OF DIBENZOFURAN/TCNQ TO CHECK THE REPRODUCIBILITY ON REPACKING

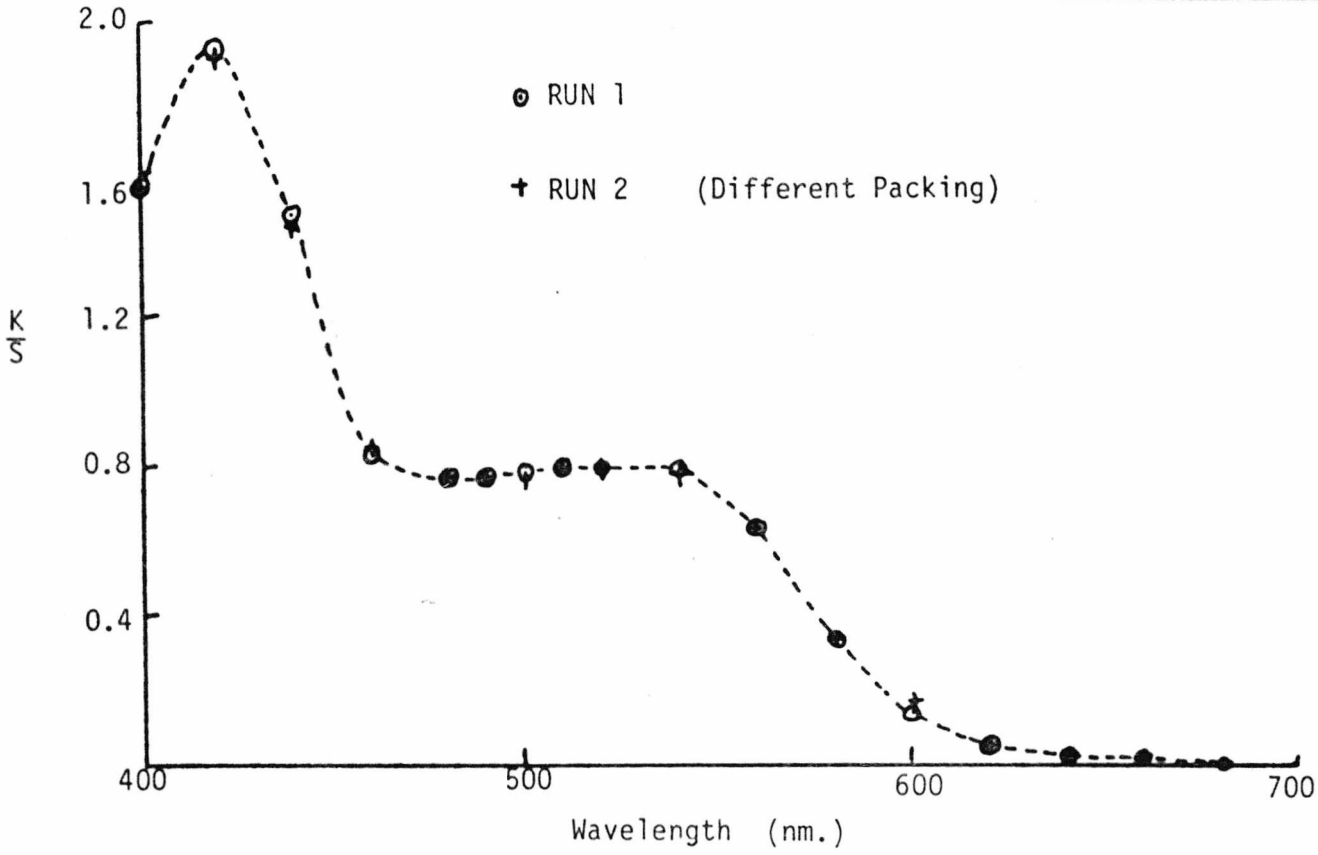

FIG. 4.10 THE REFLECTANCE SPECTRUM OF ANTHRACENE/TCNQ

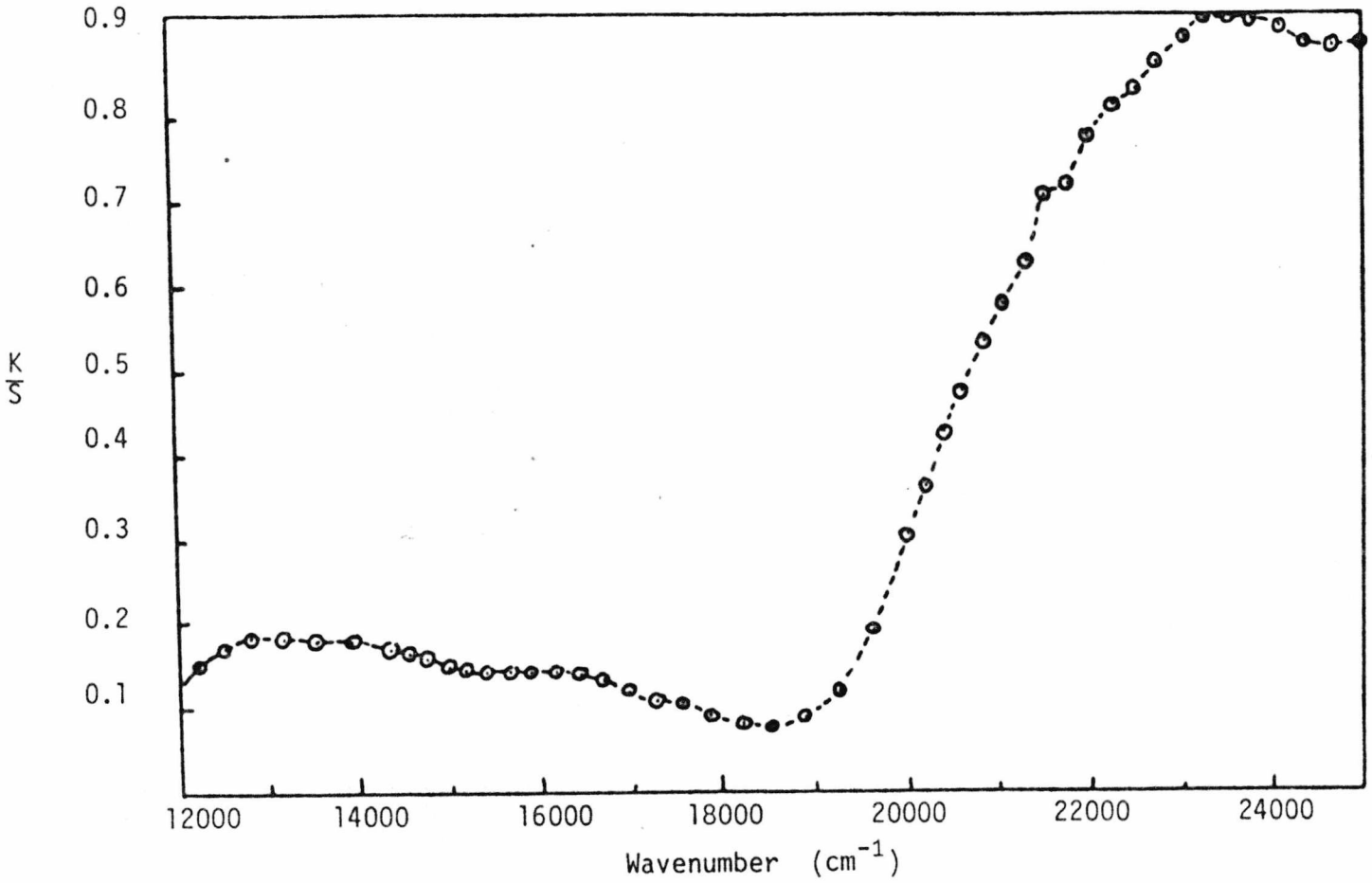

FIG. 4.11 THE REFLECTANCE SPECTRUM OF ANTHRACENE/TCNQ

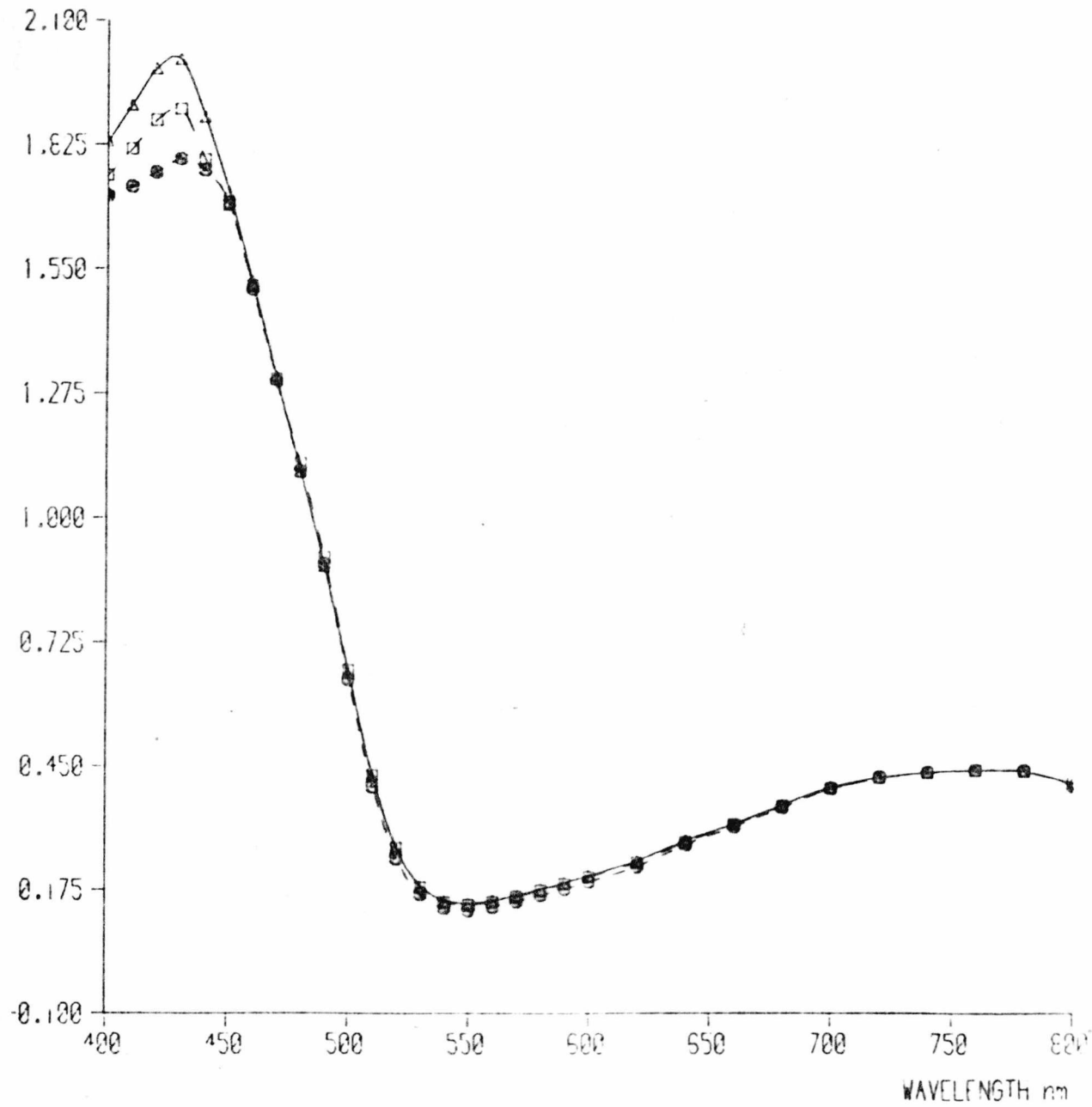

FIG. 4.12 THE REFLECTANCE SPECTRUM OF CHRYSENE/TCNQ

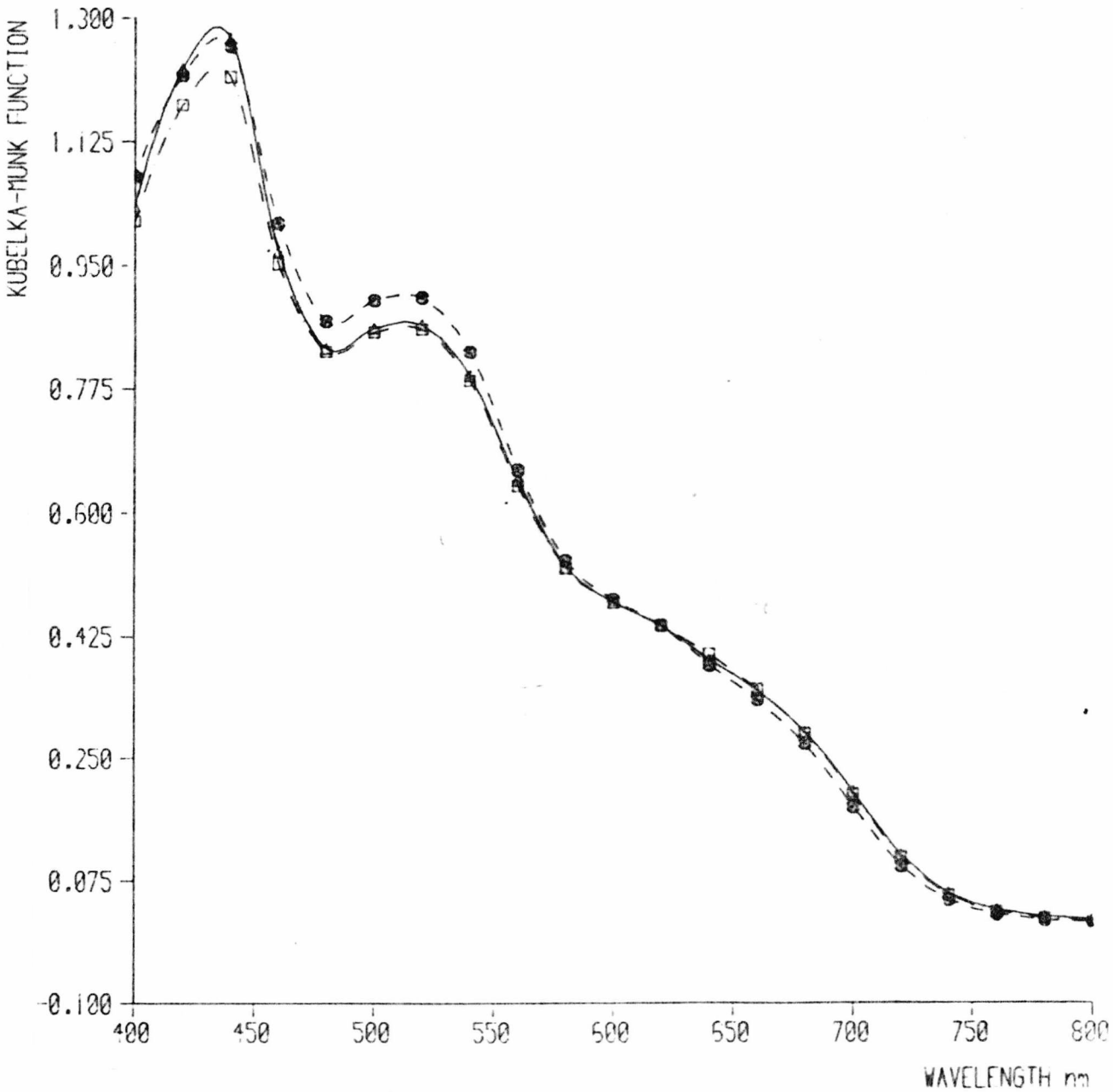

FIG. 4.13 THE REFLECTANCE SPECTRUM OF PYRENE/TCNQ

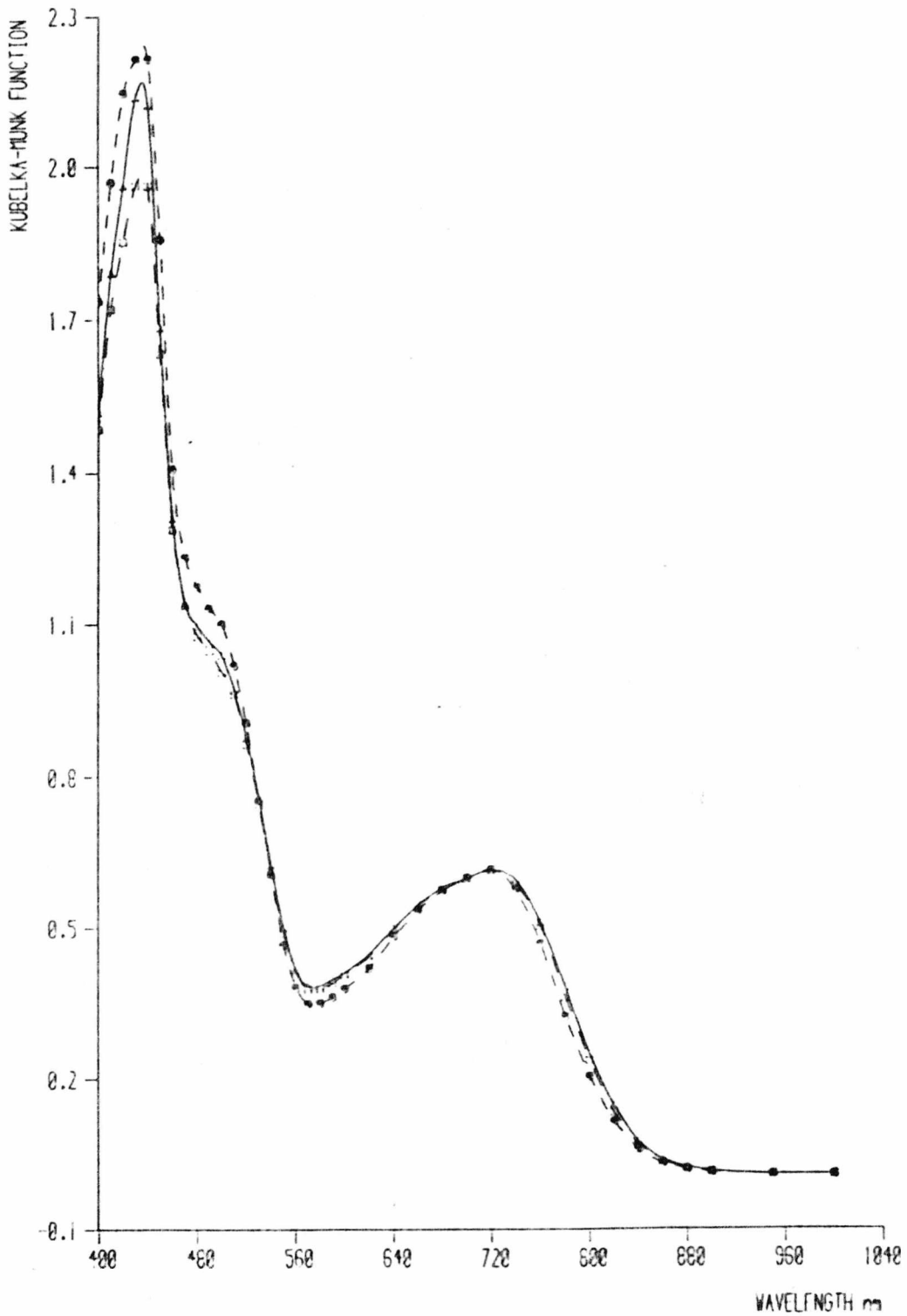

FIG. 4.14 THE REFLECTANCE SPECTRUM OF PERYLENE/TCNQ

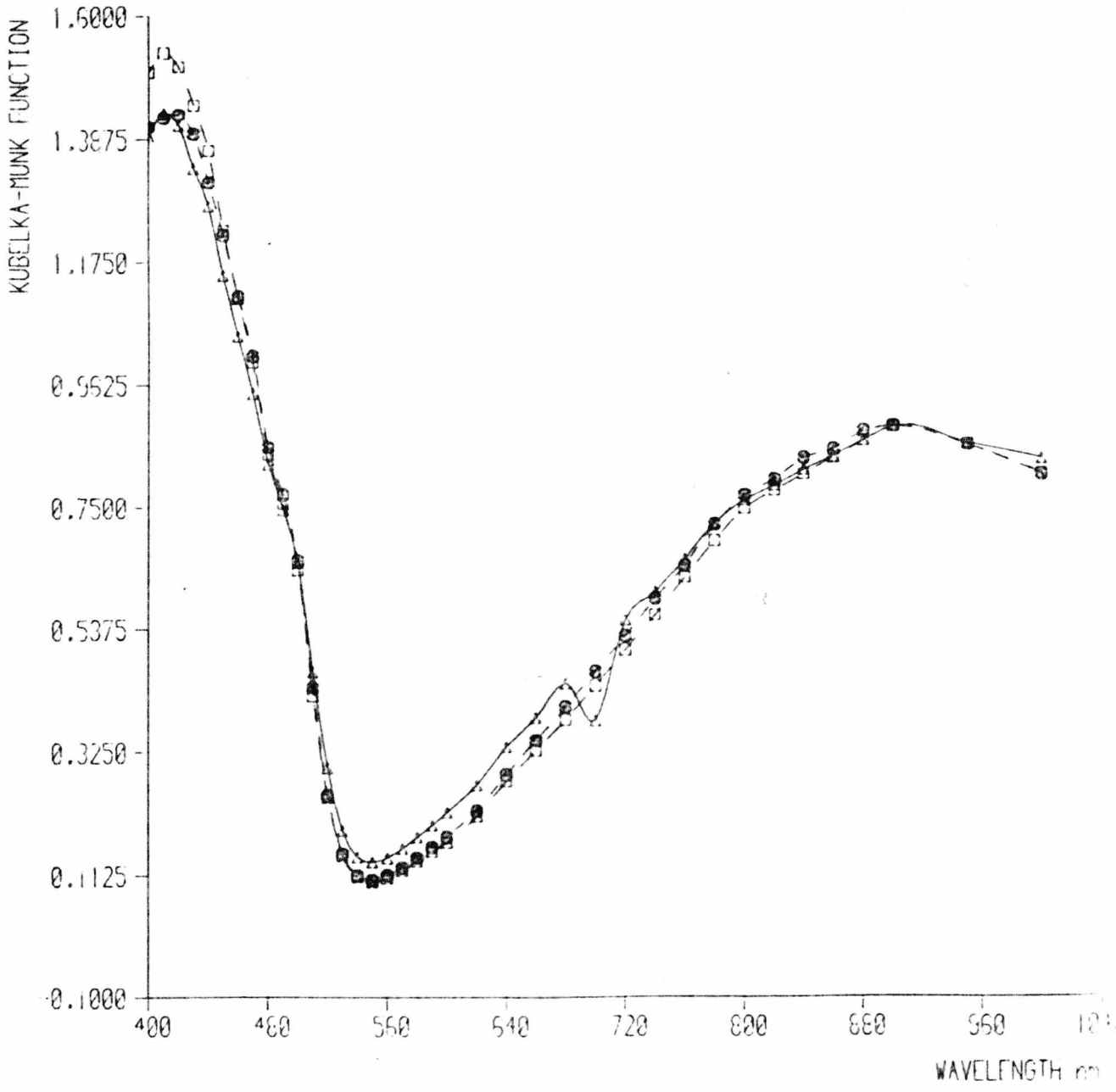

FIG. 4.15 THE BEER-LAMBERT PLOT OF ANTHRACENE/TCNB

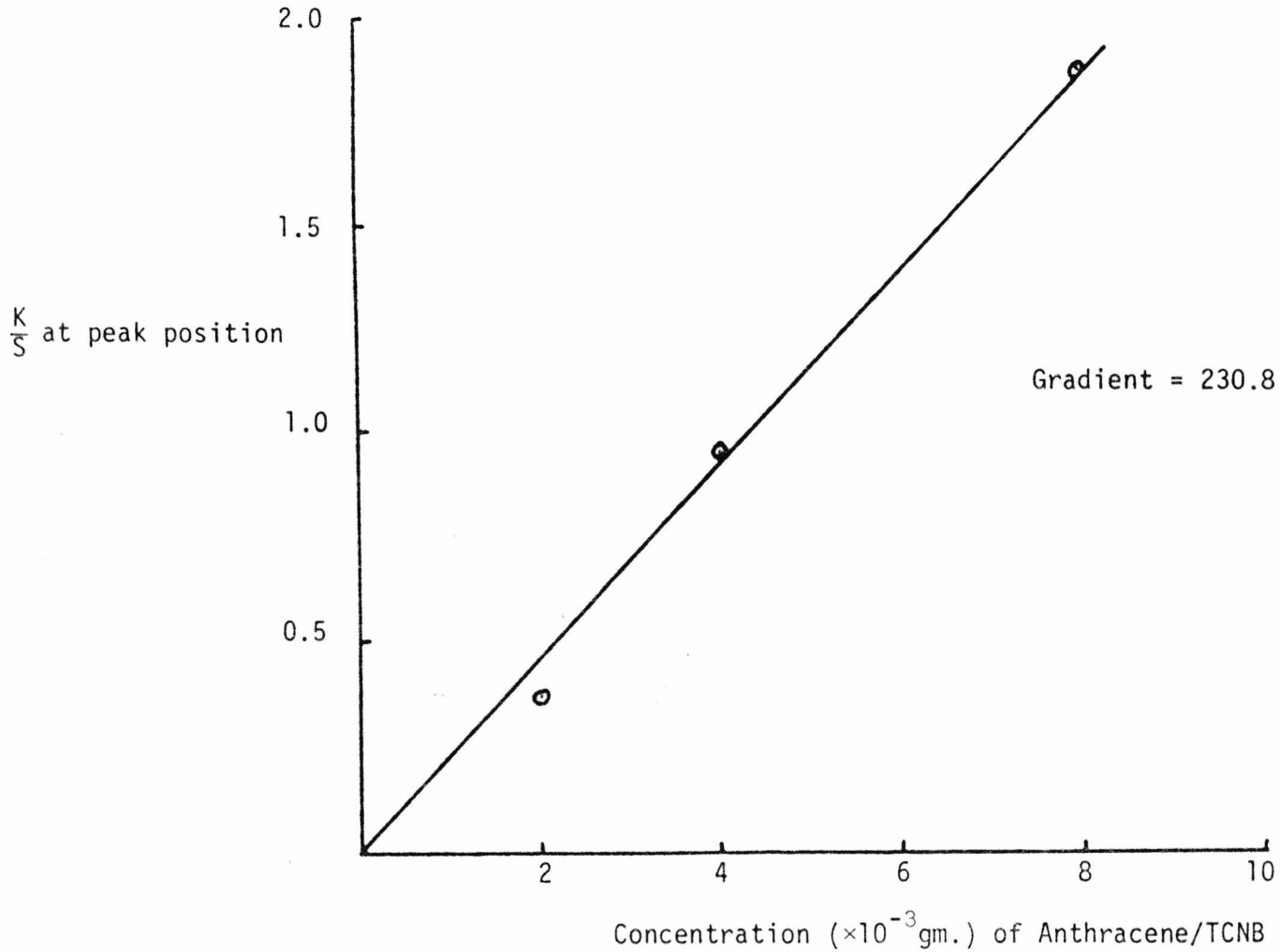

FIG. 4.16 THE BEER-LAMBERT PLOT OF PHENANTHRENE/TCNB

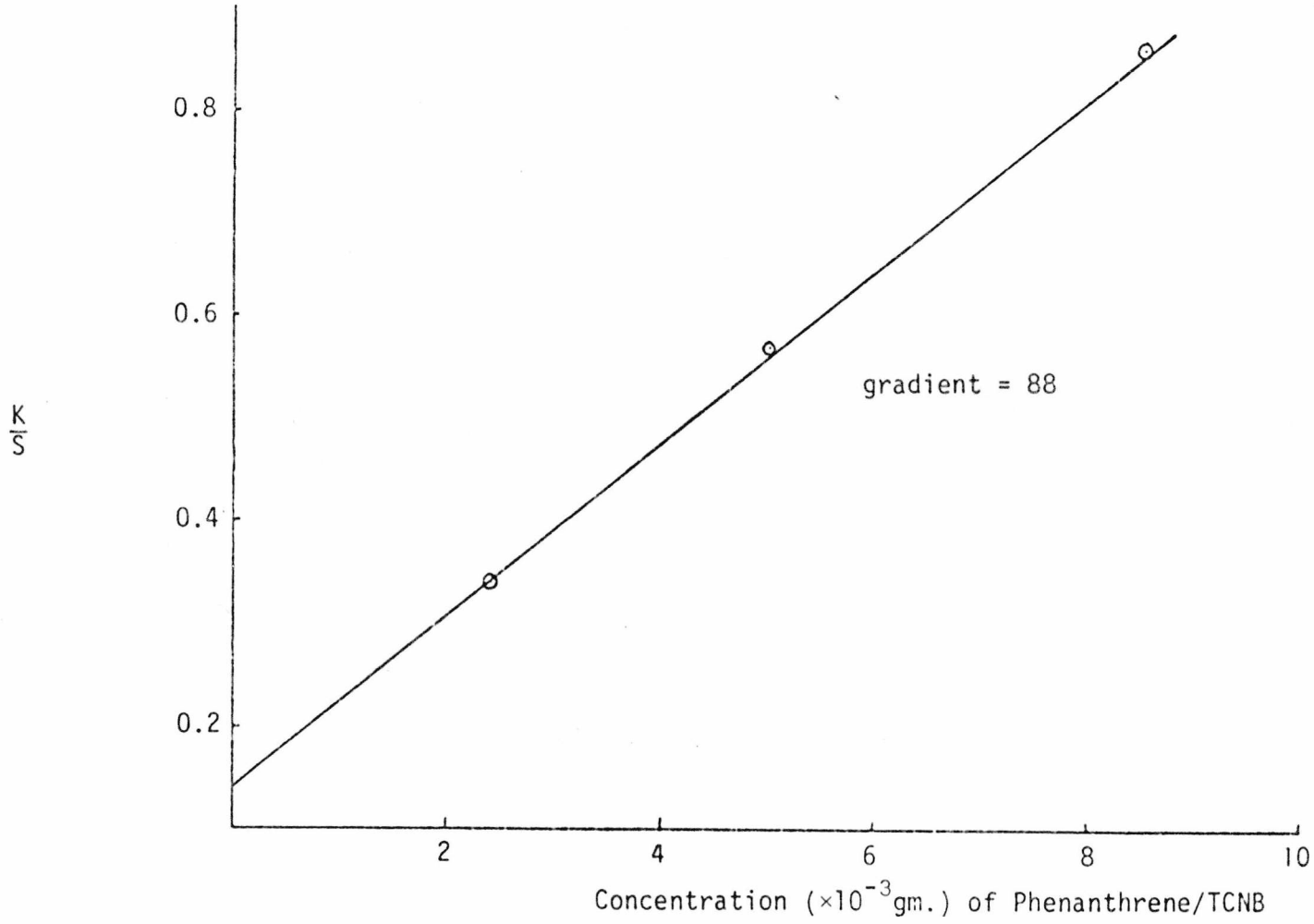

FIG. 4.17 THE BEER-LAMBERT PLOT OF DIBENZOFURAN/TCNQ

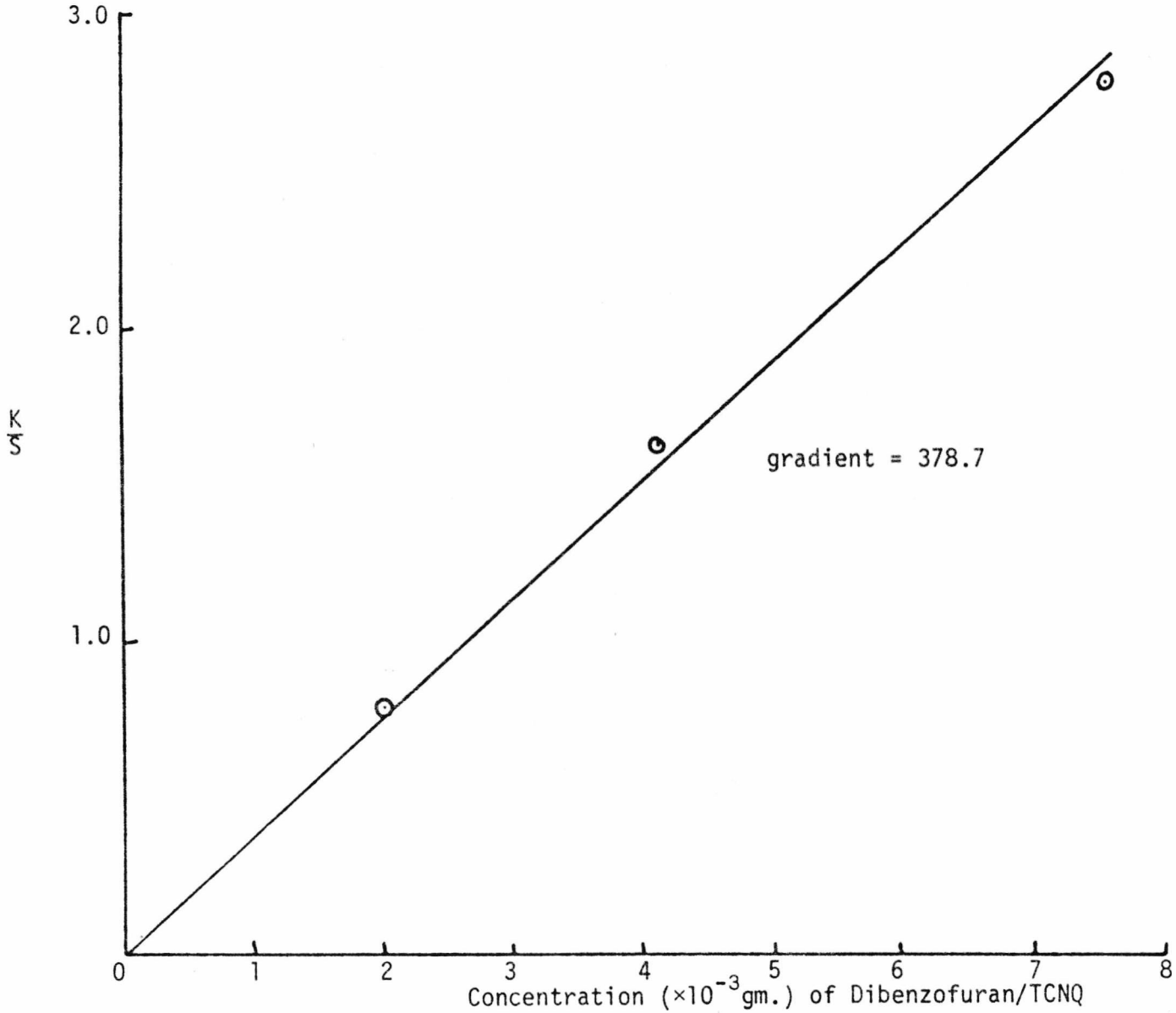

FIG. 4.18 THE BEER-LAMBERT PLOT OF DIBENZOTHIOPHEN/TCNQ AND ANTHRACENE/TCNQ

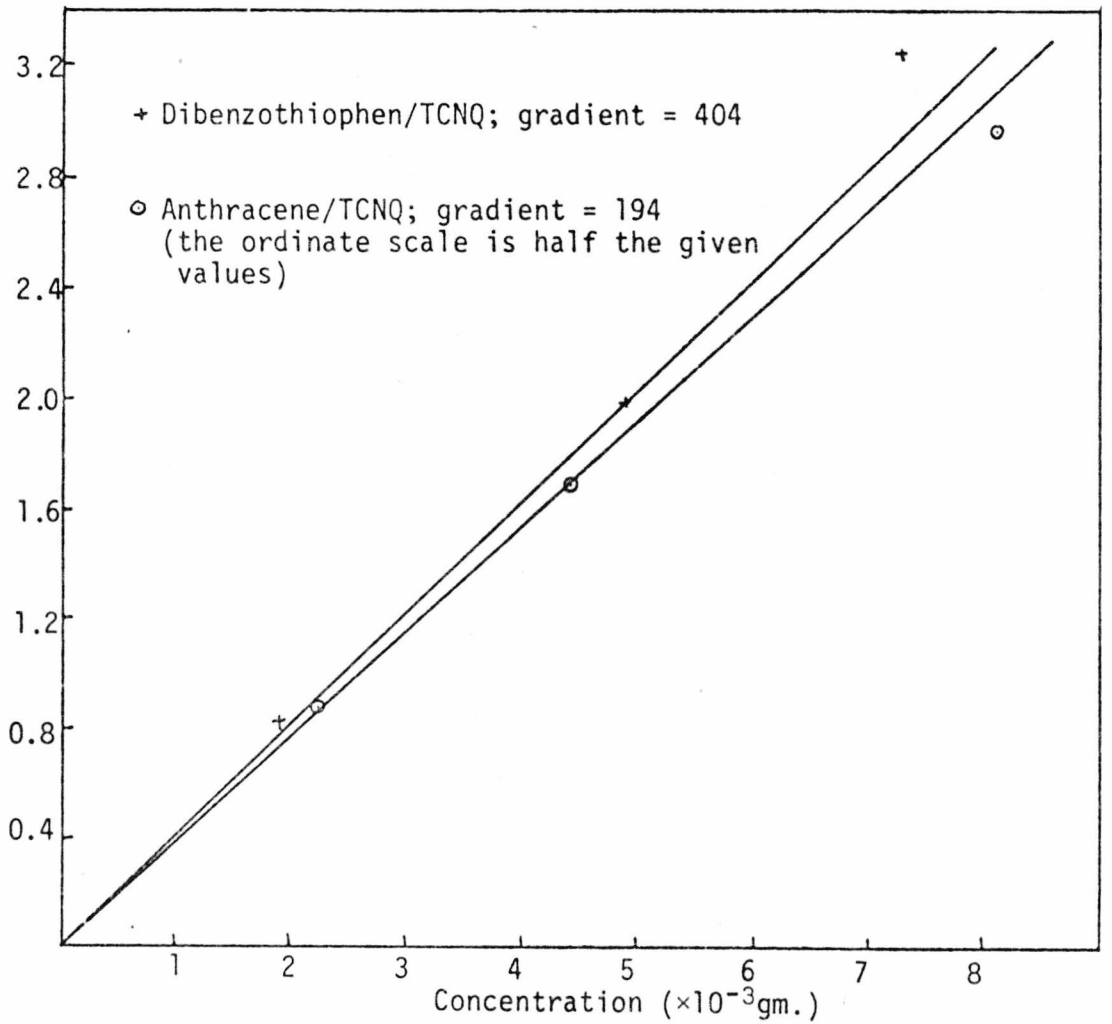

FIG. 4.19 THE BEER-LAMBERT PLOT OF CHRYSENE/TCNQ

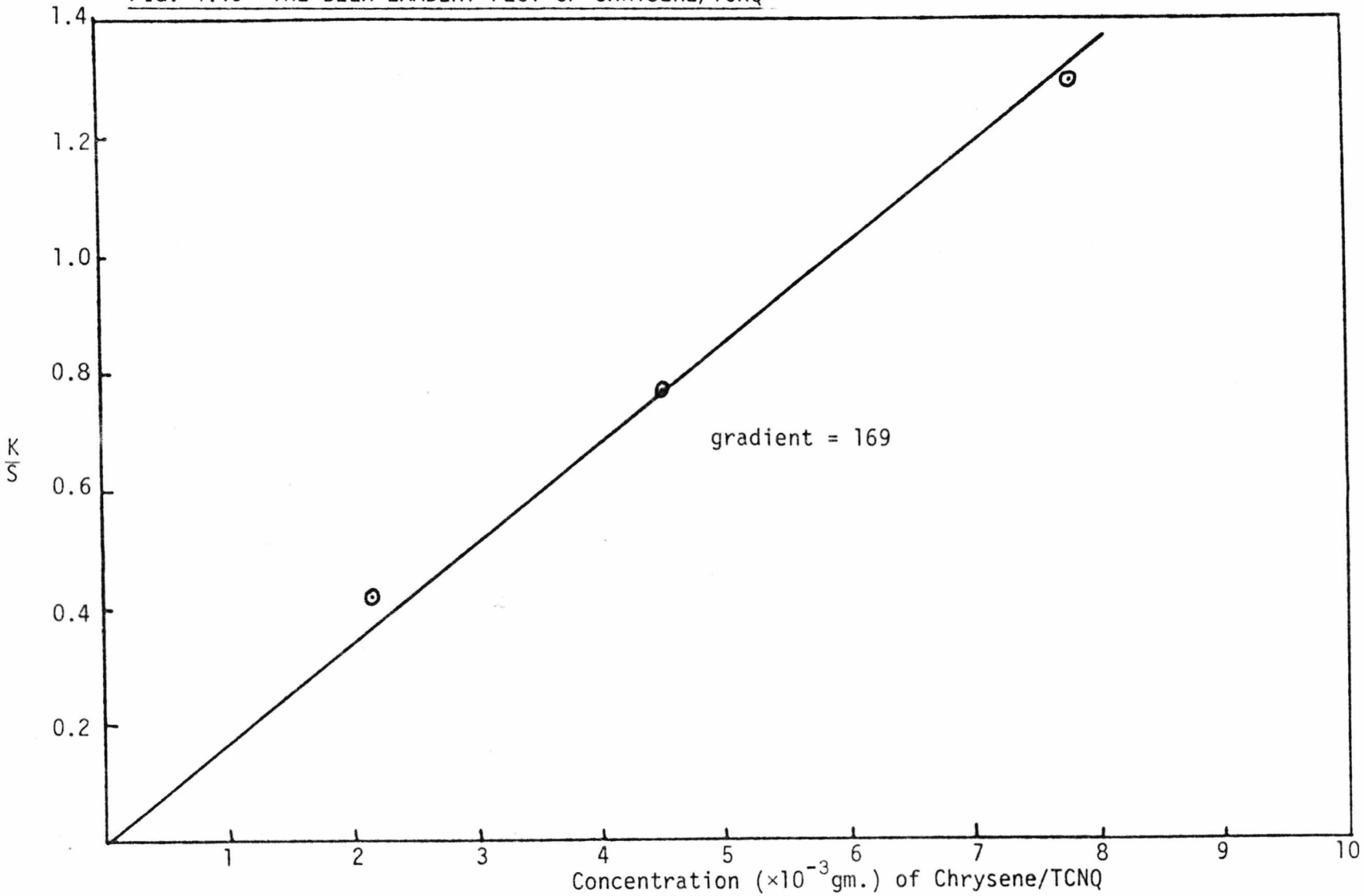

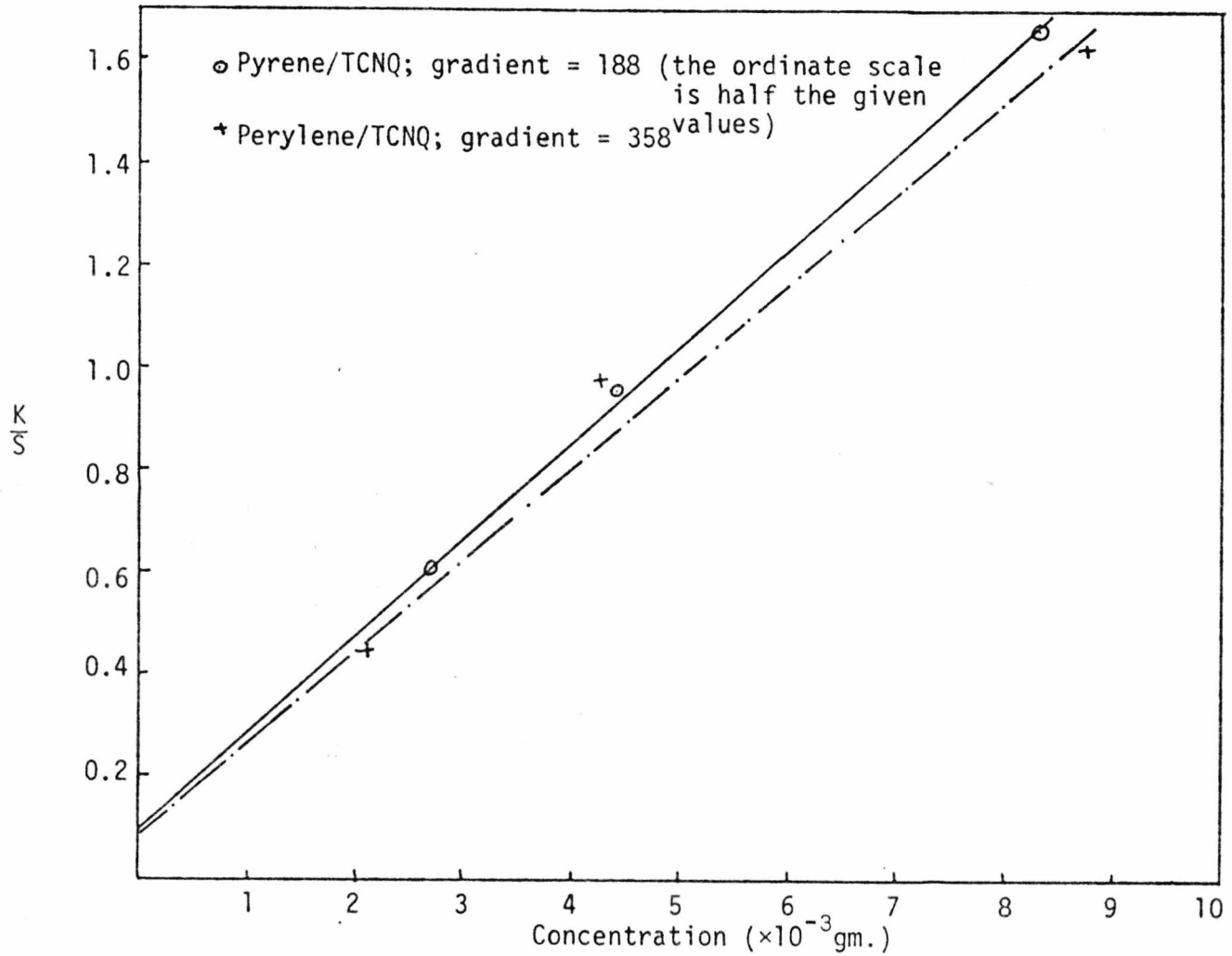

FIG. 4.20 THE BEER-LAMBERT PLOT OF PYRENE/TCNQ AND PERYLENE/TCNQ

FIG. 4.21 SCALED REFLECTANCE SPECTRA OF a) ANTHRACENE/TCNB (b-f) MIXED COMPLEXES OF ANTH.$_x$/PHEN.$_{1-x}$/TCNB b) x=.63; c)x=.45; d)x=.35; e)x=.25; f)x=.17

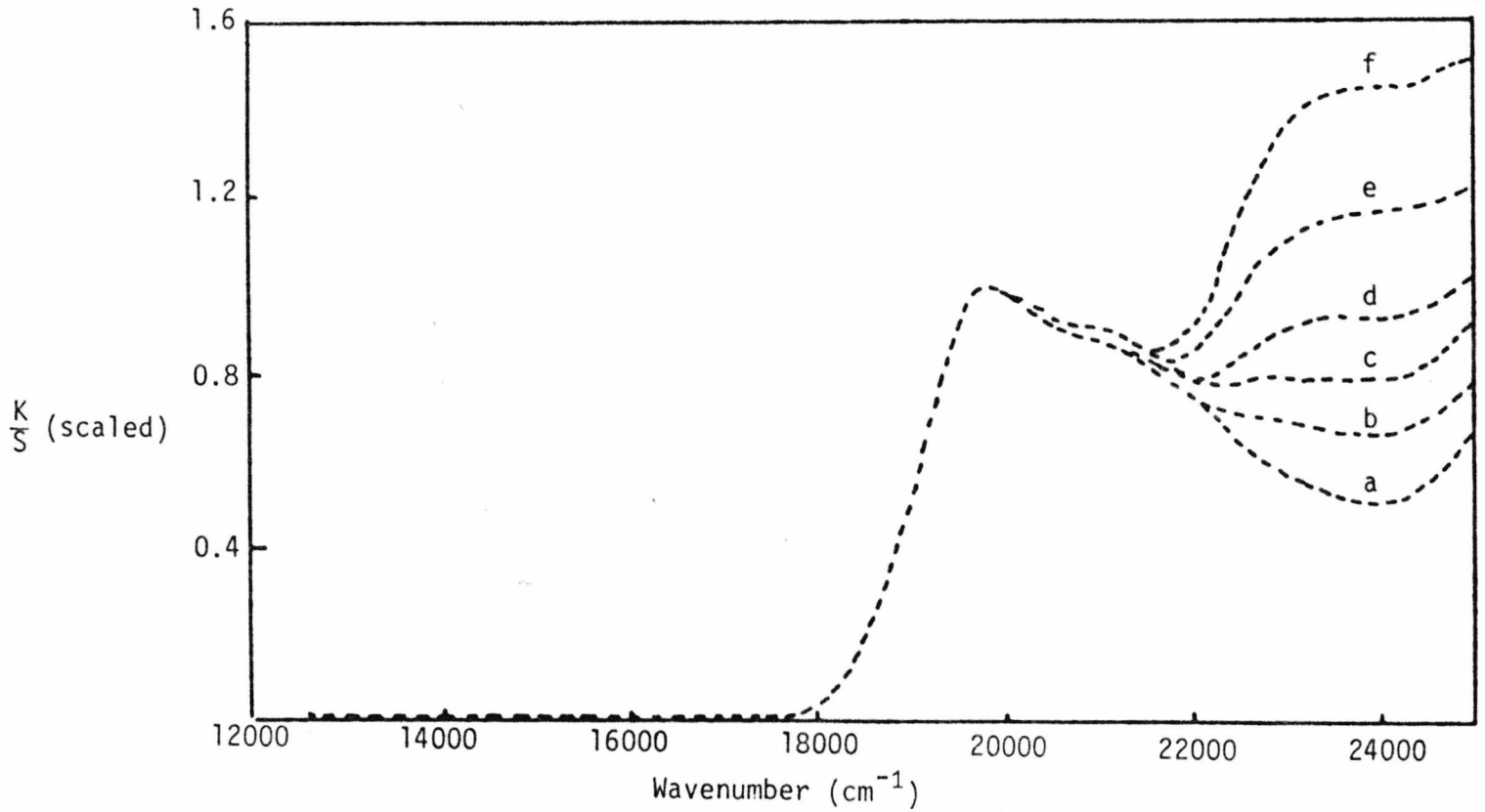

FIG. 4.22 THE DIFFERENCE SPECTRUM
(ANTH.$_{.17}$/PHEN.$_{.83}$/TCNB)

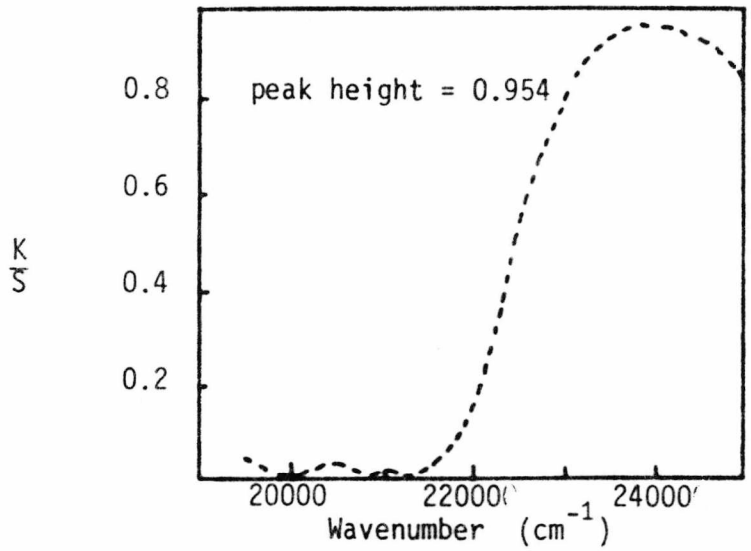

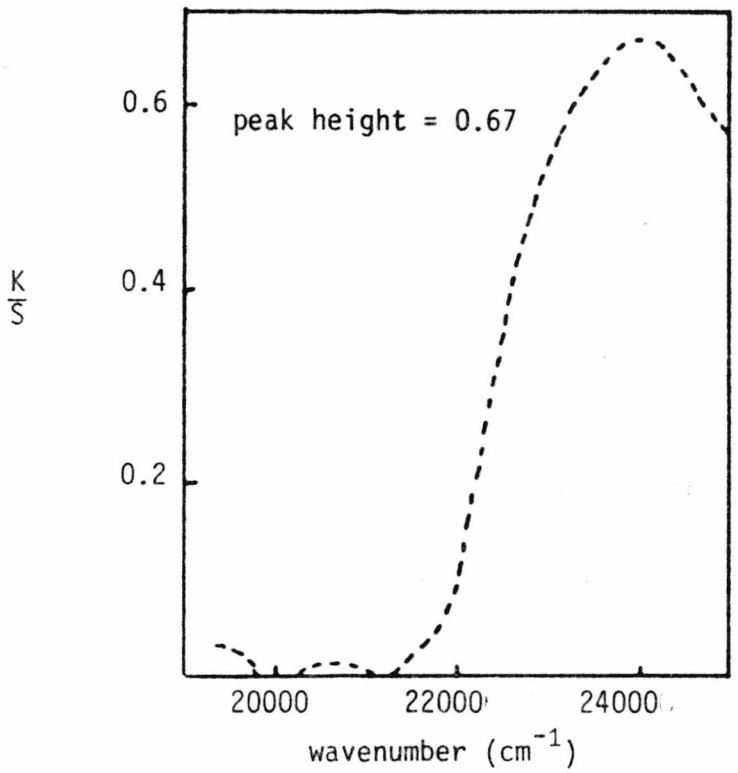

FIG. 4.23 THE DIFFERENCE SPECTRUM
(ANTH.$_{.25}$/PHEN.$_{.75}$/TCNB)

FIG. 4.24 THE DIFFERENCE SPECTRUM (ANTH.$_{.35}$/PHEN.$_{.65}$/TCNB

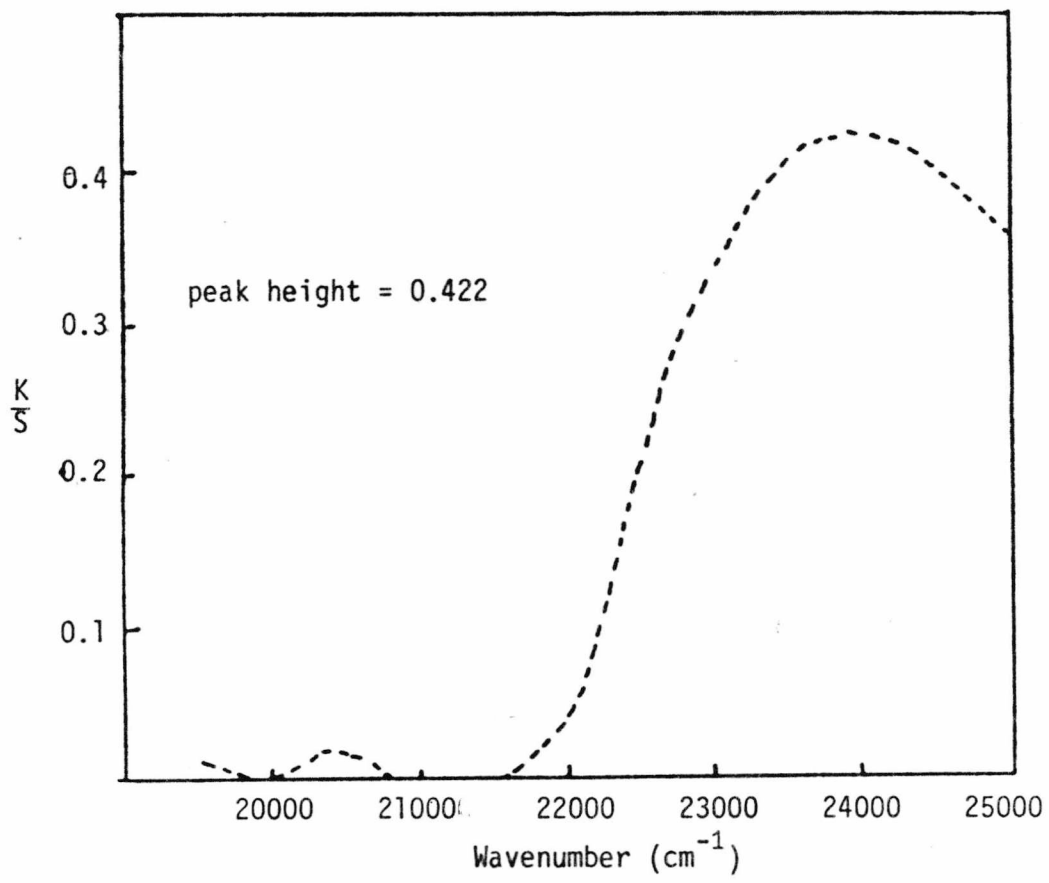

FIG. 4.25 THE DIFFERENCE SPECTRUM (ANTH.$_{.45}$/PHEN.$_{.55}$/TCNB

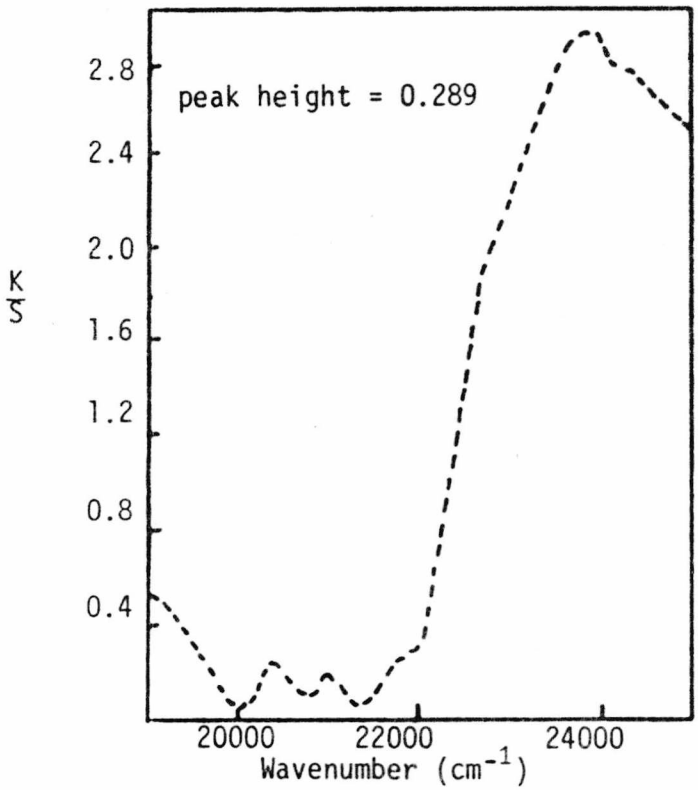

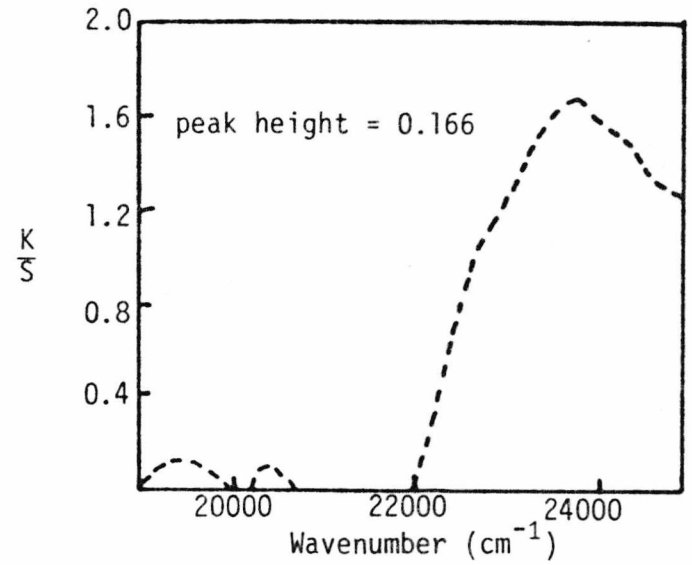

FIG. 4.26 THE DIFFERENCE SPECTRUM (ANTH.$_{.45}$/PHEN.$_{.55}$/TCNB)

FIG. 4.27 INTENSITY RATIO OF THE TWO CHARGE TRANSFER BANDS AS A FUNCTION OF MOLE RATIO OF THE TWO DONORS OF MIXED COMPLEX $ANTH_x/PHEN_{1-x}/TCNB$

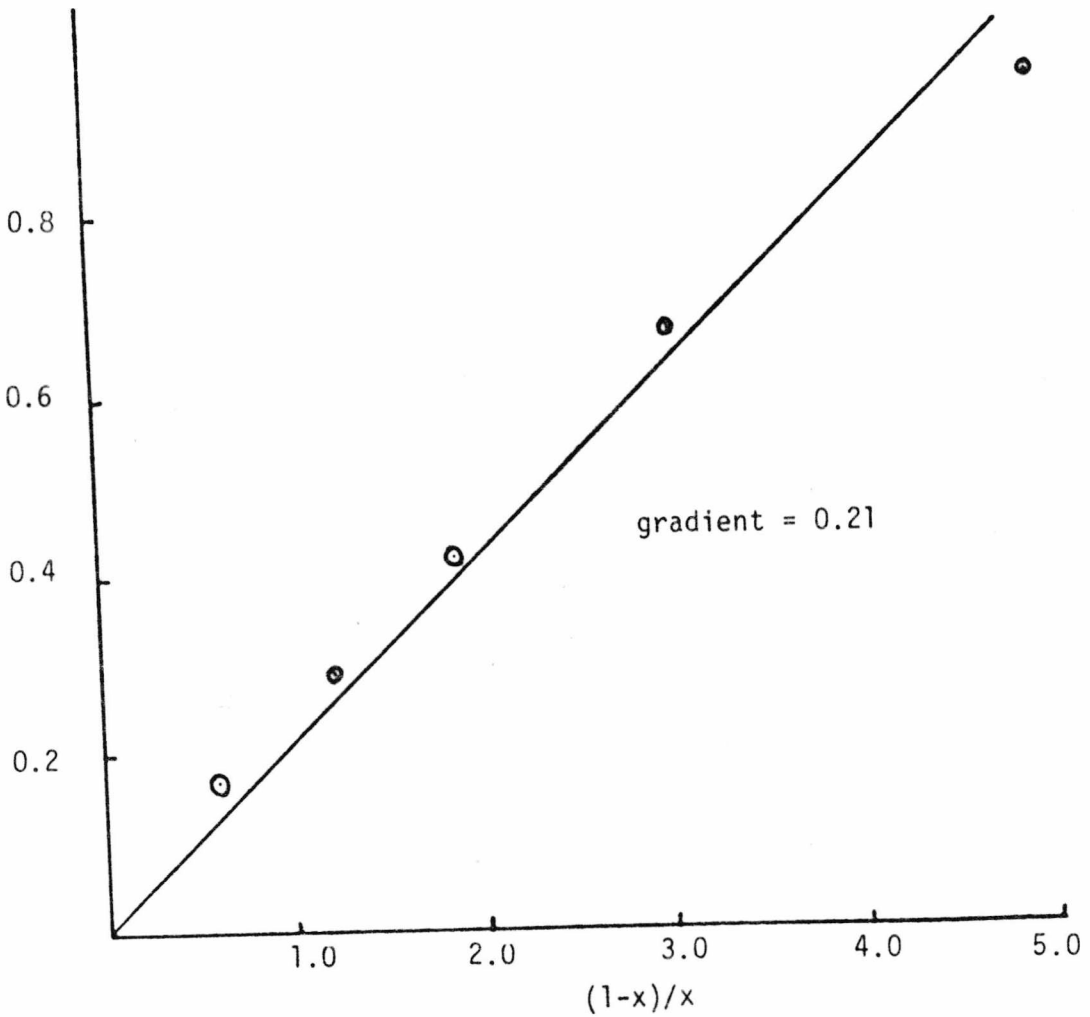

FIG. 4.28 SCALED REFLECTANCE SPECTRA OF a)Anth./TCNQ , (b-d) Anth.$_x$/Dibenzothiophen$_{1-x}$/TCNQ
b) x=0.53 ; c) x=0.37; d) x=0.26.

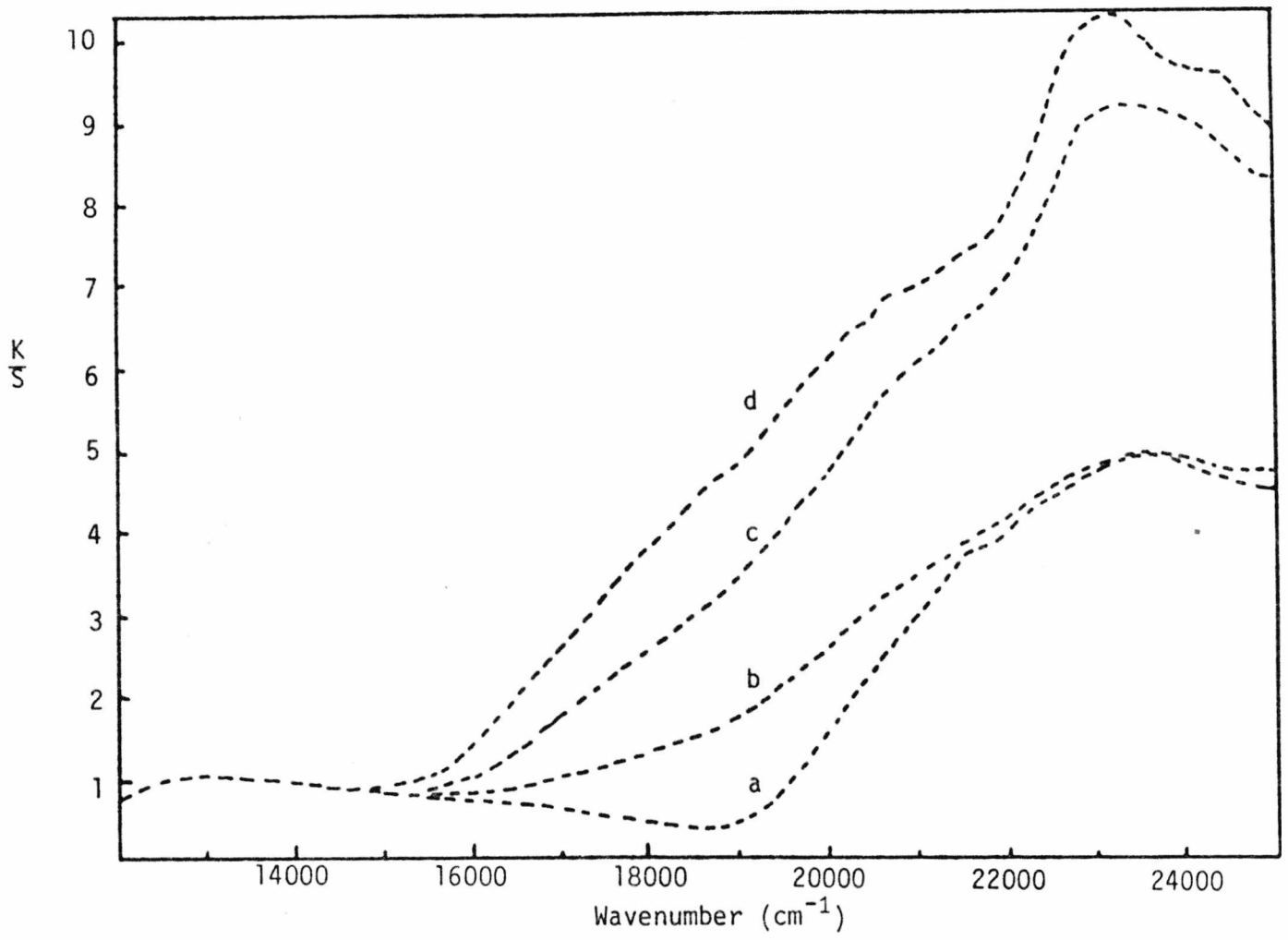

FIG. 4.29 THE DIFFERENCE SPECTRUM
$(A_{.26}/DBT_{.74}/TCNQ)$

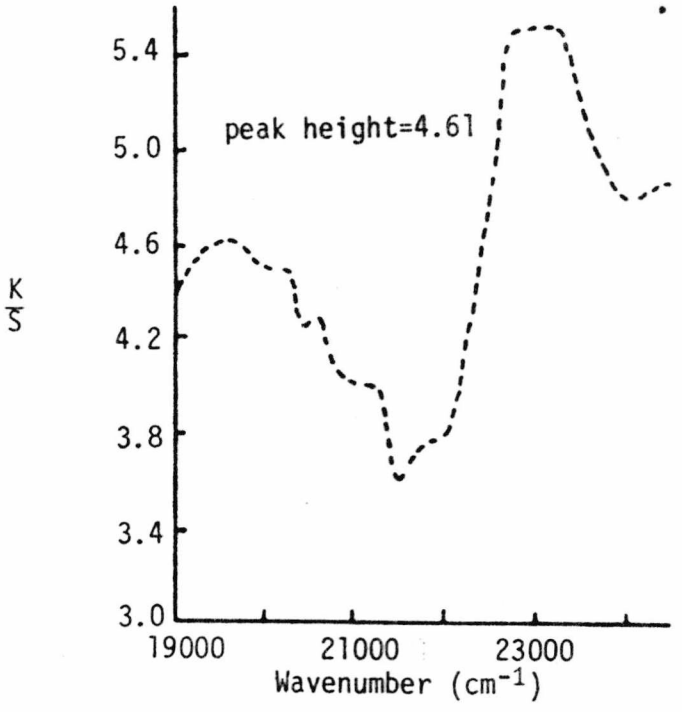

FIG. 4.30 THE DIFFERENCE SPECTRUM
$(A_{.37}/DBT_{.63}/TCNQ)$

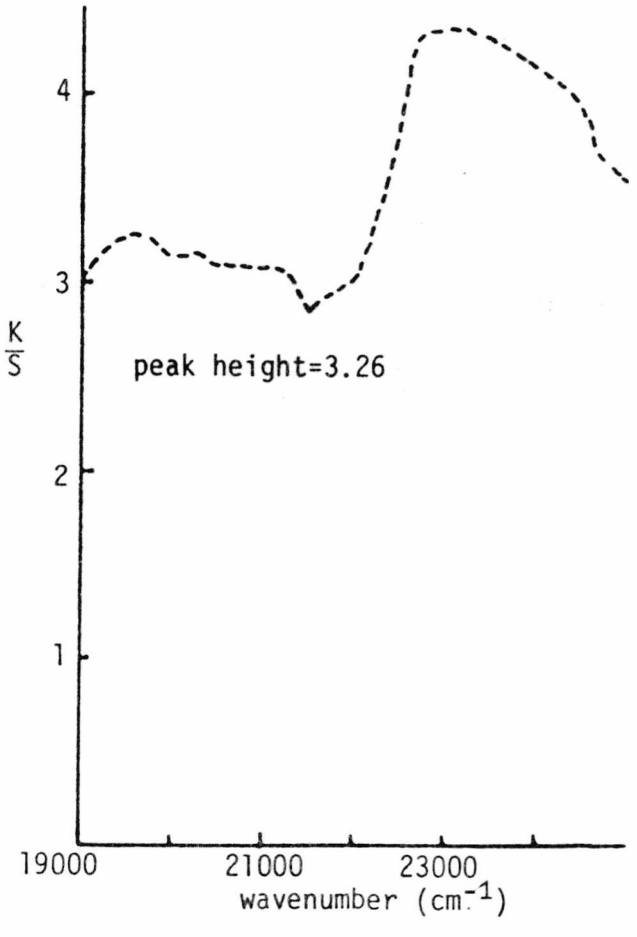

FIG. 4.31 THE DIFFERENCE SPECTRUM $(A_{.53}/DBT_{.47}/TCNQ)$

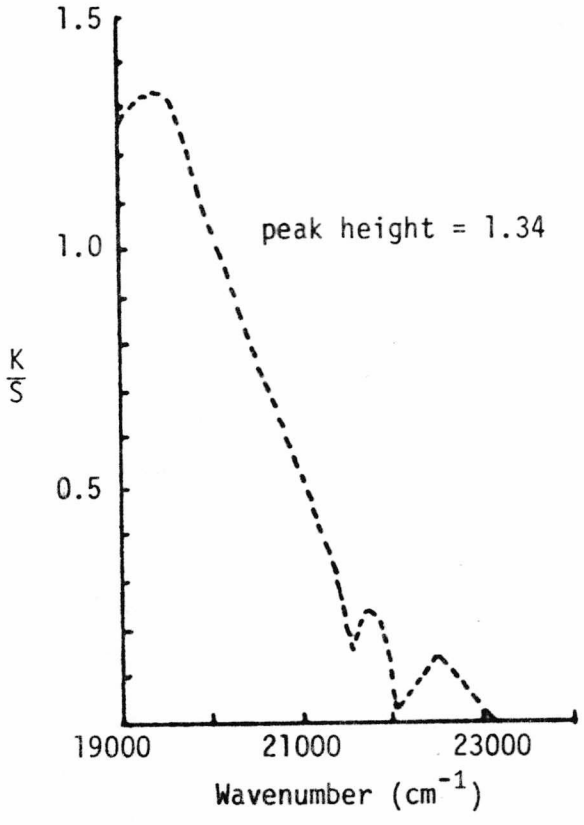

FIG. 4.32 INTENSITY RATIO OF THE TWO CHARGE TRANSFER BANDS AS A FUNCTION OF MOLE RATIO OF THE TWO DONORS OF MIXED COMPLEX ANTHRACENE$_x$/DIBENZOTHIOPHEN$_{1-x}$/TCNQ

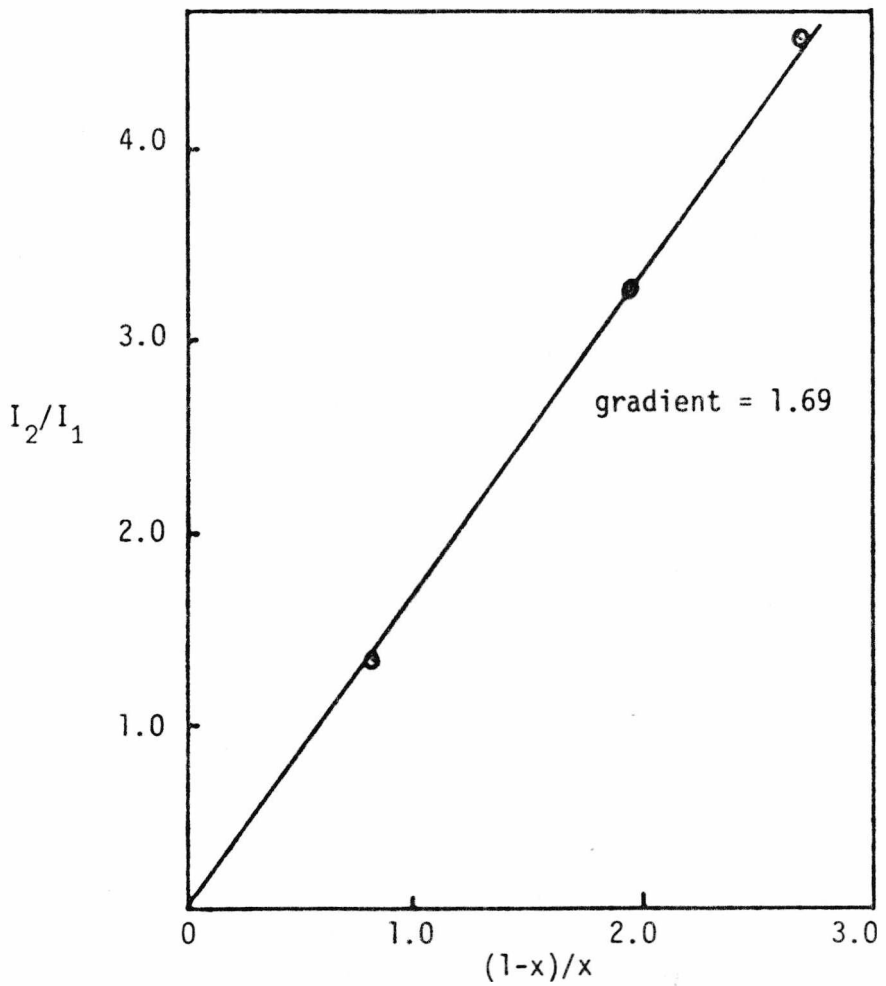

FIG. 4.33 THE REFLECTANCE SPECTRUM OF DIBENZOTHIOPHEN$_{.41}$/DIBENZOFURAN$_{.59}$/TCNQ

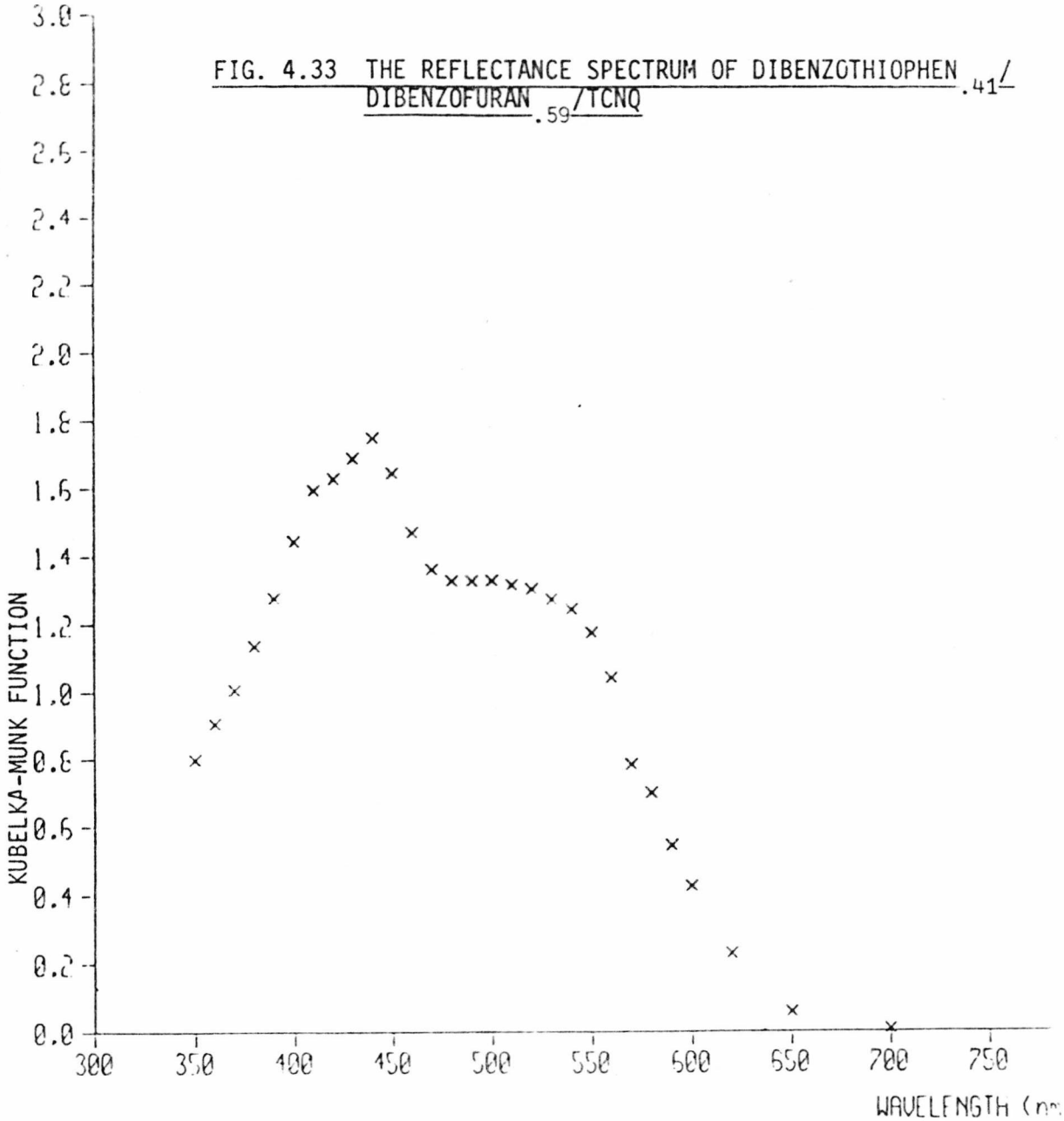

FIG. 4.34 THE REFLECTANCE SPECTRUM OF DIBENZOTHIOPHEN /[51] DIBENZOFURAN /[49] /TCNQ

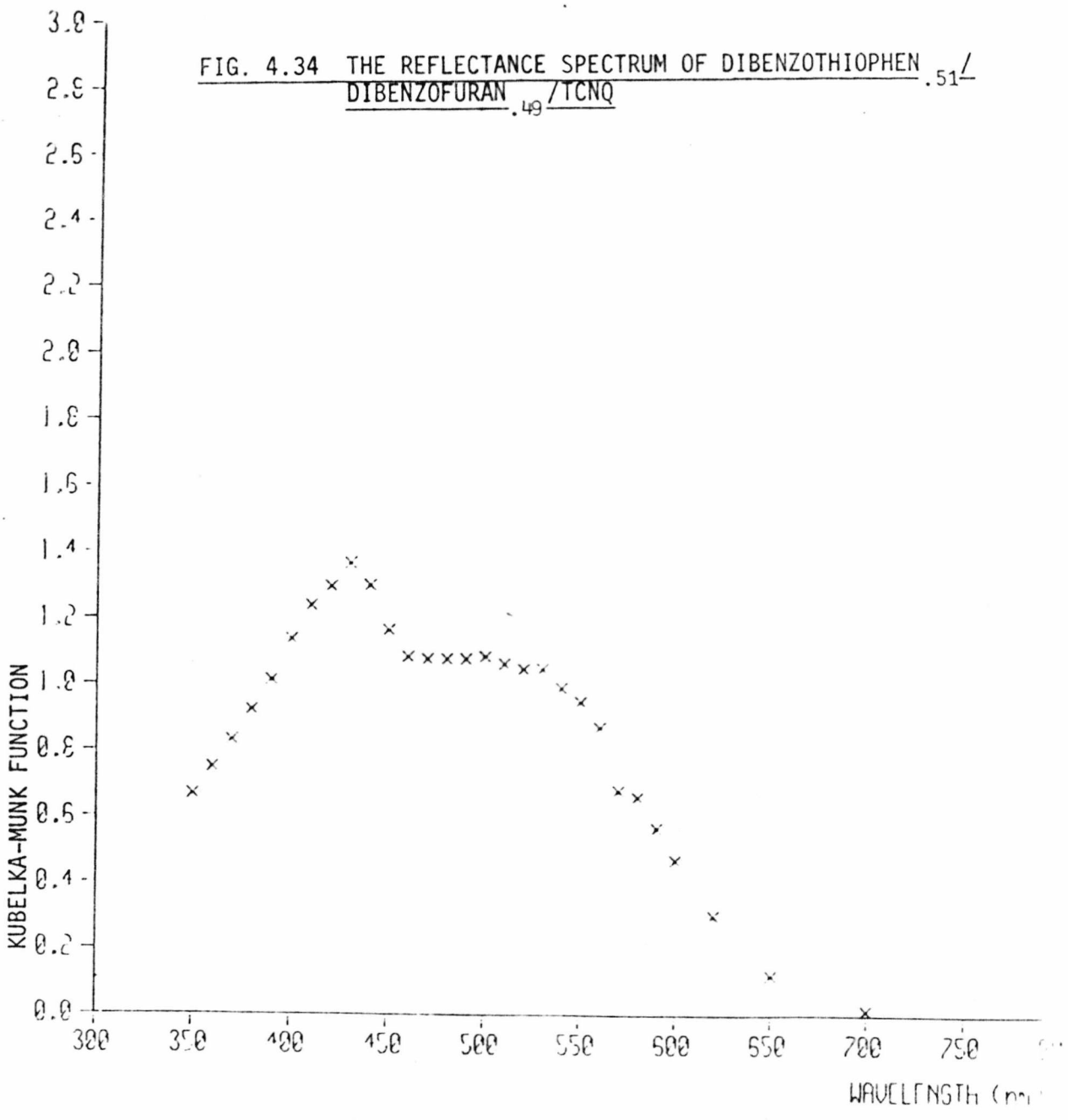

FIG. 4.35 THE REFLECTANCE SPECTRUM OF DIBENZOTHIOPHEN $_{.76}$/ DIBENZOFURAN $_{.24}$/TCNQ

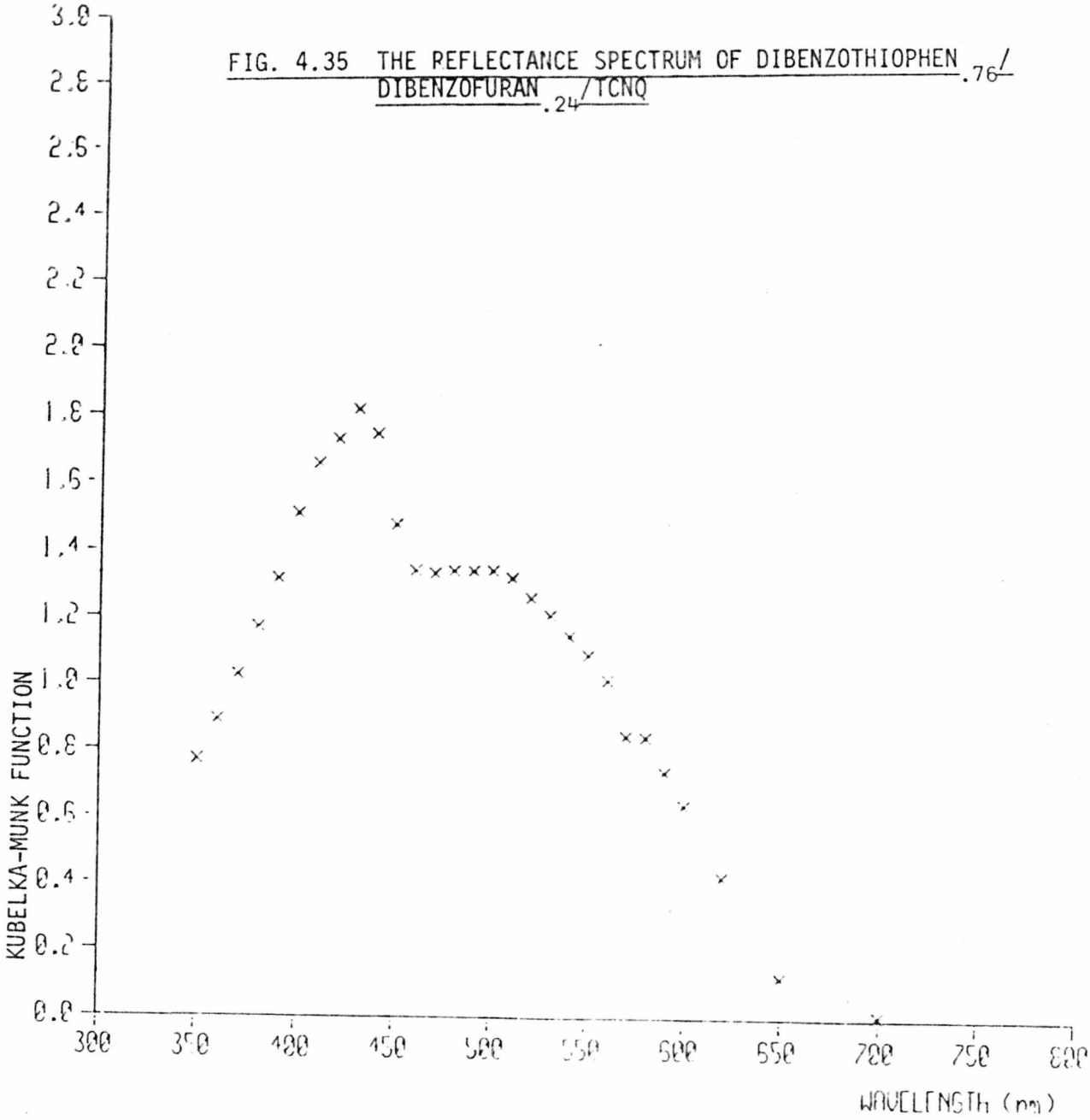

FIG. 4.36 THE REFLECTANCE SPECTRUM OF ANTHRACENE$_{.10}$/CHRYSENE$_{.90}$/TCNQ

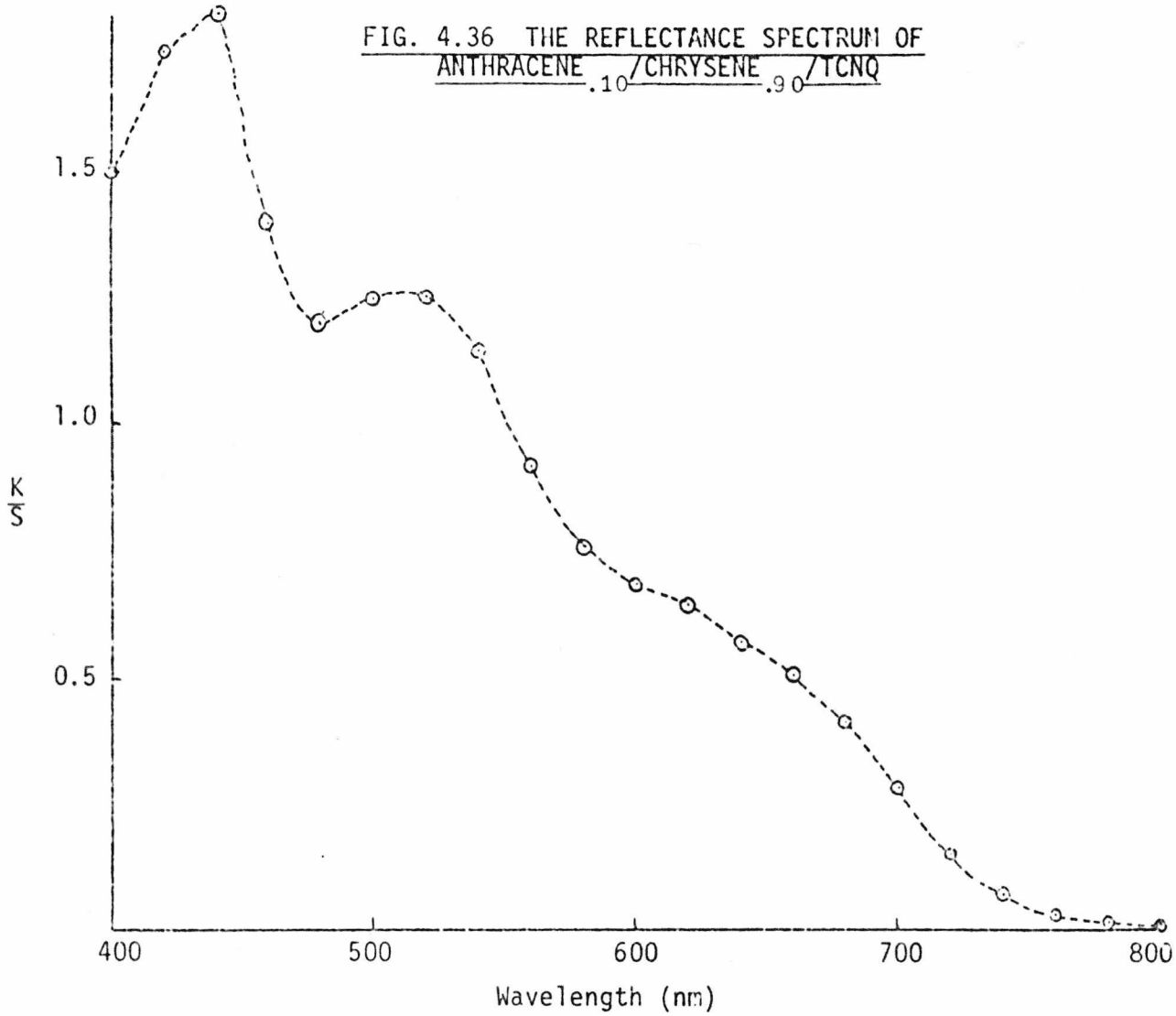

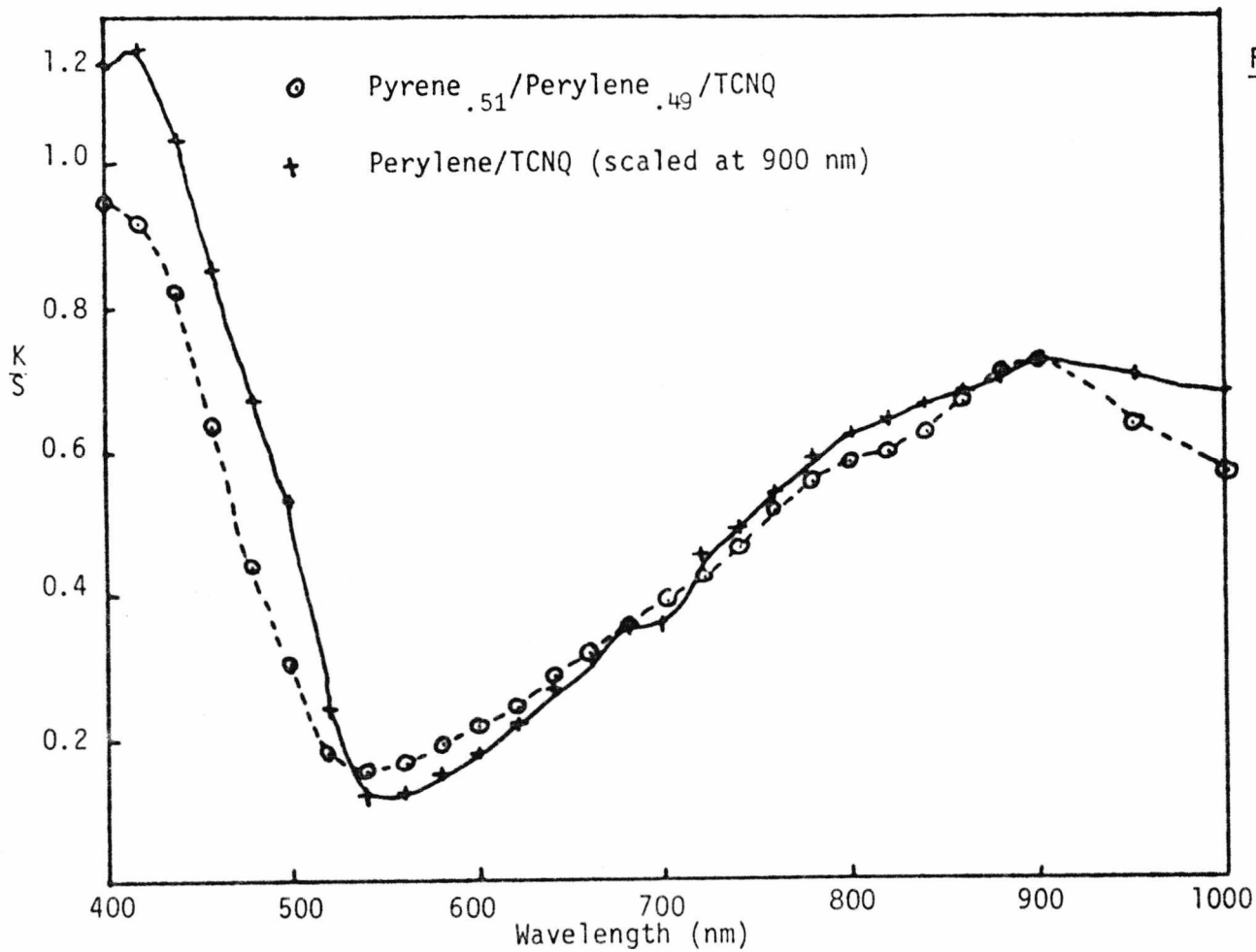

FIG. 4.37 THE REFLECTANCE SPECTRUM OF MIXED COMPLEX OF $Py_{.51}/Pe_{.49}$/TCNQ IS COMPARED WITH THE REFLECTANCE SPECTRUM OF PERYLENE/TCNQ SCALED TO SAME VALUE AT 900 nm

4.5 Discussion

4.5.1 Spectra of Parent Complexes

The spectra of the parent complexes showed a broad intense band characteristic of a charge transfer absorption. From the graph of I.P. against $h\nu_{CT}$ a linear relationship is obtained (Fig. 4.39) as predicted by Mulliken's theory of charge transfer. This relationship confirms that the charge transfer absorption maxima in all the complexes have been correctly assigned. All complexes except chrysene/TCNQ give an obvious charge transfer absorption maximum. In chrysene/TCNQ, two charge transfer bands occur: an inflexion at 620 nm and a peak at 520 nm . These could arise from transitions involving two different donor or two different acceptor molecular orbitals. If a donor or an acceptor is providing two levels, then the energy gap between the two charge transfer bands is constant for complexes with the same donor or the same acceptor respectively. Fig. 4.38 indicates the energy gap ΔE_{ν} arising from a donor or an acceptor providing two levels.

Work reported by Amano, Kuroda and Akamatu (1969) on benzidine and tetramethylbenzidine complexes of various acceptors indicated that only the lowest vacant orbital of TCNQ is involved in charge transfer. Hence in the chrysene/TCNQ complex the two levels are assumed to be provided by the donor.

Further confirmation of the correct assignment of all the first charge transfer absorption bands is provided by a correlation between these transition energies and the energies of the highest occupied orbitals of the donors calculated by the molecular orbital method.

The Molecular-Orbital Method

If the π-orbitals of the molecules are taken as a linear combination

FIG. 4.38 a) DONOR HAS TWO LEVELS
b) ACCEPTOR HAS TWO LEVELS FOR TWO CHARGE TRANSFER BANDS

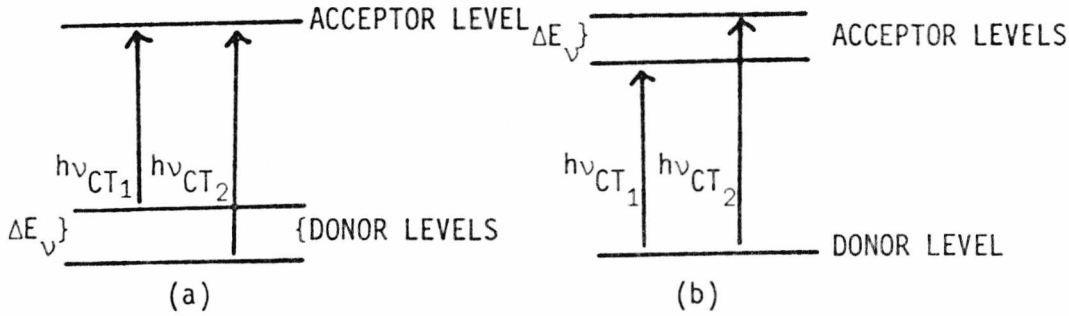

Complex	I.P. of Donor (ev)	λ of Peak (nm)	$h\nu_{CT}$ (ev)	χ
Anthracene/TCNQ	7.39	760	1.63	.414
Chrysene/TCNQ	7.75	620	2.00	.520
Pyrene/TCNQ	7.47	720	1.72	.445
Perylene/TCNQ	7.15	900	1.38	.347
Dibenzothiophen/TCNQ	8.10	500	2.48	
Dibenzofuran/TCNQ	8.18	510	2.43	

TABLE 4.1 FIRST CHARGE TRANSFER BAND MAXIMA, DONOR IONISATION POTENTIALS AND HUCKEL MOLECULAR ORBITAL ENERGY CONSTANTS (χ), FOR THE PARENT MOLECULAR COMPLEXES

FIG. 4.39 GRAPH OF I.P. AGAINST $h\nu_{CT}$ FOR COMPLEXES OF TCNQ

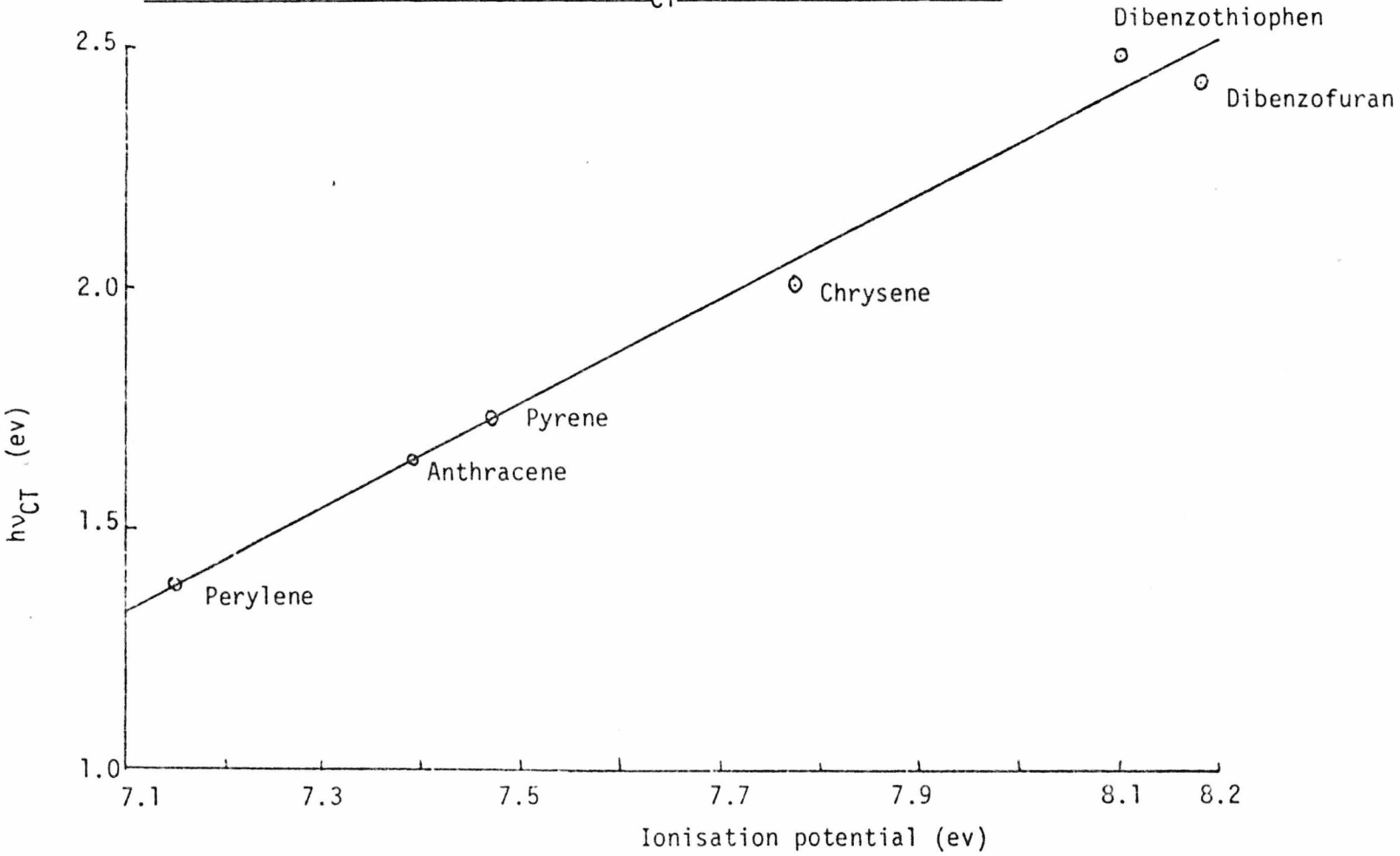

of atomic orbitals, in this case, the $2p_z$ orbitals of carbon then

$$\psi_i = \sum_r C_{ir} \phi_r$$

where

ψ_i = molecular orbital

ϕ_r = atomic orbital

by normalising such that $\Sigma_r C_{ir}^2 = 1$ then the coefficients must satisfy the secular equations

$$C_{i1}(H_{11}-S_{11}e_i) + C_{i2}(H_{12}-S_{12}e_i)+\ldots+C_{in}(H_{1n}-S_{1n}e_i) = 0$$
$$C_{i1}(H_{21}-S_{21}e_i) + C_{i2}(H_{22}-S_{22}e_i)+\ldots+C_{in}(H_{2n}-S_{2n}e_i) = 0$$
$$\vdots$$
$$C_{i1}(H_{n1}-S_{n1}e_i) + C_{i2}(H_{n2}-S_{n2}e_i)+\ldots+C_{in}(H_{nn}-S_{nn}e_i) = 0$$

where

e_i = the energy of the i^{th} molecular orbital ψ_i

H_{rs} = the Hamiltonian integral $\int \phi_r H \phi_s d\tau$

S_{rs} = the overlap integral $\int \phi_r \phi_s d\tau$.

The overlap integral S_{rs} is a measure of how much the orbitals r and s overlap. To simplify the equations an approximation is made where S_{rs} is equal to zero when $r \neq s$ and is 1 when $r=s$.

The coulomb integral H_{rr} measures the electron attracting power or the electronegativity of the atom and is equal to α.

The resonance integral $H_{rs}=\beta$ is a measure of the energy of an electron under the influence of two atoms and is a measure of bond strength.

This integral is assumed zero if the atoms are not adjacent.

From the above definition the secular equation can be written in terms of α and β .

$$
\begin{aligned}
C_{i1}(\alpha_1-e_i) + C_{i2}(\beta_{12}) + \ldots + C_{in}\beta_{1n} &= 0 \\
C_{i1}(\beta_{21}) + C_{i2}(\alpha_2-e_i) + \ldots + C_{in}\beta_{2n} &= 0 \\
&\vdots \\
C_{i1}(\beta_{n1}) + C_{i2}(\beta_{n2}) + \ldots + C_{in}(\alpha_n-e_i) &= 0
\end{aligned}
$$

The roots of the above equations are $e_i=\alpha+\chi\beta$ (1)
If the zero energy is taken to be that of an electron at rest at infinity, then the coulomb term α is negative. (This is because otherwise the electron would not be bound to the atom.) β is also negative (at any rate for neighbours). Therefore the roots of (1) for which χ is positive are the most stable ones. If $\chi>0$ it is a bonding orbital and if $\chi<0$ then it is an antibonding orbital.

The values of χ for most donors are given in the literature (Coulson & Streitwieser, 1965). A graph of energy of charge transfer against χ is given (Fig. 4.40). The linear relationship confirms that the peaks of charge transfer are correctly assigned.

Molecular orbital calculations may also be used to predict spectroscopic transition energies and intensities in π-π^* molecular complexes. Ohta, Kuroda and Kunii (1970) applied a semiempirical self-consistent field molecular orbital method, with configuration interaction calculations, to such complexes, and showed that the calculated transition energies and intensities agreed well with observed spectra. Wright, Ohta and

FIG. 4.40 GRAPH OF $h\nu_{CT_1}$ AGAINST χ , THE HUCKEL CONSTANT

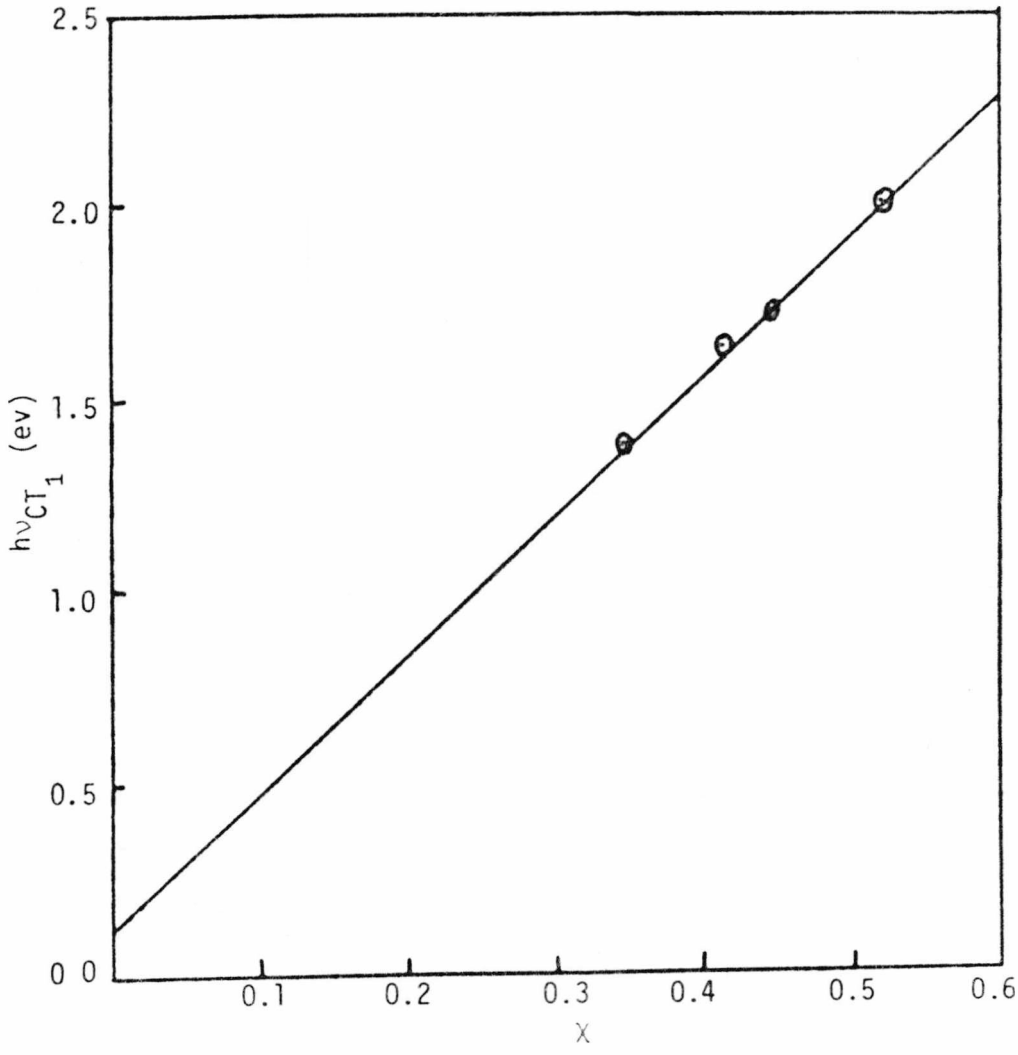

Kuroda (1976) extended this method to three-molecule systems, Donor 1-Acceptor-Donor 2. In such calculations, the whole complex is treated as a single molecule, with molecular orbitals calculated as linear combination of the 2p atomic orbitals of the atoms in the system:

$$\psi_i = \sum_{\mu}^{(D_1)} C_{i\mu}\phi_\mu + \sum_{\mu'}^{(A)} C_{i\mu'}\phi_{\mu'} + \sum_{\mu''}^{(D_2)} C_{i\mu''}\phi_{\mu''}$$

where the first, second and third summations are over the atomic orbitals in D_1,A and D_2 respectively. Using known or assumed intermolecular spacings and relative orientations of donor and acceptor, the energy levels of all occupied and vacant molecular orbitals ψ_i of the complex are first calculated using semiempirical methods. In principle there are many different excited state configurations corresponding to excitation of one electron from any of the occupied orbitals to any of the vacant orbitals. Spectroscopic transition energies and intensities are calculated following a calculation in which interactions between the lowest n (typically 40) excited state configurations are estimated. A detailed discussion of the theoretical methods and approximations involved in these calculations is beyond the scope of this thesis. However, it has been shown that although the calculations do not predict transition energies and intensities with high absolute accuracy, they are useful in estimating relative energies and intensities in different complexes or for different relative orientations of donor and acceptor (Ohta, Kuroda & Kunii, 1970; Wright, Ohta & Kuroda, 1976; Zsom, Schroff, Bakker, Verhoeven, de Boer, Wright & Kuroda, 1978).

In Table 4.2, the relative intensities of the first charge transfer transitions of the parent complexes studied in this work are compared. As stated in Section 4.4, the slopes of the Beer-Lambert plots (Figs.

4.15-4.20) provide an experimental estimate of these relative intensities. Oscillator strengths calculated by the methods outlined above by J. D. Wright (using a version of the program written by Ohta, Kuroda and Kunii adopted for use on the University of London CDC 7600 computer) are also included in Table 4.2. The experimental and calculated values show the same trends, and the ratio of (Beer-Lambert plot slope):(calculated oscillator strength) varies only by a factor of 2.5 for all the complexes. This variation is to be expected, considering experimental error and the approximate nature of the calculations. Also, the calculations are for fixed relative orientations of donor and acceptor. In practise, the molecules are undergoing anisotropic thermal motion in the solid state. Thus, strictly some contribution from orientations other than those assumed in the ideal static model should be included in the calculations. This would involve excessive computing time, however.

The results of Table 4.2 can to a first approximation be discussed with reference to the known crystal structures and the symmetries of donor highest occupied π orbitals and acceptor lowest unoccupied orbitals (Figs. 4.41 & 4.42). This is justified since the configuration interaction calculation show that the first charge transfer bands owe at least 90% of their character to charge transfer transitions involving these orbitals. Examination of Figs. 4.41 and 4.42 and Table 4.2 leads to the following conclusions:

1) The perylene/TCNQ structure provides very good overlap of the perylene HOMO and TCNQ LUMO , accounting for the high oscillator strength of the first charge transfer band.

2) The overlap becomes progressively worse in the series pyrene-TCNQ, chrysene-TCNQ and anthracene-TCNQ , as reflected in the calculated oscillator strengths.

3) Although the overlap of donor HOMO and acceptor LUMO appears to be zero in anthracene-TCNQ and near zero in dibenzofuran-TCNQ and dibenzothiophen-TCNQ , this is not reflected in the experimental Beer-Lambert plot slopes. The higher intensity observed probably arises because of thermal motion effects as mentioned above.

4) The different orbital symmetries in anthracene and phenanthrene lead to clearly worse overlap in phenanthrene-TCNB (Fig. 4.41 & 4.42) than in anthracene-TCNB. This is reflected in the lower observed and calculated transition intensity in the phenanthrene-TCNB complex compared to anthracene-TCNB.

4.5.2 Spectra of Mixed Complexes

4.5.2.1 Dibenzothiophen/Dibenzofuran/TCNQ

The spectra of these complexes are shown in Figs. 4.33-4.35. As shown in Chapter 3, the structure and relative orientations of donor and acceptor are effectively the same for all these complexes. Thus the only change in the spectra as composition is varied should be a slight increase in the intensity of the first charge transfer band and a slight shift in the position of this band on going across the series from the dibenzofuran complex to the dibenzothiophen complex.

Complex	Beer Lambert Plot Slope	Calculated Oscillator Strength†	Ratio
Anthracene/TCNQ	194	0.0	-
Chrysene/TCNQ	169	0.045	3760
Pyrene/TCNQ	188	0.056	3360
Perylene/TCNQ	358	0.191	1870
Anthracene/TCNB	231	0.155	1490
Phenanthrene/TCNB	88	0.055	1600
Dibenzofuran/TCNQ	379	-	-
Dibenzothiophen/TCNQ	404	-	-

†The oscillator strength f is defined as $f = \frac{2.303mc^2}{\pi e^2 N_0} \int e_\nu d\nu$; where e_ν is the extinction coefficient for light of frequency ν . The calculated values are for relative orientations and separation of donor and acceptor as observed in the crystal structure of the complexes.

TABLE 4.2

FIG. 4.41 SYMMETRIES OF DONOR HOMO AND ACCEPTOR LUMO

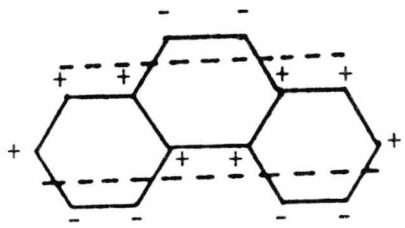

Phenanthrene

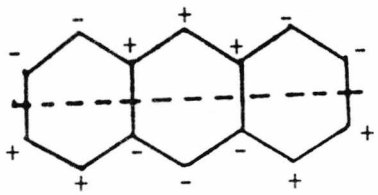

Anthracene

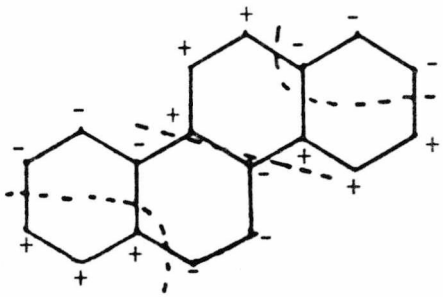

Chrysene

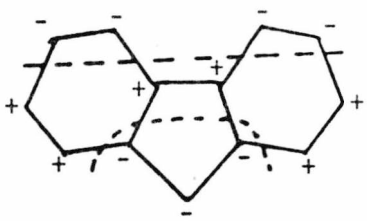

Dibenzothiophen
and
Dibenzofuran

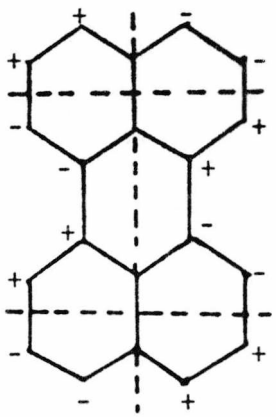

Perylene

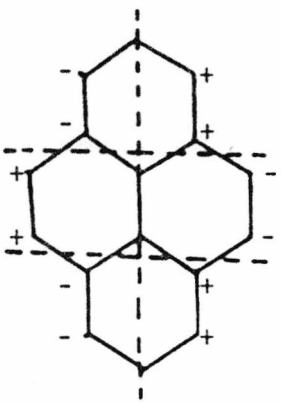

Pyrene

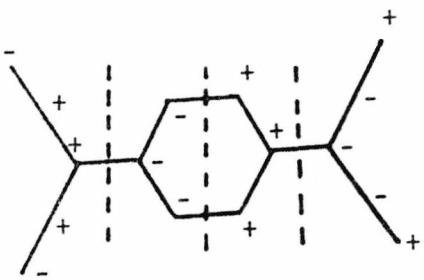

TCNQ

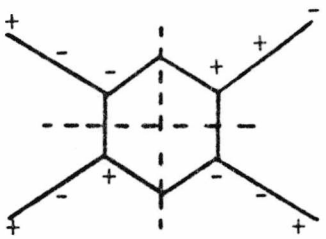

TCNB

FIG. 4.42 DIAGRAMS OF ACTUAL OVERLAP OF DONOR AND ACCEPTOR OF THE COMPLEXES STUDIED

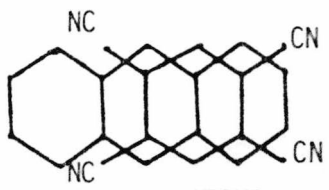

Anthracene/TCNB

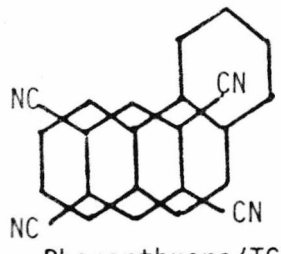

Phenanthrene/TCNB

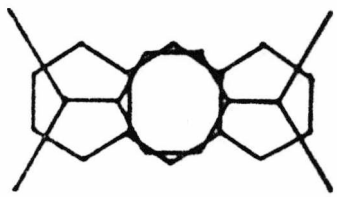

Anthracene/TCNQ

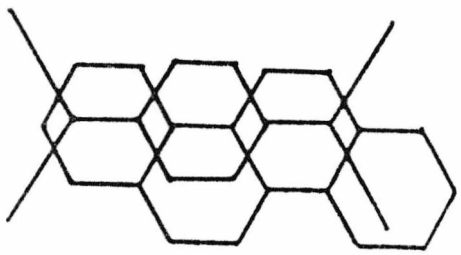

Chrysene/TCNQ

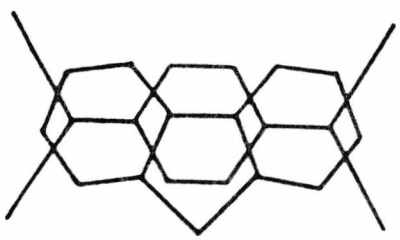

Dibenzothiophen/TCNQ

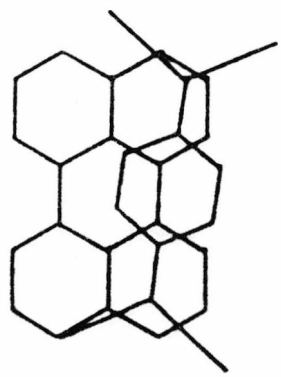

Perylene/TCNQ

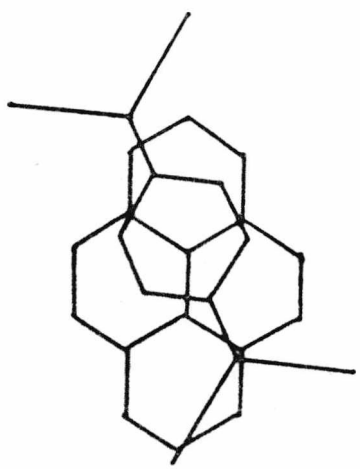

Pyrene/TCNQ

4.5.2.2 Anthracene/Dibenzothiophen/TCNQ

The spectra of these complexes, scaled to a common value at the wavelength of maximum absorption of the anthracene-TCNQ complex (at which the dibenzothiophen-TCNQ complex does not absorb) are shown in Fig. 4.28. Subtraction of the scaled anthracene-TCNQ spectrum from these curves produced difference spectra with absorption maxima in the region expected for the first CT band of dibenzothiophen-TCNQ , although these spectra did not always correspond to the spectrum of dibenzothiophen-TCNQ at shorter wavelengths (<450 nm). Thus the graphical decomposition process yielded less satisfactory results than in the case of anthracene/phenanthrene/TCNB. This may be because the anthracene-TCNQ charge transfer absorption maximum occurs at longer wavelength than for anthracene-TCNB. Any wavelength dependence of the scattering coefficients, or differences in scattering coefficients from sample to sample, will result in more serious errors at short wavelengths for curves scaled at longer wavelengths than for curves scaled at intermediate wavelengths. Even for curves scaled at long wavelengths as in this case, the errors are probably small at 500 nm in the region of the dibenzothiophen-TCNQ first CT band, as confirmed by the general agreement of the scaled spectra of different concentrations of the parent complexes as shown in Figs. 4.3-4.14. Hence a plot of I_2/I_1 vs. $(1-x)/x$ (Fig. 4.32) was made as described earlier for anthracene/phenanthrene/TCNB . This is a good straight line through the origin, with gradient 1.69. The corresponding ratio of the slopes of the Beer-Lambert plots for the two parent complexes (Figs. 4.18) is 2.08. Thus the ratio of the intensities of the first CT transitions of dibenzothiophen/TCNQ and anthracene/TCNQ is essentially the same in the mixed complexes as for the two parent complexes in their own, different, crystal lattice. X-ray powder diffraction shows that these

mixed complexes have the anthracene-TCNQ lattice structure (Chapter 3). The spectroscopic results therefore suggest that the relative orientation of dibenzothiophen and TCNQ is the same when the complex is present in the mixed systems with the anthracene-TCNQ lattice as it is in its own lattice. The relative orientations of donor and acceptor in anthracene/TCNQ and dibenzothiophen/TCNQ are similar, with the quinoid double bonds over the centres of polarisable aromatic rings in both cases. Also, the two donors are of similar overall size. It is therefore not surprising that the dibenzothiophen-TCNQ orientation should be unchanged in the anthracene-TCNQ lattice.

4.5.2.3 Anthracene/Chrysene/TCNQ

The reflectance spectrum of anthracene$_{.10}$/chrysene$_{.90}$/TCNQ (Fig. 4.36) is very similar to that of Chrysene/TCNQ itself, and the low degree of incorporation of Anthracene/TCNQ into the mixed complex prevents reliable graphical decomposition of the mixed complex spectrum by the method described earlier. The X-ray powder diffraction photographs (Chapter 3) show that the mixed complexes have the Chrysene-TCNQ structure. In this lattice, anthracene is not a tight fit on the chrysene site, and possible alternative orientations have been discussed in Chapter 6. Thermal motion of anthracene on the chrysene site is expected to be larger than that of anthracene in Anthracene-TCNQ. This creates difficulties in predicting theoretically the expected Anthracene/TCNQ CT band intensity in the mixed complex. The only conclusion from the reflectance spectrum of this mixed complex is therefore that the intensity of the Anthracene-TCNQ CT band is not greatly enhanced in the mixed complex, since the spectrum of the mixed complex is similar to that of Chrysene-TCNQ.

4.5.2.4 Pyrene/Perylene/TCNQ

The reflectance spectrum of pyrene$_{.51}$/perylene$_{.49}$/TCNQ is shown in Fig. 4.37. The pyrene-TCNQ complex does not absorb at 900 nm , which is the position of the maximum of the first CT band of perylene-TCNQ. Fig. 4.37 also shows the spectrum of perylene-TCNQ scaled to the same K/S value as the mixed complex at 900 nm . Comparison of these spectra shows that there is no contribution to the spectrum of the mixed complex from pyrene-TCNQ in the region of its first CT band at 720 nm, despite the fact that the analytical results of Chapter 2 clearly show the presence of around 50% of pyrene-TCNQ in all these mixed complexes. The X-ray powder diffraction photographs of these mixed complexes show that they form a crystal lattice different from those of either of the parent complexes. The relative orientations of pyrene, perylene and TCNQ in this new phase are not known. The reflectance spectrum of the mixed complex shows clearly that

1) the orientation of pyrene relative to TCNQ must be very unfavourable for charge transfer and
2) the orientation of perylene relative to TCNQ must be similar to that in the parent complex. This result also accounts for the observation, to be discussed in Chapter 6, that these mixed complexes do not photoconduct in the region of photoconduction associated with the first CT band in pyrene/TCNQ itself.

4.6 Conclusions

Diffuse reflectance spectra of charge transfer complexes have been shown to provide useful information on the relative intensities of the

charge transfer transitions in different complexes, which may be correlated with the known crystal structures of the complexes. Similar studies for mixed complexes can provide useful information on the likely orientations of donor and acceptor, which is consistent with information from studies of the composition ranges over which mixed complexes can be prepared and of their x-ray powder diffraction patterns and photoconduction action spectra.

* * * * * *

Chapter 5

Semiconductivity

5.1 Introduction

For any semiconductor, the observed conductivity is determined by the processes of charge carrier generation and migration. For π-π^* molecular-complexes, Munnoch and Wright (1976) have shown that both the observed semiconduction activation energy and the pre-exponential factor σ_0 in the equation $\sigma=\sigma_0 e^{-\Delta E/kT}$ are consistent with intrinsic conduction. Intrinsic conduction activation energies are most simply related to molecular parameters by the relation $\Delta E=I.P-E.A-P^+-P^-$ first postulated by Gutman and Lyons (1967). Charge carrier mobilities have been determined by the drift mobility pulse technique first developed by Kepler (1960) for many classes of organic solids. If the solid is pure and free of defects or traps, the carrier drift mobility is found to be 0.1-1 $cm^2/v.s.$ for a wide range of different organic solids. In practice, for large crystals which contain more significant numbers of traps or defects, the apparent carrier mobility will be lower than this.

These results show that controlled variation of ionization potential, electron affinity and polarization energies leads to corresponding changes in electrical conductivity properties. The objectives of the work reported in this chapter were to investigate the possibility of extending this approach to the control of conductivity in π-π^* molecular complexes by preparing mixed complexes containing two different donor molecules. In the ideal case of two parent complexes which are isostructural, the electrical conductivity of mixed complexes should be a smooth function of composition. In principle it should be possible to prepare materials of any desired conductivity within the range determined by the conductivities of the two

parent complexes, by preparing mixed complexes of appropriate composition. This ideal behaviour could be complicated by effects due to local lattice strains caused by the introduction of a different donor into the lattice of one of the parent complexes, or by effects due to structural changes as composition is varied, in the case of mixed complex series where the parent complexes are not isostructural. The studies reported in this chapter were designed to establish whether conductivity trends in series of mixed complexes follow the ideal pattern or follow a more random pattern due to large variations in defect and trap concentrations as composition is varied. In the latter case, it was hoped that information on any relationship between chemical composition and the density of traps or defects could be obtained from study of the electrical conductivity trends. Similarly, it was hoped that structural changes as composition varied within a series of mixed complexes might also be reflected in discontinuities in plots of resistivity or conduction activation energy as a function of composition.

Ideally, for such studies the parent complexes of the mixed series should have widely differing resistivity and conduction activation energy. However, as mentioned above, this implies the use of two donors of widely differing ionisation potential. This is difficult to achieve while simultaneously satisfying the requirements for formation of mixed complexes as single crystals (similar donor sizes, shapes and solubilities, and similar formation constants for their complexes with the acceptor-see Chapter 2). Therefore, in practice, semiconductivity studies were made on all the mixed complex series which could be prepared and characterised, as described in Chapter 2. The range of conductivity variation in the available systems was smaller than had been hoped, and in view of these materials limitations the conductivity measurements reported in this chapter

were less extensive than originally intended.

In the remainder of this chapter, following a summary of theory relevant to interpretation of charge carrier mobility, semiconduction activation energy and trapping effects, the conductivity apparatus is described and the results obtained on semiconductivity of pure and mixed complexes are presented and discussed.

5.2 Mobility

The mobility is defined as the velocity with which the carrier moves under unit electric field. It is related to the conductivity by the relation $\sigma=ne\mu$, where n=number of carriers per cubic centimetre, e=electronic charge and μ is the mobility.

The conductivity is related to the activation energy by the equation $\sigma=\sigma_0 e^{-\Delta E/kT}$. In general, the conductivity is determined by the exponential factor which is dependent on the exponential increase of a thermally liberated carriers across a potential barrier. Carrier concentrations is also found to contribute to the pre-exponential factor. In reality the above equation is represented by $\sigma=\sigma_0(T)e^{-\Delta E/kT}$, where σ_0 is temperature dependent. The experimental value obtained by plotting $\log\sigma$ against $\frac{1}{T}$ from the above equation is in actual fact the sum of two activation energies, one arising from the carrier concentration and the other from the mobility. However, the temperature dependence of mobility can often be neglected as compared to the temperature dependence of the carrier concentration, hence the activation energy obtained from equation $\sigma=\sigma_0 e^{-\Delta E/kT}$. experimentally is generally interpreted in terms of the creation energy of charge carriers.

Mobilities and their Temperature Dependences

The transient photoconductivity techniques introduced by Le Blanc (1959) and Kepler (1960) have been widely used to determine the drift mobility.

If the mobility is determined by scattering either by lattice vibrations or impurities, Schockley theory of scattering due to thermal vibrations (Bardeen & Schockley, 1950) gives a mobility temperature dependence of $T^{-3/2}$ whereas Pearson and Bardeen (1949) show a $T^{-1/2}$ dependence due to scattering by neutral impurities. For scattering due to dislocations, Dexter and Seitz (1952), found a T^{-1} dependence. However, Ioffe (1959) pointed out that mobility is not so much limited by scattering as by the carrier making an activated transition across a potential barrier, which is termed a hopping process.

Determination of mobilities on impurity-free aromatic or heteroaromatic molecules yields a T^{-n} dependence where $0<n<3$, and n is most frequently about 1 (Schein, 1977). Schein (1977) tabulated the data for relatively pure organic and inorganic molecules and he observed that independent of the particular material, the drift mobility is approximately equal to 1 cm^2 v^{-1} sec^{-1} within an order of magnitude and μ is weakly temperature dependent i.e. $\mu \propto T^{-n}$ with $n \simeq 1$. The mobility of As_2S_3 has been measured to be 1 cm^2/v sec with $\mu \propto T^{-n}$, $n<0.16$ at $207<T<465K$. It has been argued that the observed temperature dependence of μ appears to be inconsistent with the prediction of band theory for all the various scattering processes considered. However, Roberts, Apsley and Munn (1980) have argued that this conclusion may not be justified, as different estimates of some of the parameters involved would yield different conclusions. Moreover, As_2S_3 is a layered compound in which the binding is due to covalent bonds within a single layer, but molecular-like due to Van der Waal's forces between different layers (Zallen & Slade, 1974). As such Sumi

(1979) pointed out that the almost temperature independent mobility is observed only in a direction perpendicular to the layers, while along the layers transport properties can be understood with the band conduction model. Further work was done on anthracene, deuterated anthracene and As_2S_3 (Schein, 1977) using temperature ranges exceeding 300 K . The hopping model is argued not to give a satisfactory transport process. For the hopping model, the temperature dependence is represented by the equation $\mu \propto T^{-n} e^{-E/kT}$. From the experimental data Schein (1977) concluded that no evidence is found for activated behaviour at low temperatures or T^{-n} dependence at high temperatures and this signifies that even for an arbitrary choice of the activation energy, the hopping model does not lead to a satisfactory description of the transport behaviour of molecular crystals. The drift mobility data in the C' direction of single crystal naphthalene from 54 to 324 K are discussed in terms of a transition from hopping to band motion (Schein, Duke & McGhie, 1978) below 100 K where the mobility rises dramatically from its high temperature values. At higher temperature (T>100 K) the mobility is again almost temperature independent. Anthracene has a highly anisotropic conduction band structure, where the almost temperature independent mobility is observed only in the narrow band direction.

Roberts, Apsley and Munn (1980) tabulated the temperature dependence predicted for the drift mobility by various theories and this is reproduced in Table 5.1. Despite the extensive experimental and theoretical effort which has been devoted to the study of carrier mobility in a wide range of molecular crystals, there is still no theory which satisfactorily accounts for the whole range of experimental observations now available.

Temperature Dependence	Nature of Transport and Scattering
	Narrow Band
T^{-1}	Coulomb
	Neutral impurity
	Dislocation
T^{-2}	Acoustic one-phonon
T^{-3}	Acoustic two-phonon
$[\exp(E/kT)-1]$	Optic one-phonon
$[\exp(E/kT)-1]^2$	Optic two-phonon
	Polaron
$T^{-1}\exp(-E/kT)$	Adiabatic hopping
$T^{-3/2}\exp(-E/kT)$	
$T^{-2}\exp(-E/kT)$	Non-adiabatic hopping
$T^{-5/2}\exp(-E/kT)$	
$T^{-1/2}\exp(-\alpha e^{-E/kT})$	Band
	Quadratic Coupling
T^{-1}	Slow-electron hopping
$T^{-1}\exp(E/kT)$	Slow-electron band
	Slow-phonon band
T^{-4}	Slow-phonon quasi free

TABLE 5.1 TEMPERATURE DEPENDENCES OF THE DRIFT MOBILITY AS PREDICTED BY VARIOUS THEORIES

5.3 Activation Energy

Most semi-conductors obey the relationship $\sigma=\sigma_0 \exp \frac{-\Delta E}{2kT}$. The temperature dependence of conductivity depends on the charge carrier mobility and carrier generation process. Mobility (see Section 5.2)is generally almost temperature independent in high quality crystals and contributes very little to the temperature dependence of conductivity as compared to the contributions of carrier concentrations.

ΔE obtained experimentally by plotting $\log\sigma$ against $\frac{1}{T}$ may correspond to several parameters such as the forbidden gap width between valence and conduction state, energy levels of impurity states relative to the conduction level or the depth of traps. This ambiguity arises because most organic materials contain impurities. Only by vigorous purification is the impurity removed, hence care should be taken in interpreting activation energy data.

Intrinsic Semiconductors

Intrinsic conductivity occurs when the electrons are lifted from the valence band to the conduction band.

The temperature dependence of activation energy can be derived as follows: (Meier, 1974).

The number of thermal excitations per second and unit volume is given by:

$$Z' = \alpha e^{-\Delta E/kT} \qquad (1)$$

where $\Delta E=E_c-E_v$=width of the forbidden gap.

Each excitation process leads to an electron hole pair, $n=p$. At equilibrium, the rate of generation is equal to the rate of recombination hence

$$\alpha e^{-\Delta E/kT} = k_r np \qquad (2)$$

where k_r = bimolecular rate constant $(cm^3 s^{-1} N^{-1})$.

The equilibrium charge carrier density n_i which at a fixed temperature, is determined by Z' and $k_r(n_i^2 = Z'/k_r)$ is linked with the electron and hole concentrations through the law of mass action according to

$$np = n_i^2 \tag{3}$$

hence from (2) and (3)

$$n_i = n = p = \sqrt{\frac{\alpha}{k_r} \exp(-\Delta E/kT)} \tag{4}$$

If the temperature dependence of mobility can be neglected in comparison with carrier concentration temperature dependence, the temperature dependence of an intrinsic semiconduction is

$$\sigma = \sigma_0 \exp(-\Delta E/2kT) \tag{5}$$

or

$$\log\sigma = \log\sigma_0 - (\Delta E/2k)\frac{1}{T} \tag{6}$$

Extrinsic Semiconductor

Extrinsic conductivity occurs when the electrons or holes are excited from impurities or traps. The energy of activation can be derived using the same procedure but here the excitation energy depends on whether the impurities are donors or acceptors.

If the impurity is a donor,

$$\Delta E_D = E_C - E_D$$

If the impurity is an acceptor,

$$\Delta E_A = E_A - E_V$$

Having taken into account, the concentration of defects through the coefficient α or σ_o, Equation (6) can be written as:

excess conduction (n-type) $\sigma = \sigma_{0(D)} \exp(-\Delta E_D/2kT)$ (7)

defect conduction (p-type) $\sigma = \sigma_{0(A)} \exp(-\Delta E_A/2kT)$ (8)

From the equations (5),(7) and (8), if both intrinsic and extrinsic conduction contributed to the conduction, the form of equations is given by:

$$\sigma = \sigma_0 \exp(-\Delta E/2kT) + \sigma_{0(ex)} \exp(-\Delta E_{(ex)}/2kT) \quad (9)$$

If $\log\sigma$ vs $\frac{1}{T}$ is plotted from Equation (9), a deviation from a linear relationship may be observed.

5.4 Interpretation of Activation Energy Data

The plot of $\log\sigma$ against $\frac{1}{T}$ using data obtained from experiment by raising the temperature and observing the steady state current at reasonable temperature intervals will most frequently yield either a straight line or a change in slope at a certain temperature. The deviation from a straight line slope is a well-known phenomenon. It indicates either a phase change or the presence of impurity in the material. The presence of a phase change has been reported variously to affect (Kurematsu, Kaneko & Matsumoto, 1971), and not to affect (Chojnacki, 1966; Kronick & Labes, 1963) activation energy values. In cases where the phase transition leads to a plastic phase as in d-camphor and camphoroquinone, the change in conductance is attributed to the irregularity in the periodic structure of the plastic phase which is connected to an increase in molecular mobility and the high concentration of point defects (Meier, 1974). Hexamethylbenzene (HMB) undergoes a reversible phase change of lattice structure from triclinic to orthorhombic at 110°C which has been variously reported to affect and not to affect activation energy of conduction. However, the

important point is that conductivity changes are certainly connected to the structural changes occurring during phase transition. An account of the effects of phase transitions on the conductivity and references are given in detail by Meier (1974).

The presence of impurities in a material could lead to changes in activation energy of conduction. By assuming that all the impurity centres are filled with carriers except those from which carriers have been excited, the change from extrinsic to intrinsic conduction is subsequently reflected by the change from $\Delta E_{(ex)}/2kT$ to $\Delta E/_{2kT}$ in the conductivity Equation (9). The schematic diagram given below (Fig. 5.1) (Meier, 1974) summarises extrinsic conduction processes.

Organic semiconductors, unfortunately may often undergo decomposition before intrinsic excitation becomes dominant over extrinsic excitation. Hence a straight line slope in plots of $\log\sigma$ v. $\frac{1}{T}$ need not necessarily reflect intrinsic conduction and the extrinsic or intrinsic nature of conduction is often inferred from other sources. Thus, intrinsic conductivity has often been deduced from the agreement between a photoconductivity threshold and the activation energy determined thermally.

As mentioned in the introduction, for intrinsic conduction

$$\Delta E = \text{I.P.} - \text{E.A.} - (P_{D^+} + P_{A^-}) + \Delta wf \qquad (10)$$

Intrinsic semiconduction in molecular complexes may be discussed in terms of the following diagram (Fig. 5.2). (See overleaf.)

Since Δwf is small for π-π^* molecular complexes, it is generally neglected in comparison to the remaining terms. Donor ionisation potentials and acceptor electron affinities have been determined by other workers and are also quoted in Table 5.6. Hence, if polarisation energies can be

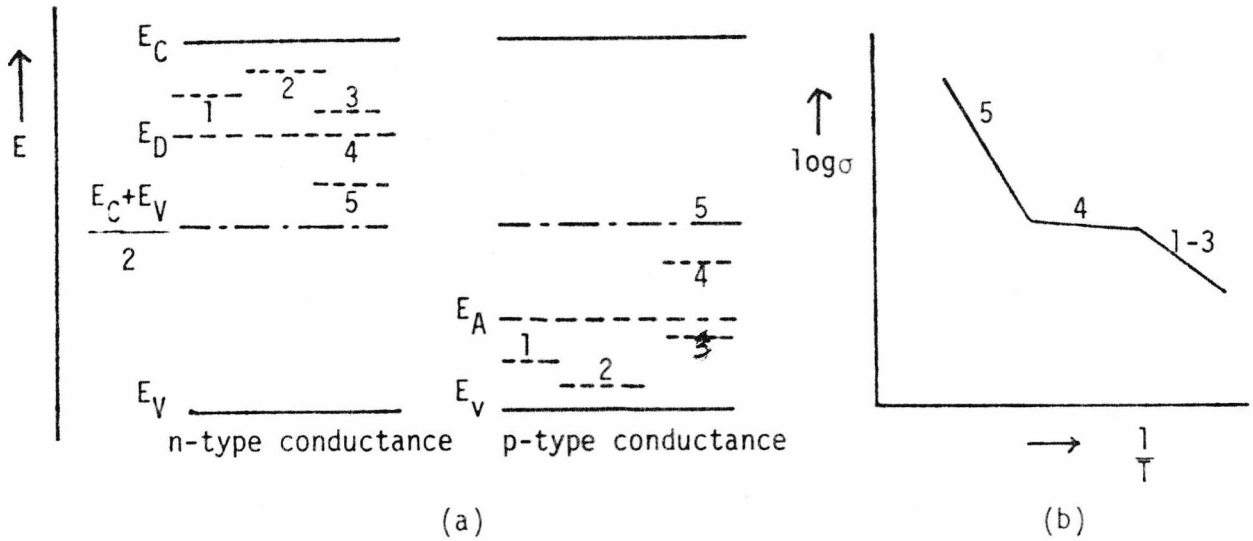

FIG. 5.1 SCHEMATIC REPRESENTATION OF CHANGE OF FERMI LEVEL (a); AND ELECTRON OR HOLE CONCENTRATION (b); ON TEMPERATURE VARIATIONS IN AN n-TYPE OR p-TYPE CONDUCTOR.

(1)-(3): excess of defects

(4) : exhaustion of defects

(5) : intrinsic conductance

determined, it is possible to derive a theoretical value for the activation energy for intrinsic conduction in molecular complexes for comparison with the experimental data.

Although polarisation energies have been determined for a wide series of organic solids by ultraviolet photoelectron spectroscopy, from the difference between the photoemission thresholds for the molecules in the gaseous and solid states, no measurements have been reported for molecular complexes. These measurements have shown that the apparent polarisation energies for many donor molecules are very similar (for example, benzene has

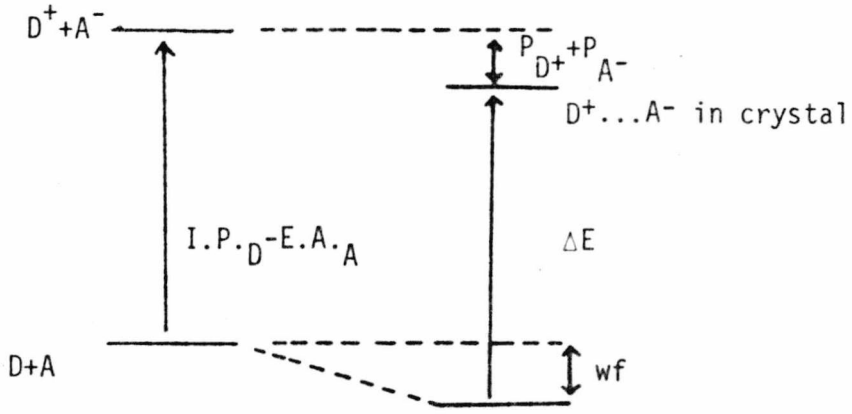

FIG. 5.2

where $I.P._D$ = ionization potential of the donor molecule

$E.A._A$ = electron affinity of the acceptor molecule

P_{D^+} and P_{A^-} are polarization energies

wf is the energy of formation of the solid complex from the free molecules D and A

ΔE = energy gap between ground state and conduction state

the same value, 1.6 ev , as violanthrene A , which has a nine-ring π system) and this similarity has been explained as due to the cancellation of the opposing effects of larger size of the ionised molecule and greater polarizability as size increases. In a π-π^* molecular complex, the polarisation energies of donor and acceptor will not in general be the same as those derived from measurements on the pure donor or acceptor crystals, since in the complex each donor has acceptors as near neighbours in the stack, and vice-versa. In principle it is possible to calculate polarization energies by

summing the interactions between a given charged molecule and the neutral molecules. The simplest approach to these calculations treats the molecule as a point charge in a spherical cavity of appropriate size in a medium of uniform polarizability, but the results of this crude model are in poor agreement with experimental values. Ideally, the charge distribution on the molecular ion should first be calculated by molecular orbital methods, and the interaction between the fractional charges on each atom and all surrounding molecules in the lattice should then be evaluated and summed to yield the polarization energy. This is a complex procedure, further complicated by the fact that crystal effective polarizabilities are not the same as free molecule polarisabilities. Bounds and Munn (1980), adopting an intermediate approach in which each aromatic ring is treated as a point polarisable sub-molecule, have obtained results close to experimental values for naphthalene, but for benzene the agreement is poor (-1.16 ev compared to the experimental value of -1.67 ev.). Thus it is very difficult to evaluate exact theoretical values for intrinsic semiconduction activation energies in molecular complexes.

5.5 Trapping

Sites where charge carriers are bound more strongly than in the rest of the crystal are known as traps. Their origin may be chemical or physical. Chemical traps are formed by impurity molecules, which are difficult to eliminate from molecular crystals. Physical traps occur in imperfect regions of the lattice, where local variations in polarisation energy occur. Both of these types of trapping centre are common in molecular crystals because of the weak intermolecular forces and low barrier to molecular reorientation in many such crystals. In mixed complexes, with two different donor or acceptor molecules, both chemical and physical trap densities would be expected to be higher than in the parent molecular complexes.

Shallow traps mainly affect the carrier mobility, leading to lower mobility and greater temperature dependence of mobility. Deep traps lead to effective carrier loss, and thermal or optical de-trapping can act as a source of carriers as discussed in the section on activation energies. Traps may act as centres for carrier recombination, thereby affecting steady state conductivity.

The distribution of trap depths and densities in a crystal may be examined by a range of techniques including space charge limited conduction, thermally stimulated currents and fluorescence phenomena. Although some of these techniques could be applied to the materials studied in the work reported in this thesis, a detailed study of traps in these materials has not been undertaken since, as already stated, materials limitations restrict the range of conductivity variation possible in mixed π-π^* molecular complexes so that detailed trap studies would be of little practical significance. The expectation of higher trap and defect densities than in the parent complexes is, however, reflected in the variations in experimental conductivity data, reported later in this chapter.

5.6 The Apparatus

Measurement of conductivity of molecular complexes needs to be done very carefully. The resistivity of these complexes is generally high, often larger than 10^{10} ohm-cm . With only small single crystals available, the noise level may exceed the actual current to be measured if precautions are not taken. Care is taken to ensure that the insulation of the apparatus is good and the cable connections are made as short as possible to minimise fluctuations and noise levels. With apparatus such as E.I.L. vibron model 62A , a vibrating reed electrometer and Keithley 610C , a MOSFET input D.C. amplifier electrometer used here, current could be measured

to as low as 10^{-16} amps.

The design of the apparatus has these particular considerations in mind:

1) The apparatus should be free from electrical noise and pickup.
2) The insulation resistance of the apparatus should exceed the resistance of the sample by at least a factor of 50 under all conditions.
3) The apparatus should permit electrical measurements over a wide temperature range for the complexes.
4) The apparatus should be capable of bringing the sample to a certain temperature as quickly as possible and maintaining that temperature as long as the experiment needs.
5) The temperature of the sample should be accurately measured.
6) The sample chamber should be able to be evacuated or filled with specific gases.
7) the light from the monochromator should be focused onto the crystals for photoconduction studies.
8) The intensity of light used for photoconduction measurement should be determined accurately.
9) The sample holder should be as light as possible and easy to handle to facilitate the changing of samples.

Power Supply

The power supply required for this work should give a stable D.C. level for a long period of time and also should be free of noise. The output is made switchable and of reversible polarity. The output comes from:

li) Harwell potentiometer unit type 1007B from 0V-10V in steps of 0.5V.
ii) Harwell potentiometer unit type 1007B, from 0V-200V in steps of 10 Volts.

2) Harwell power unit type 1359 A from 200V-4900V in steps of 100 Volts.

A digital voltmeter was used to check the calibration of the output from the above power unit.

The Measurement of Current

The principle used for the measurements of current is that of Ohm's Law (V=IR).

R_c is connected in series with R_s (Fig. 5.3) knowing the exact applied voltage, the current flowing through the circuit = V_s/R_s . Therefore the resistance of the crystal $R_c = (V_{app}-V_s)/I$. By having V_s less than 1% of the V applied, it can be ignored. Therefore $R_c = V_{app}/I$.

The two instruments available for measuring such a small current ($\simeq 10^{-10}$-10^{-16} amps.) are:

1) Keithley instruments model 610C solid state electrometer.

2) Vibron electrometer model 62A with electrometer converter unit model A62A.

The Keithley electrometer is much preferred for experiments done in this laboratory because of its convenience and automatically switched standard resistances inside the electrometer itself. The vibron is used only in measurements of very small currents with noise or fluctuations, where the possibility of varying input capacitance as well as controlling the damping of the output is particularly valuable. As the current often takes a long time to stabilise, the output of the electrometer is monitored by a chart recorder.

The Chart Recorder

The chart recorder used is a twin channel Oxford instrument series

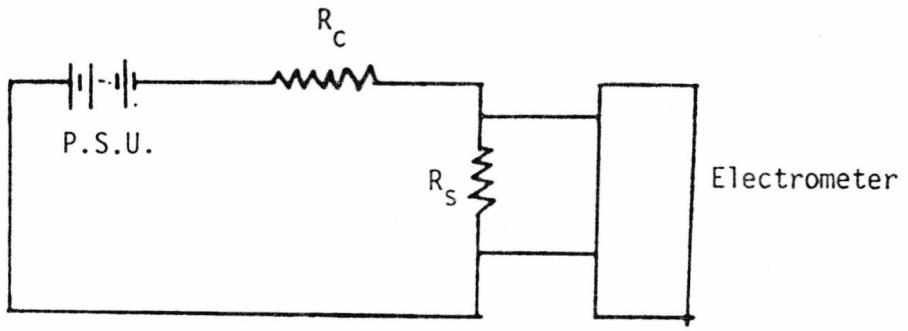

R_C = resistance of crystal

R_S = standard resistance

FIG. 5.3

3000. One pen is used to monitor the temperature (output from the thermocouple inside the cell) and the other is used to measure the current. This recorder has an offset facility which enables relatively small photocurrents to be measured accurately when there is a large dark current.

The Sample Holder

The sample holder must fulfil the conditions given earlier. A diagram of the cell is given in Fig. 5.4.

The cell was painted black to prevent outside light from reaching the crystal. The glass housing with the conductivity cell was surrounded by an earthed metal cage to minimise induced currents caused by operator movement. Sapphire was used to support the electrodes because of its high electrical resistance and excellent thermal conduction. The sapphire disc was held by a phosphor bronze clip onto a hollow copper block as shown in Fig. 5.5. The conductivity cell was mounted on a copper block to prevent mechanical

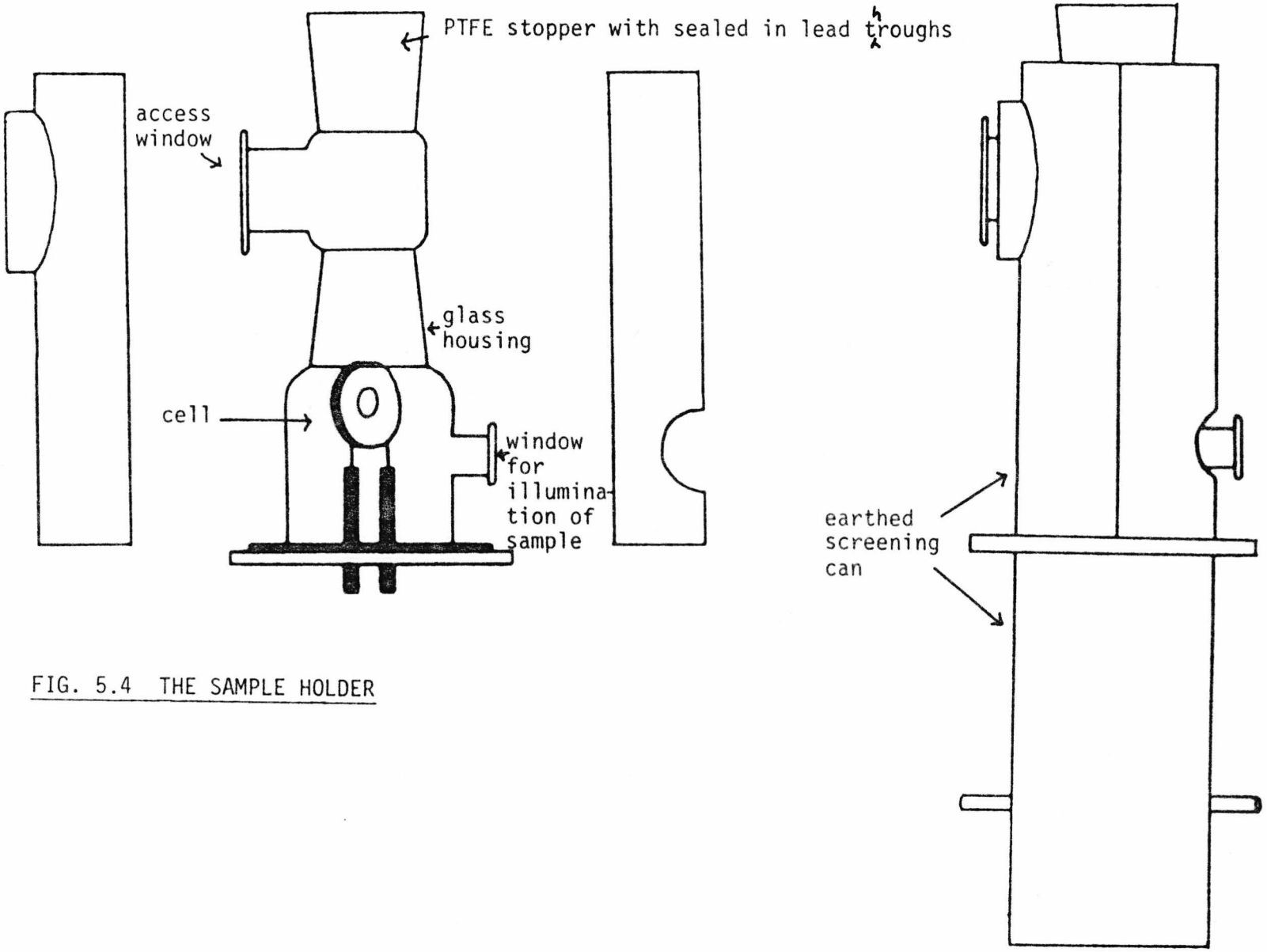

FIG. 5.4 THE SAMPLE HOLDER

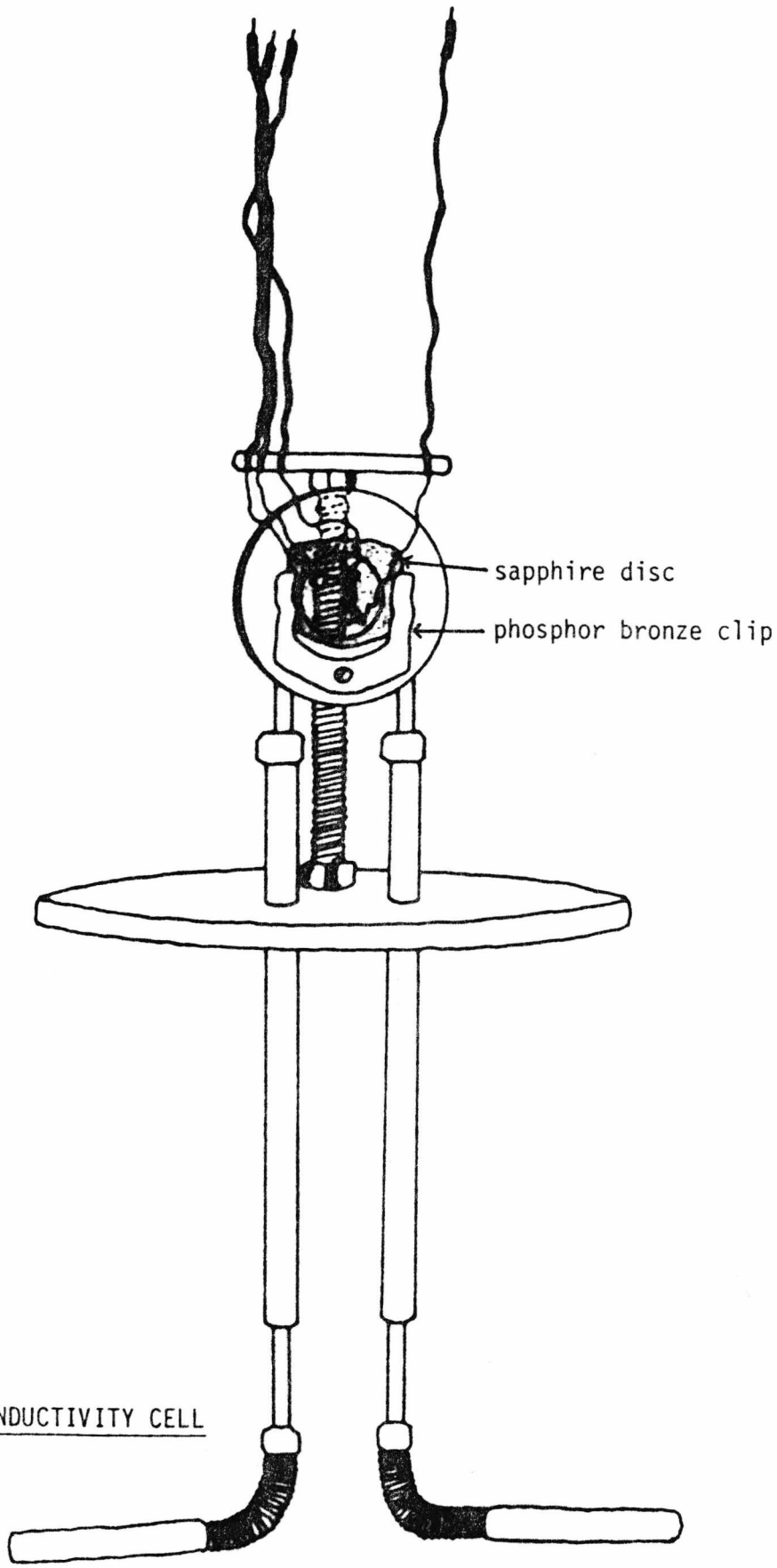

FIG. 5.5 THE CONDUCTIVITY CELL

vibrations which could induce noise when measuring the conductivity of highly resistive materials. Connections to the temperature control system were made by convoluted thin-walled brass bellows. Leads from the EHT supply were introduced into the cell via a PTFE stopper installed at the top of the cell. These leads could be connected internally to the sample via a side window. Another outlet from the glass housing was connected to the vacuum line for evacuation of the cell.

The Vacuum Line

The vacuum line is essential because of the conductivity of some molecular complexes is influenced by gases adsorbed on the crystal surface (Van Ewyk, Chadwick & Wright, 1980). A constant vacuum or the introduction of an inert gas (for example, nitrogen) should help to eliminate these effects. The vacuum system used had the following features:

1) The system was to be free from grease. All taps and joints were the "O" ring type.
2) The vacuum system was made in sections and also flexible, to prevent strain.
3) The system permitted the introduction of various gases into the system.

The layout of the vacuum system used is shown in Fig. 5.6.

Temperature Control of the Cell

The temperature controller used for this work was designed by Munnoch (1974). The description of operation and details of the circuit are given in his thesis. A brief description with important diagrams will be given here.

For measurements above room temperature, the in-line heater was used

to heat air from the compressed air line. The heater was a brass can containing a 1 kw bowl fire element (Fig. 5.7). The air inlet and outlet were opposite one another to ensure good heat transfer from the element to the air stream. A thermistor was used to monitor the temperature. A thermistor is a semiconductor device whose resistance changes considerably with temperature. The use of a thermistor is good because commercially this sensing element is available in a wide range of resistances, hence enabling

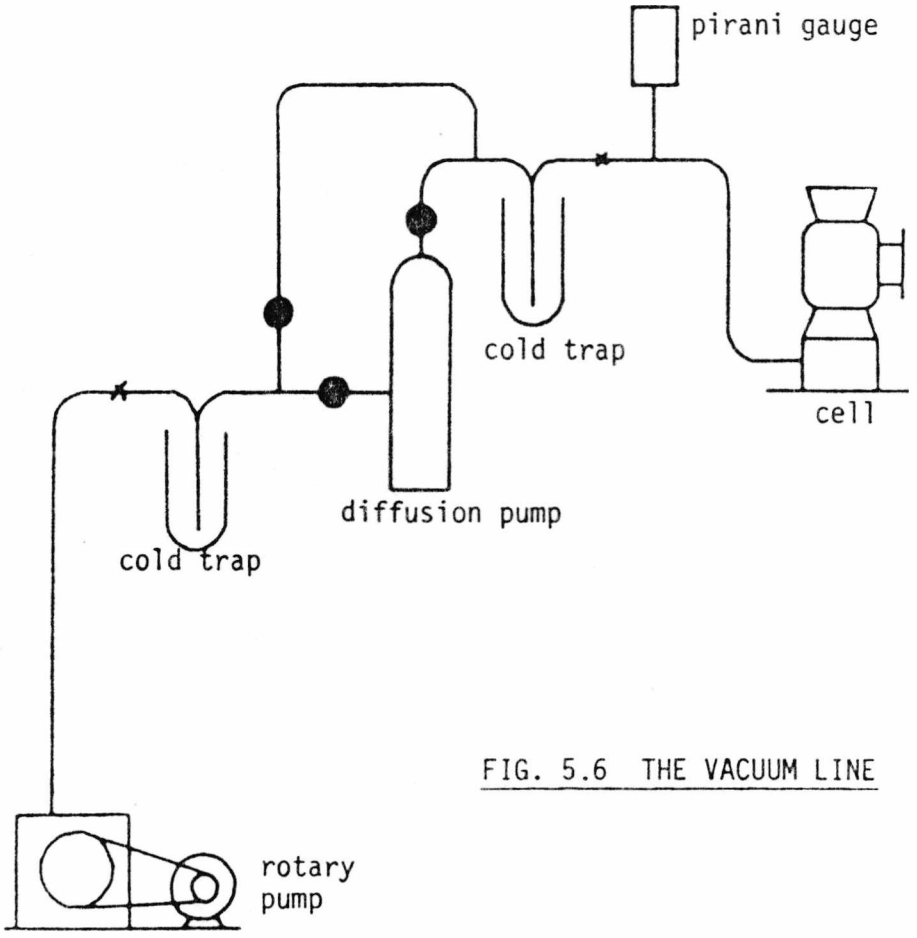

FIG. 5.6 THE VACUUM LINE

the use of the same control unit for different temperature settings, with only the need to change the thermistor. A thermocouple was used to determine the temperature inside the cell chamber. It was used both for above and below room temperature. The thermocouple was a copper constantan junction

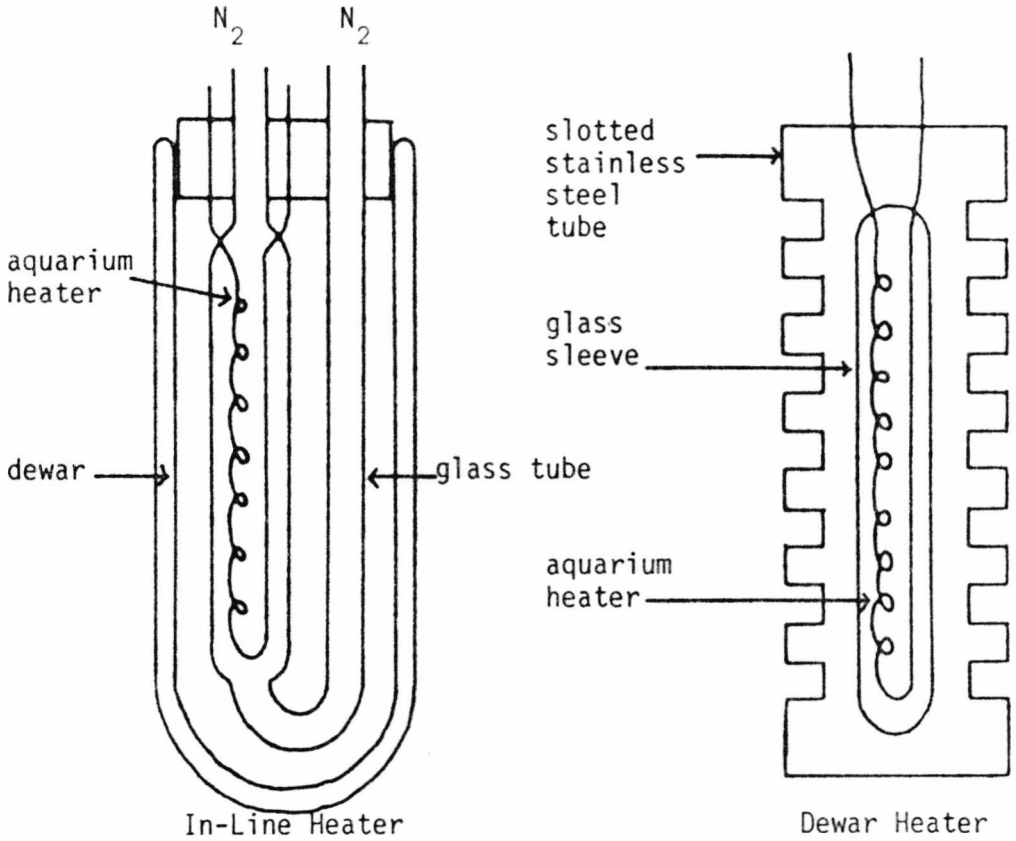

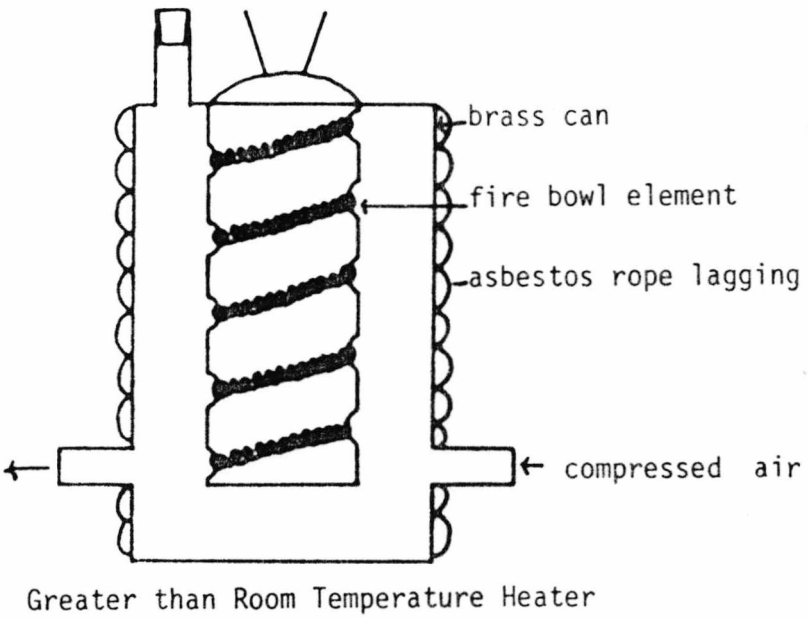

FIG. 5.7 THE VARIOUS HEATERS USED FOR TEMPERATURE CONTROL OF THE CELL

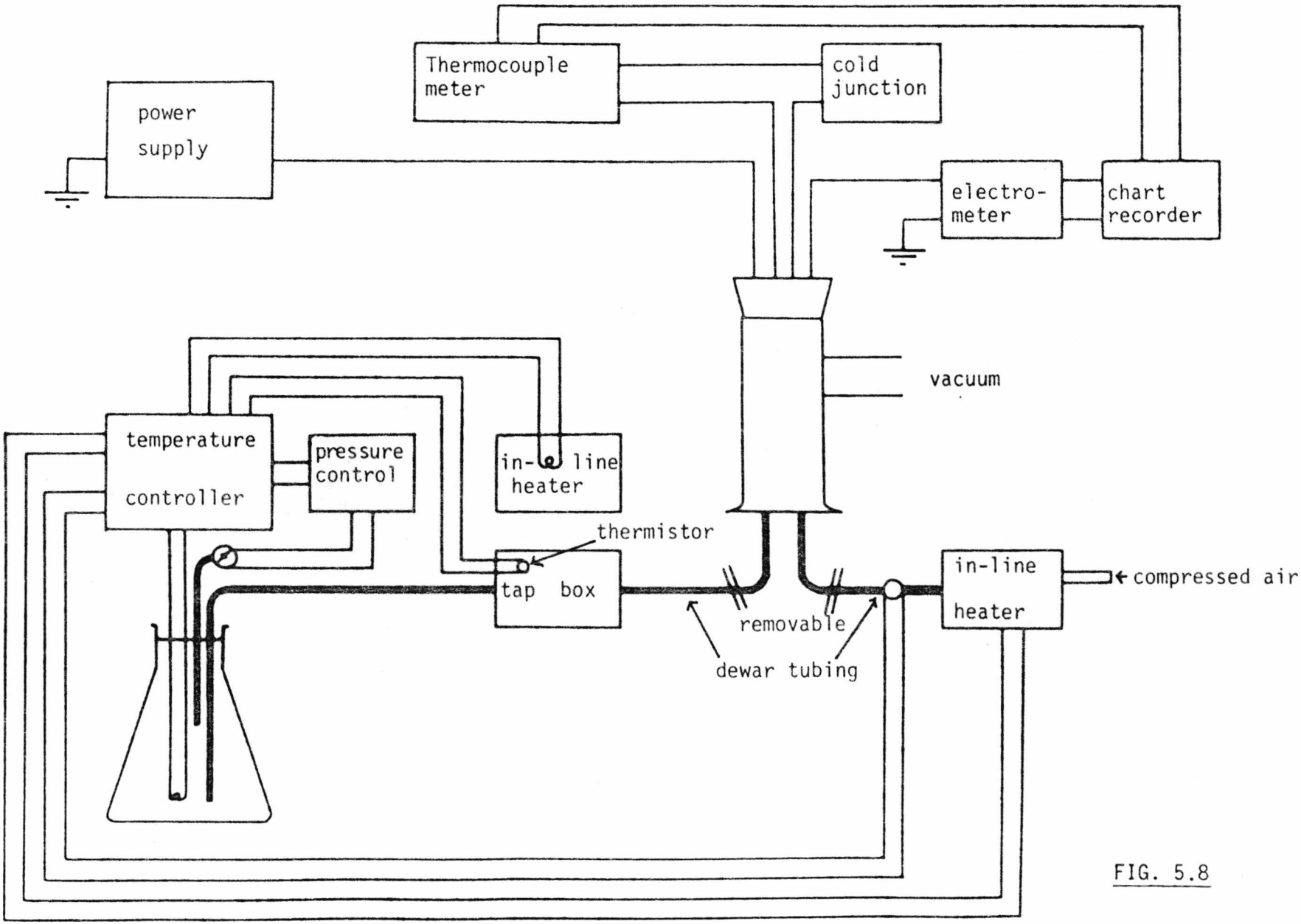
Thermocouple meter
cold junction
power supply
electro-meter
chart recorder
vacuum
temperature controller
pressure control
in-line heater
thermistor
tap box
in-line heater
compressed air
removable
dewar tubing

FIG. 5.8

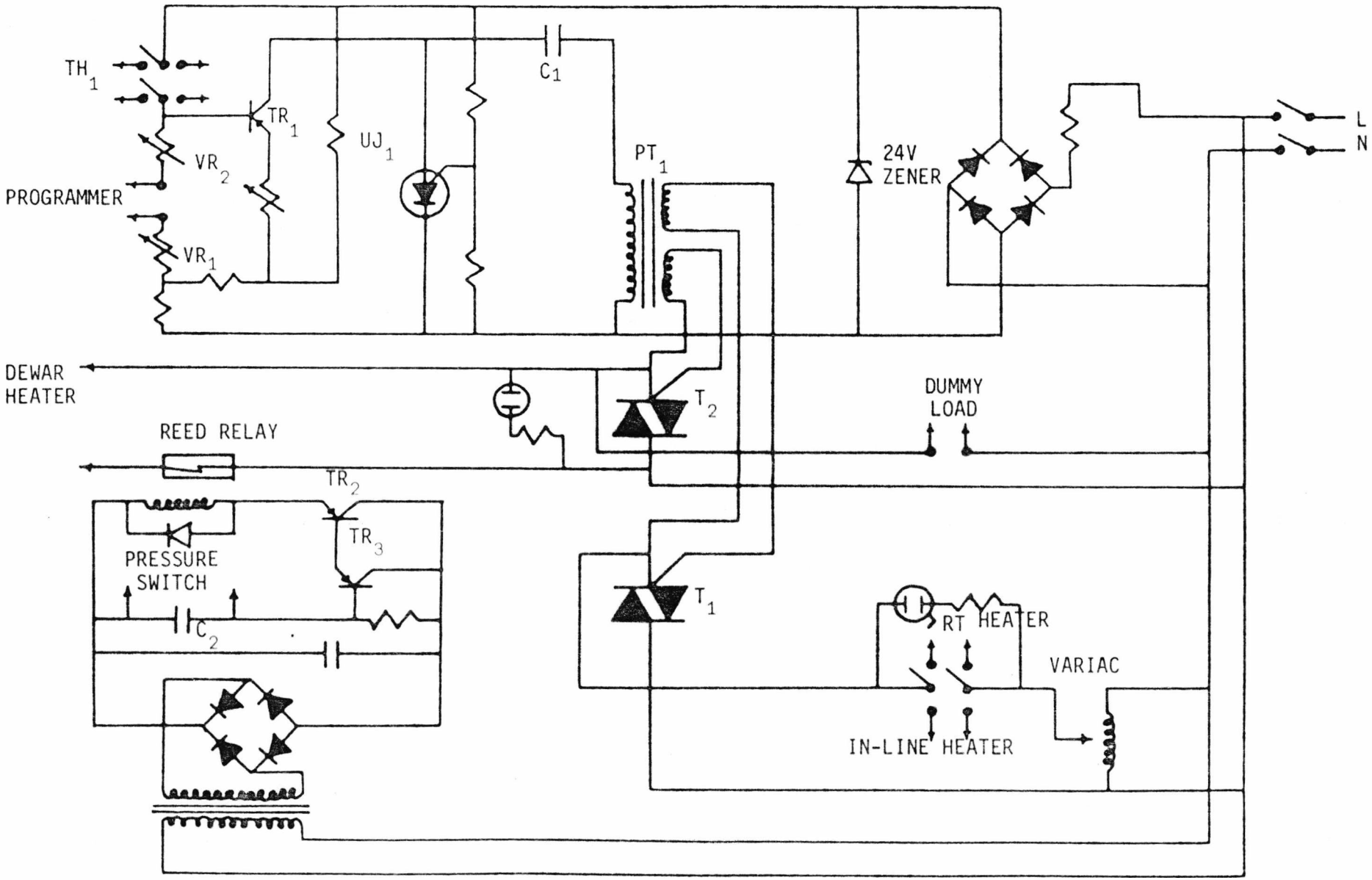
TH1
TR1
UJ1
C1
PT1
24V
ZENER
L
N
PROGRAMMER
VR2
VR1
DEWAR
HEATER
REED RELAY
T2
DUMMY
LOAD
TR2
TR3
PRESSURE
SWITCH
C2
T1
RT HEATER
VARIAC
IN-LINE HEATER

FIG. 5.9

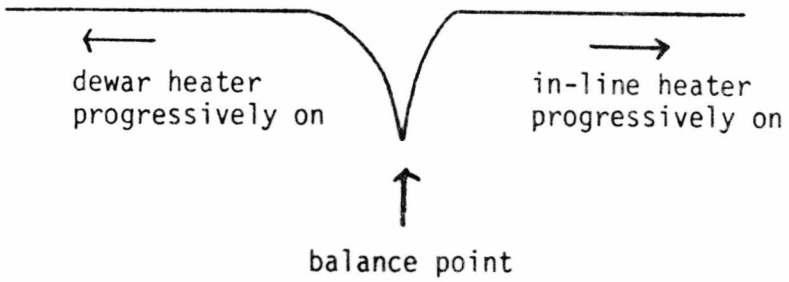

FIG. 5.10

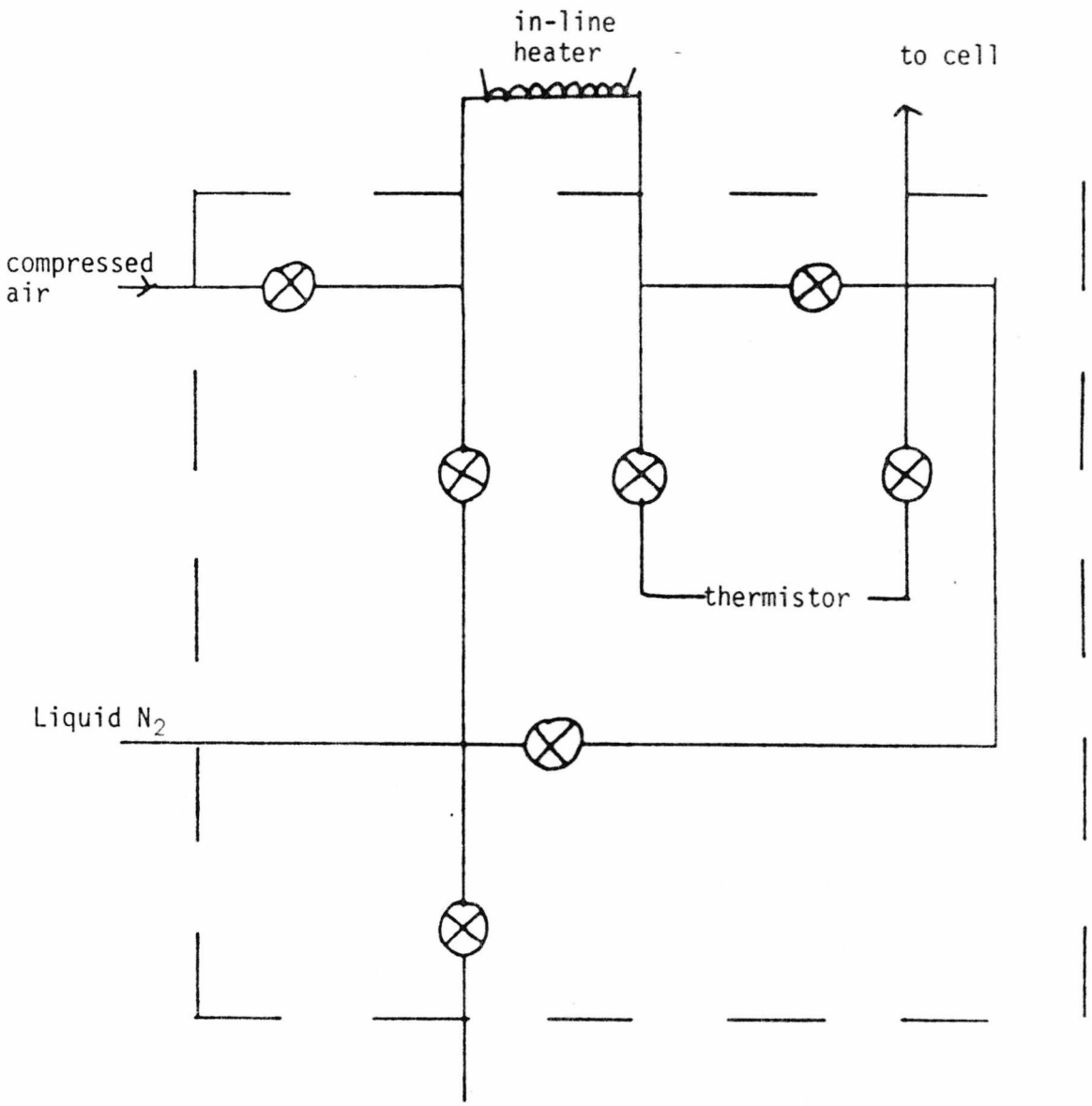

FIG. 5.11 TAP BOX

whose output was monitored by a chart recorder. For below room temperature, the system used is shown in Figs. 5.7 and 5.8.

Cold nitrogen gas was produced by the electric heater immersed in the liquid N_2 in the dewar, and passed into the system via the in-line heater and the thermistor. The in-line heater was controlled by a Triac T_1 and a dummy load (three 150 watt lamps) was powered by T_2 (Fig. 5.9). If the temperature was below the balance point T_2 was shunted and the dewar heater was turned off. However, T_1 was turned on, hence the in-line heater would be on. This would increase the temperature of the system. When the temperature of the system was above the balance point, both T_1 and T_2 were turned off, and the dewar heater on thus increasing the flow of cold nitrogen. The system responded symmetrically as follows (Fig. 5.10) thus achieving the balance temperature.

The pressure inside the dewar was preset using a pressure controller which consisted of a contact to the earthed needle of a standard bourdon tube pressure gauge. A reed relay switch was used to cut the supply to the dewar heater when the pressure inside the dewar reached a certain preset value.

The tap box system in Fig. 5.11 was used to connect the cell, dewar, in-line heater and a thermistor. Rapid cooling was obtained by direct injection of cold nitrogen to the cell and rapid warming was obtained by direct introduction of compressed air to the cell.

5.7 Experimental

Small crystals, which were single, regularly shaped and with shiny surfaces were selected from each batch using a binocular microscope. Larger crystals were often observed to be defective and irregular in shape and hence could lead to instability of observed currents due to electrical noise.

The crystals were mounted with the needle axis forming the length between the electrodes. Since the crystals were generally fragile and brittle extra care was taken during their mounting. A copper spring was used to attach the crystal to the sapphire disc.

The use of a copper spring helps to reduce strain in the crystal as the temperature is varied. High conductivity silver paint was used to attach the two electrodes to the crystal, and to attach a thermocouple junction to the sapphire disc to permit temperature measurement. The silver paint contacts on the crystal were allowed to dry for at least 6 h. During this period, the apparent conductivity frequently changed but the conductivity was constant after the initial drying was complete.

5.8 Results

Electrical measurements have been carried out on parent complexes and mixed complexes of $A_x/C_{1-x}/TCNQ$, $Py_x/Pe_{1-x}/TCNQ$, $DBT_x/DBF_{1-x}/TCNQ$ and $Phe_x/DBF_{1-x}/TCNQ$.

A current voltage plot was done on every crystal. For an ohmic crystal, resistivity is calculated using the equation:

$$\rho = \frac{RA}{L} = \frac{VA}{IL}$$

where

ρ = resistivity in Ωcm.

V = voltage applied in volts.

I = current in amperes

A = cross sectional area of crystal (width×thickness) in cm^2

L = electrode separation in cm .

The results are tabulated in Tables 5.2-5.5. Typical plots

Crystal No.	Composition	Dimensions (cm) L	W	T	Resistivity (Ωcm)	Activation Energy (ev)
1	$A_{.10}/C_{.90}$/TCNQ	.197	.033	.028	4.08×10^{9}	
2	$A_{.10}/C_{.90}$/TCNQ	.243	.035	.027	1.04×10^{10}	.51
3	$A_{.10}/C_{.90}$/TCNQ	.186	.024	.024	9.68×10^{8}	.51
4	$A_{.10}/C_{.90}$/TCNQ	.211	.026	.022	1.08×10^{9}	.63,.58,.62
5	$A_{.10}/C_{.90}$/TCNQ	.297	.021	.021	1.86×10^{8}	.41
6	$A_{.08}/C_{.92}$/TCNQ	.351	.041	-	-	slope 1 = .52 slope 2 = .83 slope 3 = .29
11	$A_{.16}/C_{.84}$/TCNQ	.162	.023	-	-	.51
12	$A_{.16}/C_{.84}$/TCNQ	.127	.020	-	-	.54
15	Anthracene/TCNQ	.174	.073	.037	2.27×10^{10}	-
16	Anthracene/TCNQ	.221	.048	.013	1.41×10^{13}	-
17	Chrysene/TCNQ	.194	.026	.026	8.7×10^{9}	-
18	Chrysene/TCNQ	.221	.047	.011	1.0×10^{9}	-
19	Chrysene/TCNQ	.148	.017	.015	3.3×10^{7}	-

TABLE 5.2 RESISTIVITIES AND ACTIVATION ENERGIES OF PARENT AND MIXED COMPLEXES OF A/C/TCNQ

$ANTHRACENE_x/CHRYSENE_{1-x}$/TCNQ

Crystal No.	Composition	Dimensions (cm) L	W	T	Resistivity (Ωcm)	Activation Energy (ev)
1	Perylene/TCNQ	.246	.045	.033	1.68×10^{11}	.65
2	Perylene/TCNQ	.380	.059	.059	6.00×10^{11}	-
4	Pyrene/TCNQ	.405	.156	.136	4.56×10^{9}	.55
5	$Py_{.39}/Pe_{.61}$ /TCNQ	.254	.034	.025	5.58×10^{11}	.61
7	$Py_{.39}/Pe_{.61}$ /TCNQ	.137	.046	.035	1.96×10^{12}	.62
8	$Py_{.39}/Pe_{.61}$ /TCNQ	.291	.085	.069	1.12×10^{13}	.82
9	$Py_{.52}/Pe_{.48}$ /TCNQ	.307	.045	.020	2.44×10^{11}	.77,.77
10	$Py_{.52}/Pe_{.48}$ /TCNQ	.366	.059	.024	4.29×10^{11}	.59
11	$Py_{.41}/Pe_{.59}$ /TCNQ	.130	.026	.010	2.5×10^{11}	-
12	$Py_{.51}/Pe_{.49}$ /TCNQ	.214	.022	.023	6.76×10^{11}	-
13	No Detectable Pyrene in complexes	.403	.082	.042	3.22×10^{11}	.67
14		.364	.088	.068	6.45×10^{11}	.68
15	" "	.312	.05	.02	4.78×10^{10}	.65,.63
16	" "	.384	.066	.034	5.4×10^{10}	.68
17	" "	.268	.054	.035	4.4×10^{10}	.67

TABLE 5.3 RESISTIVITIES AND ACTIVATION ENERGIES OF PARENT AND MIXED COMPLEXES OF Py/Pe/TCNQ

$PYRENE_x/PERYLENE_{1-x}/TCNQ$

Crystal No.	Composition	Dimensions (cm) L	W	T	Resistivity (Ωcm)	E (ev)
1	Dibenzothiophen / TCNQ	.254	.061	.022	8.3×10^{9}	.59
2	Dibenzothiophen / TCNQ	.173	.013	.008	5.73×10^{10}	
4	Dibenzofuran/TCNQ	.16	.038	.025	3.13×10^{11}	.68
5	Dibenzofuran/TCNQ	.465	.155	.039	2.25×10^{11}	
8	$DBT_{.29}/DBF_{.71}/TCNQ$	.198	.012	.012	2.69×10^{9}	
9	$DBT_{.29}/DBF_{.71}/TCNQ$	.194	.015	.010	1.45×10^{9}	
10	$DBT_{.29}/DBF_{.71}/TCNQ$	.095	.013	.013	2.27×10^{9}	
11	$DBT_{.41}/DBF_{.59}/TCNQ$	.228	.029	.017	3.7×10^{12}	
12	$DBT_{.41}/DBF_{.59}/TCNQ$	.176	.027	.019	1.71×10^{11}	
13	$DBT_{.51}/DBF_{.49}/TCNQ$	.118	.023	.010	1.78×10^{9}	
14	$DBT_{.51}/DBF_{.49}/TCNQ$	.116	.023	.020	5.7×10^{11}	
15	$DBT_{.73}/DBF_{.27}/TCNQ$	.073	.016	.010	5.3×10^{11}	
16	$DBT_{.73}/DBF_{.27}/TCNQ$	.059	.019	.012	1.4×10^{12}	
17	$DBT_{.76}/DBF_{.24}/TCNQ$	.215	.028	.018	3.0×10^{12}	
18	$DBT_{.76}/DBF_{.24}/TCNQ$	.047	.032	.017	3.2×10^{12}	

DBT = Dibenzothiophen ; DBF = Dibenzofuran

TABLE 5.4 RESISTIVITIES AND ACTIVATION ENERGIES OF PARENT AND MIXED COMPLEXES OF DBT/DBF/TCNQ

Crystal No.	Composition	Dimensions (cm) L	W	T	Resistivity (Ωcm.)	E (ev)
1	Phenazine/TCNQ	.252	.097	.039	1.07×10^{10}	
2	Phenazine/TCNQ	.409	.10	.017	6.93×10^{9}	
3	Phenazine/TCNQ	.392	.078	.018	1.43×10^{8}	.47
4	Phenazine/TCNQ	.450	.128	.044	5.1×10^{9}	
5	$PHE_{.84}/DBF_{.16}/TCNQ$	.300	.176	.077	1.13×10^{13}	
6	$PHE_{.89}/DBF_{.11}/TCNQ$	.257	.172	.061	2.7×10^{12}	
7	$PHE_{.85}/DBF_{.15}/TCNQ$	.407	.195	.084	4.47×10^{12}	
8	$PHE_{.90}/DBF_{.10}/TCNQ$	.582	.093	.058	1.03×10^{12}	

PHE = Phenazine ; DBF = Dibenzofuran

TABLE 5.5 RESISTIVITIES AND ACTIVATION ENERGY OF PARENT AND MIXED COMPLEXES OF PHENAZINE/DBF/TCNQ

FIG. 5.12 OHMIC PLOT FOR A C TCNQ CRYSTAL 5

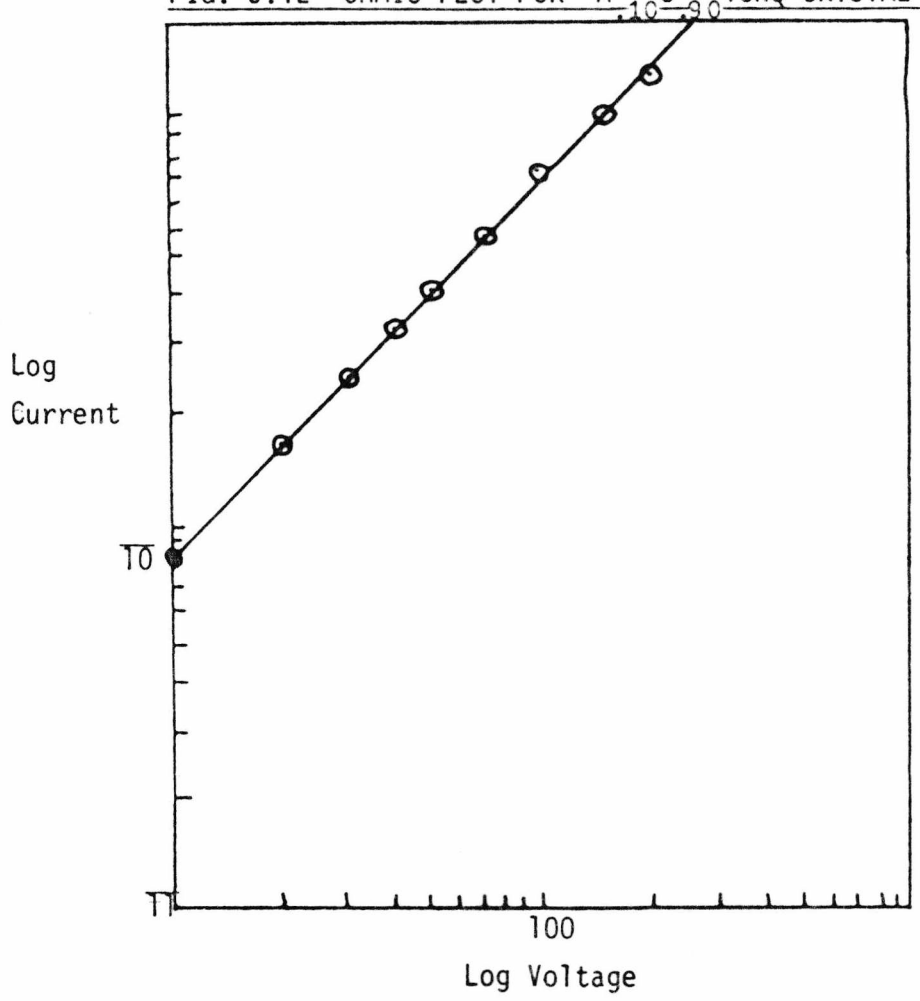

FIG. 5.13 OHMIC PLOT FOR Py/TCNQ CRYSTAL 4

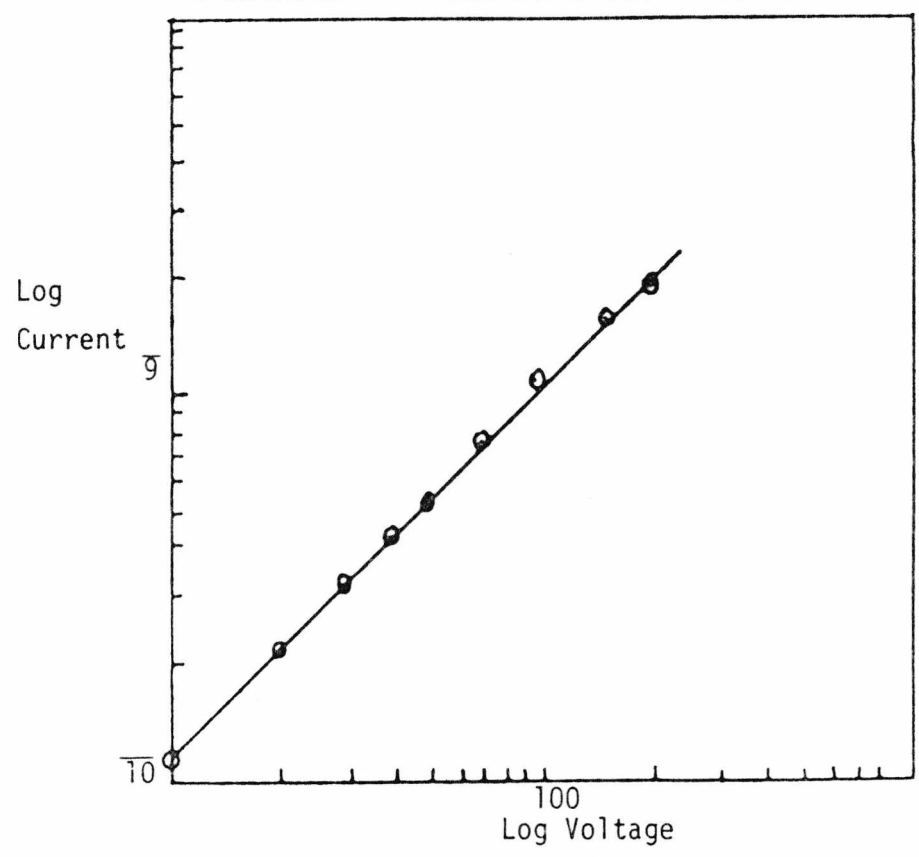

FIGURE 5.14 OHMIC PLOT FOR MIXED COMPLEXES OF Py/Pe/TCNQ

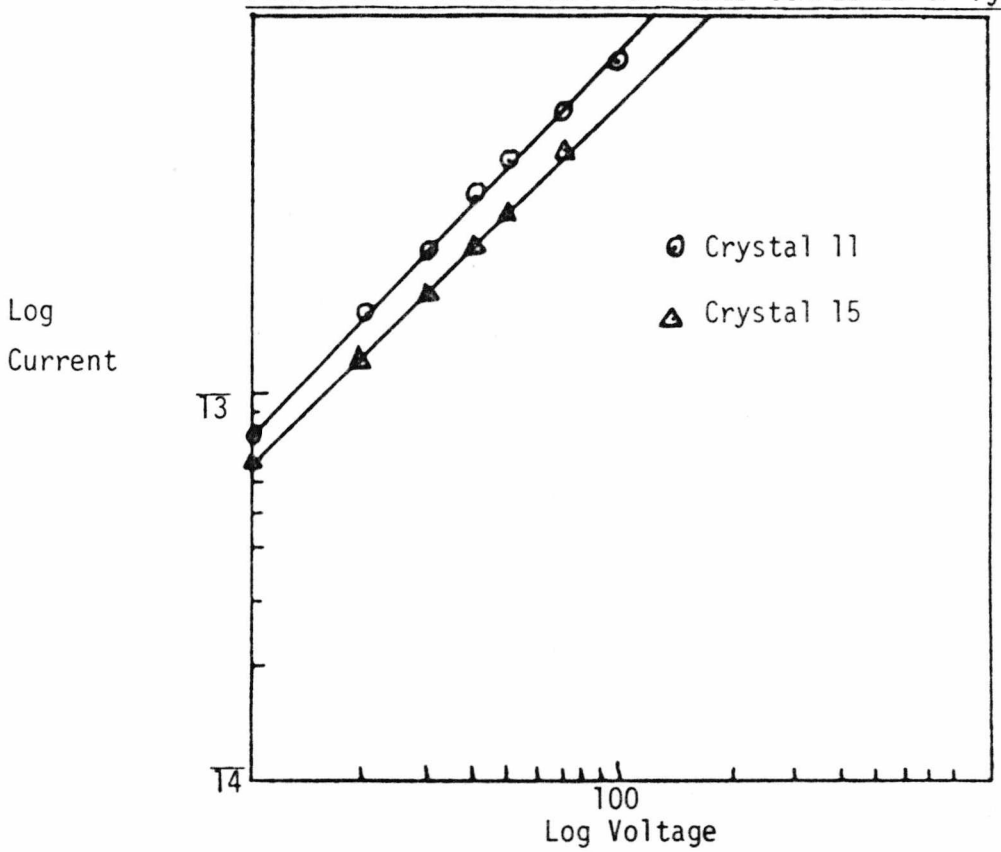

FIGURE 5.15 OHMIC PLOT FOR DBF/TCNQ CRYSTAL 4

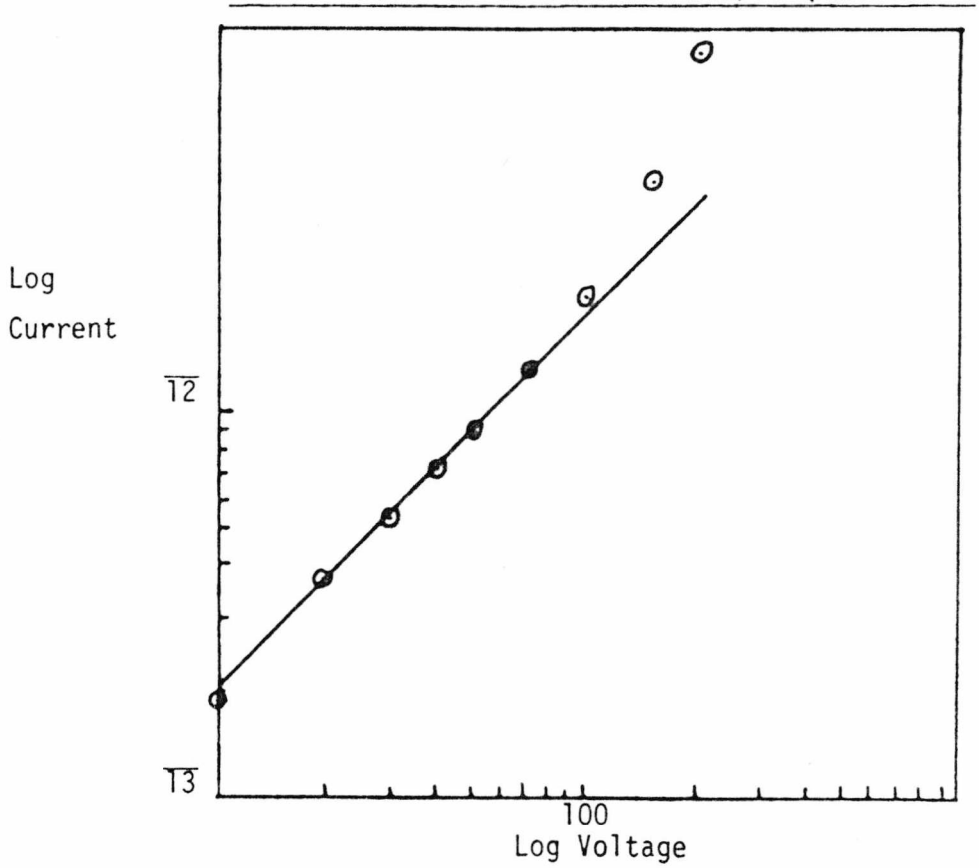

FIG. 5.16 OHMIC PLOT FOR DBT/TCNQ CRYSTAL 1

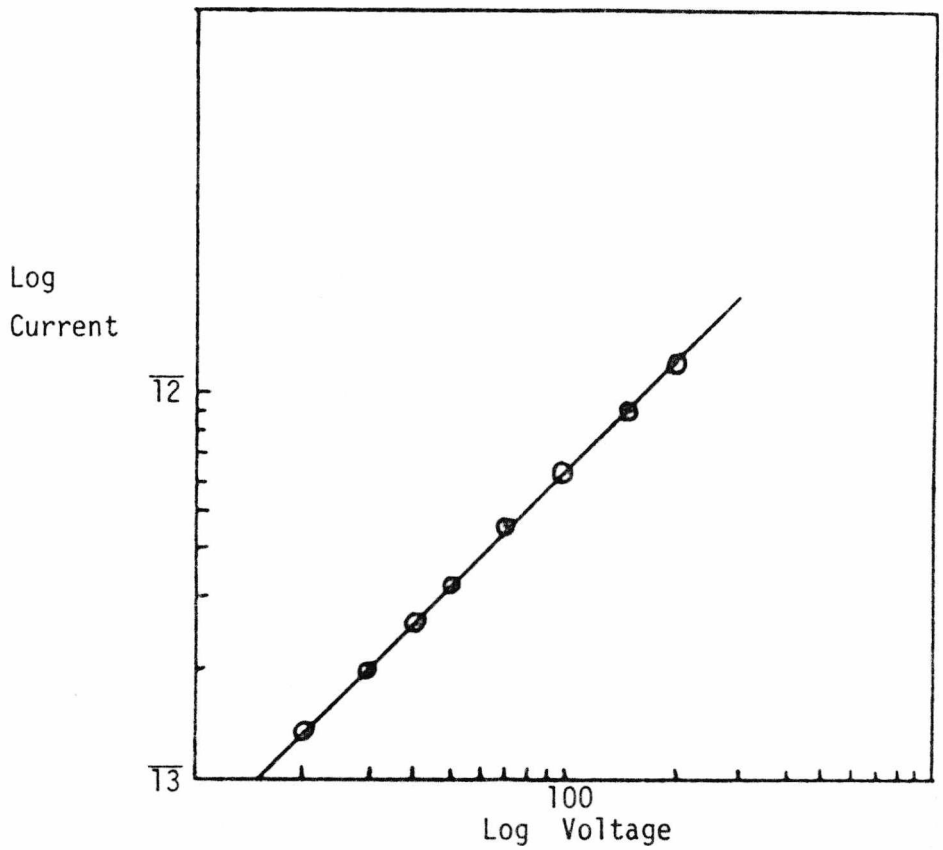

FIG. 5.17 OHMIC PLOT FOR $DBT_{.29}/DBF_{.71}$/TCNQ CRYSTAL 1

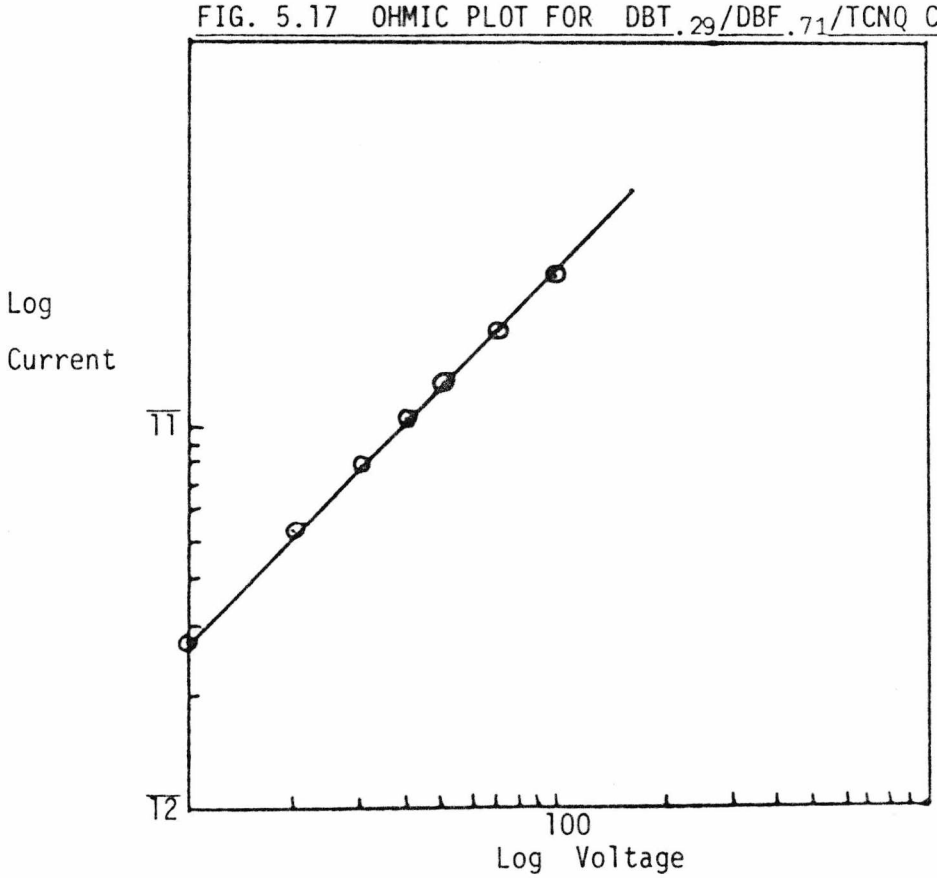

FIG. 5.18 $A_{.10}/C_{.9}$/TCNQ CRYSTAL 2

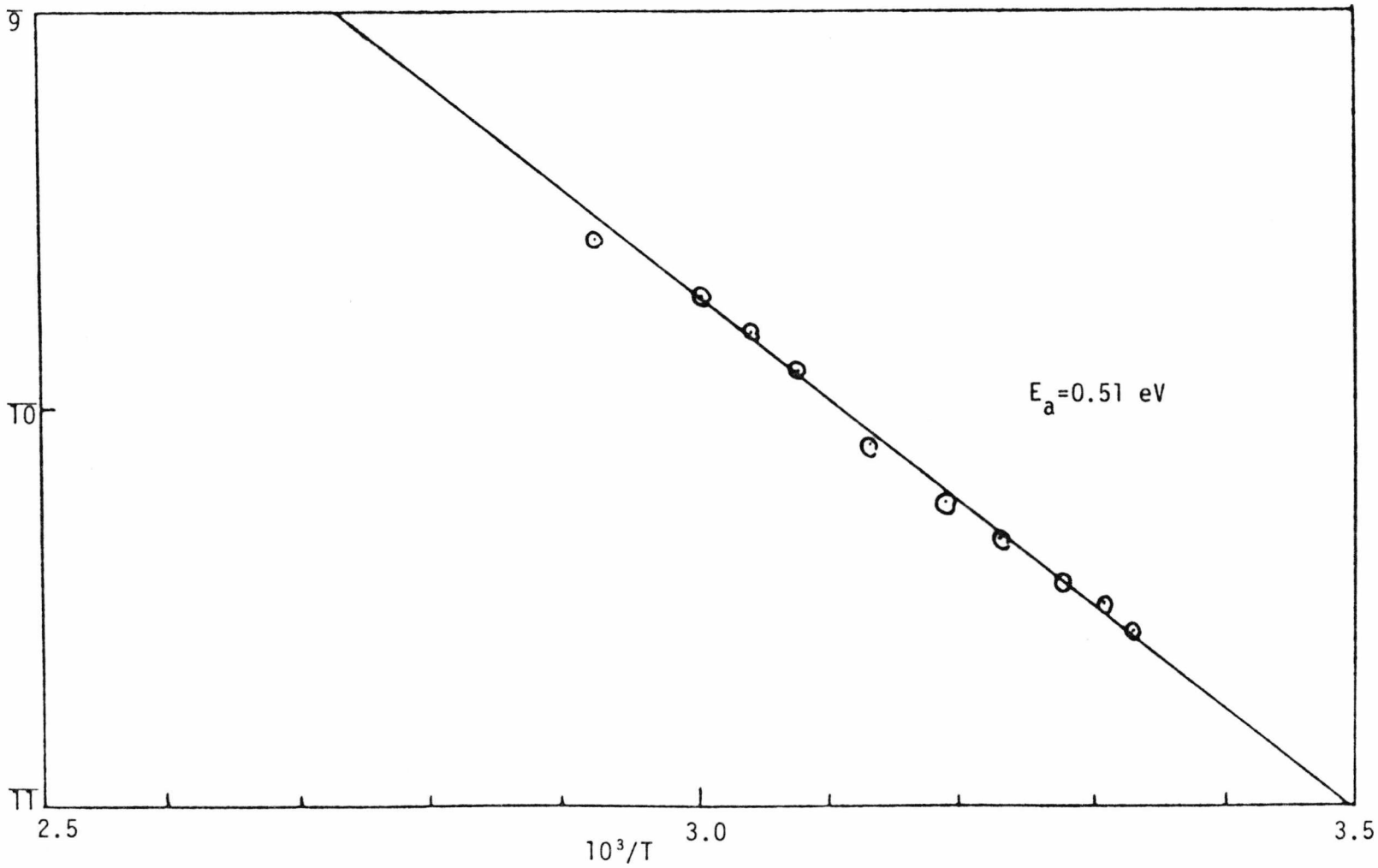

FIG. 5.19 $A_{.10}/C_{.90}$/TCNQ CRYSTAL 3

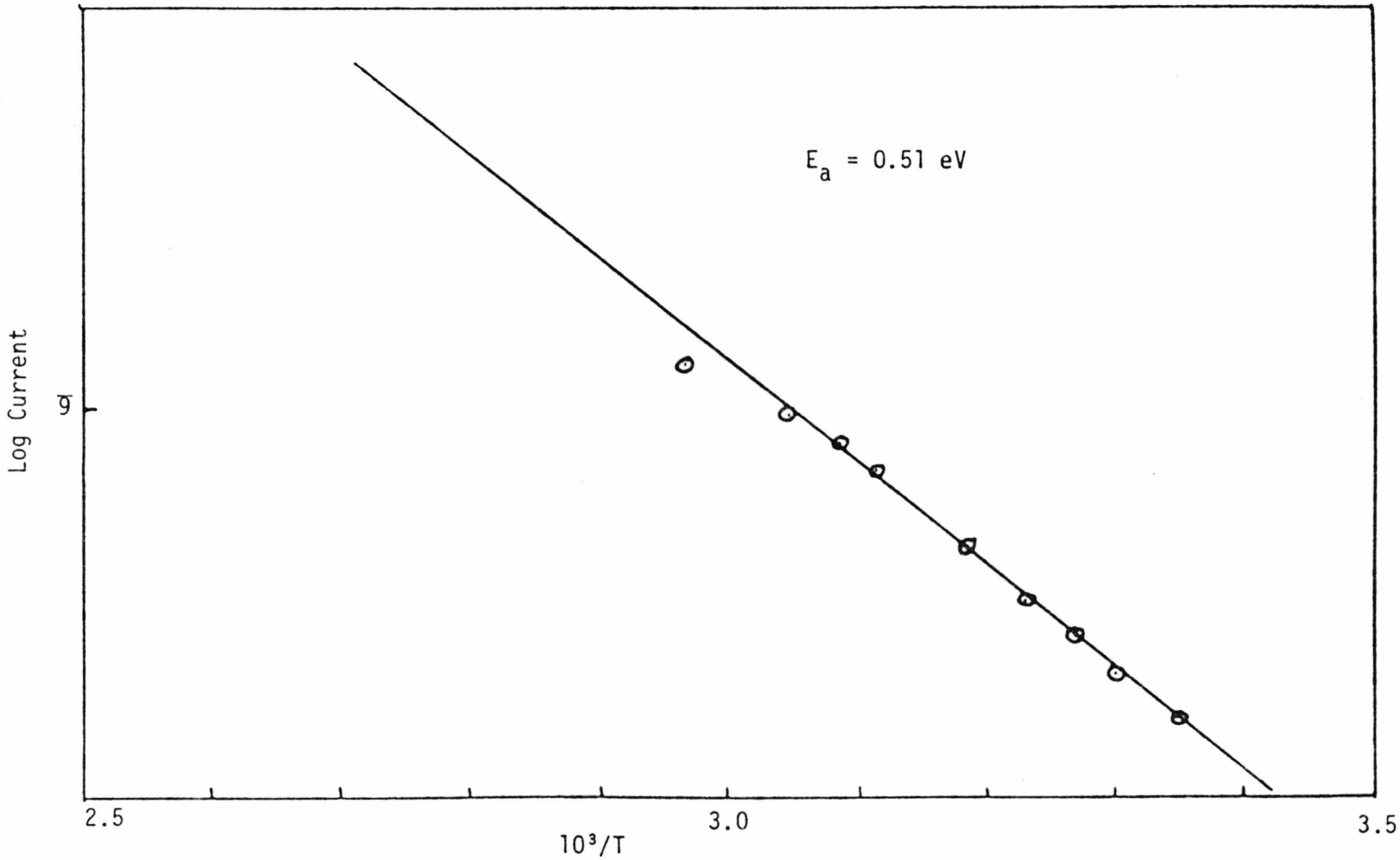

FIG. 5.20 A$_{.10}$/C$_{.90}$/TCNQ CYRSTAL 4

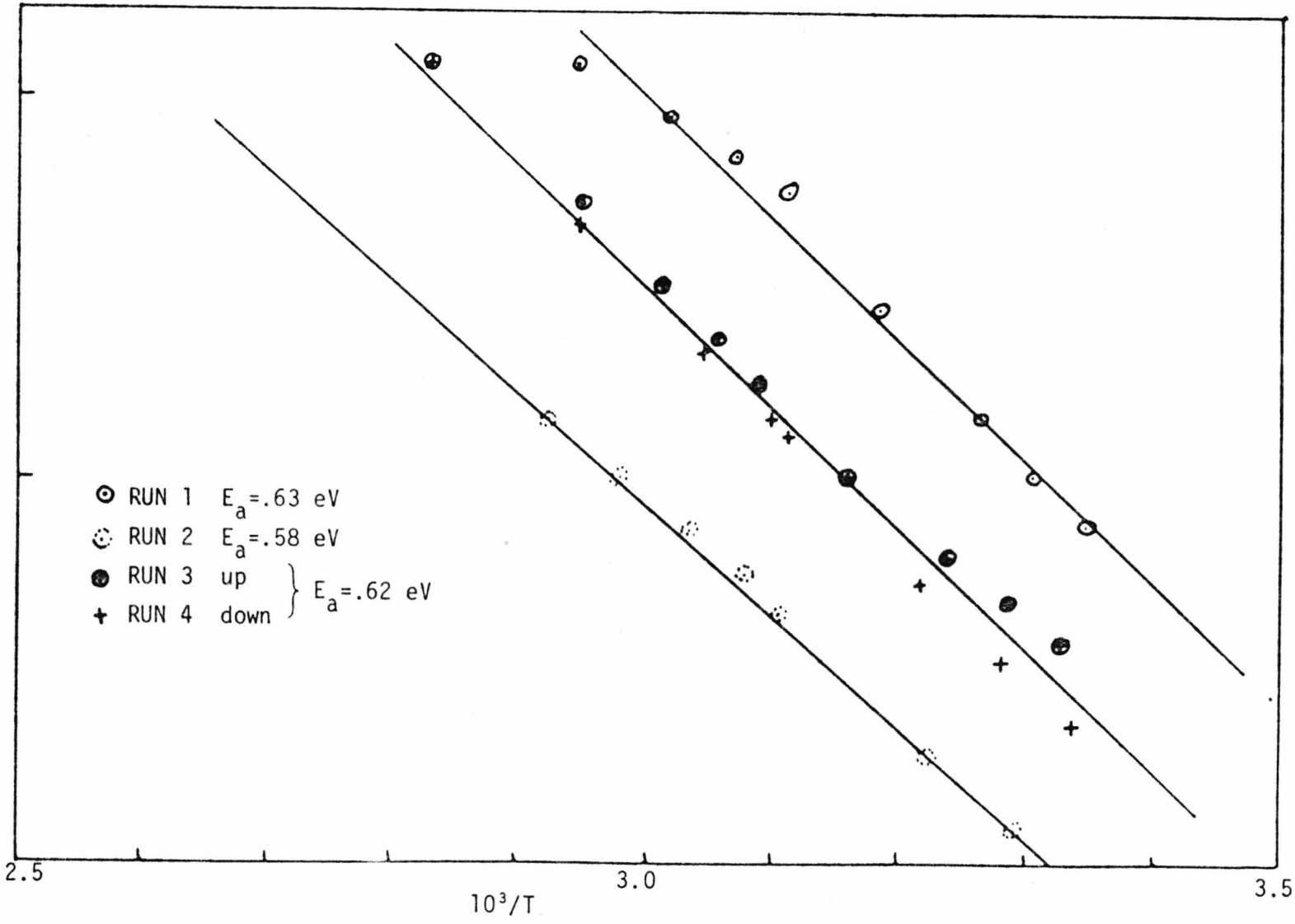

FIG. 5.21 $A_{.10}/C_{.9}$ /TCNQ CRYSTAL 5

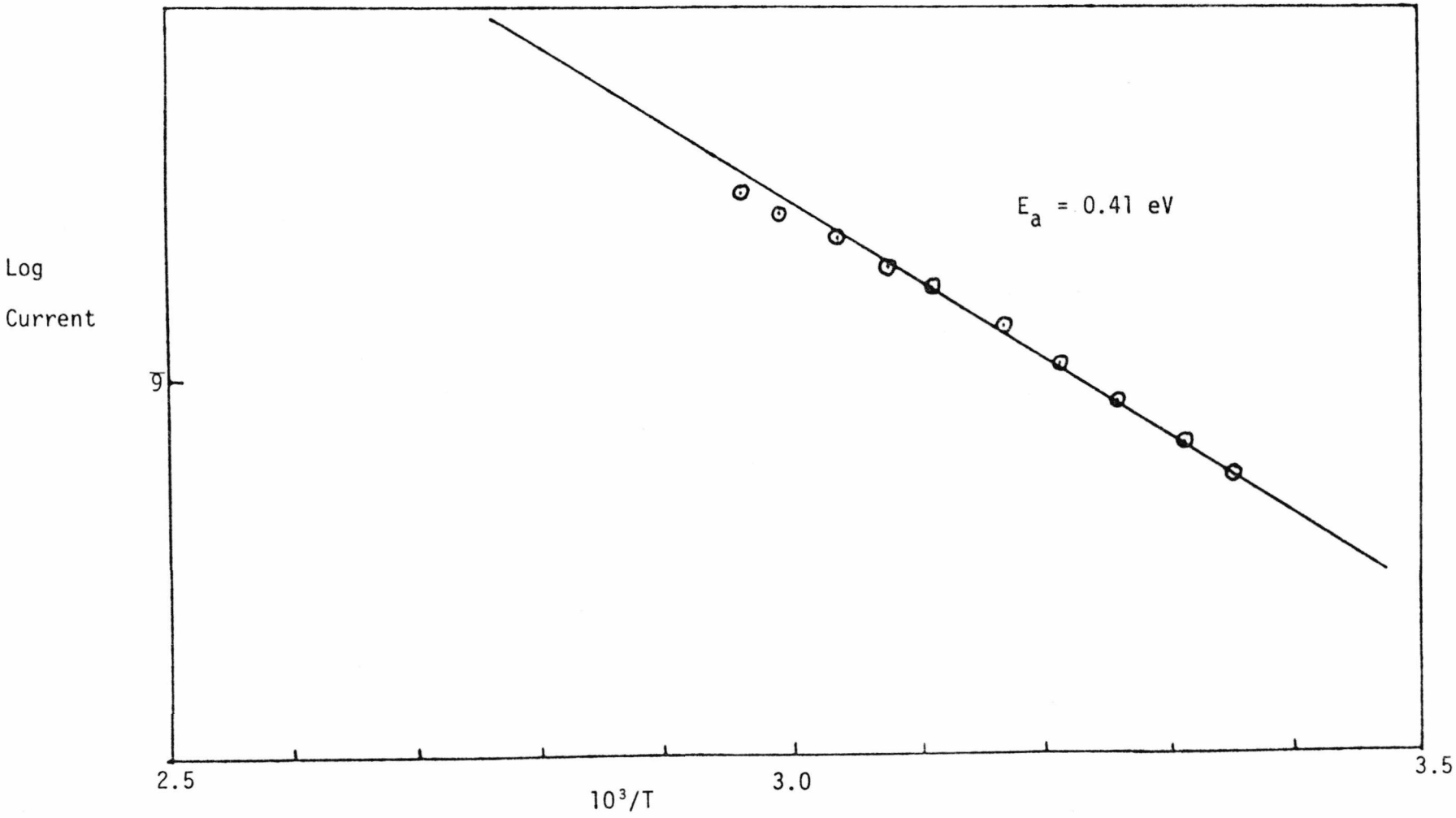

FIG. 5.22 $A_{.08}/C_{.92}$/TCNQ CRYSTAL 6

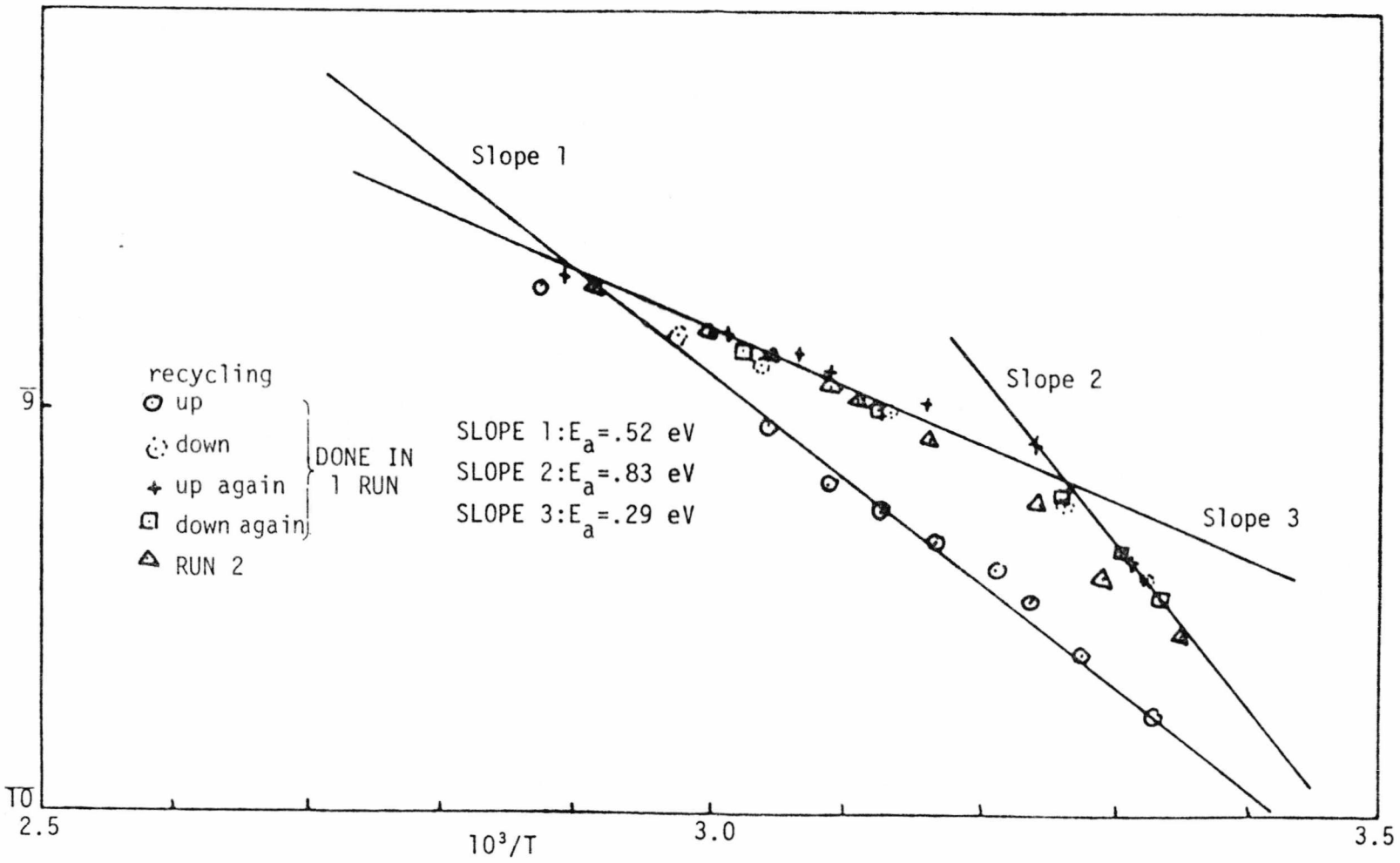

FIG. 5.23 $A_{.16}/C_{.84}$/TCNQ CRYSTAL 11

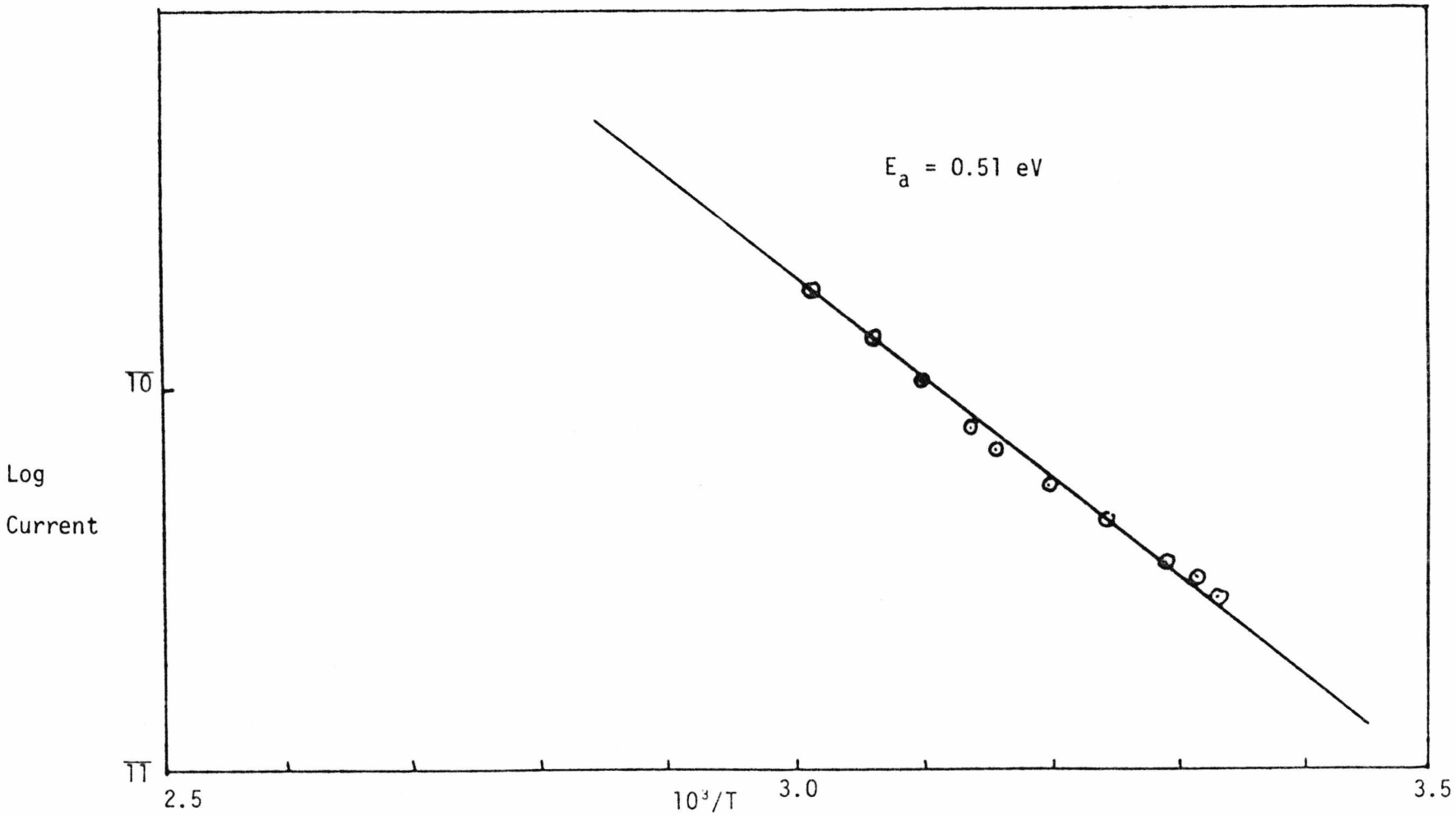

FIG. 5.24 $A_{.16}C_{84}$/TCNQ CRYSTAL 12

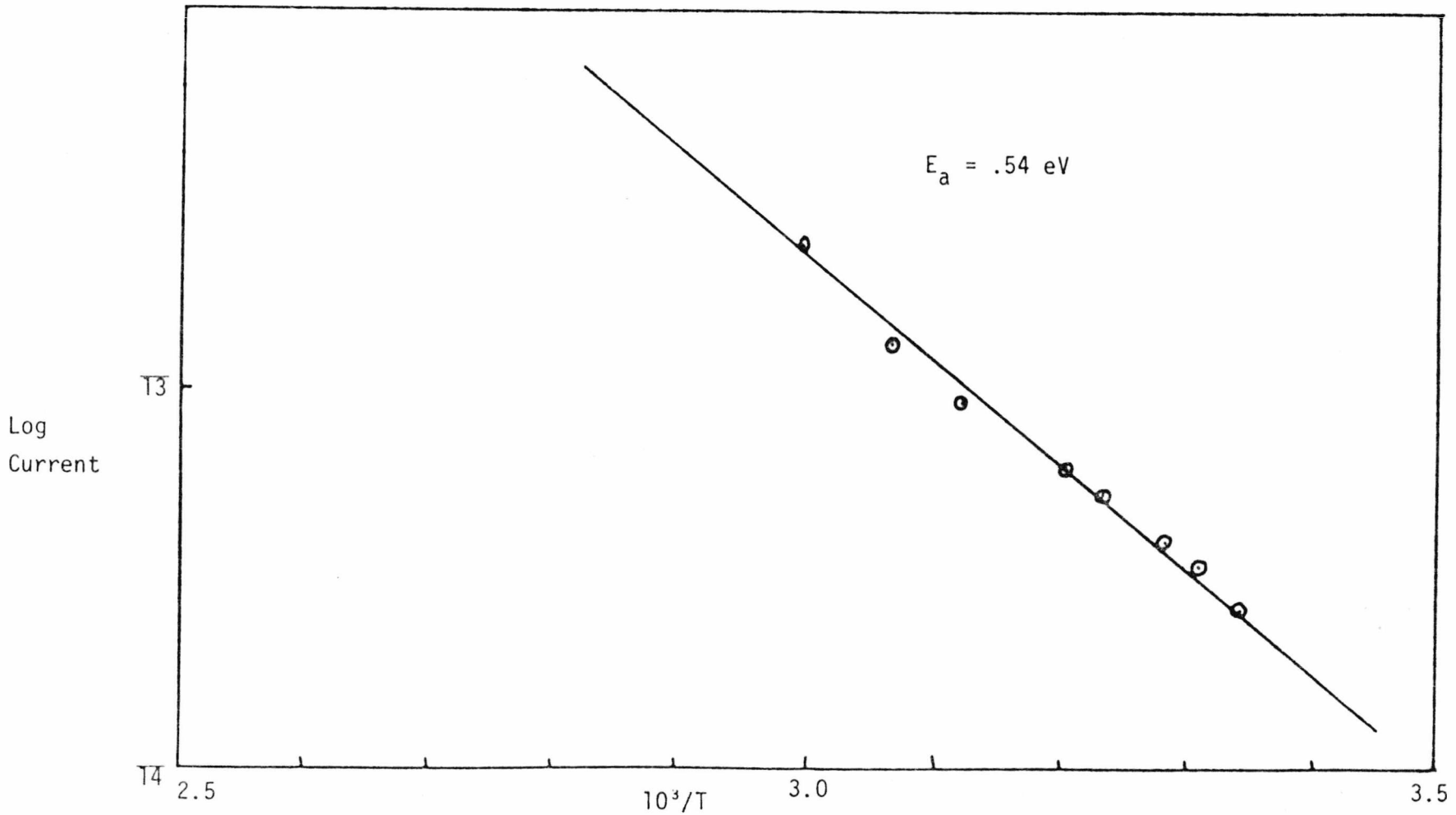

FIG. 5.25 Py/TCNQ CRYSTAL 4

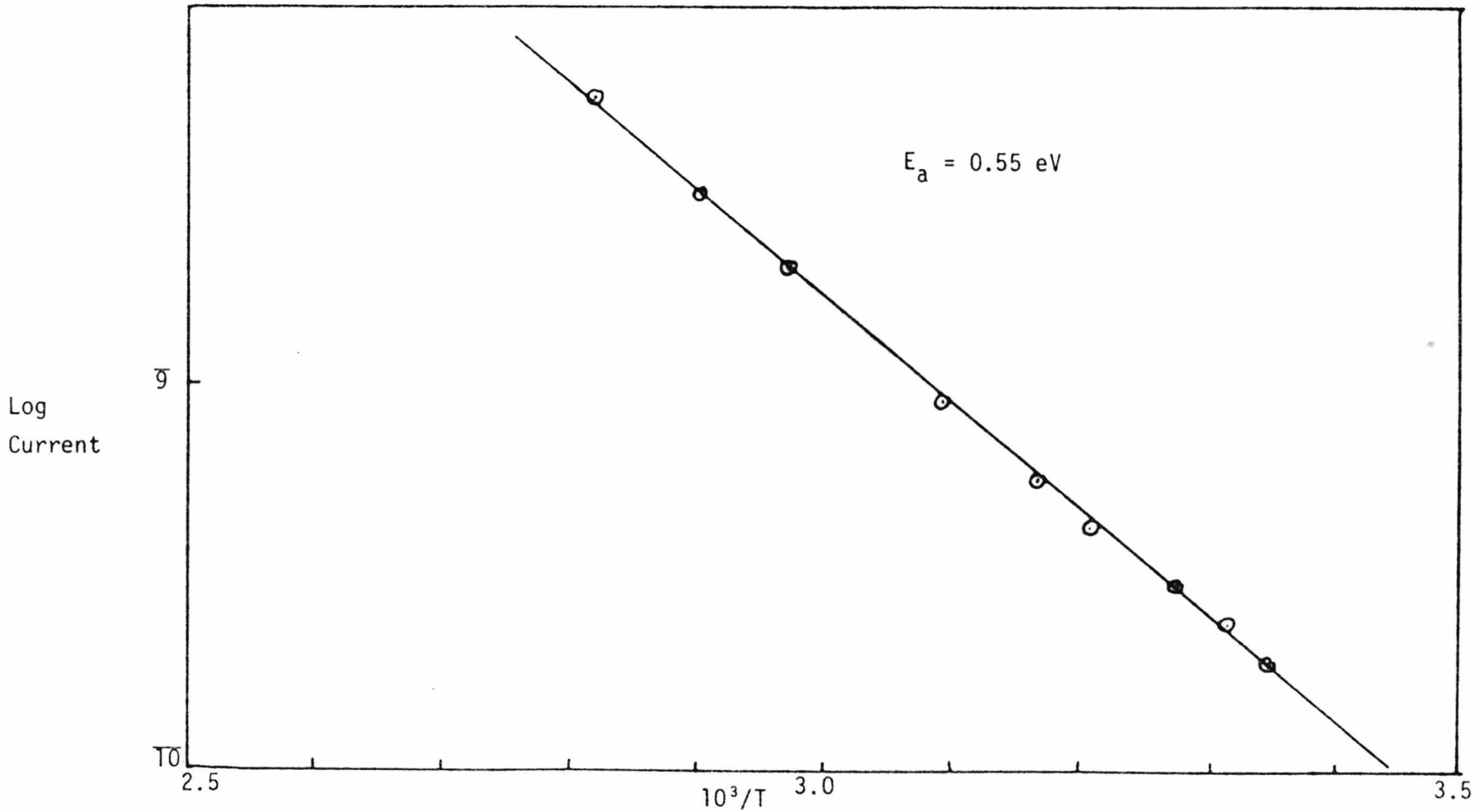

FIG. 5.26 PERYLENE/TCNQ - CRYSTAL 1

$Py_{.52}/Pe_{.48}$/TCNQ - CRYSTAL 10

$Py_{0}/Pe_{1.0}$/TCNQ - CRYSTAL 13 and 14

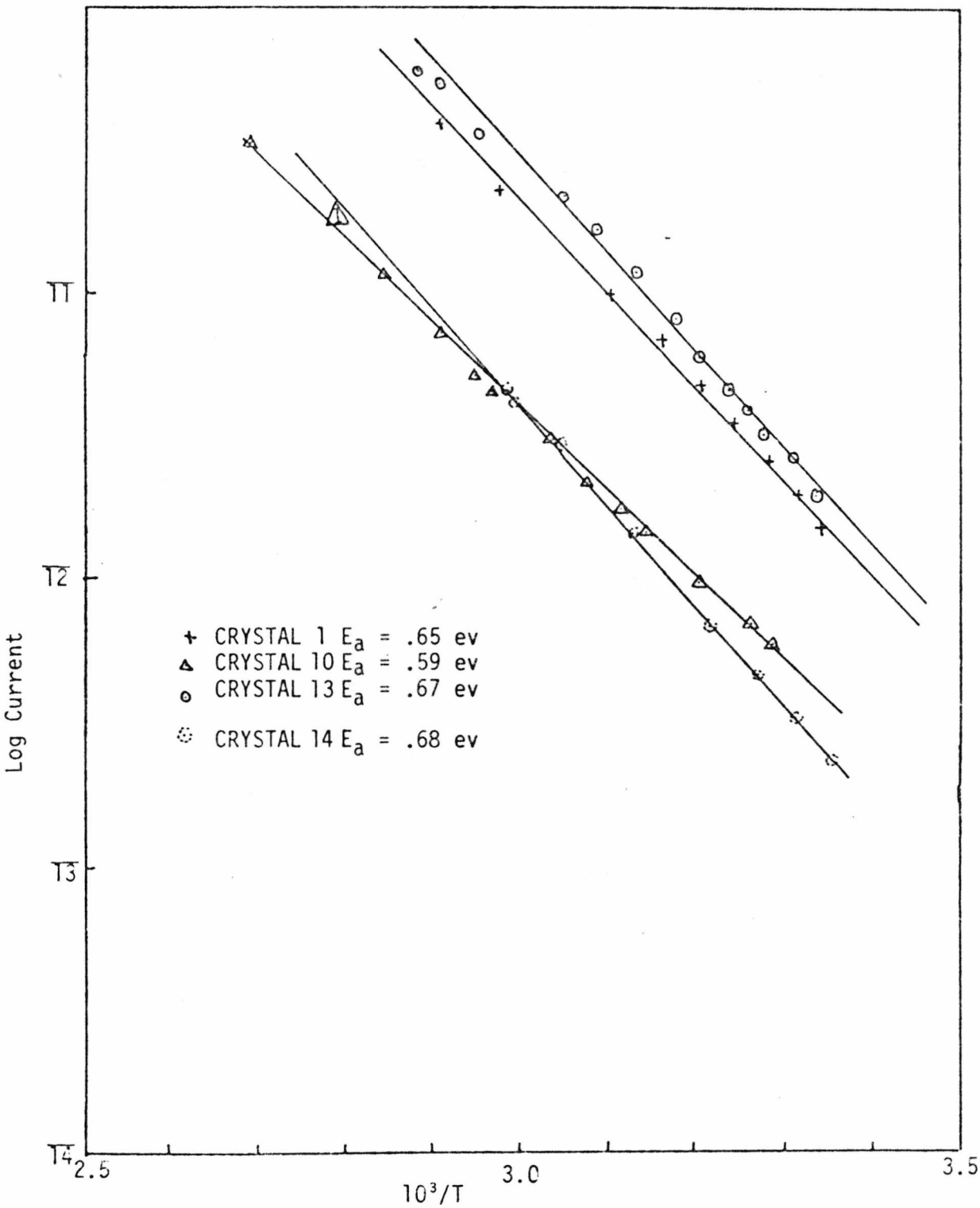

FIG. 5.27 $Py_{.39}/Pe_{.61}/TCNQ$

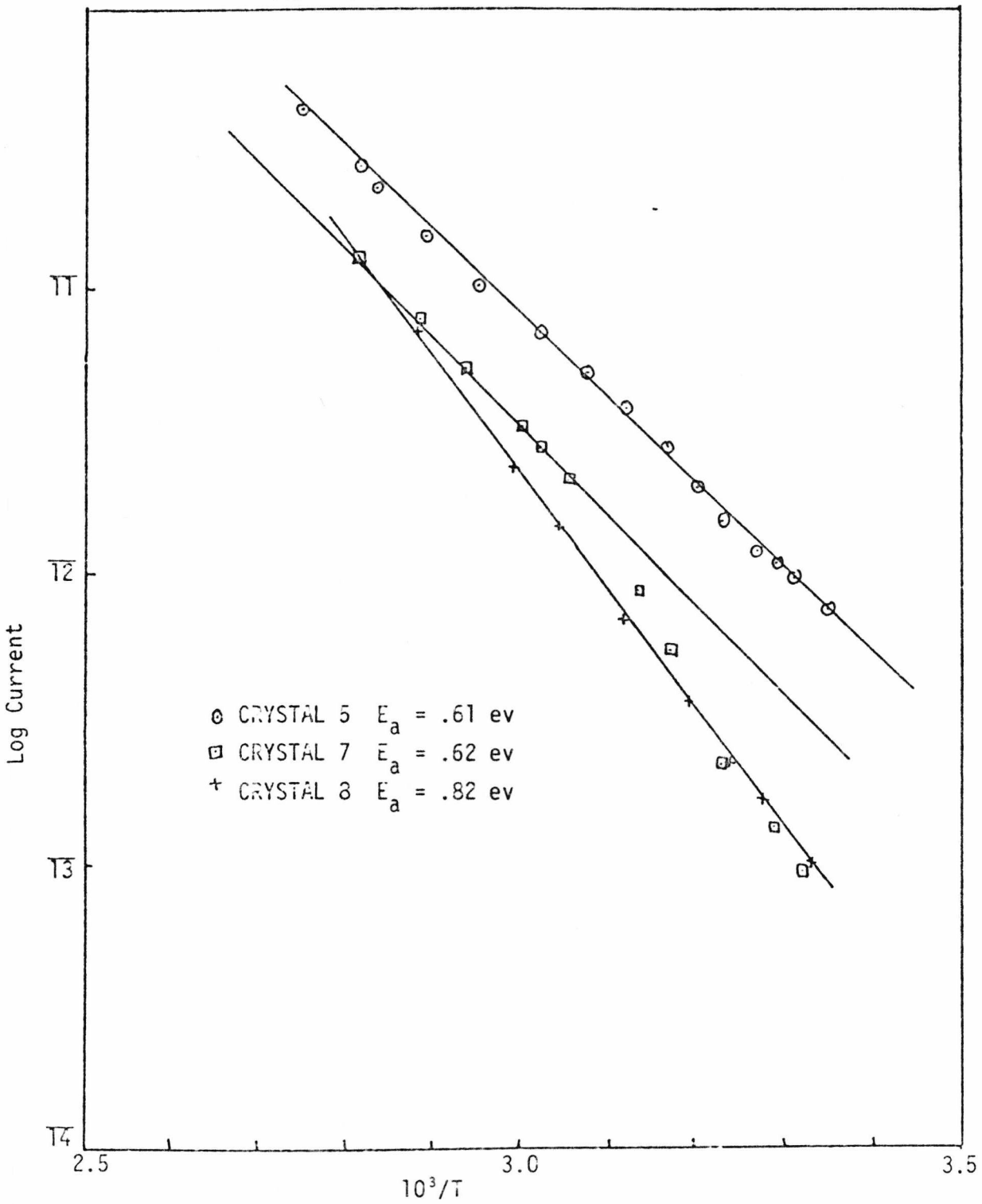

FIG. 5.28 $Py_{.52}/Pe_{.48}/TCNQ$ CRYSTAL 9 and $Py_{0}/Pe_{1.0}/TCNQ$ CRYSTAL 15 and 16

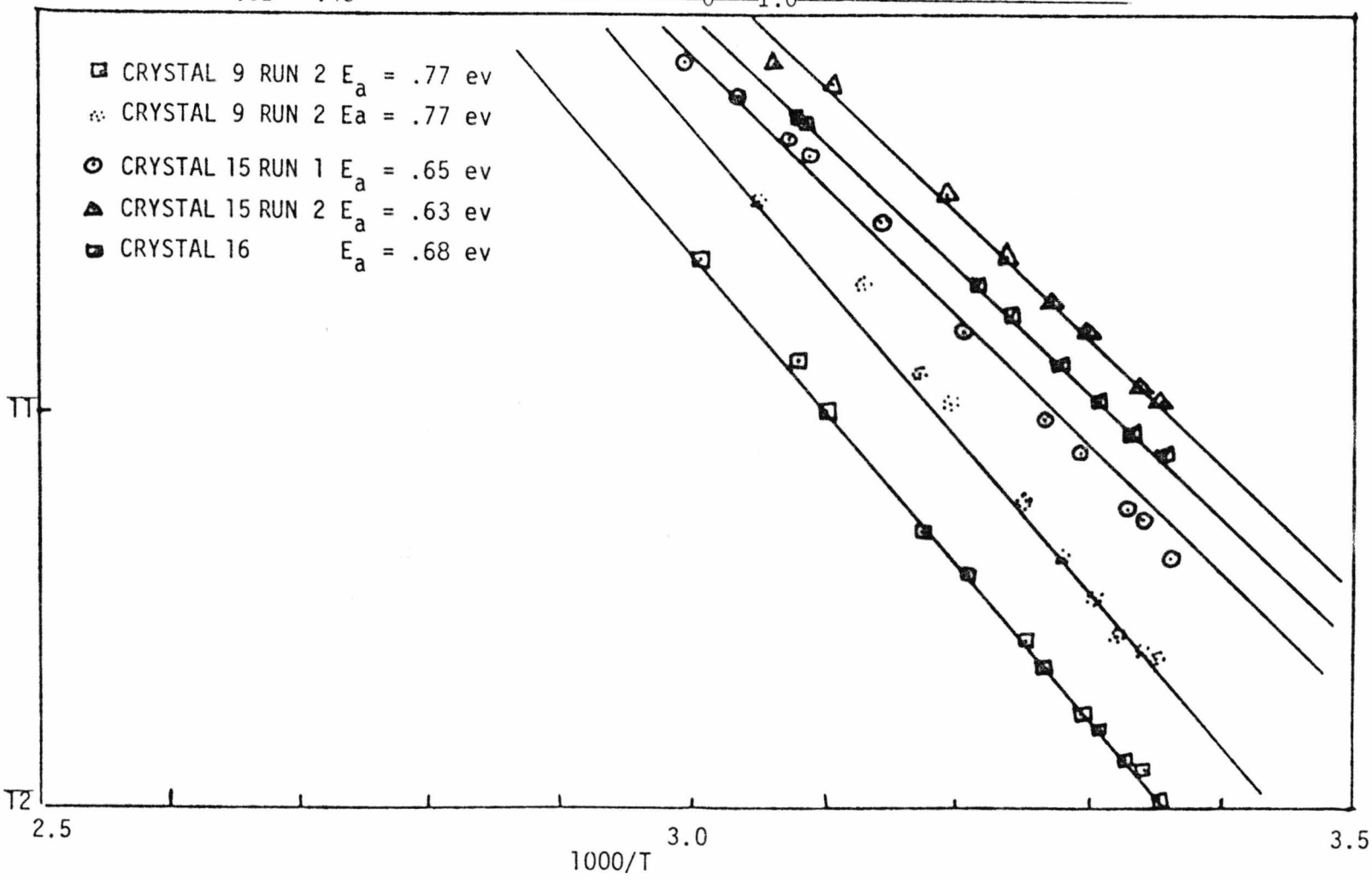

FIG. 5.29 $Py_{0.0}$/Pe/TCNQ CRYSTAL 17

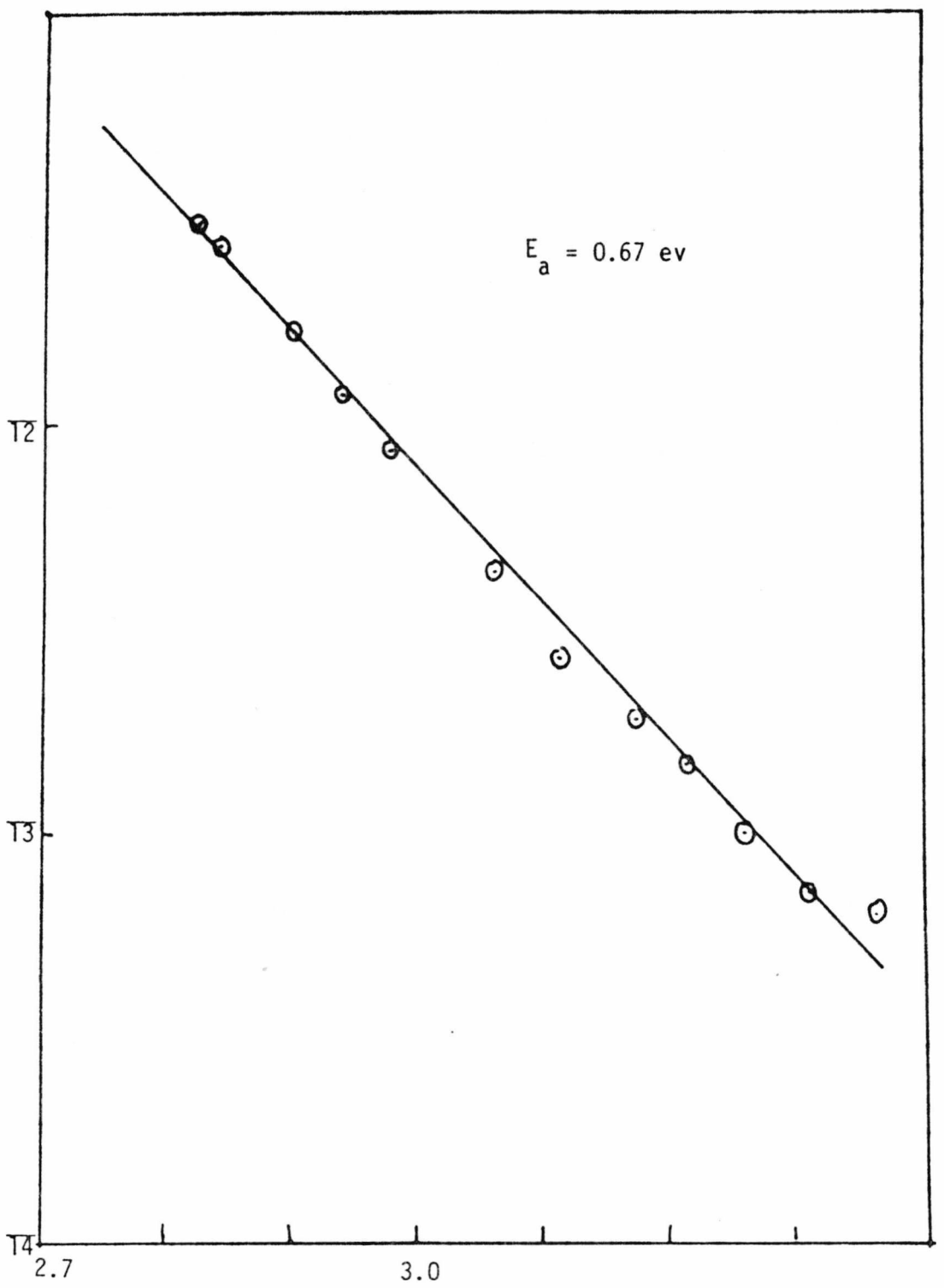

Log
Current

FIG. 5.30

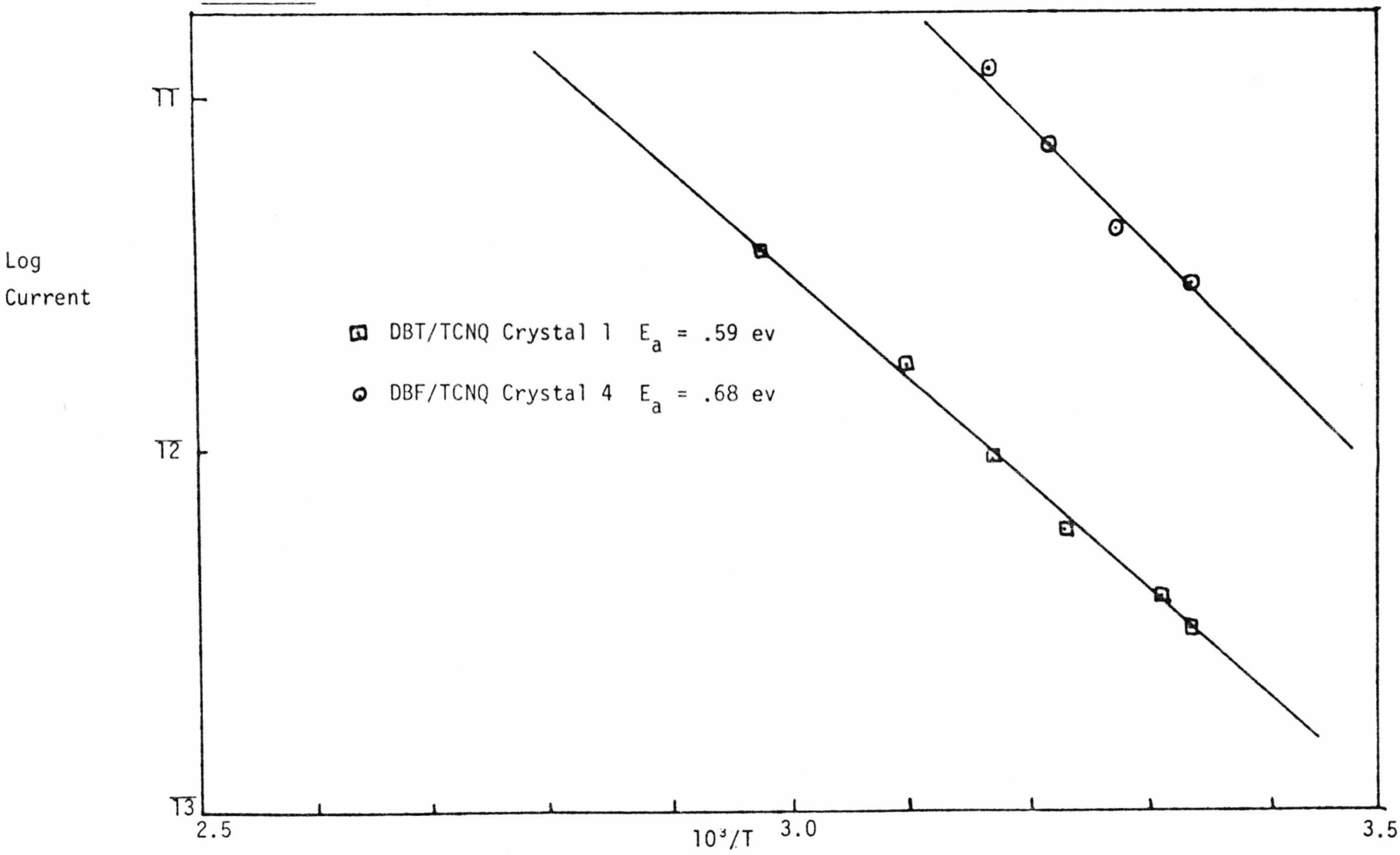
Log
Current
10^{-11}
10^{-12}
10^{-13}
DBT/TCNQ Crystal 1 E_a = .59 ev
DBF/TCNQ Crystal 4 E_a = .68 ev
2.5
3.0
3.5
$10^3/T$

FIG. 5.31

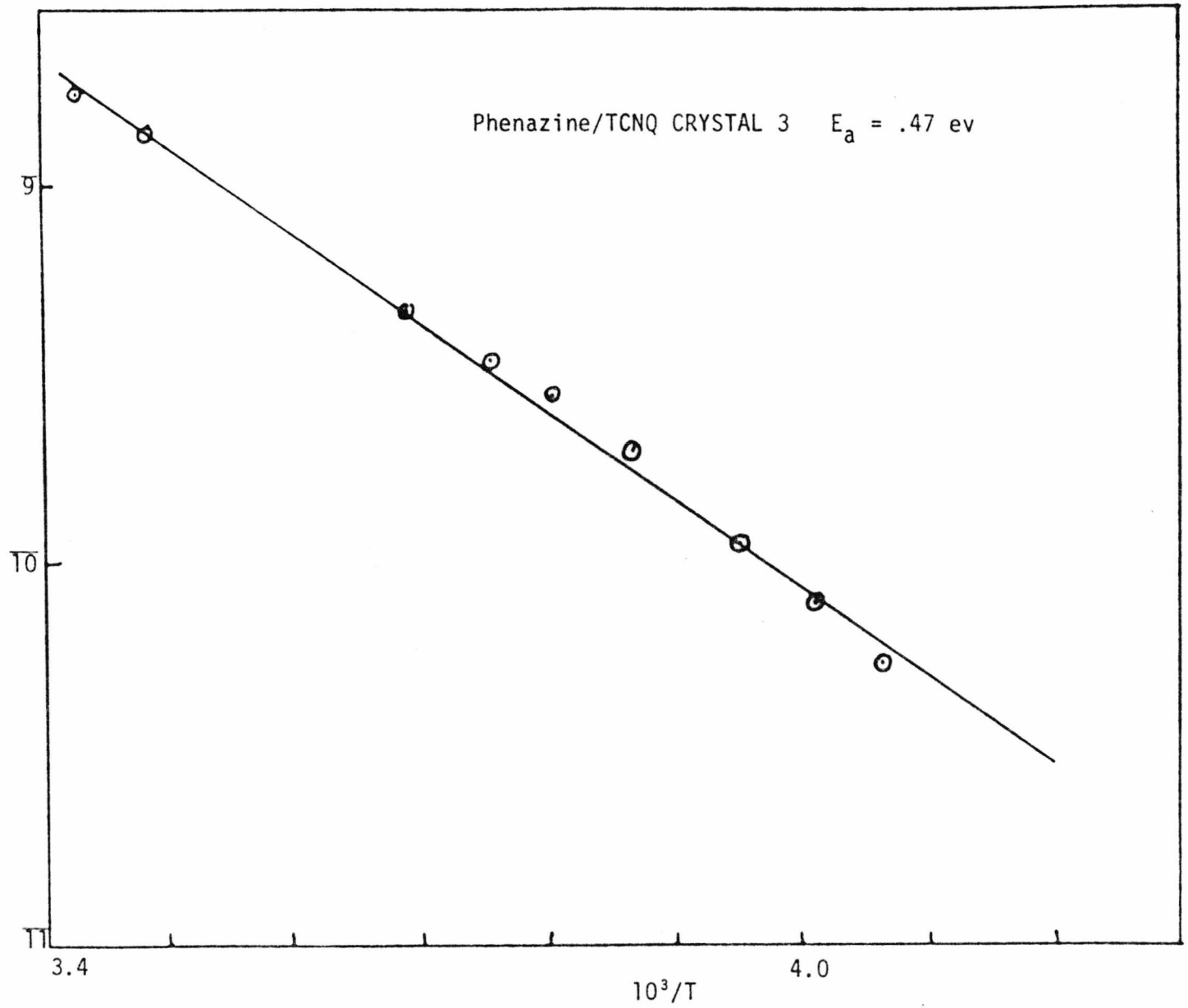
Phenazine/TCNQ CRYSTAL 3 E_a = .47 ev
Log Current
9
10
11
3.4
4.0
$10^3/T$

of log voltage vs log current are presented in Figs. 5.12-5.17.

Activation energies of conduction obtained from the plots of log I vs $\frac{10^3}{T}$ are also tabulated in Tables 5.2-5.5. The plots are also given (Figs. 5.18-5.31). Figure 5.22 indicates the effect of multiple recycling. The change of slope is due to insufficient time given for a steady state to be reached. Figure 5.20, RUN 3 shows recycling with ample time given. Also, Figures 5.20 and 5.28 show the reproducibility of slope between different runs.

5.9 Discussion

Parent Complexes

In Table 5.6 the activation energies for semiconductors in the parent molecular complexes studied in this work are compared with those of other workers. Since, as discussed in Section 5.4, there are no reliable data on polarization energies in molecular complex crystals, only approximate estimates of ΔE are available using Equation 10. In Table 5.6, ΔE values have been calculated assuming that the polarization energies of the components in the complex are the same as those in the pure crystals of the component molecules. Considering that this is an approximation, the agreement between calculated and observed semiconduction activation energies is generally good, consistent with intrinsic conduction. However, as has been pointed out by Munnoch and Wright (1976), activation energies of a similar magnitude could also be accounted for in terms of an extrinsic model, with carriers generated from $TCNQ^-$ impurities. Examination of the preexponential factors for semi-conduction can help to resolve this ambiguity.

For intrinsic conduction,

$$\sigma_0 = 2N_0 e\mu$$

where

μ = carrier mobility

and N_0 = density of states (=density of molecules in the crystal)

For extrinsic conduction,

$$\sigma_0 = (\tfrac{1}{2}N_0 N_i)^{\frac{1}{2}} e\mu$$

where

N_i = density of impurity levels leading to carriers.

In Table 5.7, the apparent mobilities derived on the assumption of intrinsic conduction are listed. These values are of the same order as those found for other complexes by Munnoch and Wright (1976), who also showed that the concentrations of acceptor$^-$ species were such as to require unreasonably large values of μ in order to account for the observed preexponential factors in terms of extrinsic conduction. Since the materials in the present work were purified by the same methods as used by Munnoch and Wright (1976), it is to be expected that this conclusion is also valid for the present materials. The apparent mobilities assuming intrinsic conduction are lower than the experimental room temperature value of 10^{-2} cm.^{2}/vs found for phenanthrene/PMDA , (Mohwald, Haarer & Castro, 1975), and this is to be expected as our crystals are less perfect than those used for drift mobility measurements. As explained in Section 5.5, defects and impurities are expected to reduce mobility.

Semiconduction in the parent complexes therefore has magnitude and activation energy consistent with intrinsic conduction.

Mixed Complexes

As stated in Section 5.1 of this chapter, one of the main objectives

Complexes	Donors I.P. (ev)	E.A. TCNQ (ev)	$P_D^+ + P_A^-$ (ev)	$\frac{I.P. - E.A. - P^+ - P^-}{2}$ (ev)	E This work (ev)	E Literature	Resistivity (Ωcm)
A/TCNQ	7.39	2.88[a]	1.7[b]+2.1[b]	.36	-	.49[c]	2.27×10^{10}[d]
						.75[e]	1.41×10^{13}[d]
							5.3×10^{10}[c]
							5.0×10^{11}[e]
C/TCNQ	7.75	2.88[a]	2.1[f]+2.1	.34	-	.39[c]	8.7×10^{9}[d]
							1.0×10^{9}[d]
							3.3×10^{7}[d]
							2.9×10^{6}[c]
							1.5×10^{8}[c]
Py/TCNQ	7.47	2.88[a]	1.6+2.1	.45	.55	.73[g]	4.5×10^{9}[d]
							3.6×10^{10}[c]
							6.0×10^{10}[i]
Pe/TCNQ	7.15	2.88[a]	1.7+2.1	.24	.65	.64[e]	1.68×10^{11}[d]
						.46[c]	6.00×10^{11}[d]
						.57[i]	1.4×10^{11}[c]
							5.34×10^{11}[i]

TABLE 5.6 COMPARISON OF EXPERIMENTAL VALUES WITH LITERATURE VALUES

TABLE 5.6 COMPARISON OF EXPERIMENTAL VALUES WITH LITERATURE VALUES (Cont'd.)

Complexes	Donors I.P. (ev)	E.A. TCNQ (ev)	$P_D^+ + P_A^-$ (ev)	$\frac{I.P. - E.A. - P^+ - P^-}{2}$ (ev)	E This work (ev)	E Literature	Resistivity (Ωcm)
DBT/TCNQ	8.10	2.88[a]	-	-	.59	.67[e]	8.3×10^{9}[d]
							5.73×10^{10}[d]
							1.0×10^{10}[e]
DBF/TCNQ	8.18	2.88[a]	-	-	.68	.80[e]	3.13×10^{11}[d]
							2.25×10^{11}[d]
							1.0×10^{13}[e]
PHE/TCNQ	8.0	2.88[a]	-	-	.47	.56[e]	1.07×10^{10}[d]
							6.93×10^{9}[d]
							1.43×10^{8}[d]
							5.1×10^{9}[d]
							3.0×10^{8}[e]

[a]Farragher and Page (1967); [b]Seki, Sato and Inokuchi (1980); [c]Vincent and Wright (1974); [d]This work; [e]Organic Semiconductors (1970); [f]Gutman and Lyons (1967); [g]Kokado, Hasegawa and Schneider (1964); [h]Kolninov (1969); [i]Munnoch (1974)

Complex	Density g $cm.^{-3}$	Molecular Weight	RT Resistivity (Ωcm)	Activation Energy (ev)	Pre-Exponential Factor	Apparent Mobility (cm^2/vs)
Anthracene/TCNQ	1.26	382.43	5.0×10^{11}	.75	9.7	1.52×10^{-2}
			5.3×10^{10}	.49	0.04	5.7×10^{-6}
Chrysene/TCNQ	1.362	432.4	1.5×10^{8}	.39	0.03	4.5×10^{-5}
Pyrene/TCNQ	1.302	406.5	4.56×10^{9}	.55	0.44	7.05×10^{-4}
Perylene/TCNQ	1.312	456.5	1.68×10^{11}	.65	0.59	1.05×10^{-3}
Dibenzothiophen/TCNQ	1.357	388.4	8.3×10^{9}	.59	1.15	1.7×10^{-3}
Dibenzofuron/TCNQ	1.325	372.4	3.13×10^{11}	.68	1.01	1.47×10^{-3}
Phenazine/TCNQ	1.344	384.4	1.43×10^{8}	.47	0.62	9.2×10^{-4}

TABLE 5.7

in studying semiconductivity of mixed complexes was to examine changes in resistivity and activation energy as a function of composition. The simplest ideal treatment of such changes assumes constant carrier mobility as composition is varied from one parent complex, across the mixed series, to the other parent complex, as well as constant total density of states involved in carrier generation. (The similarity in the pre-exponential factors found in this work for different complexes (Table 5.7) suggests that these assumptions are justified at least for the parent complexes.) Then for a mixed complex $(\text{Donor 1})_x(\text{Donor 2})_{1-x}\text{Acceptor}$,

$$\begin{aligned} \text{Conductivity} &= x\,\sigma_0 e^{-\Delta E_1/kT} + (1-x)\,\sigma_0 e^{-\Delta E_2/kT} \\ &= x\,\sigma_1 + (1-x)\sigma_2 \end{aligned} \qquad (11)$$

where σ_1 and σ_2 are the conductivities of the two parent complexes and ΔE_1 and ΔE_2 are their semiconduction activation energies.

In Figs. 5.32, 5.33 and 5.34, the actual conductivities of mixed complexes as a function of composition are compared with the ideal trend obtained using the above equation, for Anthracene/Chrysene/TCNQ , Pyrene/Perylene/TCNQ and Dibenzothiophen/Dibenzofuran/TCNQ . From these results, it can be seen that in these systems the conductivity is not a linear or smooth function of composition, nor do the deviations from the ideal trend correlate in any regular way with composition. Since the analytical results reported in Chapter 2 show reproducible composition within a given batch of material, these deviations in conductivity are unlikely to be due to wide variations in the actual compositions of individual crystals selected for conductivity measurements. Furthermore, although there is a range of conductivity values for different crystals of the same composition, this scatter is no greater than that commonly found for crystals

of the parent complexes. Close examination of the data, however, reveals two significant trends. Firstly, as shown in Table 5.8, in almost all cases the variations in conductivity for crystals of a given composition are such that the crystals of larger cross section area have the lowest conductivity. Secondly, in the majority of cases, the conductivities of the mixed complexes are lower than the values expected on the basis of the simple idealised model mentioned above. Both of these observations suggest that the deviations from ideal behaviour are due to irregularities in the crystal lattice, or physical defects in the crystals of mixed complexes. Large crystals are more likely to contain defects than well-formed small crystals. (Cross-section area is chosen as a measure of crystal size because crystals of molecular complexes of this type generally have a needle-shaped habit and conductivity measurements are made along the needle axis. The effective length for conductivity purposes is thus determined by the exact placing of the electrodes on the crystal rather than by the actual original length of the sample before attaching the electrodes. Cross-section area, in contrast, is not determined by the electrodes as the silver paint always completely covers each end of the crystal.) Any irregularity in the crystal lattice will lead to reduction in carrier mobility, and hence to lower conductivity. The fact that in most cases the conductivities of the mixed complexes are less than the ideal expected values, based on the properties of the parent complexes, suggests that there are more defects and irregularities in the lattices of the mixed complexes than in those of the parent complexes. This is expected, since the two different donor molecules will in general not fit onto the available lattice site for a donor molecule with equal facility, and local regions of strain will tend to be produced due to this

FIG. 5.32 CONDUCTIVITIES OF A/C/TCNQ AS A FUNCTION OF COMPOSITION

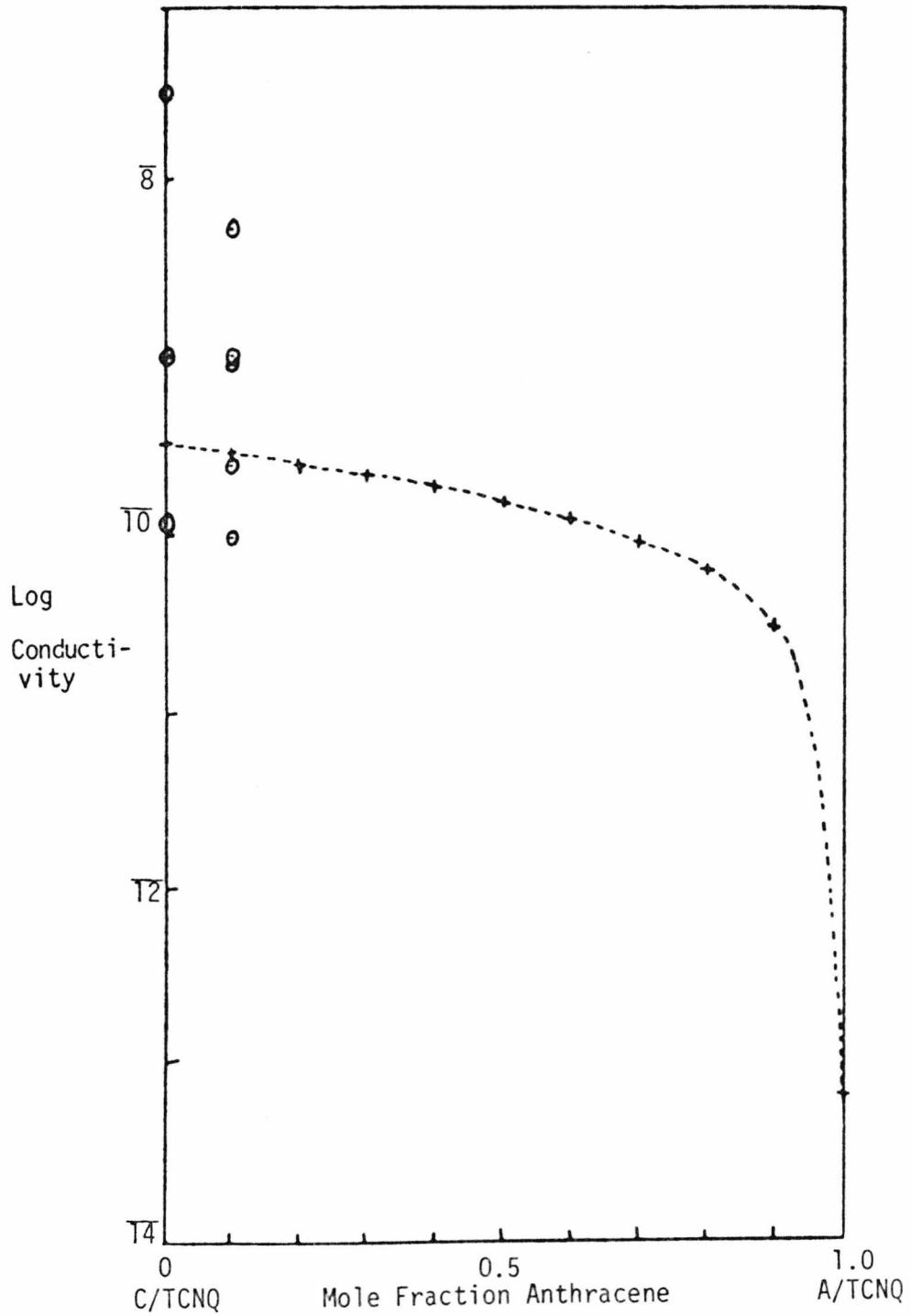

FIG. 5.33 CONDUCTIVITIES OF Py/Pe/TCNQ AS A FUNCTION OF COMPOSITION

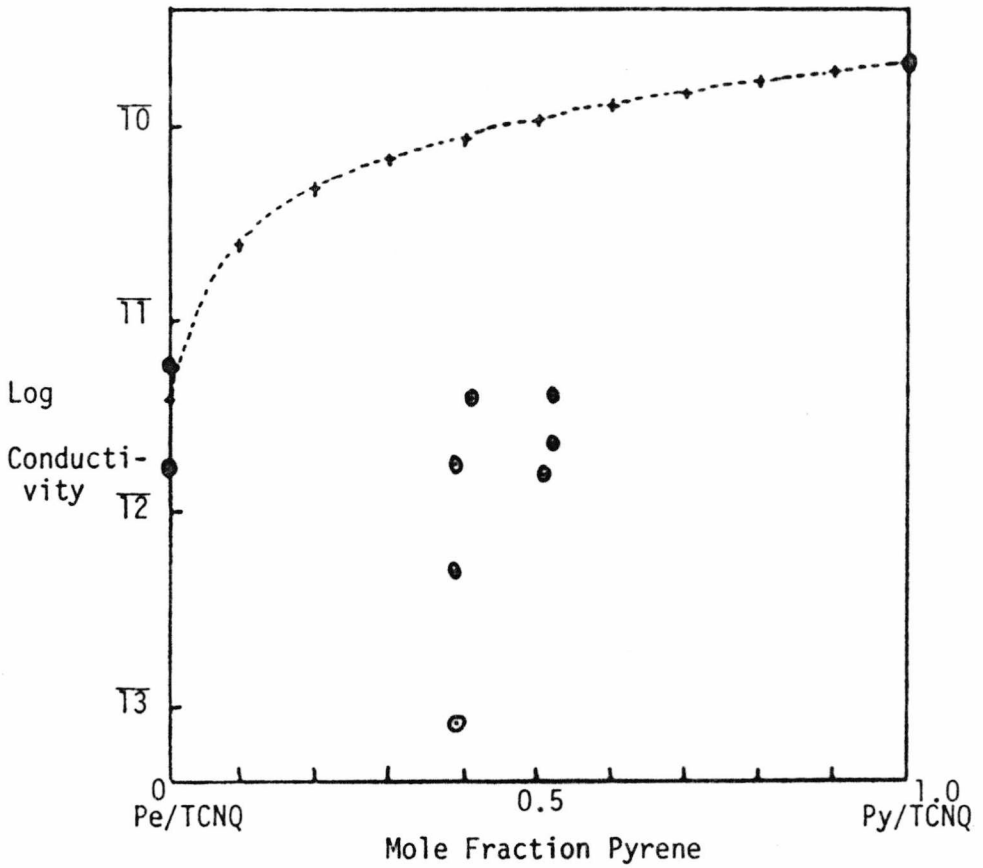

FIG. 5.34 CONDUCTIVITIES OF DBT/DBF/TCNQ AS A FUNCTION OF COMPOSITION

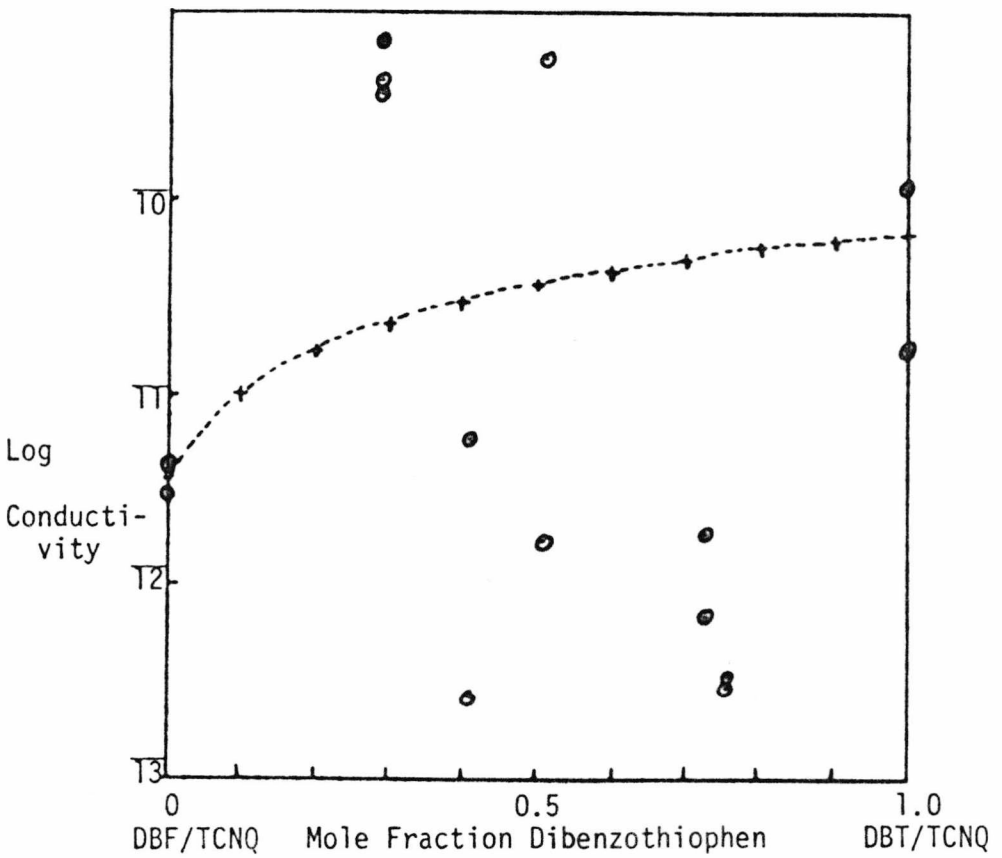

Mixed Complexes	Resistivity (Ωcm.)	Cross Section Area (cm^2)
Anthracene$_{.10}$/	1.86×10^{8}	0.000441
Chrysene$_{.9}$/TCNQ	9.68×10^{8}	0.000576
	1.08×10^{9}	0.000572
	4.08×10^{9}	0.000924
	1.04×10^{10}	0.000945
Pyrene$_{.39}$/Perylene$_{.61}$/	5.58×10^{11}	0.00085
TCNQ	1.96×10^{12}	0.00161
	1.12×10^{13}	0.00587
Pyrene$_{.52}$/Perylene$_{.48}$/	2.44×10^{11}	0.0009
TCNQ	4.29×10^{11}	0.0014
Dibenzothiophen$_{.29}$/	1.45×10^{9}	0.00015
Dibenzofuran$_{.71}$/TCNQ	2.27×10^{9}	0.00017
	2.69×10^{9}	0.00016
Dibenzothiophen$_{.41}$/	1.71×10^{11}	0.000513
Dibenzofuran$_{.59}$/TCNQ	3.7×10^{12}	0.000493
Dibenzothiophen$_{.51}$/	1.78×10^{9}	0.00023
Dibenzofuran$_{.49}$/TCNQ	5.7×10^{11}	0.00046
Dibenzothiophen$_{.73}$/	5.3×10^{11}	0.00016
Dibenzofuran$_{.27}$/TCNQ	1.4×10^{12}	0.00023
Dibenzothiophen$_{.76}$/	3.0×10^{12}	0.000504
Dibenzofuran$_{.24}$/TCNQ	3.2×10^{12}	0.000544

TABLE 5.8 COMPARISON OF RESISTIVITY AND CROSS-SECTIONAL AREA

effect. Similar effects have been observed in mixed charge transfer salts of tetrathionaphthacene (TTN) with various substituted tetracyanoquinodimethanes (Wheland, 1976), where the mixed salts had conductivities that were never significantly better, and frequently worse, than those of either of the parent salts. It is perhaps surprising that the deviations from the ideal behaviour are similar for compounds where the two parent complexes have very similar lattice types and donor shape and size (Dibenzothiophen/Dibenzofuran/TCNQ) and compounds where the two parents have different lattices and donor shapes and sizes (Pyrene/Perylene/TCNQ). Larger deviations would be expected for the latter type. However, crystal structure studies (Chapter 3) have shown that the dibenzofuran/TCNQ complex lattice structure permits disorder at the donor site, and both the semiconductivity results reported in this Chapter and the photoconduction results of Chapter 6 support the conclusions that crystals of the Dibenzothiophen/Dibenzofuran/TCNQ system contain high defect concentrations which may arise from the disorder possibility. X-ray powder diffraction also shows that the mixed complexes of Pyrene/Perylene/TCNQ have a new lattice structure, different from either of the parent complexes. This new structure is evidently more stable than structures obtained by fitting a different donor molecule onto the donor site in either of the parent complex structures, and may therefore be expected to involve less lattice strain and defect formation than in the latter structure.

For an ideal system, the temperature dependence of semiconductivity should also follow Equation (11), that is, the $\log(\sigma)$ v $\frac{1}{T}$ plot should correspond to the appropriate sum of two lines with slopes determined by ΔE_1 and ΔE_2. In general, over a wide enough temperature range, this should not yield a single straight line plot of $\log\sigma$ v $\frac{1}{T}$. However,

for the systems studied here the temperature range accessible is very limited, at the upper end by the tendency of some complexes to decompose on heating, and at the lower end by the low conductivity of the materials rendering measurements impossible. These limitations only permitted measurements as a function of temperature for the Pyrene/Perylene/TCNQ and Anthracene/Chrysene/TCNQ systems, and over the limited temperature range the data obtained could be fitted well by a single straight line on a $\log\sigma$ v $\frac{1}{T}$ plot (see Figs. 5.18-5.31). The apparent semiconduction activation energies obtained from the slopes of these lines are shown in Figs. 5.35 and 5.36, as a function of complex composition. Within experimental error, the majority of these values lie in the range between the values found for the parent complexes. The exceptions are two crystals of Pyrene/Perylene/TCNQ , with apparently higher activation energies than expected. These data should be treated with caution, however, for the following reasons:

1) The temperature range over which measurements were made is small, so the accuracy of the derived activation energies is limited.
2) Raising the temperature may anneal out defects in the crystals, leading to contributions affecting the temperature dependence of conductivity.
3) The overall temperature dependence of semiconductivity is determined by the temperature dependence of mobility as well as by the activation energy for charge carrier generation. Although measurements by Schein (1977);Schein, Duke and McGhie (1978) on anthracene and naphthalene etc. suggest temperature independent

FIG. 5.35 ACTIVATION ENERGY AGAINST COMPOSITION FOR ANTHRACENE/CHRYSENE/TCNQ

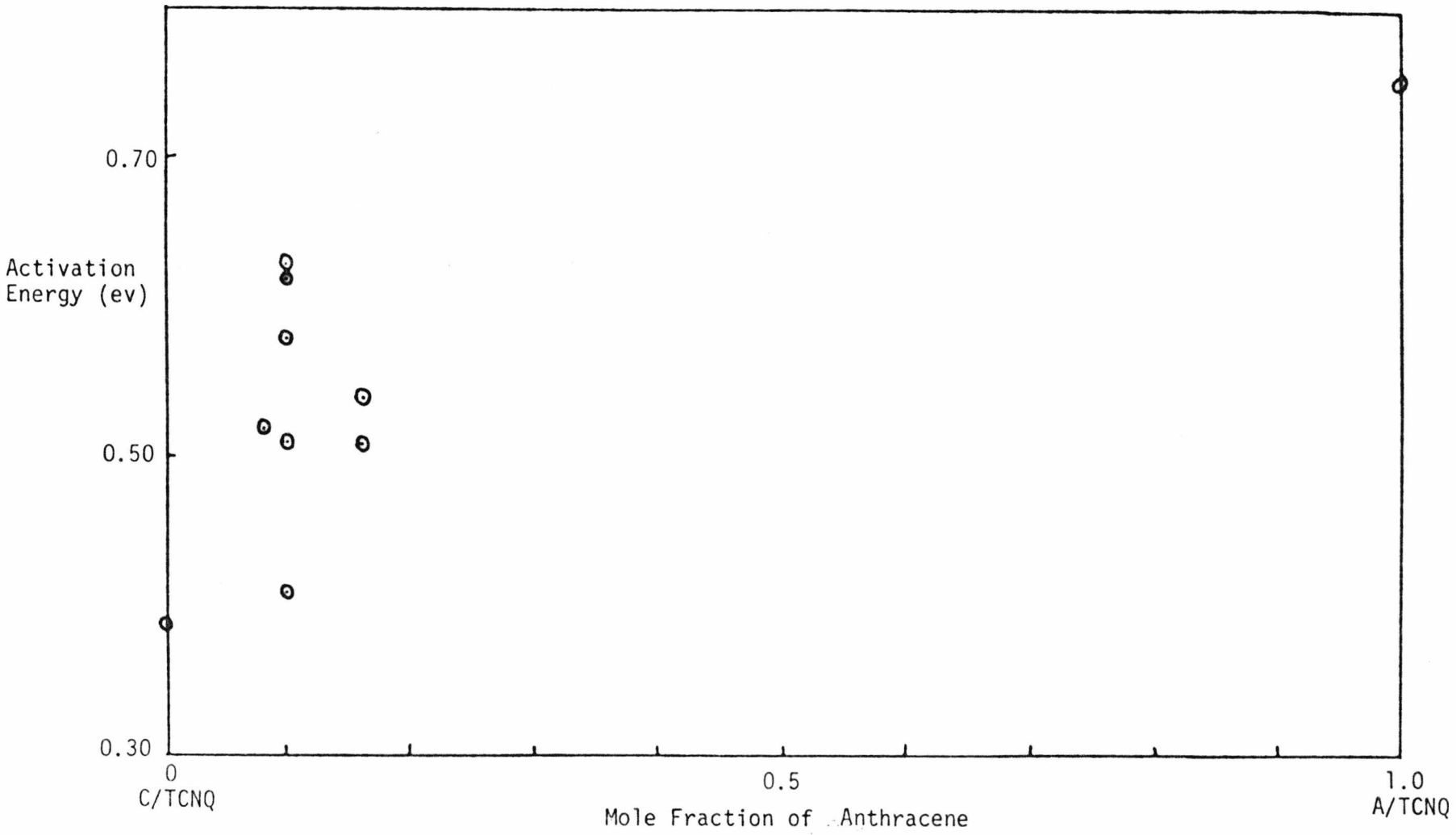

FIG. 5.36 ACTIVATION ENERGY AGAINST COMPOSITION FOR PYRENE/PERYLENE/TCNQ

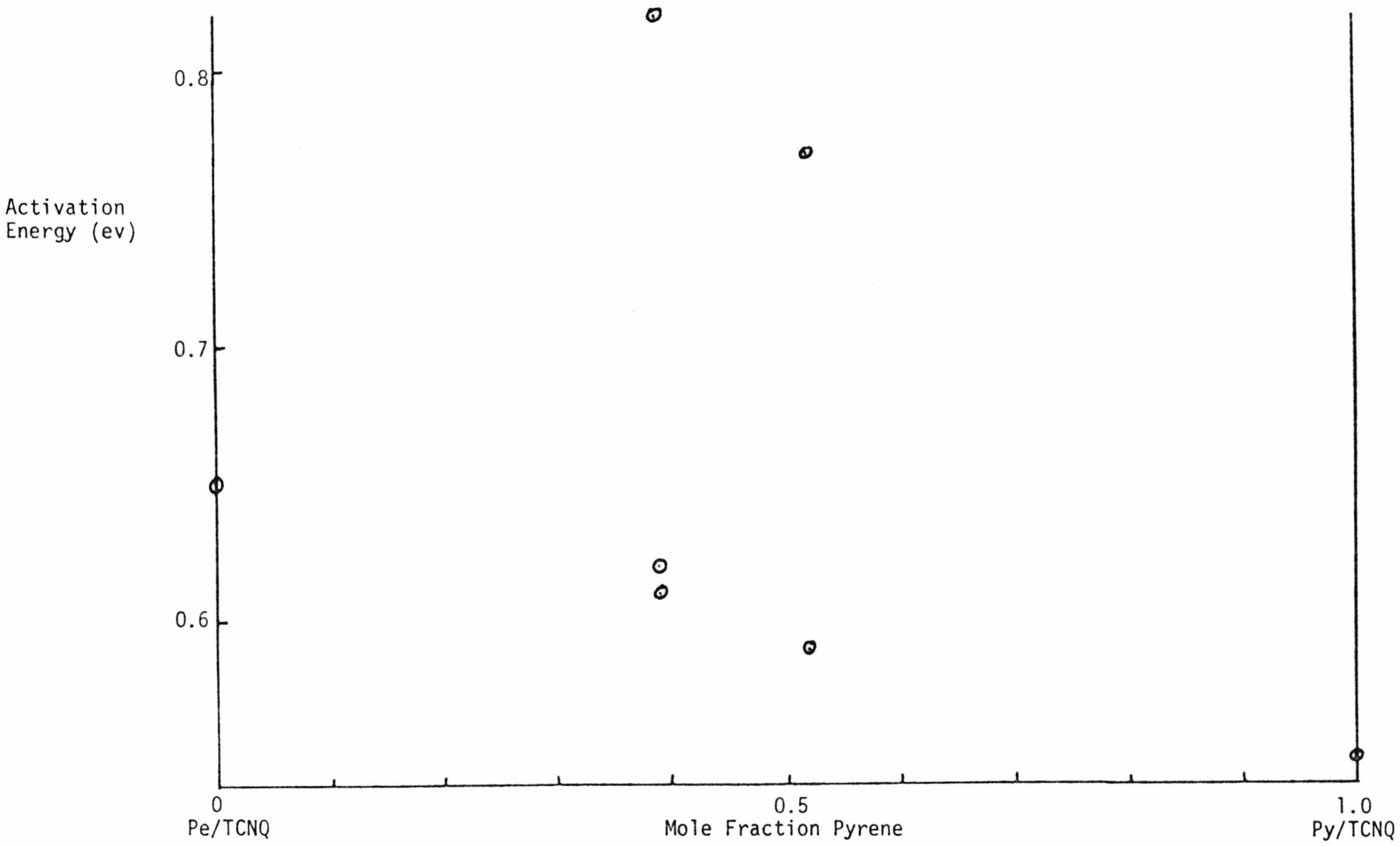

mobility in the temperature range of our studies, the presence of defects (as indicated by the low mobilities derived from pre-exponential factors as discussed earlier) will lead to larger temperature dependence of mobility in the materials studied here.

4) Temperature dependent trapping phenomena also affect variation of conductivity with temperature.

Two experimental observations in the present work are relevant to these factors. Firstly, for two of the Pyrene/Perylene/TCNQ mixed complex crystals, repeating the measurement of conductivity as a function of temperature gave data for which the slopes of $\log\sigma$ v $\frac{1}{T}$ plots were identical. Thus, factor 1) and 2) are probably of minor significance. Secondly, in many cases, it took a long time for the current to reach a final steady value after a change in temperature. This suggests that trapping phenomena, which enter into 3) and 4) are significant. A full investigation of the density and distribution of traps and defects in the sample, which would be required for detailed interpretation of these results, would be difficult for these materials, and was not felt to be justified in view of the materials limitations discussed earlier.

5.10 Conclusions

The semiconductivity properties of the mixed complexes studied are consistent with the predictions of a simple model combining the properties of the parent complexes in proportion to their composition ratio in the complexes, modified by the presence of traps and physical defects in the crystals. The limitations on the range of materials that can be prepared as single crystal mixed complexes severely limit the scope for producing controlled conductivity variations by doping one molecular complex with

another of different conductivity. This is in marked contrast to the wide range of variation achieved by doping of inorganic semiconductors. There are no clear correlations between composition of a mixed complex and the irregular variations in conductivity properties ascribed to the influence of traps and defects, nor are there any marked discontinuities in conductivity properties which might reflect structural change as composition is varied.

During the course of the present work, two publications appeared from other groups, showing that larger conductivity variations can be produced by doping of charge transfer salts in favourable cases. The most dramatic effect concerned the increase of 10^9 in the conductivity of N-ethylphenazinium/TCNQ produced when the compound was crystallized in the presence of 15% phenazine (Sandman, 1979). This was attributed to the conversion of a normal mixed stack 1:1 salt into a segregated stack structure, initiated by complexing between phenazine and N-ethylphenazinium cations. The role of phenazine is reported to be quite selective - other similar molecules do not produce the same effect. Thus, although in principle other poorly conducting 1:1 salts might be converted to highly conducting segregated stack forms, it is not a simple matter to identify the ideal neutral molecule which will produce the effect for a given salt. The other work reported preparation of a series of complexes (N-methylphenazinium)$_x$(Phenazine)$_{1-x}$TCNQ with $0.5<x\leqslant 1.0$, in which the degree of band filling varied continuously with composition, reflected in the conducting properties. (Epstein & Miller, 1978.) As in the previous case, it is likely that this specific example is a relatively isolated case, owing to the requirement that the neutral molecule must have similar solubility and molecular shape.

It may be concluded that the scope for wide, controlled variation of conductivity properties of molecular complexes and charge transfer salts by preparing mixed complexes or salts is very limited. More success in producing conductivity variations in molecular crystals has been achieved by doping crystals of donor molecules with electron acceptors, either in the form of bulk doping (example: doped polyacetylene, I_2 doped phthalocyanine, etc.) or surface doping (example: the effect of adsorbed electron accepting gases on conductivity of phthalocyanine, perylene, etc. (Van Ewyk, Chadwick & Wright, 1980)).

* * * * * *

Chapter 6

Photoconductivity

6.1 Introduction

Although structural and spectroscopic studies of mixed molecular complexes have been reported (Koizumi & Matsunaga, 1973;,1974; Wright, Ohta & Kuroda, 1976), very little work has been reported on their photoconductivity. Studies of photoconductivity in π-π^* molecular complexes have mainly focussed on two component systems of π donor and π acceptor.

In this chapter, studies of the spectral responses and the relative magnitude of photoconduction and their dependences on light intensity are reported for several mixed complex systems and correlated with spectroscopic, structural and defect properties of the complexes.

In charge transfer complexes, an exciton state exists between the ground and the conduction states. The exciton state is of the form D^+A^- (Wannier exciton) which is a coulombically bound species of D^+ and A^-. A pair of charge carriers is generated when this exciton is separated to isolated D^+ and A^- species. D^+A^- states are produced by single photon excitation of charge transfer transitions of the complex. Once such excitons are created they may undergo the following processes:

1) Return to ground state by a radiationless transition.
2) Return to ground state accompanied by fluorescence emission.
3) Dissociation into two charge carriers by a thermal process (interaction with a phonon).
4) Dissociation into two charge carriers by collision between two excitons, where one returns to the ground state while the energy liberated separates the other.

5) Dissociation into two charge carriers by absorption of a photon (photoionization).

6) Dissociation into two charge carriers by the Poole-Frenkel effect (effect of electric field).

7) Dissociation into two charge carriers by interaction with an impurity, the electrodes or the surface.

8) Dissociation by interaction with an excited state of just the donor or just the acceptor.

Processes 3,6,7 are one-photon processes, while processes 4,5,8 are two-photon processes. The proportion of charge transfer excitons that are separated into charge carriers can be represented by a quantum yield parameter (Section 6.2). For steady state photoconductivity, the rate of carrier generation is equal to the rate of carrier loss. Carrier loss may occur via three main processes namely:

1) electrode loss

2) trapping loss

3) recombination loss.

The effect of trapping in steady state measurements is neglected because this effect only affects (reduces) the mobility, provided long enough time is given to reach equilibrium or steady state. The effect of electrode loss and recombination loss will be discussed in Section 6.2 in conjunction with discussion on intensity dependences and quantum yield parameter.

6.2 Steady State Photoconductivity

In the steady state, rate of carrier generation = rate of carrier loss.

The magnitude of the steady state photocurrent depends on the charge carrier concentration at which these two rates become equal. As outlined above, there are in principle carrier generation processes involving both one and two photons per pair of charge carriers generated, as well as carrier loss processes dependent on carrier concentration and (carrier concentration)^2. Specific combinations of these generation and loss processes lead to characteristic dependences of photocurrent (Iph) on light intensity (L).

$$I\ ph \propto L^n$$

Four idealised cases may be distinguished:

1) For a charge carrier generation process involving a single photon per charge carrier pair, with carrier loss by recombination negligible compared to carrier loss to the electrodes (i.e. transit time much shorter than lifetime)

Generation rate $\propto L^{1.0}$

Loss rate $\propto$ steady state charge carrier concentration N .

Now, $\sigma = Ne\mu$

therefore $N = \sigma/e\mu = i\ell/ve\mu wt$

where

ℓ = interelectrode spacing

w = crystal width

t = crystal thickness

i = steady state current

v = applied voltage

For crystals mounted in the manner used in this work (needle shaped crystals with electrodes on the needle ends, and illumination of needle faces between the electrodes).

i.e. $N \alpha$ steady state current (i)

therefore when generation rate = loss rate

$k_1 L^{1.0} = k_2 i$ where k_1 and k_2 are constants

hence $i \alpha L^{1.0}$

b) For two-photon charge carrier generation processes in the same circumstances,

generation rate $\alpha L^{2.0}$

loss rate $\alpha N \alpha i$

therefore $i \alpha L^{2.0}$

c) For single photon charge carrier generation with carrier loss dominated by bimolecular recombination (carrier lifetime short compared to transit time)

generation rate $\alpha L^{1.0}$

loss rate $\alpha N^2 \alpha i^2$

therefore $i \alpha L^{0.5}$

d) For two photon charge carrier generation in the same circumstances

generation rate $\alpha L^{2.0}$

loss rate $\alpha N^2 \alpha i^2$

therefore $i \alpha L^{1.0}$.

In practice, many real systems do not correspond exactly to any of these ideal cases since charge carriers are lost by recombination as well as to the electrodes, and, less commonly, they may be generated by several mechanisms operating at the same time, some involving single photons and others involving

two photons. For molecular complexes of the type studied in this work, previous workers (Akamatu & Kuroda, 1963; Vincent & Wright, 1974) have observed that, so long as the crystals are thick enough for near 100% absorption of incident light irrespective of polarisation direction of the light, the photoconduction action spectrum shape and magnitude are independent of the polarisation direction of incident light relative to the crystal axes. Since charge transfer transitions in the crystalline complexes are strongly polarised, this observation shows that the mechanism of carrier generation from charge transfer excited states is dependent on the total number of such states rather than on their density. This strongly supports single photon mechanisms of charge carrier generation. Hence, depending on the balance of recombination losses and carrier loss to the electrodes, the power law of the dependence of photocurrent on light intensity is expected to be in the range 0.5-1.0. This is found in the studies reported later in this chapter, although n is never close to 0.5 or 1.0, always nearer 0.7 (strictly the combination of both unimolecular and bimolecular carrier loss processes, should not yield a linear log i v log L plot, but over the limited range of intensity accessible in the present work no curvature is evident). These results suggest that the two types of carrier loss processes occur to roughly comparable extents in π-π^* molecular complex crystals.

Using this approximation, the total carrier loss is estimated as twice the loss rate of carriers to the electrodes. Hence

$$QLA = \frac{2I_{ph}}{e}$$

where

A = illuminated area of crystal

L = light intensity (photons/unit area/sec.)

and Q = is a parameter related to the quantum yield for charge carrier generation from the optically excited charge transfer states.

An independent test of the validity of this approximation has been provided by Vincent and Wright (1974) using an approach based on a simple collision model for carrier recombination.

The number of collisions per second per unit volume resulting in recombination is given by $Z = \frac{\pi d^2 N^2 \overline{C}}{\sqrt{2}}$

where

$\overline{C}$ is the mean carrier velocity

and d is the distance below which carriers spontaneously recombine.

Now

$$\overline{C} = \frac{v\mu}{\ell}$$

and

$$N = \frac{i\,\ell}{ve\mu wt}$$

Hence

$$Z = \frac{\pi d^2 \cdot i^2\, \ell^2}{\sqrt{2} wte^2 \mu v}$$

This should be approximately equal to the loss rate to the electrodes, i/e.

Hence

$$i/e \approx \frac{\pi\, d^2 i^2 \ell^2}{\sqrt{2} wte^2 \mu v}$$

or

$$\frac{d^2}{\mu} \approx \frac{\sqrt{2} wtev}{\pi i\, \ell^2}$$

Data for many actual crystals (where w, t, ℓ, i and v are known) yield values of $\frac{d^2}{\mu}$ consistent with literature estimates of $d = 10$ nm and $\mu \geq 10^{-7} m^2/v.s.$.

Although this quantum yield parameter is approximate, comparisons of its value for different materials can be justified if:

1) The same field gradient is used throughout the experiments, or if the results are corrected to values at this field gradient provided Ohm's law is followed.

and 2) Charge carrier effective mobilities are similar for all samples. (This requires that trap densities and distributions are not grossly different in different samples.)

Variations in effective carrier mobility from sample to sample generally result in some scatter of Q values for any material, and limit discussion of variations in Q from one method to another to cases where the differences are large.

6.3 Photoconductivity and Charge Transfer Spectra

The photoconduction spectral responses can be categorised into two groups:

1) Those that photoconduct in the charge transfer absorption region or in the region where the absorption is mainly due to a donor or an acceptor singlet transition (high energy region).
2) Those that photoconduct in the long wavelength region (low energy region).

A photoconduction spectrum that follows the charge transfer absorption is due to the presence of $D^{+}A^{-}$ states, analogous to Wannier excitons, being generated by the light.

The photoconduction on the high energy side of the first charge transfer band can be explained in terms of an energy level diagram for photoconduction in crystalline molecular complex as shown in Fig. 6.1 (Vincent & Wright, 1974).

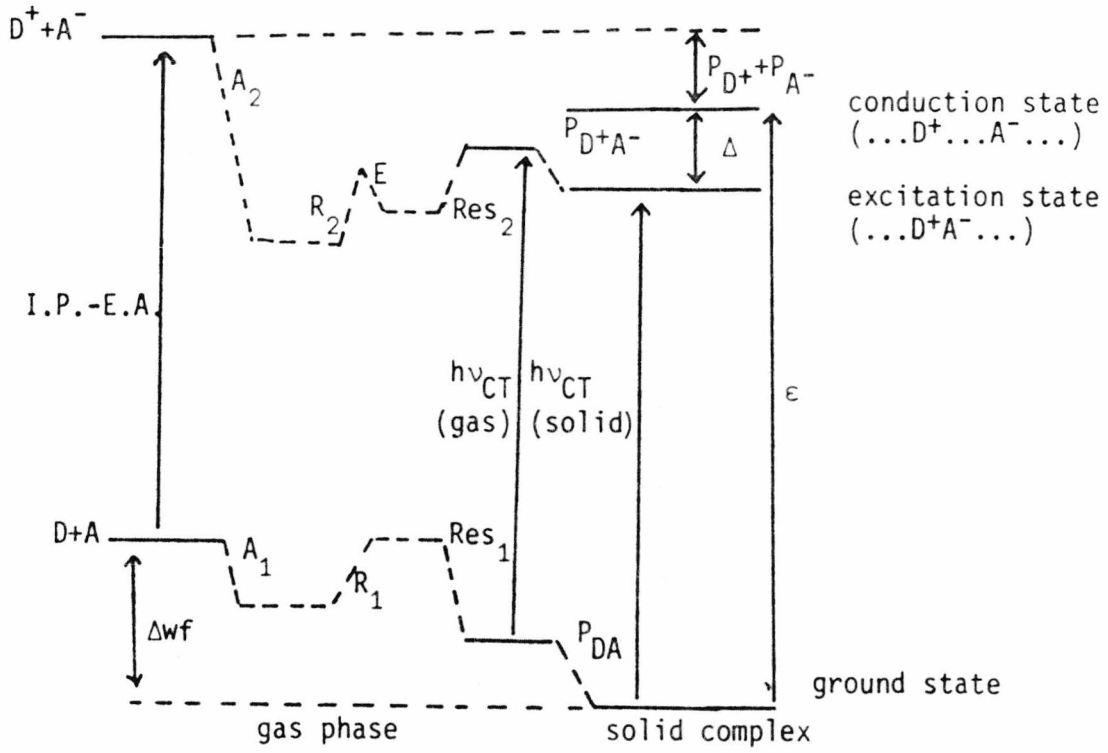

FIG. 6.1 ENERGY LEVEL DIAGRAM FOR PHOTOCONDUCTION IN CRYSTALLINE MOLECULAR COMPLEXES. (Δwf=energy of formation of complex DA in solid phase. A_1 and A_2 are attractive forces, other than charge-transfer resonance forces, in ground and excited state species, respectively. R_1 and R_2 are the corresponding repulsive forces. E=exchange energy in excited state. Res_1 and Res_2 are pertubations of ground and excited states due to charge transfer resonance. P_{DA}, $P_{D^+A^-}$, P_{D^+} and P_{A^-} are the interaction energies between DA, D^+A^-, D^+ and A^-, respectively, and the crystal lattice.)

Peak photoconduction can occur to the high energy side of the charge transfer maximum if the conduction state is of higher energy than the excited state and/or the separation of the charge carriers has a high activation energy. The energy gap Δ of the separated charge carriers and the charge transfer excited state is given by:

$$\Delta = \varepsilon - h\nu_{CT} \quad (1)$$

$$\varepsilon = \text{I.P.} - \text{E.A.} - P_{D^+} - P_{A^-} + \Delta wf \quad (2)$$

$$h\nu_{CT} = \text{I.P.} - \text{E.A.} - A_2 + R_2 - E + Res_2 - P_{D^+A^-} + \Delta wf \quad (3)$$

therefore

$$\Delta = A_2 - R_2 + E - Res_2 + (P_{D^+A^-} - P_{D^+} - P_{A^-}) \quad (4)$$

Δ depends on many factors which are difficult to account for and is therefore very difficult to predict the value of Δ. However Δ is not the only factor which determines the maximum photoconduction as the hopping process needs an activation energy for the charge carriers to move and this must be provided irrespective of the value of Δ if carrier generation is to occur. In cases where both of these energy requirements are met, the photoconduction action spectrum follows the charge transfer absorption spectrum. In other cases the required energy may be provided by excitation to higher vibrational energy levels of the charge transfer excited state. However, appreciable photoconduction is often observed when the singlet transition of donor and/or acceptor overlap with charge transfer band. In such cases, a mechanism involving interaction of charge transfer and singlet excited states may be important. A possible mechanism has previously been proposed (Vincent & Wright, 1974).

Such a mechanism would require overlap between adjacent donor (or acceptor) molecules, but the excitation need not be on adjacent molecules

FIG. 6.2 D^+A^- ION PAIR SEPARATION BY INTERACTION WITH DONOR OR ACCEPTOR SINGLET EXCITED STATES

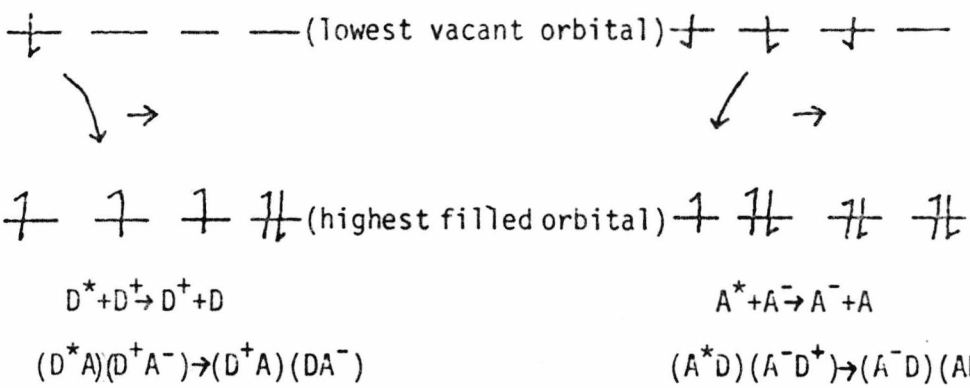

initially since the singlet (Frenkel) exciton is mobile in the lattice and could readily diffuse to the less mobile charge transfer (Wannier) exciton.

Photoconduction responses in the long wavelength region have been observed by several workers (e.g. Akamatu & Kuroda, 1963; Bauser & Ruf, 1969; Mukherjee, 1970). Akamatu and Kuroda observed that in pyrene with TCNE , bromanil and trinitrobenzene, the photoconduction action spectra do not coincide with the charge transfer bands and suggested that in these weak charge transfer complexes, the excited state associated with the charge transfer band cannot contribute to conduction. The two photoconduction peaks for each complex are assigned to primary and secondary photoconduction at shorter and longer wavelengths respectively. Two possible mechanisms were proposed for secondary photoconduction; direct optical excitation of trapped carriers to conduction levels, and exciton dissociation at defects. A general observation is that in all the three complexes,

the maximum secondary photoconduction was observed at the threshold of a charge transfer band. This led to the conclusion that a charge carrier is produced as a result of energy transfer from a charge transfer exciton to an electron trapped at a defect. Bauser and Ruf (1969) observed an inverse relationship between photoconduction action spectrum and absorption spectrum with also an additional long wavelength peak. It was suggested that the photocurrent depended on crystal purity, injection capability of the anode, applied voltage and light intensity. An interpretation was given in terms of two competitive processes; generation of carriers at the surface via singlet excitons, and detrapping in the bulk mainly by triplet excitons. Mukherjee (1970) reported work on complexes of dibenzothiophen with different acceptors. Correlation of photocurrent maxima vs CT absorption maxima and the photocurrent maxima vs CT absorption edges yielded straight line plots. This suggests that carrier generation is initiated by the optical excitation of the CT complexes.

6.4 Photoconductivity and Crystal Structure

As discussed in Section 6.3, the energy level diagram for photoconduction shows that many factors are involved in determining the relative energy levels of the charge transfer excited state and the conduction state. Many of these factors are influenced by crystal structure.

The orientation of the molecules in a crystal is determined by a balance of a number of intermolecular forces; including the charge transfer stabilization energy. The various forces involved are discussed in Chapter 3. A theoretical study of the influence of charge transfer interactions on the structures of π-π^* electron donor acceptor molecular complexes led Mayoh and Prout (1972) to conclude that

i) the presence of hydrogen bonding, strong dipole-dipole or charge-dipole interactions determine the donor-acceptor orientation. Interaction between bulky groups on donor and acceptor may occasionally be of importance;

ii) in the absence of these large directional intermolecular forces CT stabilization energy must be nearly maximised in the observed orientation, unless

iii) the largest CT stabilization energies are obtained for a near centre-on-centre stacking of donor and acceptor molecules. In this case the necessity for close packing may force an alternative orientation if donor and acceptor molecules are of dissimilar size and shape.

Generally the optimum charge-transfer overlap is preferred unless there are very unfavourable circumstances as mentioned above. Vincent and Wright (1974) proposed that for good photoconductivity, there are two structural requirements:

i) π orbitals of adjacent donor molecules or adjacent acceptor molecules(but not both) should overlap appreciably in the crystal and

ii) the relative orientation of the donor with respect to the acceptor should only produce poor overlap of π orbitals involved in charge transfer transition.

Projections of donor-donor overlap or acceptor-acceptor overlap provide a good means of predicting photoconductivity. For several of the

complexes in the present work, the acceptor-acceptor overlap may be the largest because of the more open structure of TCNQ . For example, the cyanide arms of TCNQ have a better chance of overlapping with neighbouring TCNQ molecules than is the case for the more compact donor molecules. Moreover, in the excited state, the acceptor has an occupied anti-bonding orbital which will extend the size of its excluded volume while the donors, having lost an electron becoming a positive ion, will contract relative to their ground states.

Disorder and twinning are also common in many molecular complex crystals, and contribute to defect formation.

The structures of the complexes studied in this work are discussed in Chapter 3, and the relevance of these structures to the results reported in this chapter is discussed in Section 6.8.

6.5 Apparatus

The Optical System (Fig. 6.3)

In addition to the apparatus used in Chapter 5, an optical system is also required for measurements of photoconduction of molecular complexes. The crystal should be illuminated with a uniform monochromatic light of known intensity throughout the region under investigation. The source used was a white light source consisting of a 55 watt , 12 volt quartz halogen bulb powered by a mains transformer and a variac. A Grubb Parsons M2 grating monochromator was used in preference to a prism monochromator because it minimised light loss. This model has an optical bench attachment. Suitable mirrors could be placed on the optical bench so as to focus the light onto the crystals through the side window of the glass cell, mentioned in Chapter 5, Section 5.6. Provisions were made for the

FIG. 6.3 THE OPTICAL SYSTEM

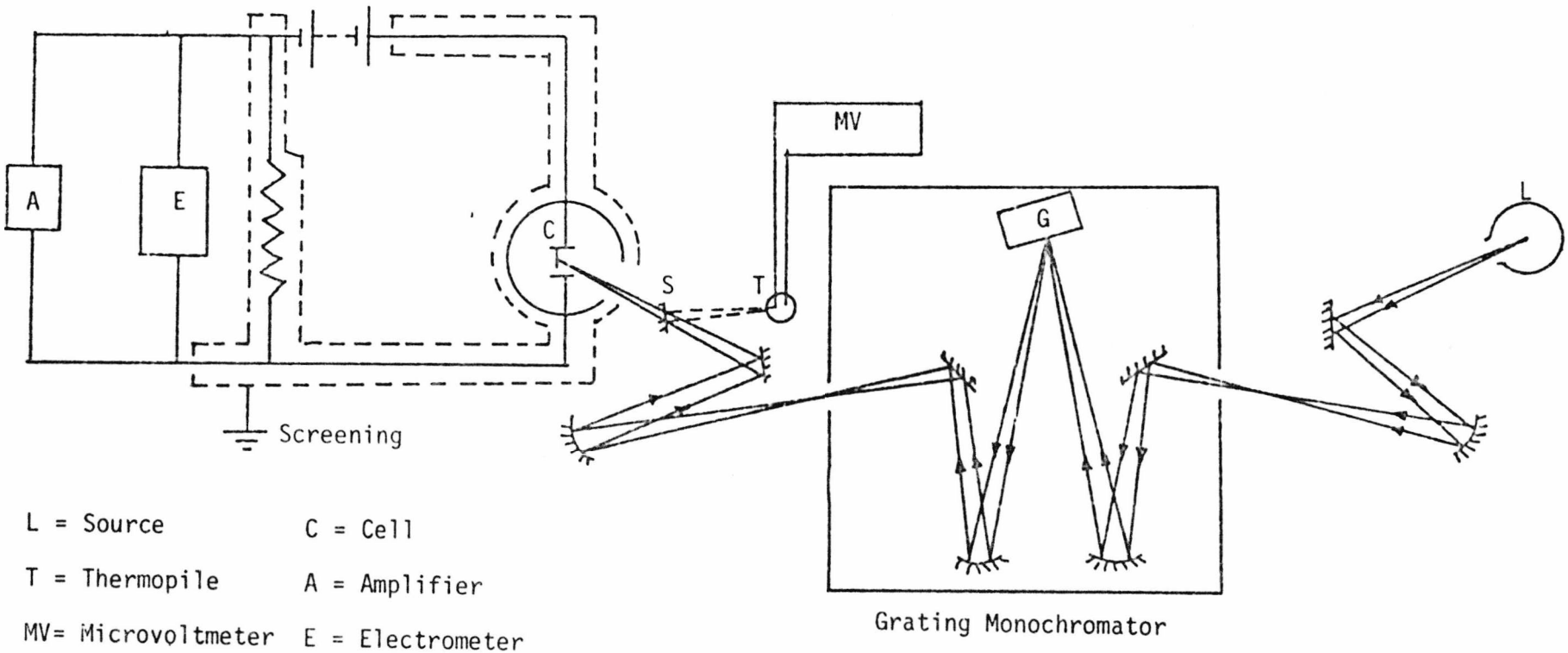

L = Source C = Cell

T = Thermopile A = Amplifier

MV= Microvoltmeter E = Electrometer

G = Grating S = Solenoid operated mirror

measurement of light intensity used. A thermopile was chosen to measure the intensity because it acted as a black body and its sensitivity was wavelength-independent. The thermopile used was a room temperature compensated Hilger Schwartz thermopile. The output of the thermopile was monitored by a Comark microvoltmeter. The monochromated light was redirected to the thermopile by means of a solenoid operated mirror. The intensity of light was varied by adjusting the power supplied to the lampsource by a variac.

The slit width of a monochromator was fixed and suitable filters were used to prevent any interference from second order diffraction.

6.6 Experimental

Photoconduction Spectral Response Run

Each spectral response run was carried out over the range 450-1000 nm. Filters were used to cut off ultraviolet light and also to eliminate second order diffraction effects. A suitable magnitude of light intensity (10μv thermopile output, typically 10^{18} photons/m^2/s) was chosen. The same intensity of light and slit width were used throughout the experiment. With a known applied voltage or field gradient, the steady state dark current was measured. A known intensity of light, was directed to the crystal in the cell and the total current registered was measured. A chart recorder was used to monitor the steady state current. The photocurrent is the difference between the total and the dark current. The light was then taken away from the crystal and the current was allowed to come to its steady state dark value again. The procedure was repeated at 10 or 20 nm intervals until enough points were obtained. For each wavelength the intensity of light was readjusted to 10μv and the dark current was allowed to come down to its original value or a steady state value.

The photoconduction spectral response was obtained by plotting

photocurrents (corrected to 500 v/cm field gradient and unit area of illumination) against wavelengths.

Intensity Dependence Study

The intensity dependence study was done by varying the light intensity and observing the photocurrent at each intensity. The study was done at several fixed wavelengths. The wavelengths chosen, usually spanned the peak in the spectral response curve. Studies over this region would indicate that the response was not due to a varying recombination rate if the intensity dependence was found constant.

The results are presented as plots of log[Iph] against log[light intensity]. As mentioned earlier, such plots should strictly only be exactly linear for the special cases where the power law of intensity dependence of photocurrent is 0.5 , 1.0 or 2.0 , but over the limited range of light intensity covered in these studies, effectively linear plots of slopes different from these ideal cases were obtained.

6.7 Results

Crystal No.	Dimensions L	W	T	Iph at 530 nm corrected to 500v/cm/unit area	Q
1(Subl.)	.190	.080	.036	4.0×10^{-12}	3.7×10^{-7}
2(Subl.)	.177	.051	.028	run 1 7.3×10^{-12}	6.8×10^{-7}
				run 2 7.2×10^{-12}	6.7×10^{-7}
3(Soln.)	.161	.024	.019	run 1 3.5×10^{-11}	3.3×10^{-6}
				run 2 2.38×10^{-11}	2.2×10^{-6}
4(Soln.)	.140	.024	-	run 1 1.58×10^{-10}	1.5×10^{-5}
				run 2 1.98×10^{-10}	1.9×10^{-5}

TABLE 6.1 MAGNITUDES OF QUANTUM YIELD PARAMETERS (Q) AND PHOTOCURRENTS OF SOLUTION AND SUBLIMATION GROWN CRYSTALS OF ANTHRACENE/PMDA

FIG. 6.4 SCALED PHOTOCONDUCTION ACTION SPECTRA OF ANTHRACENE/PMDA

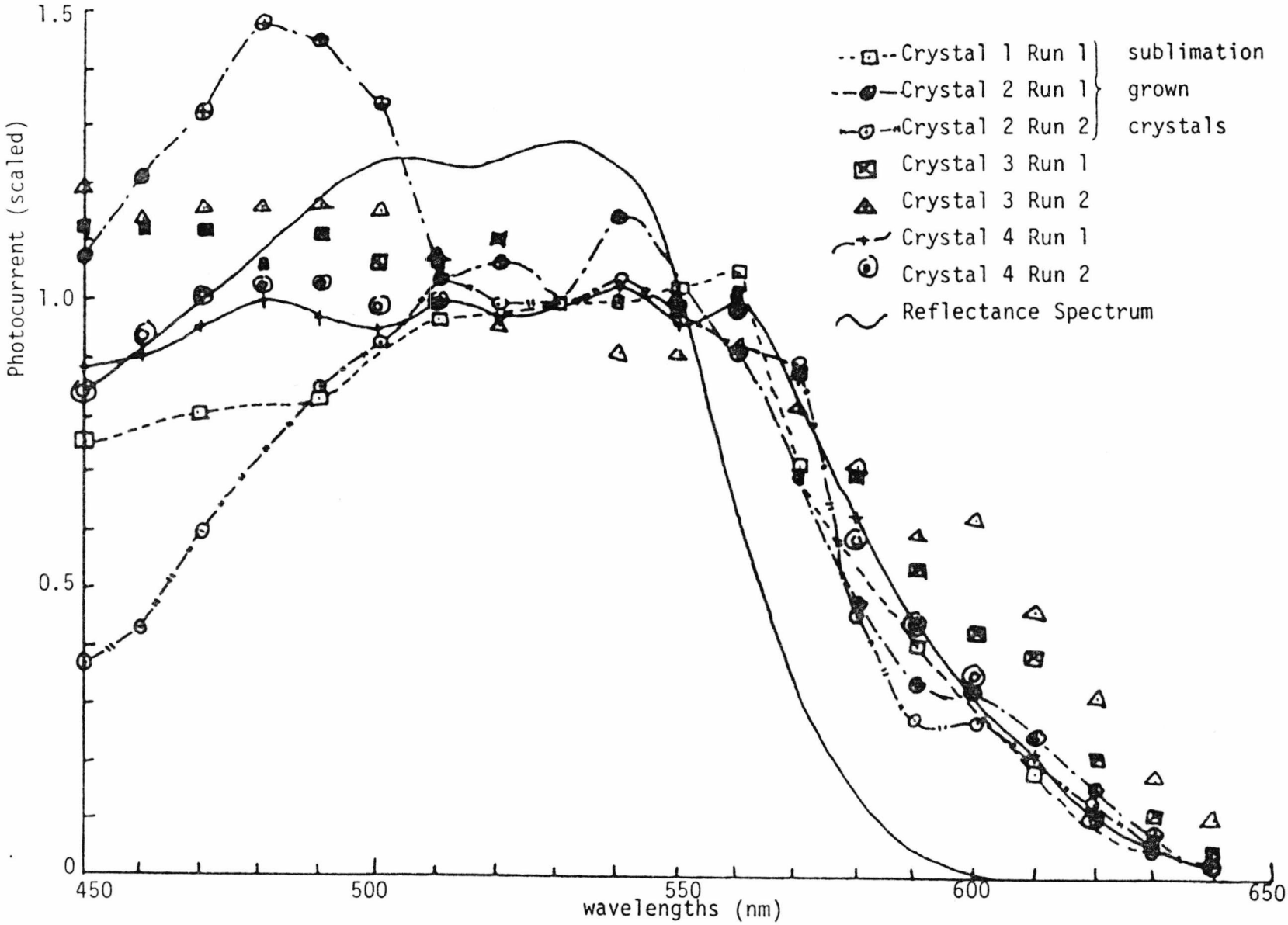

FIG. 6.5 PHOTOCONDUCTION ACTION SPECTRA OF ANTHRACENE/PMDA

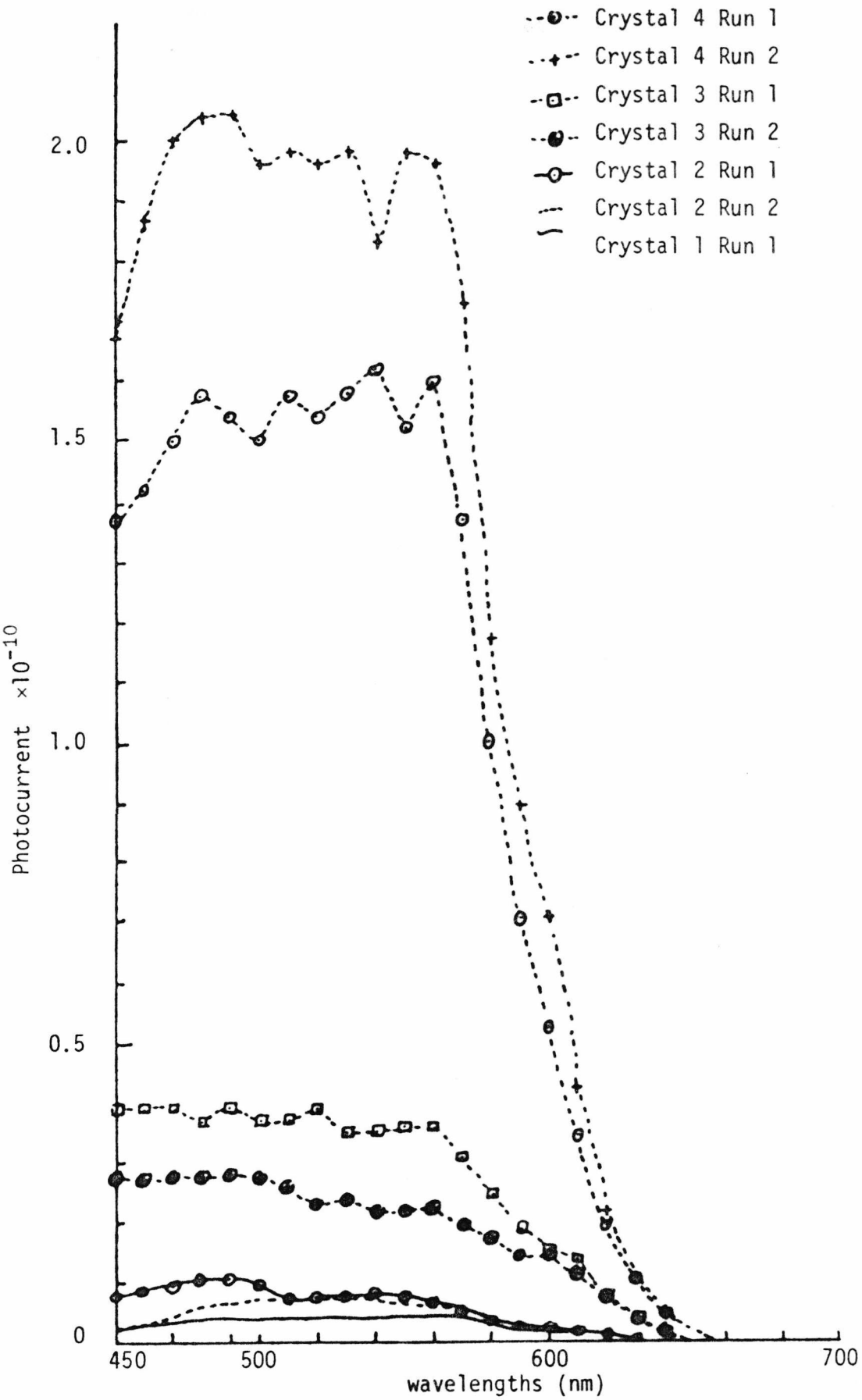

FIG. 6.6 ANTHRACENE/PMDA - INTENSITY DEPENDENCES AT DIFFERENT WAVELENGTHS

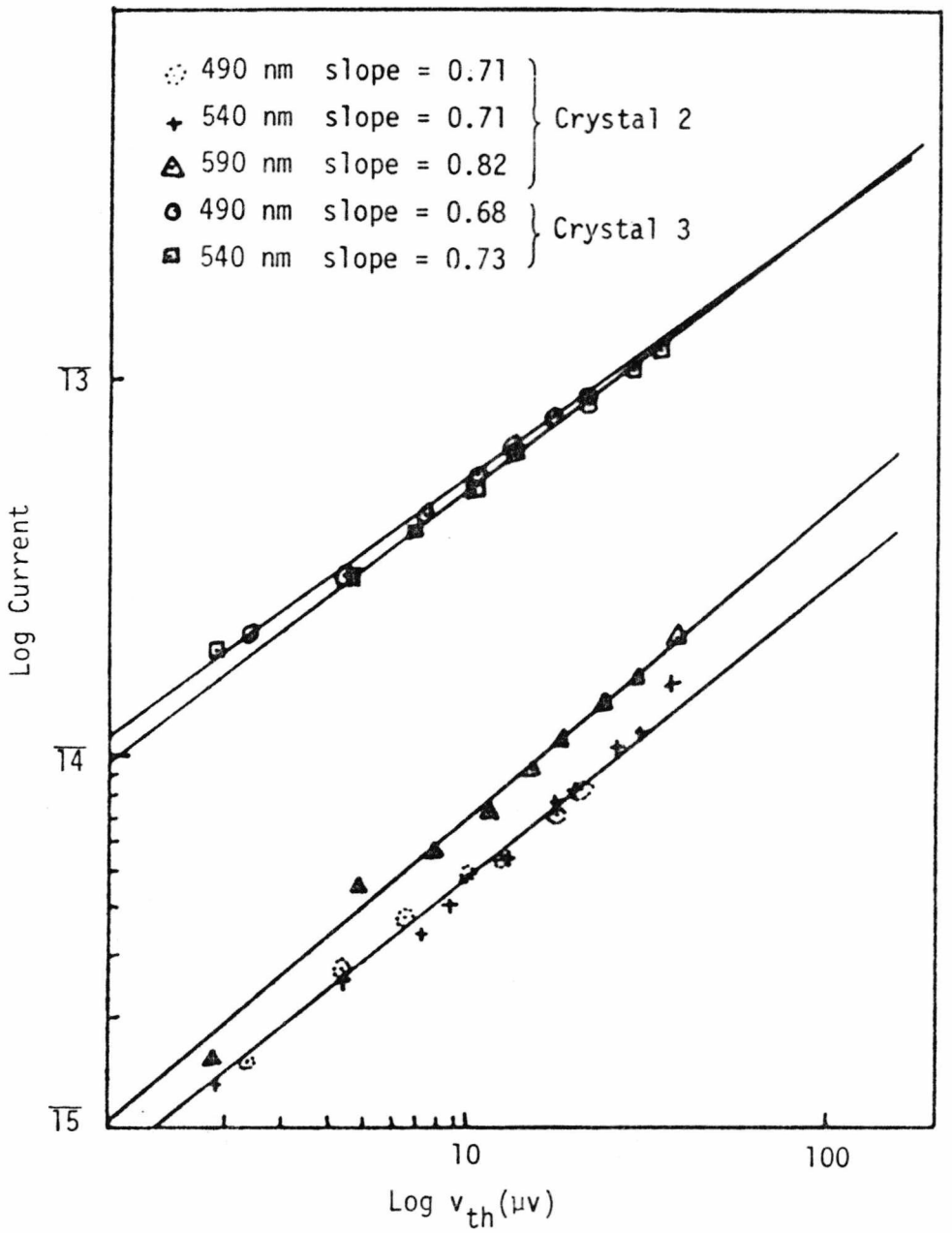

FIG. 6.7 ANTHRACENE/PMDA - INTENSITY DEPENDENCES

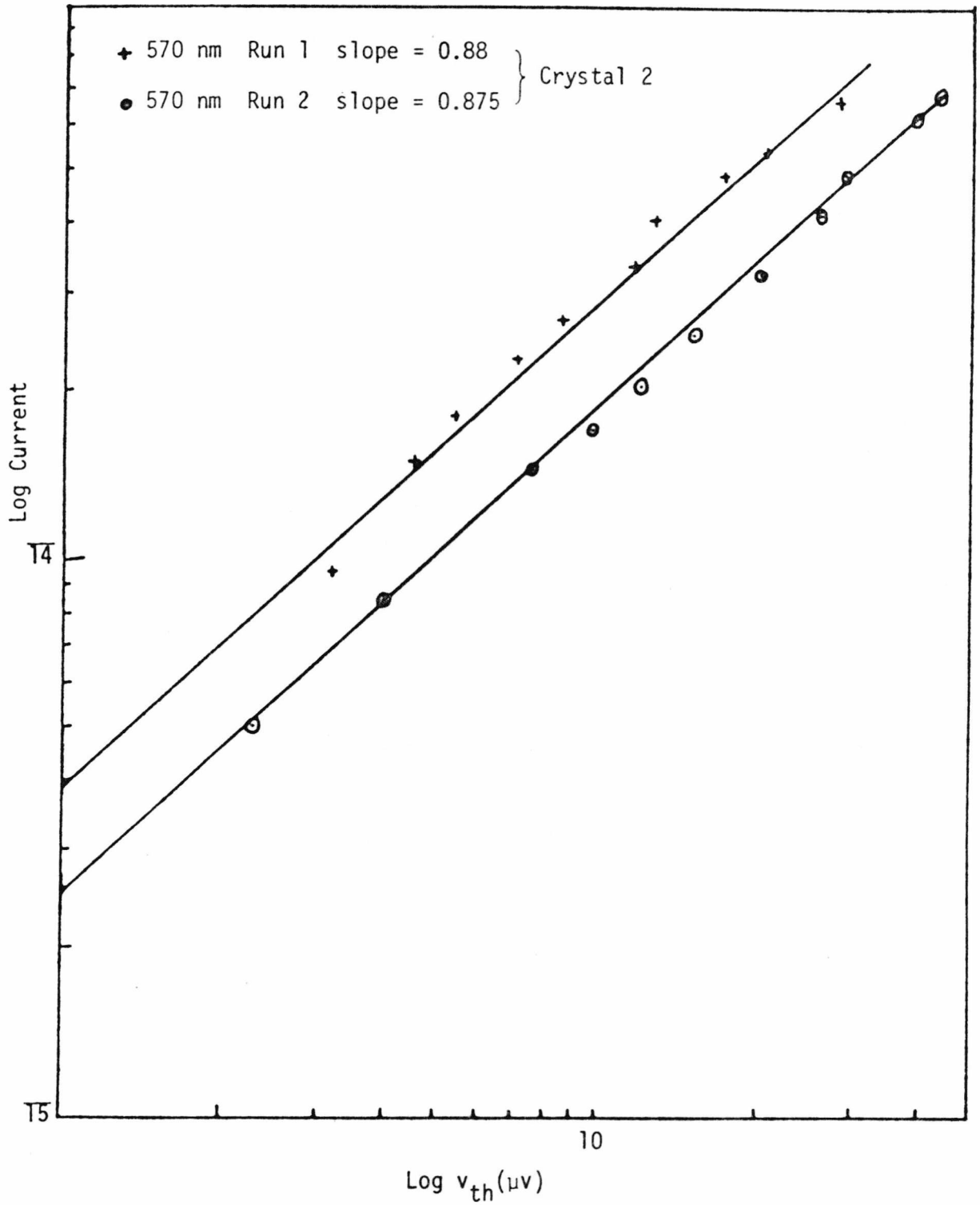

Crystal No.	Complex	Dimensions (cm) L	W	T	Q
1	DBT/TCNQ	.254	.061	.022	2.34×10^{-5}
2	DBT/TCNQ	.173	.013	.008	2.03×10^{-5}
	DBT/TCNQ	.173	.013	.008	1.86×10^{-5}
3	DBT/TCNQ	.151	.027	.022	3.11×10^{-5}
	DBT/TCNQ	.151	.027	.022	2.94×10^{-5}
6	DBF/TCNQ	.137	.07	.027	1.45×10^{-5}
	DBF/TCNQ	.137	.07	.027	1.62×10^{-5}
7	DBF/TCNQ	.168	.02		9.9×10^{-5}
	DBF/TCNQ	.168	.02		1.07×10^{-4}
8	$DBT_{.29}/DBF_{.71}/TCNQ$	.198	.012	.012	2.52×10^{-4}
	$DBT_{.29}/DBF_{.71}/TCNQ$	.198	.012	.012	2.68×10^{-4}
10	$DBT_{.29}/DBF_{.71}/TCNQ$	.095	.013	.013	4.12×10^{-4}
11	$DBT_{.41}/DBF_{.59}/TCNQ$	.228	.029	.017	1.3×10^{-5}
12	$DBT_{.41}/DBF_{.59}/TCNQ$	.176	.027	.019	1.81×10^{-5}
	$DBT_{.41}/DBF_{.59}/TCNQ$	.176	.027	.019	1.91×10^{-5}
13	$DBT_{.51}/DBF_{.49}/TCNQ$	.118	.023	.010	2.3×10^{-5}
14	$DBT_{.51}/DBF_{.49}/TCNQ$	.116	.023	.020	2.65×10^{-5}
	$DBT_{.51}/DBF_{.49}/TCNQ$	.116	.023	.020	2.49×10^{-5}
15	$DBT_{.73}/DBF_{.27}/TCNQ$	.073	.016	.010	5.02×10^{-5}
	$DBT_{.73}/DBF_{.27}/TCNQ$	.073	.016	.010	4.96×10^{-5}
16	$DBT_{.73}/DBF_{.27}/TCNQ$	.059	.019	.012	2.37×10^{-5}
17	$DBT_{.76}/DBF_{.24}/TCNQ$	.215	.028	.018	1.40×10^{-5}
	$DBT_{.76}/DBF_{.24}/TCNQ$	.047	.032	.017	1.15×10^{-5}

TABLE 6.2 QUANTUM YIELD PARAMETER VALUES (Q) OF DIBENZOTHIOPHEN/TCNQ (DBT/TCNQ), DIBENZOFURAN/TCNQ (DBF/TCNQ) AND MIXED COMPLEXES OF $DIBENZOTHIOPHEN_x/DIBENZOFURAN_{1-x}/TCNQ$ ($DBT_x/DBF_{1-x}/TCNQ$) WHERE $0<x<1$.

FIG. 6.8 PHOTOCONDUCTION ACTION SPECTRA OF DBT/TCNQ AND DBF/TCNQ

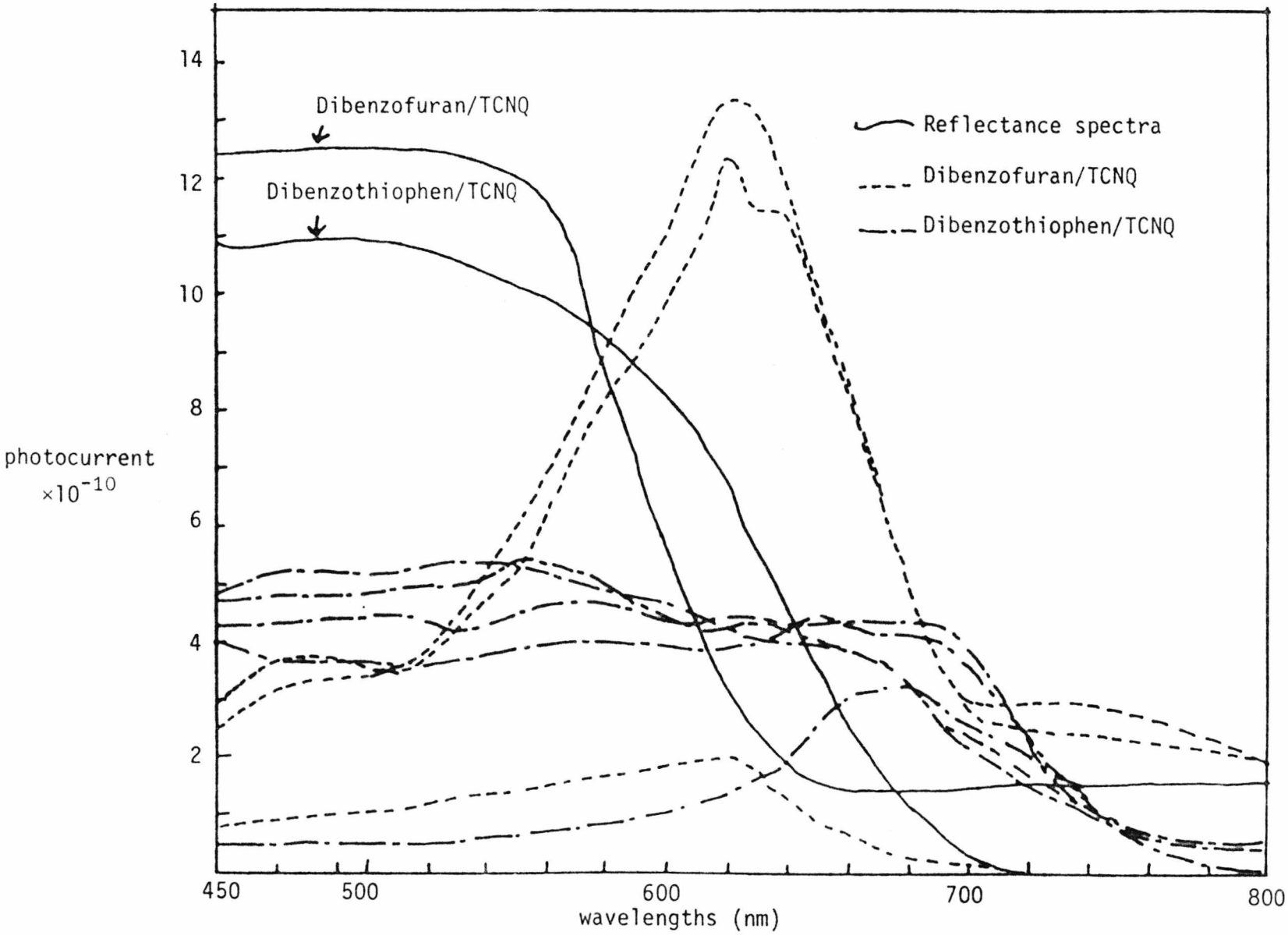

FIG. 6.9 DIBENZOFURAN/TCNQ - INTENSITY DEPENDENCES AT DIFFERENT WAVELENGTHS

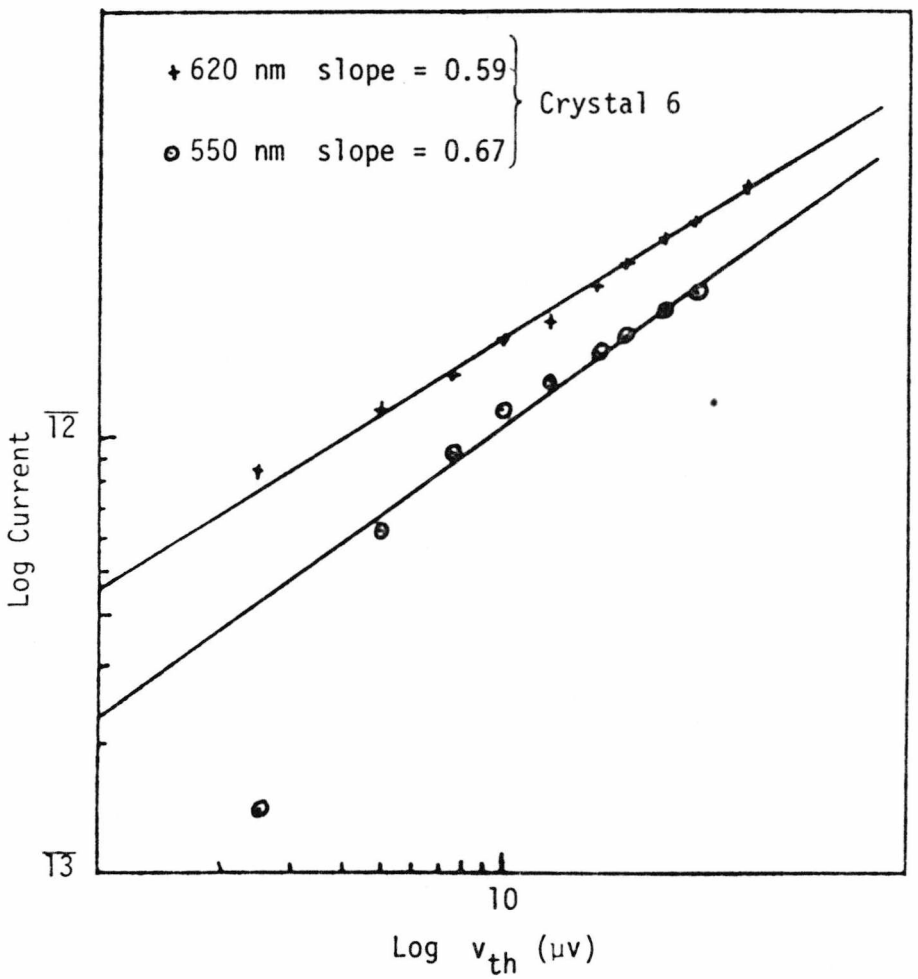

FIG. 6.10 DIBENZOTHIOPHEN/TCNQ - INTENSITY DEPENDENCES AT DIFFERENT WAVELENGTH (CRYSTAL 1)

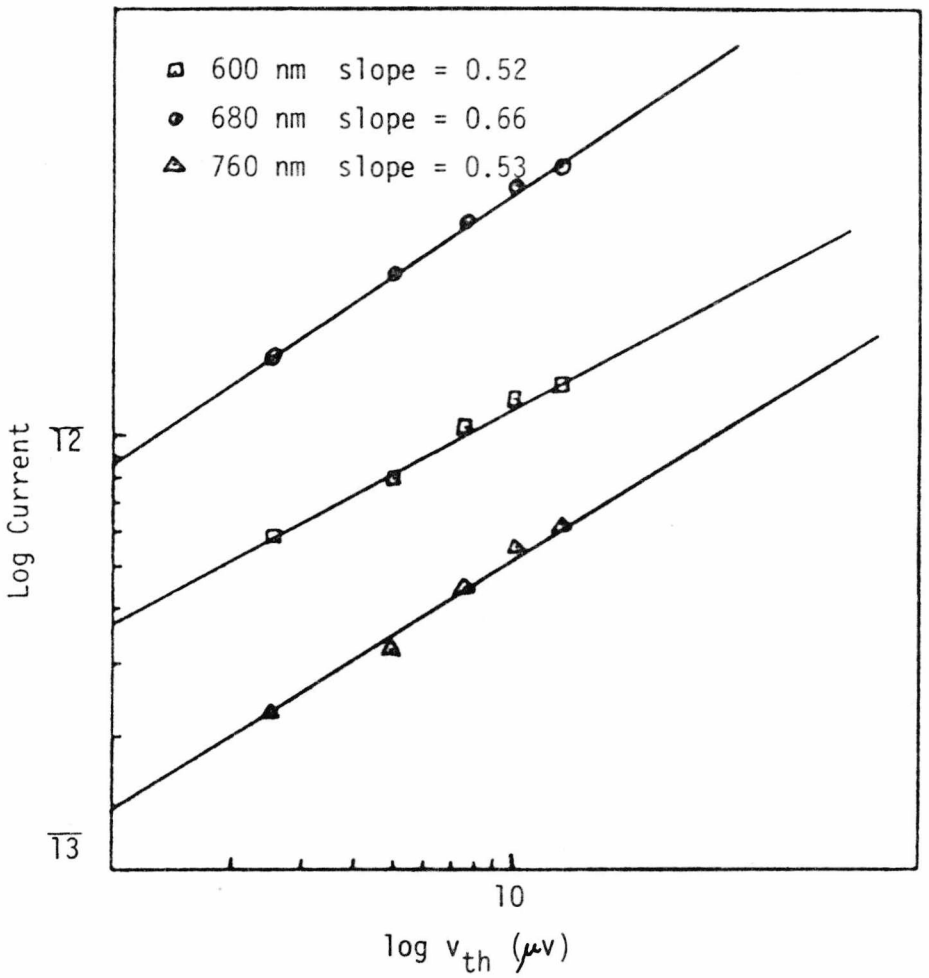

FIG. 6.11 PHOTOCONDUCTION ACTION SPECTRA OF $DBT_{0.29}/DBF_{.71}/TCNQ$

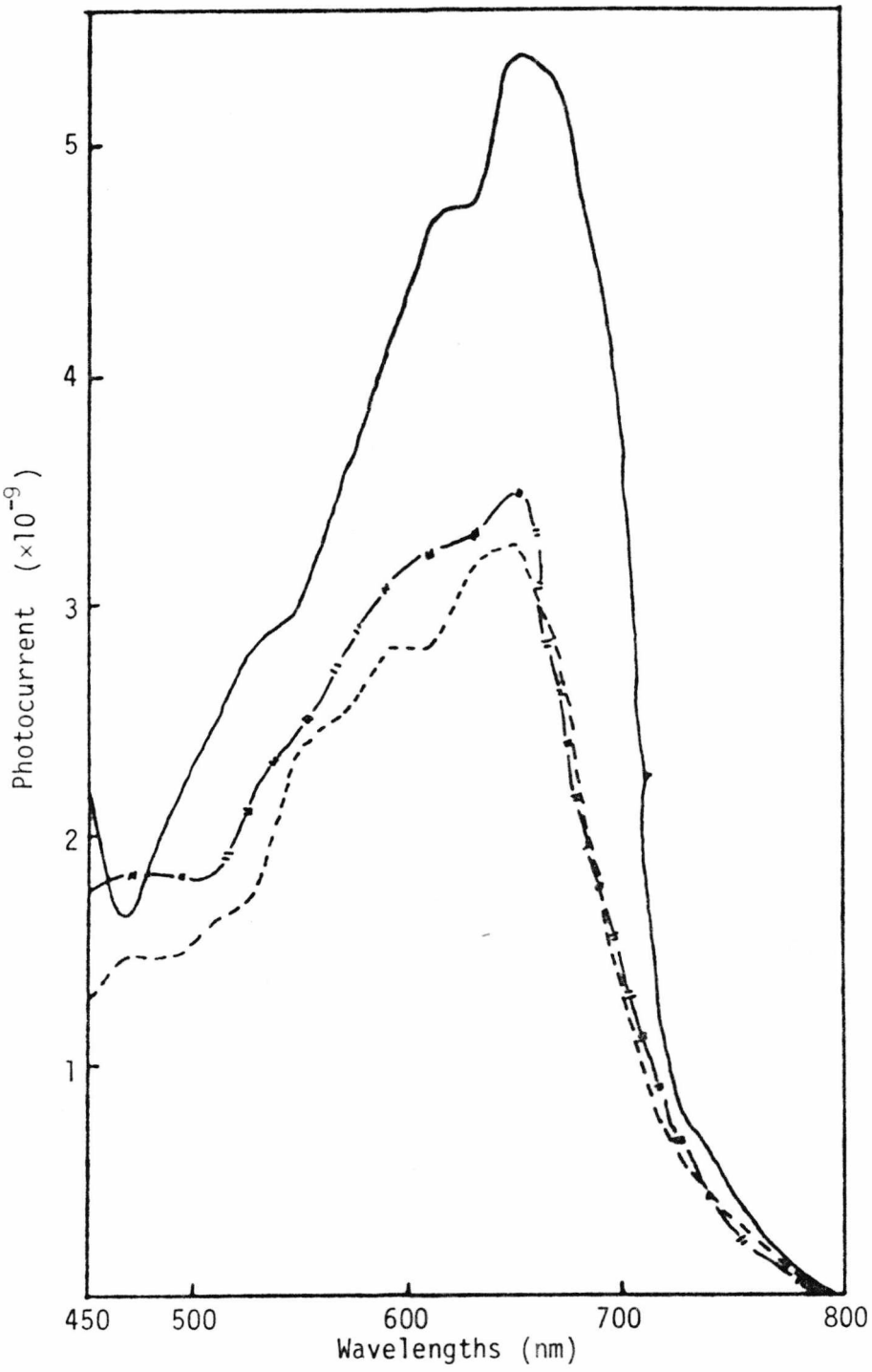

FIG. 6.12 PHOTOCONDUCTION ACTION SPECTRA OF $\underline{DBT}_{.41}/\underline{DBF}_{.59}/\underline{TCNQ}$

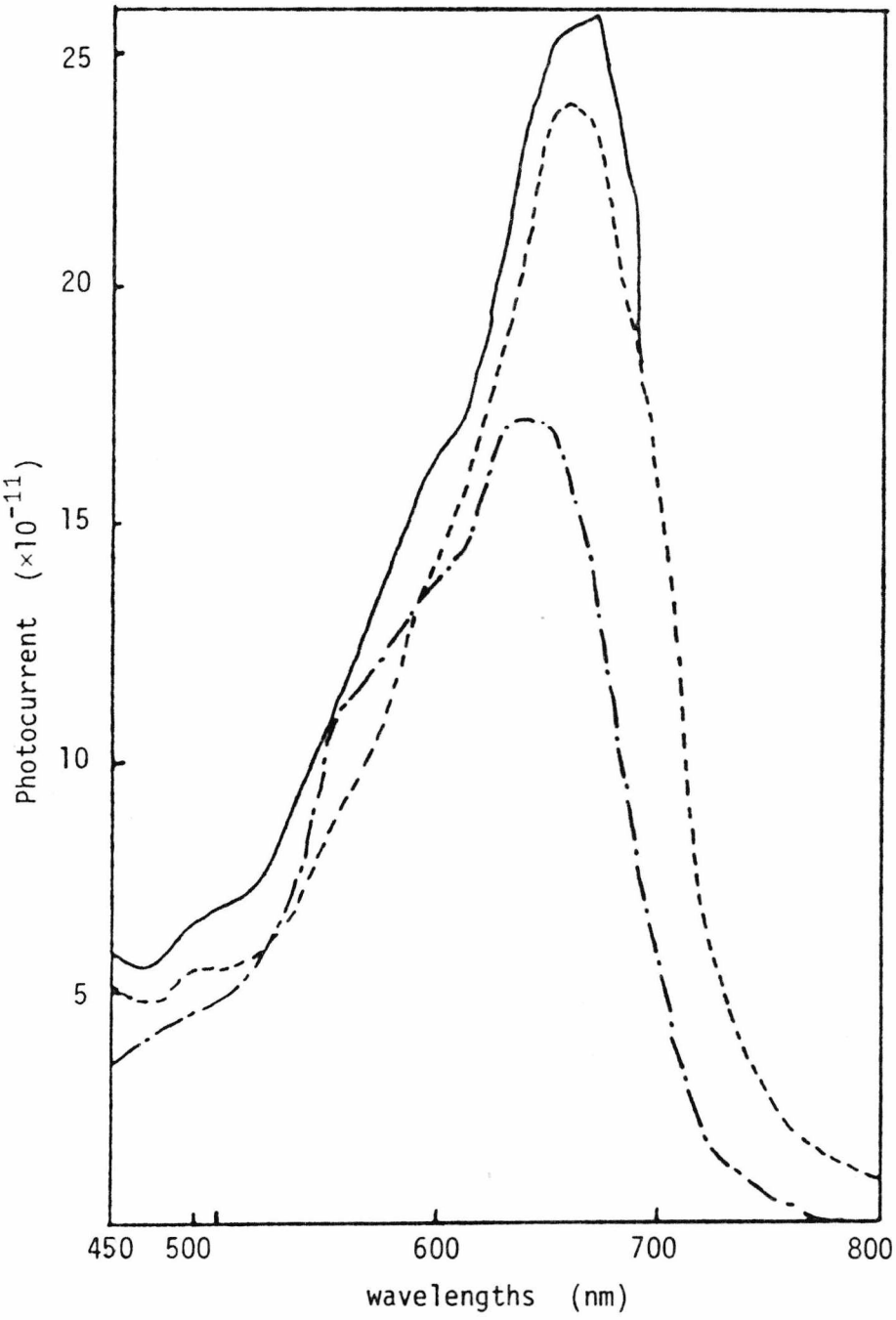

FIG. 6.13 PHOTOCONDUCTION ACTION SPECTRA OF $\underline{\text{DBT}}_{.51}/\underline{\text{DBF}}_{.49}/\underline{\text{TCNQ}}$

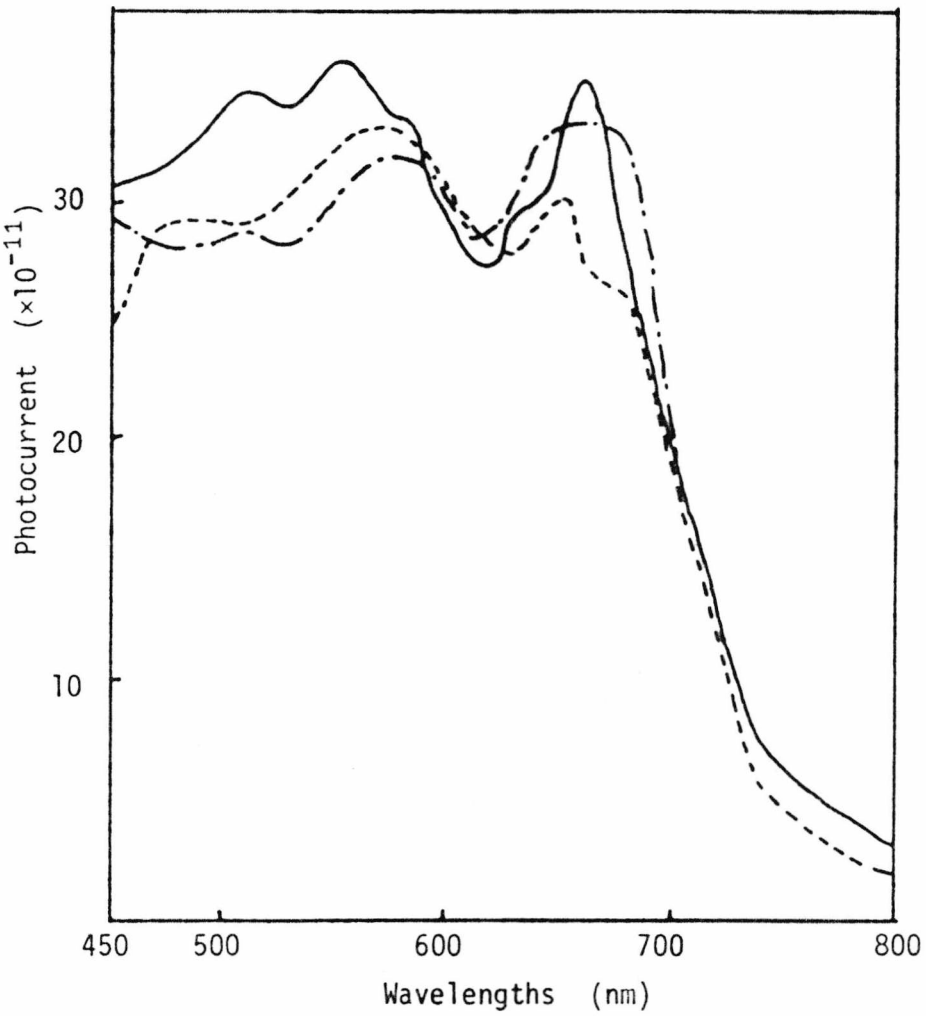

FIG. 6.14 PHOTOCONDUCTION ACTION SPECTRA OF $DBT_{.73}/DBF_{.27}/TCNQ$

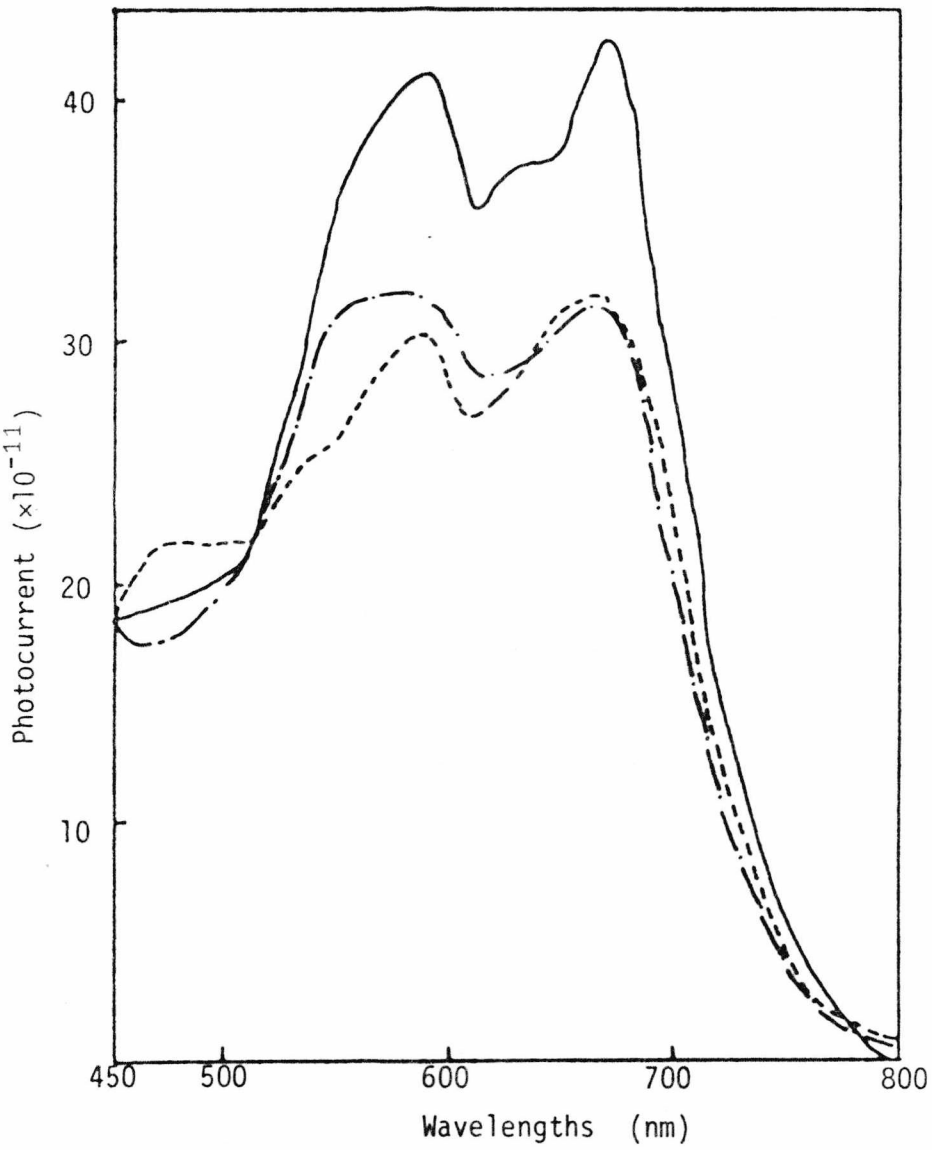

FIG. 6.15 PHOTOCONDUCTION ACTION SPECTRA OF DBT$_{.76}$/DBF$_{.24}$/TCNQ

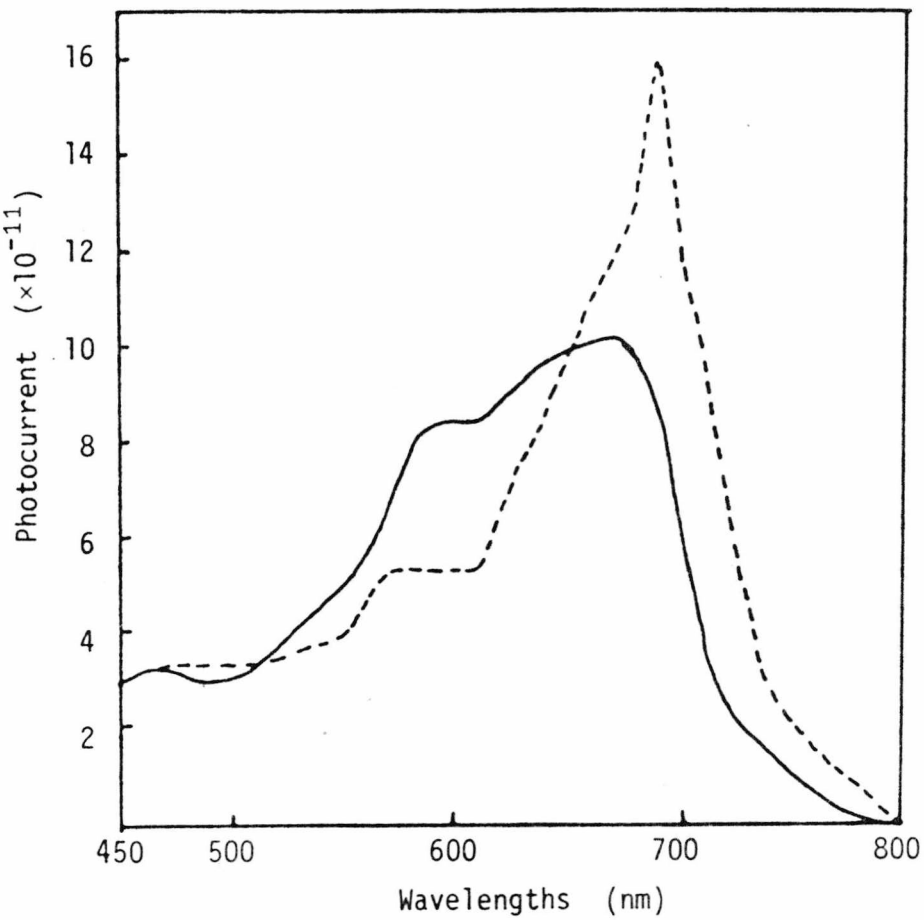

Crystal No.	Complex	Dimensions L	W	T	Q.Y.P. at 550 nm	Q.Y.P. (max.)
1	Pe/TCNQ	.246	.045	.033	3.54×10^{-5}	
3	Pe/TCNQ	.245	.045	-	1.44×10^{-5}	
4	Py/TCNQ	.405	.156	.136	3.03×10^{-5}	5.05×10^{-5}(780)
5	$Py_{.39}/Pe_{.61}$/TCNQ	.254	.034	.025	4.18×10^{-5}	4.23×10^{-5}(540)
5	$Py_{.39}/Pe_{.61}$/TCNQ	.254	.034	.025	5.79×10^{-5}	6.56×10^{-5}(540)
6	$Py_{.39}/Pe_{.61}$/TCNQ	.311	.035		9.38×10^{-5}	
7	$Py_{.39}/Pe_{.61}$/TCNQ	.137	.046	.035	4.29×10^{-5}	
8	$Py_{.39}/Pe_{.61}$/TCNQ	.291	.085	.069	1.34×10^{-5}	1.39×10^{-5}(560)
10	$Py_{.52}/Pe_{.48}$/TCNQ	.366	.059	.024	3.67×10^{-6}	4.53×10^{-6}(520)
10	$Py_{.52}/Pe_{.48}$/TCNQ	.366	.059	.024	5.83×10^{-6}	7.99×10^{-6}(470)
9	$Py_{.52}/Pe_{.48}$/TCNQ	.307	.045	.020	2.49×10^{-7}	2.76×10^{-7}(510)
9	$Py_{.52}/Pe_{.48}$/TCNQ	.307	.045	.020	2.62×10^{-7}	3.18×10^{-7}(510)

TABLE 6.3 QUANTUM YIELD PARAMETER VALUES (Q) OF Pe/TCNQ , Py/TCNQ and Py/Pe/TCNQ

TABLE 6.3 QUANTUM YIELD PARAMETER VALUES (Q) OF Pe/TCNQ , Py/TCNQ and Py/Pe/TCNQ (Cont'd.)

Crystal	Complex	Dimensions L	W	T	Q.Y,P. at 550 nm	Q.Y.P. (max.)
11	$Py_{.41}/Pe_{.59}/TCNQ$	.130	.026	.010	6.76×10^{-5}	
18	$Py_{.41}/Pe_{.59}/TCNQ$	.121	.02	-	3.15×10^{-5}	3.87×10^{-5}(510)
18	$Py_{.41}/Pe_{.59}/TCNQ$	.121	.02	-	5.32×10^{-5}	5.81×10^{-5}(530)
19	$Py_{.51}/Pe_{.49}/TCNQ$	.135	.021	-	6.5×10^{-5}	

FIG. 6.16 PHOTOCONDUCTION ACTION SPECTRA OF $PYRENE_x/PERYLENE_{1-x}/TCNQ$

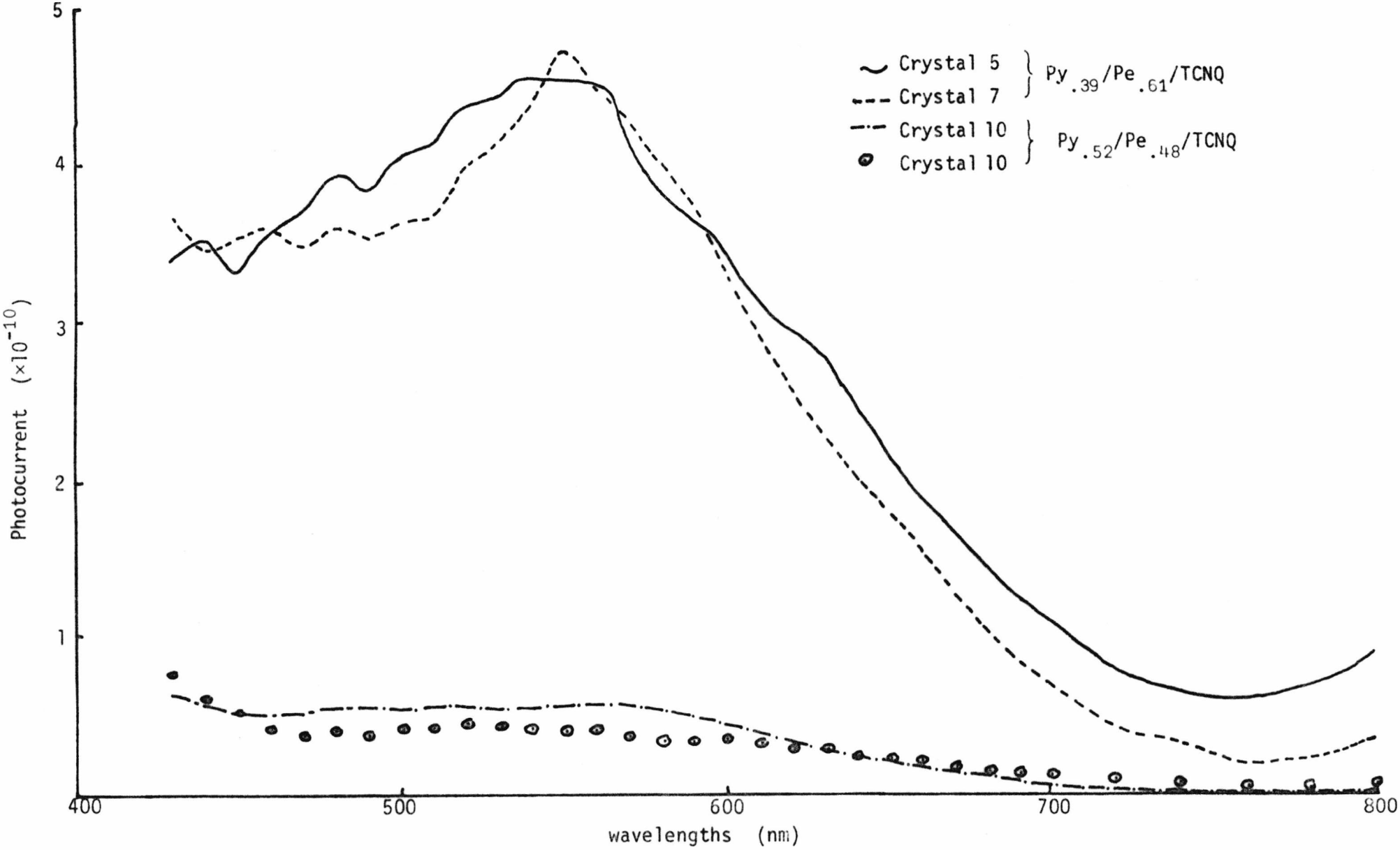

FIG. 6.17 PHOTOCONDUCTION ACTION SPECTRA OF Py/Pe/TCNQ

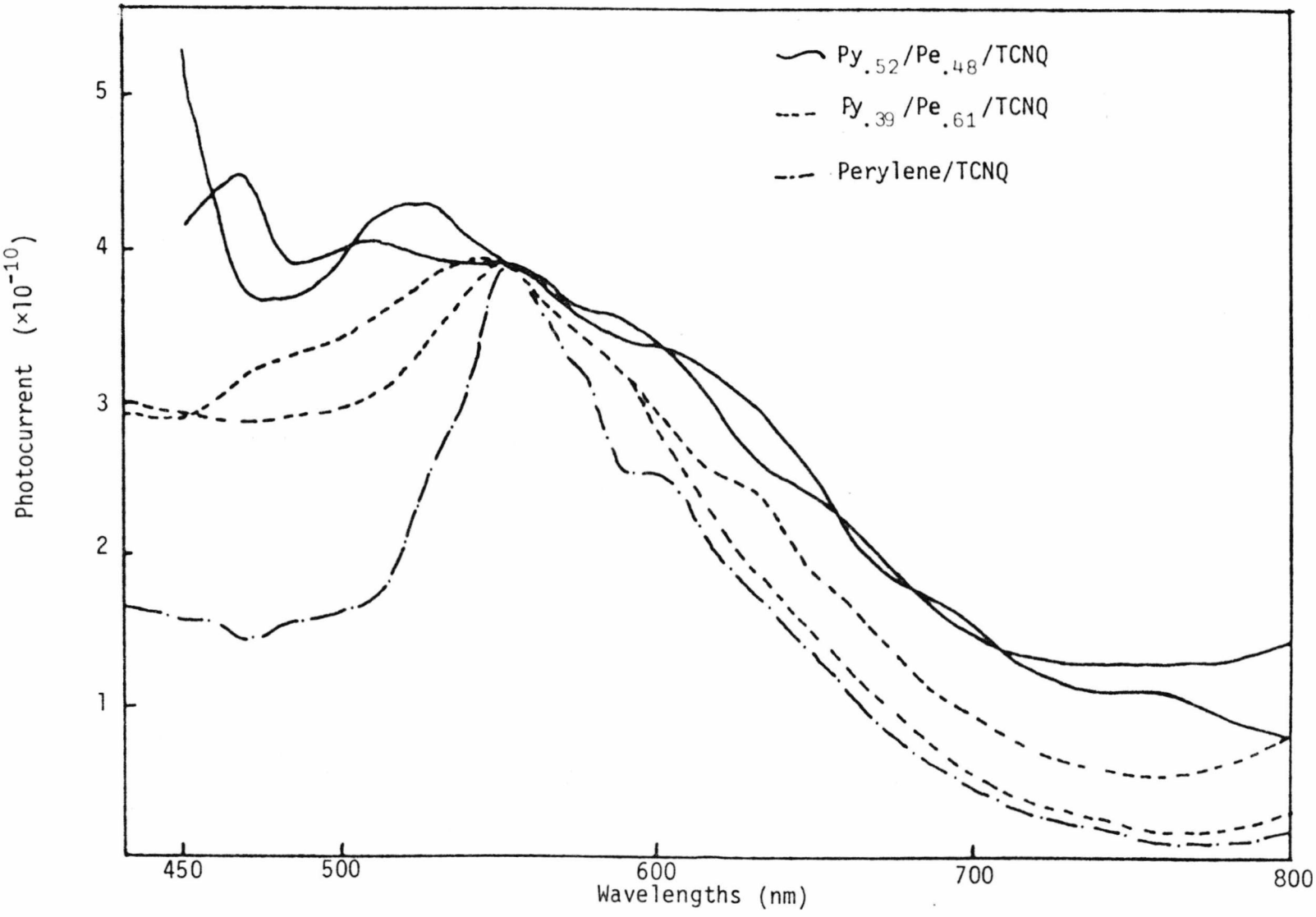

FIG. 6.18 $Py_{.39}/Pe_{.61}/TCNQ$ - INTENSITY DEPENDENCE AT DIFFERENT WAVELENGTHS (CRYSTAL 5)

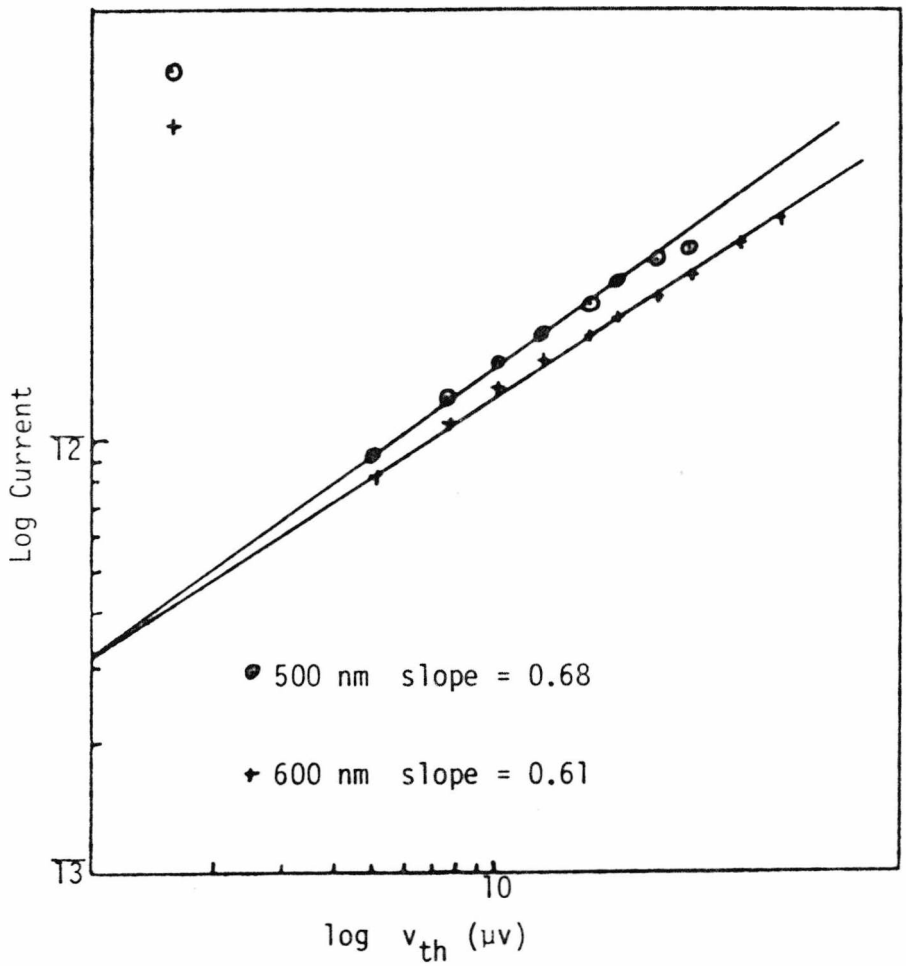

FIG. 6.19 PHOTOCONDUCTION ACTION SPECTRA OF ANTHRACENE$_{.08}$/CHRYSENE$_{.92}$/TCNQ

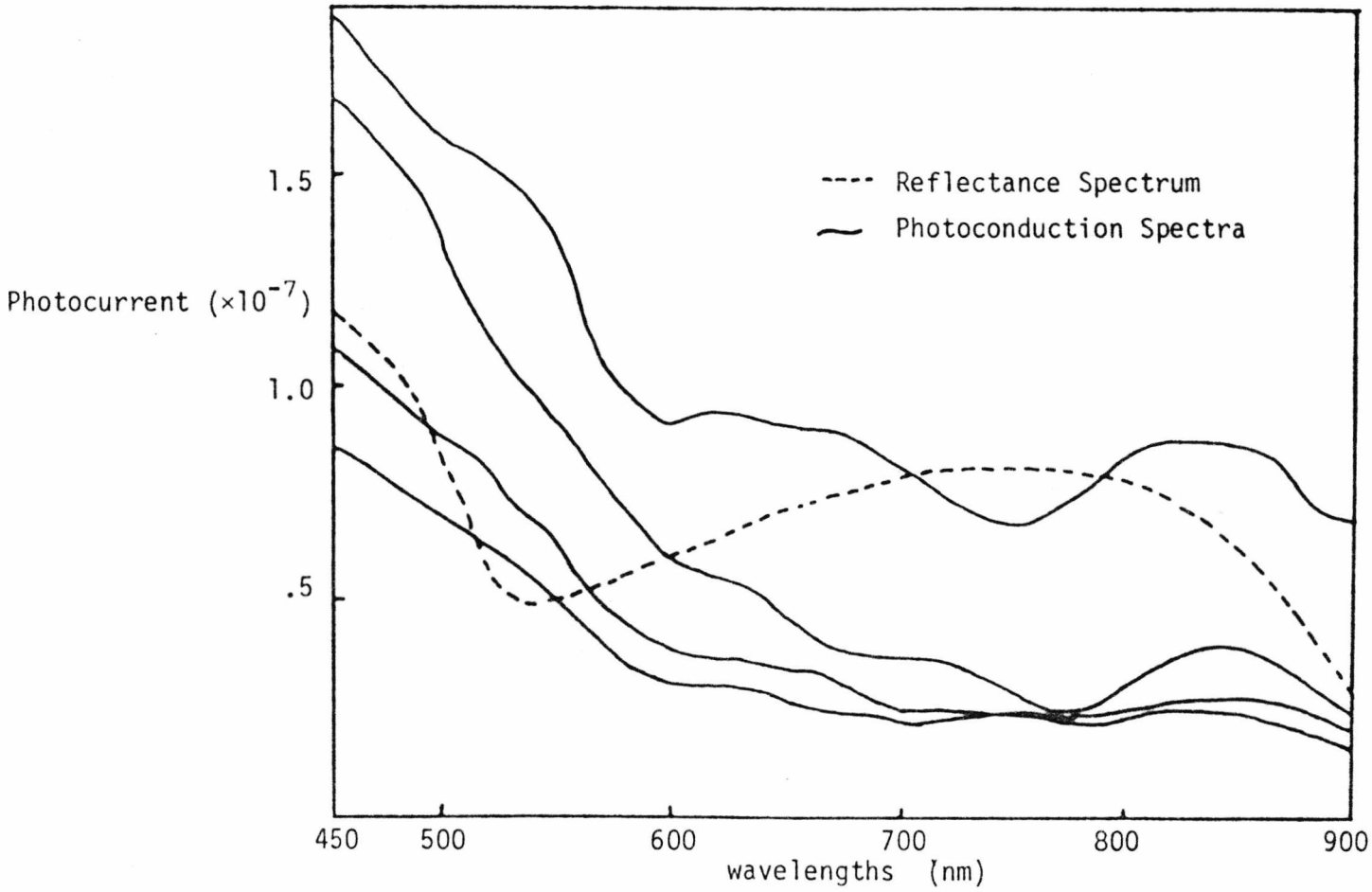

FIG. 6.20 PHOTOCONDUCTION ACTION SPECTRA OF ANTHRACENE$_{.12}$/CHRYSENE$_{.88}$/TCNQ

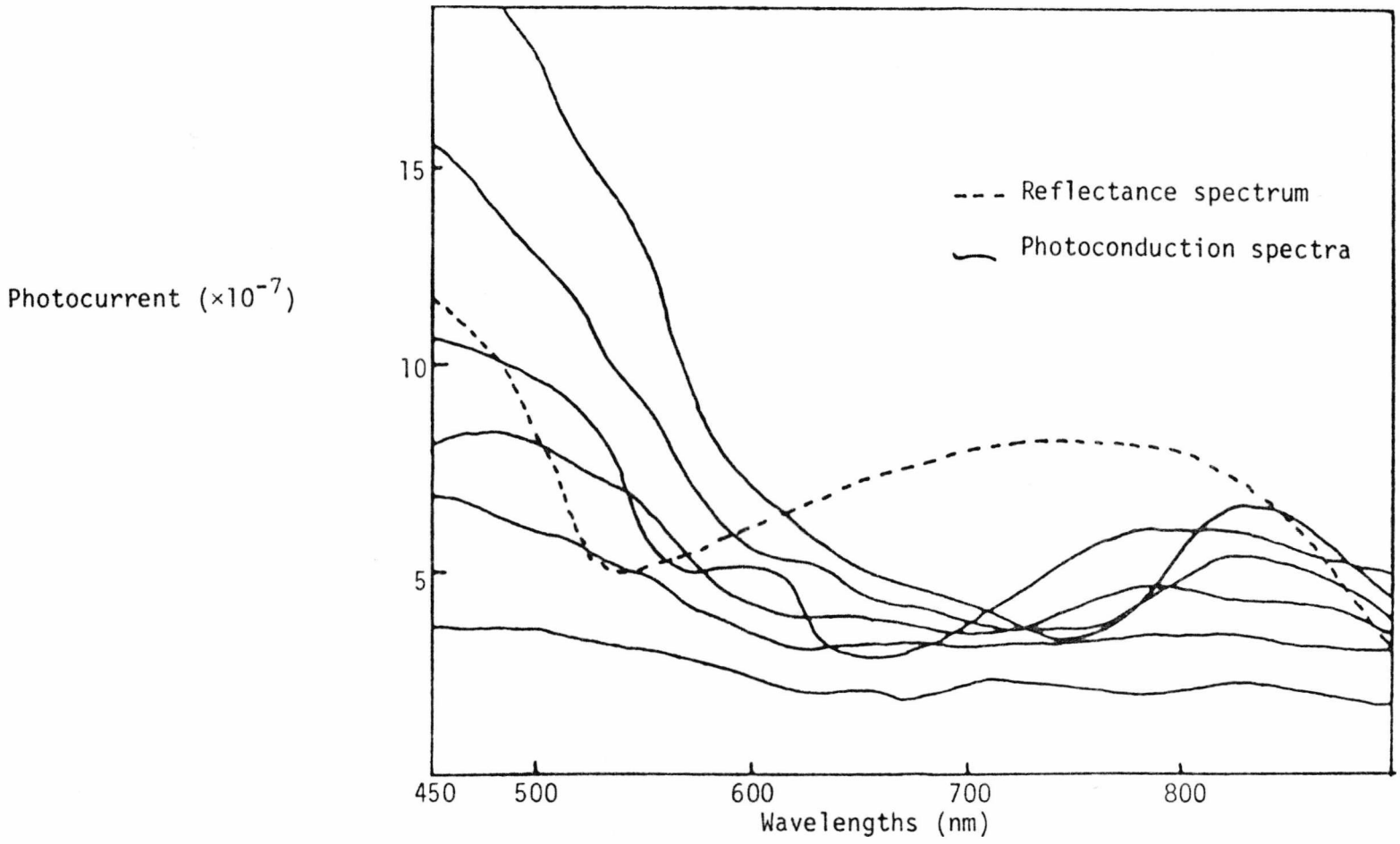

FIG. 6.21 PHOTOCONDUCTION SPECTRUM OF ANTHRACENE$_{.10}$/CHRYSENE$_{.90}$/TCNQ (CRYSTAL 2) - FILTER IS USED

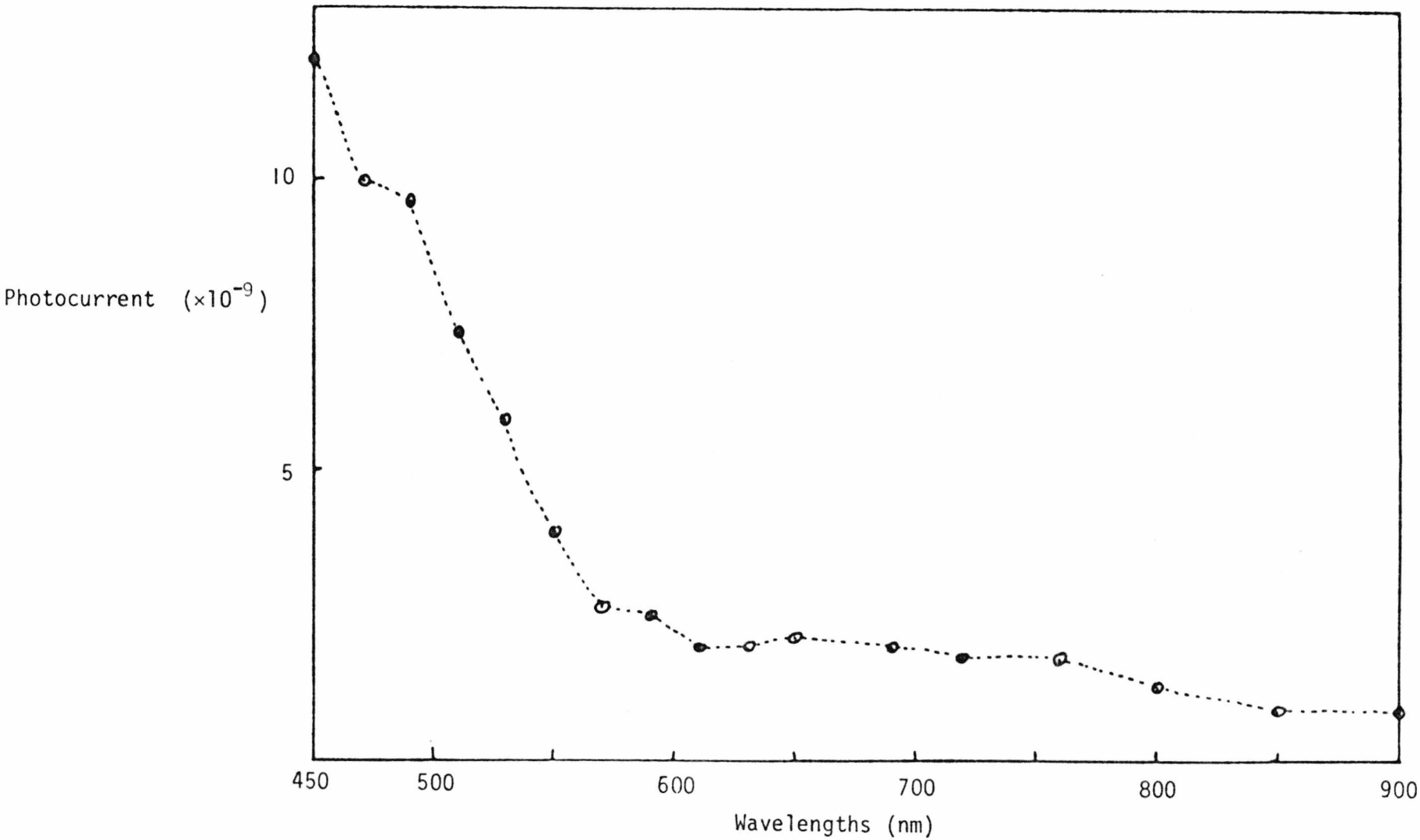

6.8 Discussion

Anthracene/Pyromellitic Dianhydride (Ant/PMDA)

The photoconduction of crystals of this complex, prepared from solution and by sublimation as described in Chapter 2, was studied in order to investigate the influence of crystal quality on the magnitude of photoconduction and the form of the action spectrum of photoconduction. Fig. 6.4 shows the action spectra for two sublimation grown crystals and two solution grown crystals, scaled to a common value of 1.0 for the photocurrent observed at 530 nm , together with the diffuse reflectance spectrum of the complex obtained as described in Chapter 4. This figure shows that the shape of the action spectrum is similar for samples prepared by these two methods, and closely related to the charge transfer absorption spectrum. Figure 6.5 shows the same action spectra with the photocurrent corrected to a common scale to remove effects due to the different applied field gradients and illuminated areas of the different samples and permit comparison of the relative magnitudes of photoconduction. This graph shows that the solution grown crystals gave photocurrents significantly larger than those of the sublimation grown crystals. Table 6.1 gives details of crystal dimensions, photocurrents and derived quantum yield parameters. Figures 6.6 and 6.7 show the results of studies of the dependence of photocurrent on incident light intensity at several wavelengths across the response region. In all cases, photocurrent $\propto$(light intensity)^n , with $0.68<n<0.88$. There are no major differences in the value of n for the two groups of crystals or for different wavelengths.

The action spectra of Figs. 6.4 and 6.5 are similar to that reported by Karl and Ziegler (1975), (Figs. 6.22), who also reported that the spectrum is independent of polarisation of incident light in the range covered in our work (450-650 nm). The latter observation suggests that,

FIG. 6.22 PHOTOCURRENT EXCITATION SPECTRUM OF A-PMDA FOR THE EXTERNAL ELECTRIC VECTOR OF THE LIGHT PARALLEL AND PERPENDICULAR TO TO THE STACK AXIS (RELATIVE UNITS, ROOM TEMPERATURE CORRECTED FOR THE LIGHT INTENSITY

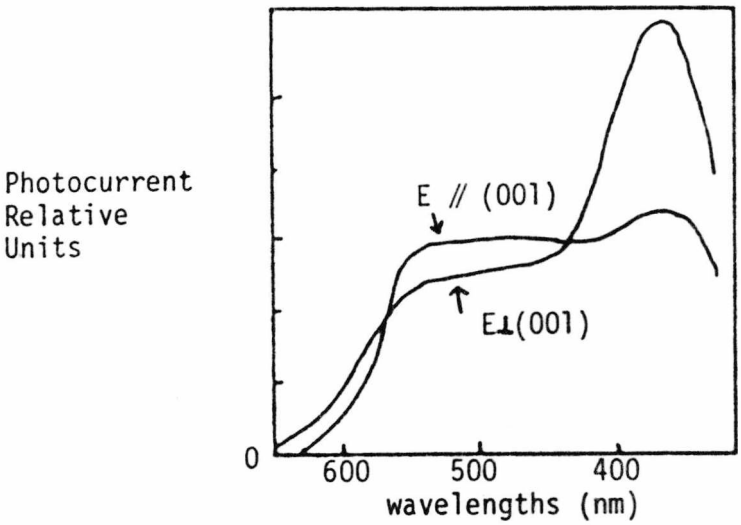

FIG. 6.23 TEMPERATURE DEPENDENCE OF THE EXPERIMENTAL VALUES OF THE CHARGE CARRIER MOBILITIES IN THE 1:1 CT COMPLEX ANT-PMDA

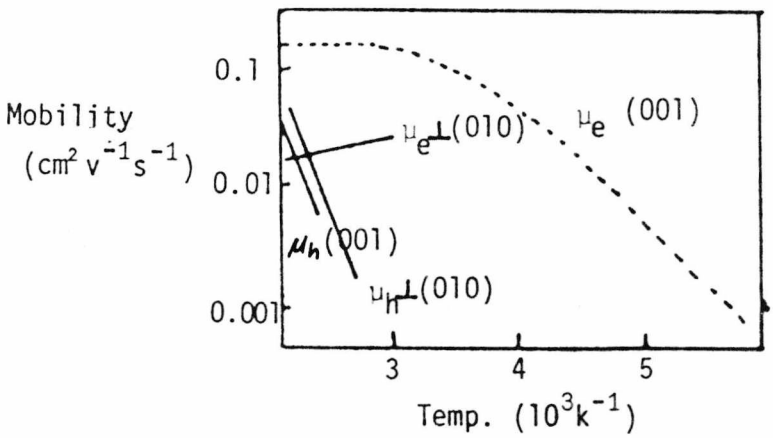

for the thick samples used in both Karl and Ziegler's work and in the present work, the photocurrent is not dependent on the density of excited charge transfer states but only on the total number of such states. This shows that charge carrier generation is a single photon process. The power law of the dependence of photocurrent on light intensity thus indicates a balance between carrier loss processes dependent on carrier concentration (e.g. loss to electrodes) and those dependent on (carrier concentration)^2 (e.g. bimolecular recombination). The observation of enhanced photoconduction in solution grown crystals compared to that in sublimation grown crystals, while the intensity dependence remains unchanged, provides evidence on the reason for the enhanced photoconduction. An enhanced photocurrent could be due to increased carrier mobility or higher steady state carrier concentration. Charge carrier drift mobility measurements (Karl & Ziegler, 1975) on single crystals prepared by sublimation show electron mobility to be 0.15 cm^2/vs at room temperature, with hole mobility much smaller and more temperature dependent (Fig. 6.23). This electron mobility is a typical value for molecular crystals and it is unreasonable to suppose that solution grown crystals would have mobilities significantly larger than this. Thus it is most likely that the increased photocurrent in solution grown crystals is due to higher steady state charge carrier concentrations. However, since bimolecular charge carrier recombination should increase as the square of the steady state concentration, the balance of carrier loss processes would be altered unless the recombination takes place at recombination centres in the crystals, of which there are less in solution grown crystals than in sublimation grown samples. The observation of similar power laws for intensity dependence of photocurrent in both sets of samples thus supports the hypothesis that solution grown crystals contain less recombination centres. Karl and

Ziegler's (1975) observation that hole mobility is much smaller and more temperature dependent than electron mobility in sublimed samples also suggests that such samples contain hole traps, which could act as recombination centres. Although the origin of such hole traps is not known, it is to be expected that the higher temperatures used in sublimation growth would assist the creation of chemical or physical defects to a greater extent than the milder conditions of solution growth.

The quantum yield parameters for all samples are low compared to those for many other molecular complexes, and this is consistent with the crystal structure (Boeyens & Herbstein, 1965; Robertson & Stezowski, 1978) which does not provide significant interstack π-π^* overlap of donor with donor or acceptor with acceptor (Vincent & Wright, 1974). The variations in quantum yield parameters in Table 6.1 for different samples probably reflect variations in carrier recombination rate, (which is taken as approximately constant in the method used to derive the quantum yield parameter as explained in Section 6.2), rather than genuine variations in quantum yield of the carrier generation process.

Dibenzothiophen/TCNQ and Dibenzofuran/TCNQ

Of the various parent molecular complexes on which mixed complexes for photoconductivity studies were based, these two complexes were the only ones for which no photoconduction data were available. Photoconduction action spectra and dependence of photocurrent on light intensity at various wavelengths were therefore measured for several crystals of each complex. Although small single crystals of good quality, suitable for x-ray diffraction studies, could be found by careful selection from batches of solution grown crystals of both complexes, crystals of size suitable for mounting for conductivity measurements were observed to be of

poorer quality than for most single molecular complexes. Crystal faces showed a fine line structure rather than a smooth shiny appearance, and the larger crystals were frequently found in aggregates suggesting highly twinned material. Triclinic crystals readily form twinned samples, and this and the disorder possible in the dibenzofuran complex accounts for the poor crystal quality.

Photoconduction action spectra of both complexes are shown in Fig. 6.8, together with the diffuse reflectance spectra of the complexes for comparison. The shapes of these action spectra vary from crystal to crystal of the same compound, and show a fairly featureless response in the region of the first charge transfer transition, together with a response on the low energy edge of the charge transfer band. The magnitude of this low energy response relative to that of the higher energy response is variable. Photoconduction peaks on the low energy edge of the charge transfer absorption band have been previously reported for other complexes by Akamatu and Kuroda (1963) and Mukherjee (1970). In the case of some of the complexes for which this effect was observed by Akamatu and Kuroda (1963), later studies on well-formed single crystals (Vincent & Wright, 1974) showed no low energy photoconduction response. This response thus appears to involve crystal imperfections. Mukherjee (1970) showed that for a series of dibenzothiophen complexes with different acceptors, the position of this low energy response varied in the same way as the charge transfer transition energy varied, suggesting the involvement of optically excited charge transfer states rather than mechanisms involving direct optical excitation of trapped charge to conduction levels. The low energy photoconduction therefore involves interaction of D^+A^- excited states with defects, and a plausible mechanism is trapping of one of the charges at the defect (thereby lowering its energy) with a

corresponding increase in the probability of the separation of the other charge, leading to carrier generation. Such a mechanism would not be effective for more highly excited charge transfer states produced by absorption of light of significantly higher energy than the threshold for the charge transfer transition, if the excess energy of the charge transfer state was greater than the trap depth. Hence a photoconduction response arising from this mechanism would only occur on the low energy edge of the charge transfer band, for crystals containing shallow traps. The magnitude and peak position of the response would depend on trap density and distribution of trap depths, which depend on crystal quality. Hence the variation in the relative magnitude of low energy photoconduction in different crystals can be explained.

Two alternative effects which would produce a similar photoconduction peak on the low energy edge of the absorption band are as follows:

i) Weak absorptions of light on the low energy edge of the charge transfer band could produce mainly bulk photoconduction, while more strongly absorbed light near the peak absorption region could lead to surface photoconduction. Differences in surface and bulk trap densities would then account for different relative magnitudes of the responses in these two regions. This interpretation is ruled out by the observation of Akamatu and Kuroda (1963) and Vincent and Wright (1974) on the effect of varying the polarisation direction of the incident light with respect to the crystal axes. No major change in the shape of the photoconduction action spectra of any of the complexes studied in this way was observed, whether the light was polarised along the

direction of polarisation of the charge transfer transition or perpendicular to this direction. Since charge transfer transitions are strongly polarised, these experiments should alter the amounts of incident light absorbed near the surface and in the bulk. The absence of any change in the action spectrum thus rules out interpretations based on surface vs bulk photoconduction.

ii) The decline in photocurrent on going from low energy, weakly absorbed light to higher energy strongly absorbed light could arise from the increased rate of charge carrier recombination in regions of high excitation density, leading to a fall in steady state current. To test this hypothesis, studies of the dependence of photocurrent on light intensity were carried out at several wavelengths across the spectral response region of interest (Figs. 6.9 & 6.10). These results show no significant decrease in the power law of dependence of photocurrent on light intensity in regions of strong optical absorption. Increased charge carrier recombination should lead to a decrease in the power law of dependence on light intensity, and the absence of the effect thus eliminates this explanation.

Mixed Complexes

The results obtained using polarised light and from intensity dependences, suggest that only a single photon is needed to produce charge carriers. While a single photon mechanism is possible with mobile excited states, a two photon mechanism would also be expected (at high absorption region in particular) if excited states are mobile.

Since the excited states produced by charge transfer absorption are not mobile within the crystal, photoconduction at a particular wavelength should depend on:

i) Number of excited species produced (not density). The number of excited states depends on

   a) the extinction coefficients of the parent complexes at that wavelength

   b) the relative concentration of the two complexes.

   If there are no structural changes as composition is varied, the extinction coefficients of the two complexes will remain constant, and the number of excited species will be proportional to $n(x\varepsilon_1+(1-x)\varepsilon_2)$ where x is the fraction of complex 1; n is the total number of complex molecules.

   If there are structural changes, ε_1 and ε_2 may depend on x, and the number of excited complexes 1 and 2 will no longer depend linearly on x.

ii) Probability of excited state species dissociating to produce charge carriers.

   This is related to lattice structure (Vincent, 1972).

   Two cases could occur:

   a) interstack D-D or A-A overlap is similar for both complexes

   b) interstack D-D or A-A overlap is different for the two complexes.

   In case (a), there will be no change in the dissociation, probability on going from one complex, through mixed complexes, to the other pure complex.

In case (b), if there is poor interstack D_1-D_1 overlap for the D_1A complex, use of a larger D_2 may produce better (D_1-D_2) interstack overlap in the mixed complex, and allow excited D_1A species to dissociate and show photoconduction not present in the pure D_1A complex.

iii) Recombination rate and loss rate to electrode: if the introduction of a second complex into the lattice of the first produces regions of lattice strain, or defects, these may act as charge carrier traps. These will have the effect of slowing down carriers (i.e. reduce mobility) and hence will reduce the loss to electrodes (i.e. reduce photocurrent). They may also act as recombination centres, which will also reduce the apparent photocurrent, and should show as a decrease in intensity dependence power law.

Dibenzothiophen/Dibenzofuran/TCNQ

This system was studied as it represented an ideal mixed complex system for comparison with other less ideal systems. The main advantages of this system which make it an ideal case are:

i) A continuous series (Dibenzothiophen)$_x$(Dibenzofuran)$_{1-x}$ TCNQ with $0<x<1$ can be prepared in crystalline form, and analysed (Chapter 2).

ii) The two parent complexes and the mixed complexes all have very similar crystal structures (Chapter 3), in which the relative orientations of donor and acceptor within the stacks and the degree of interstack donor-donor or acceptor-acceptor overlap are constant.

iii) The photoconduction action spectra are different. Unfortunately, however, the main differences (see Fig. 6.8) occur in the long wavelength region on the low energy side of the charge transfer absorption band, in a region where, as discussed above, photoconduction is strongly influenced by crystal defects. As shown in the semiconductivity trends (Chapter 5), mixed complexes of this system have a higher defect concentration than pure complexes.

The last point above suggests that the variability of shape of the photoconduction action spectra observed for the parent complexes should be greater in the mixed complexes. The action spectra of the mixed complexes are shown in Figs. 6.11; 6.12; 6.13; 6.14; 6.15. Although all these spectra correspond to photoconduction in the same regions as shown by the parent complexes, and the shapes are moderately similar for crystals of a given composition from a given batch, there is no clear correlation between these shapes and the composition of the complex which could be interpreted in terms of points (i-iii) of the general discussion above. Any attempt to produce a meaningful correlation of this sort would require comparison of the mixed complex action spectrum with the sum of the action spectra of crystals of the two parent complexes having the same concentrations and distribution of defects, weighted in the ratio of the concentration of the two component complexes in the mixed complex. This was not feasible in the present work since characterisation of defect concentration and distribution would be a very time consuming process, particularly since the identity of the particular defects involved in the mechanism proposed above for the low energy photoconduction is not known. Also, even if such a study had been carried out, the results would not be very useful in controlled modification of photoconduction action spectra because it is difficult to control defect concentrations practically. For example, in

this mixed complex system, the parent complex and the mixed complex crystals were all grown under essentially the same conditions from solution, yet the photoconduction action spectra clearly show that the relative importance of the low energy photoconduction mechanism involving defects differs from sample to sample.

Table 6.2 gives details of the crystal dimensions and quantum yield parameters at the wavelength of maximum photoconduction for the mixed complexes in this series. For all samples, the peak photocurrents and quantum yield parameters are similar. This result is a consequence of the similarity of the two donor molecules and the common lattice structure of all the complexes. The similarity of relative orientation of donor and acceptor in the two parent complexes (Chapter 3) and the similar shapes of dibenzothiophen and dibenzofuran result in very similar extinction coefficients for the first charge transfer bands of the two complexes (Chapter 4). Since the mixed complexes have the same lattice structure as the two parent complexes, the degree of interstack donor-donor or acceptor-acceptor overlap is the same in both cases (in fact small for both possible overlaps, accounting for the low quantum yield parameter). Thus, both the number of excited charge transfer states produced in unit time by a given illumination intensity and the probability of these states dissociating to yield charge carriers is similar for all compositions, and hence the observed peak photocurrents are expected to be comparable, as observed. The insensitivity of the magnitude of the peak photocurrent to variations in defect concentrations can also be explained. As the defect concentration rises, the low energy photoconduction mechanism becomes more important, increasing the carrier generation rate. At the same time the defects will tend to reduce carrier mobility and possibly increase carrier recombination rate. The balance of these two opposing effects minimises the observed variation in peak photocurrent as defect concentrations change.

As described in Chapter 2, attempts to obtain other series of mixed complexes with the ideal characteristics mentioned above, but not suffering from the problem of defect-ridden crystals, were unsuccessful.

Pyrene/Perylene/TCNQ

This system was studied for the following reasons:

i) The photoconduction action spectra of the parent complexes have been extensively studied in this laboratory (Vincent, 1972; Munnoch, 1974) and show distinct characteristics (Fig. 6.24) with the wavelengths of peak photoconduction corresponding to regions of low photoconduction response in the other complex, but with comparable magnitude of peak photocurrent.

ii) Crystals of the parent complexes are of good quality and the action spectra do not appear to involve features attributable to defects. This, and (i) above, suggests that the mixed complexes of this system should be suitable for investigation of the possibility of modifying photoconduction action spectra by varying composition.

iii) Although analysis of the mixed complexes (Chapter 2) showed that only a small range of compositions around 50% of each complex could be prepared as single crystals, irrespective of ratio of solution concentrations, x-ray powder diffraction (Chapter 3) shows that crystals of this composition form a distinct new phase, of "structrure" different from that

FIG. 6.24

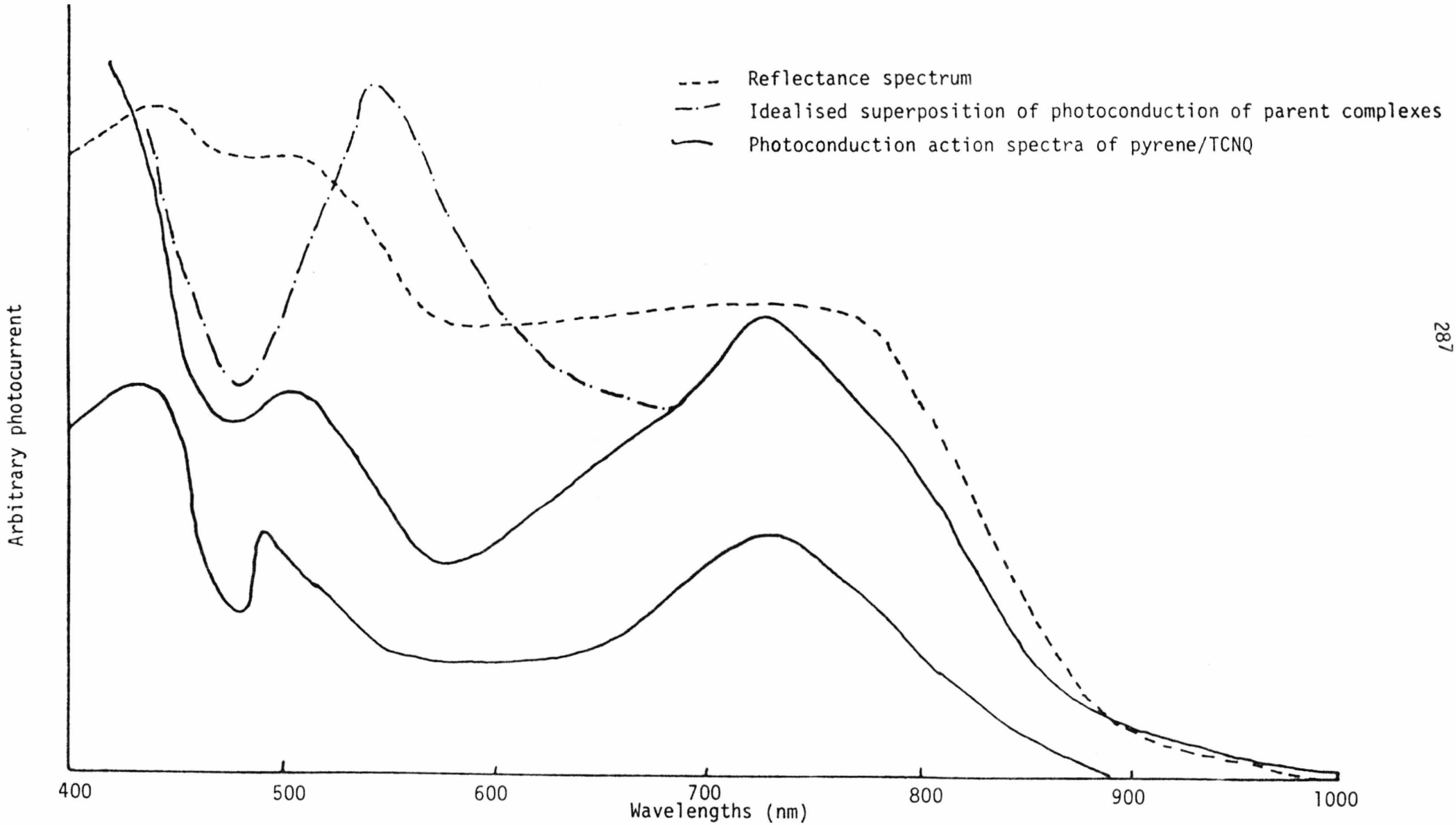
Reflectance spectrum
Idealised superposition of photoconduction of parent complexes
Photoconduction action spectra of pyrene/TCNQ
Arbitrary photocurrent
400
500
600
700
800
900
1000
Wavelengths (nm)

of either parent complex. Diffuse reflectance spectra, together with molecular orbital calculations of charge transfer transition intensities as a function of relative orientation of donor and acceptor in the parent systems, show that the relative orientation of donors and acceptor are different in the new phase from those in the parent complexes. The study of the influence of these changes on photoconduction was thought to be of interest.

Figure 6.16 shows the action spectra of the mixed complexes of this system. Table 6.3 gives details of crystal dimensions and quantum yield parameters. There is no evidence of low energy photoconduction peaks such as were observed for the dibenzothiophen/dibenzofuran/TCNQ system, and the quality of the crystals was visibly better for this system also. Thus the photoconduction charge carrier generation process in this system is the normal one discussed in the introduction to this chapter (Section 6.3) and does not appear to involve defects directly. However, variations in defect concentrations from crystal to crystal almost certainly still occur, affecting carrier mobility and recombination rate. This leads to variations in magnitude of the steady state photocurrent and quantum yield parameters which are larger than those for dibenzothiophen/dibenzofuran/TCNQ (although no larger than found for many single molecular complexes (Vincent & Wright, 1974). The action spectra in Fig. 6.17 have been scaled to comparable peak magnitude to permit better comparison of their shapes. It is clear from comparison of the action spectra of perylene/TCNQ and of the mixed pyrene/perylene/TCNQ system, that incorporation of pyrene leads to an increased photoconduction response

at wavelengths shorter than that of peak photocurrent for perylene/TCNQ. However, superposition of the action spectra of pyrene/TCNQ and perylene/TCNQ (Fig. 6.24) would produce enhancement on both short and long wavelength sides of the perylene/TCNQ peak. The action spectrum of pyrene/TCNQ closely follows the absorption spectrum (Fig. 6.24). Thus discussion of the photoconduction action spectra of the mixed complexes must consider how the absorption spectra of the two components change in the new phase observed for the mixed complexes. This is discussed in Chapter 4, where evidence is presented from diffuse reflectance spectra that the extinction coefficient of the lowest energy charge transfer band of pyrene/TCNQ in the mixed complexes is much smaller than that in the pure complex. However, orientational changes which would produce this effect are also shown, using molecular orbital calculations to lead to a similar or increased absorption intensity in the region below 500 nm, where the transitions are mixtures of the second charge transfer transition and local excitations of TCNQ . In contrast, these results also revealed that the intensity of the first charge transfer transition of the perylene/TCNQ complex is not greatly different in the mixed and pure complexes. The form of the photoconduction action spectra of the mixed complexes can be explained using these results. In the region to long wavelength side of 600 nm , the absorption of light by perylene/TCNQ in the mixed complex will be much greater than that by pyrene/TCNQ . Thus, few pyrene/TCNQ charge transfer excited states will be produced, and few charge carriers will in turn be produced from these states, so that the photocurrent in this region will not differ significantly from that of perylene/TCNQ itself. Below 500 nm , both pyrene/TCNQ and perylene/TCNQ absorb strongly in the mixed complex,so in this region the photocurrent is closer to the superposition of the action spectra of the parent complexes.

The fact that the 50:50 mixed complex has a new structure different from that of either the parent complexes may also influence photoconduction in other ways. For example, the interstack D-D overlap for the two donors may change altering the probability of carrier generation from the CT excited state. Also, structural changes may alter polarisation energies. Unfortunately, it is not possible to deduce the crystal structure of the 50-50 mixed complex from the powder diffraction data alone, so it is not possible to estimate the size of these other effects. However, since the form of the observed changes in photoconduction action spectra can be accounted for in terms of changes in absorption spectra as describedabove, it may be concluded that any additional structural effects are of relatively minor importance in this system.

Anthracene/Chrysene/TCNQ

This system was studied for the following reasons:

i) The magnitudes of maximum photoconduction of the parent complexes were found to be very different. In addition, the maximum photoconduction responses of the parent complexes were in a different spectral region. Since chrysene/TCNQ (good photoconductor) and anthracene/TCNQ (poor photoconductor) have very similar acceptor-acceptor network, with chrysene-chrysene approach closer than that of anthracene-anthracene approach the introduction of both the donors in the mixed complex could introduce interstack anthracene/chrysene overlap which could result in an enhanced photoconduction in the anthracene/TCNQ spectral response region which was otherwise very poor.

ii) Neither of the photoconduction action spectra suggest that defects are involved in photoconduction. Single crystals could easily be obtained having shiny faces characteristic of good crystals.

iii) The analysis of composition showed only 10% of anthracene is able to be incorporated into the mixed system. X-ray powder diffraction patterns showed characteristic chrysene/TCNQ patterns. Diffuse reflectance spectra of the mixed complexes are similar to that of chrysene/TCNQ with a small contribution from anthracene/TCNQ consistent with its 10% concentration.

Figures 6.19 and 6.20 show the photoconduction action spectra of mixed complexes containing 8-12% of anthracene/TCNQ in the chrysene/TCNQ lattice. Comparison of these curves with the action spectra of pure chrysene/TCNQ (Fig. 6.25) shows that there appears to be a new response peak at around 850 nm in the mixed complex crystals. However, these results were obtained without using a suitable filter to prevent second order short wavelength light reaching the sample. The importance of using such a filter is revealed by comparison with Fig. 6.21 which shows the action spectra containing 10% anthracene/TCNQ , obtained using a suitable filter to eliminate second order short wavelength light. In this case there is no response peak at 850 nm , and there is no evidence for enhanced anthracene/TCNQ photoconduction resulting from overlap of anthracene with chrysene molecules in a neighbouring stack.

Figure 6.26 shows the likely interstack anthracene-chrysene overlap diagram in this mixed complex. The powder diffraction data of Chapter 3 show that the mixed complex still has the chrysene/TCNQ lattice. The two

FIG. 6.25 PHOTORESPONSE CURVES OF CHRYSENE/TCNQ

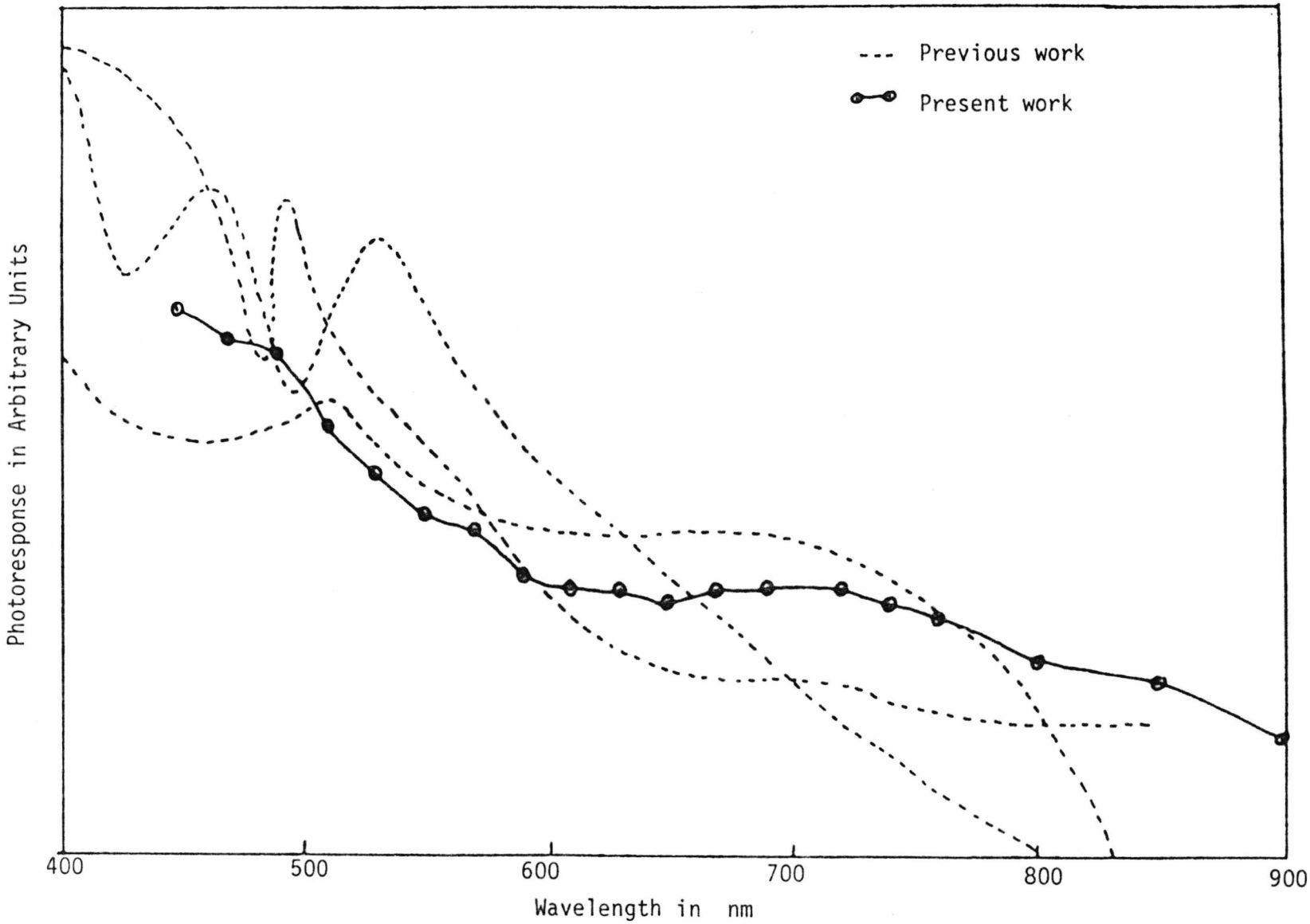

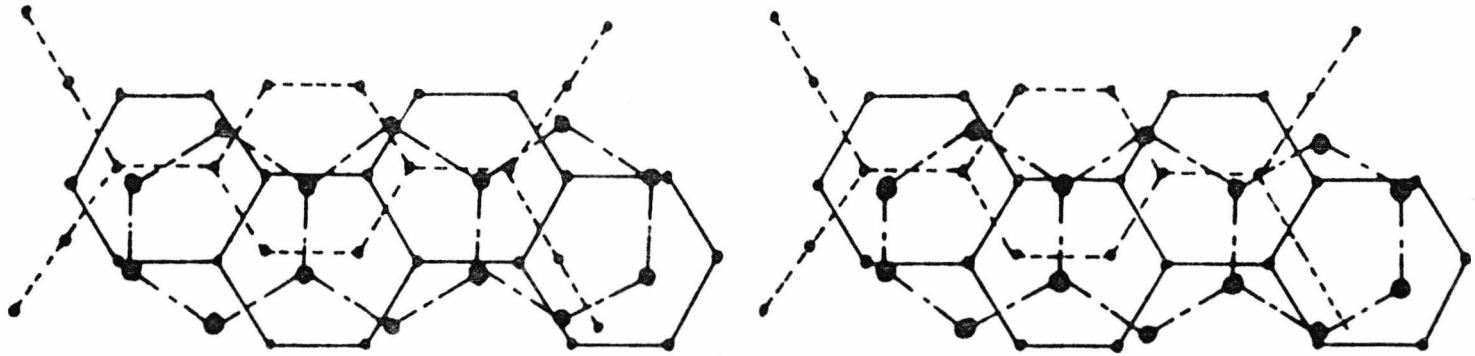

(a)

FIG. 6.26 LIKELY INTERSTACK ANTRACENE-CHRYSENE OVERLAP DIAGRAM

(a) The centre of anthracene placed at the centre of chrysene molecule

(b) The relative orientation of anthracene and TCNQ is the same as observed in the anthracene/TCNQ complex

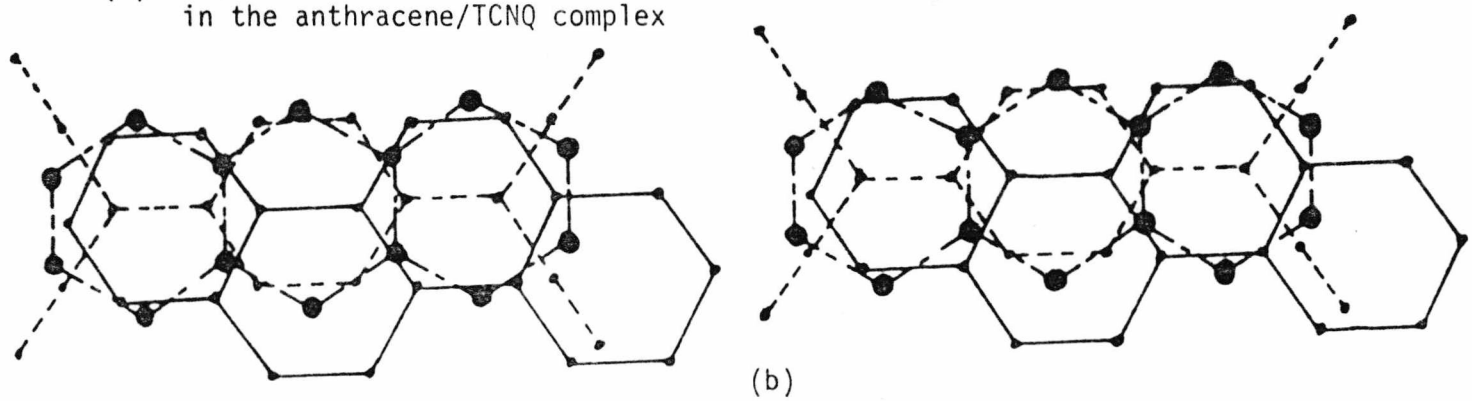

(b)

most likely sites for the anthracene molecule in this lattice are

i) at the chrysene site with the molecular centre of the anthracene placed at the same point as the centre of the chrysene molecule and the long axis of anthracene orientated so that the anthracene fits as well as possible onto the chrysene site or

ii) at the chrysene site, but aligned so that the relative orientation of anthracene and TCNQ is the same as observed in the anthracene/TCNQ complex.

In either of these orientations the overlap of anthracene with chrysene in a neighbouring stack is larger than the anthracene-anthracene overlap in anthracene/TCNQ . However, the quantum yield parameter for anthracene/TCNQ is a factor of 10^8 smaller than that for chrysene/TCNQ (VIncent & Wright, 1974) so any increase in anthracene/TCNQ photoconduction due to increased interstack overlap would need to be very large indeed in order to be visible in the presence of the chrysene/TCNQ photocurrent. The fact that only approximately 10% incorporation of anthracene/TCNQ into the chrysene/TCNQ lattice is possible further adds to this problem. The absence of any observable increase in photoconduction in the region where anthracene/TCNQ is expected to photoconduct is thus not conclusive proof that the structural effects have not enhanced the photoconduction. Although in principle such effects should be more readily observable in systems where the quantum yield parameters of the two parent complexes are less drastically different, the scatter due to approximations in the derivation of the quantum yield parameter (generally a factor of 10-100 for quantum yield parameters for different crystals of a given complex) is such that the quantum yield parameters of the parent complexes should differ by about 10^4 for any significance to be attached to observed changes in mixed complexes. Hence, further investigations along these lines were not carried out.

6.9 Conclusions

The influence of defects on photoconductivity properties of π-π^* molecular complexes has been clarified by studies of the complexes anthracene/PMDA , dibenzothiophen/TCNQ and dibenzofuran/TCNQ . Such complexes may be classified into two groups according to the relationship between the photoconduction action spectrum and the charge transfer absorption spectrum. Complexes forming good quality crystals have photoconduction action spectra whose maxima either coincide with or lie to high energy of the charge transfer absorption maxima. Anthracene/PMDA is an example of this group, and the photoconduction action spectra of crystals prepared from solution and by sublimation are similar, while the photoconduction magnitude is consistently larger in the solution grown crystals. This result is interpreted in terms of lower concentrations of defects acting as charge carrier recombination centres in the solution grown crystals. Complexes forming poorer quality crystals (e.g. dibenzothiophen/TCNQ and dibenzofuran/TCNQ) show additional features in the photoconduction action spectra, on the low energy edge of the first charge transfer absorption band. The magnitude of this response is variable from crystal to crystal of the same material and its origin is discussed in terms of a carrier generation mechanism involving dissociation of charge transfer excited states to charge carriers at defect sites in the crystal.

The photoconduction action spectra of the mixed molecular complexes studied did not show the expected ideal behaviour, namely that the mixed complex photoconduction action spectrum should be the weighted sum of the action spectra of the two parent complexes. Consideration of the factors influencing the shape and magnitude of the photoconduction response of molecular complexes shows that there are three conditions which must be satisfied if this ideal behaviour is to be observed.

1) The densities and distributions of various defects which influence photoconduction should be the same in crystals of the parent and mixed complexes. Failure to satisfy this condition will result in either the magnitude or the shape of the action spectra varying from the ideal behaviour. The mixed complex system $(\text{dibenzothiophen})_x(\text{dibenzofuran})_{1-x}$/TCNQ is an example of this type.

2) The relative orientations of donor and acceptor in the mixed complex should be the same as those in the parent complexes. Changes in these relative orientations induced by lattice packing requirements of the mixed complex structure will lead to changes in the intensity of charge transfer absorption and hence in the relative numbers of excited states of the two component complexes produced by the incident light. Even if the probability of these excited states dissociating to charge carriers is not affected by such structural changes, this will lead to changes in the relative contributions of the two component complexes to the mixed complex photoconduction action spectrum. The mixed complex system $(\text{pyrene})_x(\text{perylene})_{1-x}$/TCNQ is an example where such orientational changes affect the photoconduction of the mixed complex.

3) The degree of interstack donor-donor or acceptor-acceptor π orbital overlap should be similar for the mixed complex and the parent complexes. Changes in this overlap influence the probability of the charge transfer excited states dissociating into charge carriers. In practice, this means that the two

donors in a mixed donor complex should have similar shapes and sizes as in the case of dibenzothiophen and dibenzofuran. An attempt to exploit this effect and produce enhancement of the contribution of one of the complexes to the mixed complex photoconduction action spectrum failed for the system (anthracene)$_x$(chrysene)$_{1-x}$ TCNQ partly because it proved impossible to increase x beyond 0.16 and partly because the difference in magnitude of photocurrent in the two parent complexes is very large ($\simeq 10^8$) so that only a very dramatic enhancement of the anthracene/TCNQ photoconduction would lead to observable changes in the action spectrum of the mixed complex.

These conditions, together with the conditions discussed in Chapter 2 for formation of single crystals of mixed complexes, suggest that although the magnitude and spectral response of photoconduction may be modified by the use of mixed molecular complexes, it is very difficult to control this modification or to design specific mixed complexes having predetermined photoconduction characteristics. Polymeric materials appear to offer more promise as practical organic photoconducting materials. For example, an aggregate photoconductive film consisting of a polymer combined with a cationic organic dye and an aromatic organic compound acting as a "sensitizer-transport" component has been reported (Dulmage, Light, Marino, Salzberg, Smith & Staudenmayer, 1978; Borsenberger, Chowdry, Hoesterey & Mey, 1978) with a broad photoconduction action spectrum and a field dependent photogeneration efficiency reaching 0.5

at 10^6 v/cm . However, the present studies have provided some useful new insights into photoconduction processes in molecular complex crystals as shown above.

* * * * * *

Chapter 7

Conclusions

In this work, the preparation of parent and mixed π-π^* molecular complexes, compositional analysis of mixed complexes and the criteria for their formation as a continuous series are described. The electrical properties are interpreted with the aid of x-ray powder diffraction pattern and diffuse reflectance spectra data. The success of the present work lies in the ability to explain photoconduction action spectra by considering the above independent observations. The semiconductivity of the parent complexes is explained in terms of intrinsic conduction. For mixed complexes, there are no systematic variations in dark conductivity and semiconduction activation energy.

Mixed molecular complexes can be prepared from solution in favourable cases (Chapter 2). The mixed complexes that were prepared are listed in Table 2.3. Spectroscopic and chromatographic methods have been devised for the analysis of mixed complexes. The spectroscopic method has been the principal one used. The chromatographic method has been used to check the reproducibility and the accuracy of the spectroscopic method. Both these methods have been proved reliable and therefore are very important methods for compositional analysis of mixed molecular complexes. The above alternative methods are superior to conventional elemental analysis because most of the complexes contain only carbon, nitrogen and hydrogen and the elemental analysis is relatively insensitive to changes in composition.

As discussed in Chapter 2, the formation of a complete series of

mixed donor molecular complexes seems to require similar formation constants and solubilities for the parent complexes and similar shapes and sizes for the donors. An added advantage is to have parent complexes of similar crystal lattice structure although this is not essential.

It can be seen from Table 7.1 (see over) that there is no one set of factors which determines the formation of a continuous series of mixed complexes. This led to the suggestion that solubilities and formation constant of the parent complexes are of significance in the formation of mixed complexes.

Structural information for the mixed complexes has been obtained from x-ray powder diffraction data with the following conclusions.

Parent complexes involving two donors of similar size and/or shape (e.g. dibenzothiophen/TCNQ and dibenzofuran/TCNQ, anthracene/TCNB and phenanthrene/TCNB) often crystallise with very similar unit cells, and form a continuous series of isostructural mixed complexes. Complexes of two donors of similar size but different shape may have different unit cells but a complete series of mixed complexes may nevertheless be formed, adopting the structure of the parent complex whose lattice most readily accommodates the second donor (e.g. anthracene/dibenzothiophen/TCNQ). Where the parent complexes involve donors of very different size or shape, mixed complex formation is more restricted. In some cases (e.g. anthracene/chrysene/TCNQ) mixed complexes with small incorporation of the smaller donor into the lattice of the complex with the larger donor occur. In other cases (e.g. pyrene/perylene/TCNQ) mixed complexes having a lattice structure different from that of either of the parent complexes form over a very limited composition range.

The crystal structure of the dibenzothiophen/TCNQ complex has been determined and reveals a donor acceptor relative orientation and interplanar

Mixed Complexes	Size of Donors	Lattice Type	Cell Dimensions	Comments
Dibenzothiophen/Dibenzofuran/TCNQ	Similar	Same	Similar	Formed continuous series
Phenazine/Dibenzofuran/TCNQ	Similar	Same	Similar	Formed complex rich in phenazine/TCNQ
Anthracene/Dibenzothiophen/TCNQ	Similar	Different	Different	Formed continuous series
Anthracene/Chrysene/TCNQ	Different	Different	Different	Only 10% anthracene/TCNQ is incorporated
Pyrene/Perylene/TCNQ	Different	Same	Similar	Formed new phase of 50:50 donors

TABLE 7.1

separation consistent with weak charge transfer interactions. Interstack donor-donor and acceptor-acceptor π orbital overlap is poor. The dibenzofuran/TCNQ complex has a very similar triclinic unit cell, with the a axis length halved. This halving of the unit cell is due to the fact that dibenzofuran can be orientated on the dibenzothiophen site in two ways (by rotation through 180^0 about its longest principal axis) without causing excessively short contacts with atoms of surrounding molecules in the lattice. The slightly different shape of dibenzothiophen and the larger size of the sulfur atom do not permit such an alternative orientation in the dibenzothiophen/TCNQ complex.

Comparison of diffuse reflectance spectra and single crystal spectra of anthracene/phenanthrene/TCNB complexes has shown that diffuse reflectance spectra can yield useful information on the relative intensities of charge transfer transitions in different molecular complexes. The first charge transfer band energies of the TCNQ complexes studied have been correlated with donor ionisation potential and with calculated energies of the donor highest occupied molecular orbitals. Experimental data on the relative intensities of the first charge transfer bands of the parent complexes follow the same trends shown by calculations of these intensities using semiempirical self-consistent molecular orbital methods with configuration interaction. A qualitative impression of these trends is also obtained by examination of the symmetries of the donor HOMO and acceptor LUMO in conjunction with the observed relative orientation of donor and acceptor in each crystalline complex. Comparison of the relative intensities of charge transfer bands in mixed complexes with those of the two parent complexes provides information on the relative orientations of donors and acceptor in the mixed complexes. These relative intensities from mixed and parent complexes are in good agreement for systems where mixed and parent complexes are isostructural (e.g. anthracene/phenanthrene/TCNB) or where the mixed complex lattice permits the same relative orientation of

donor and acceptor as in the parent complexes (e.g. anthracene/dibenzothiophen/TCNQ). However, the spectrum of the new phase of pyrene/perylene/TCNQ is very similar to that of perylene/TCNQ. The orientation of pyrene relative to TCNQ in this new phase must therefore be very unfavourable for overlap of orbitals involved in the first charge transfer transition from pyrene to TCNQ.

The study of semiconduction properties of the mixed complexes showed no ideal trend in conductivity as a function of composition. However, two significant general features have been observed:

1) Larger crystals of a given composition have lower conductivity.
2) In the majority of cases, the conductivities are lower than that predicted by a simple idealised model (Chapter 5).

The conclusion that can be derived from the above observations is that the deviations from ideal behaviour are due to the physical defects in the mixed complexes.

The influence of defects on photoconductivity has also been studied. Anthracene/PMDA can be prepared both by sublimation and from solution. Sublimation grown crystals of anthracene/PMDA have more defects than solution grown crystals. Defects do not change the shape of photoconduction action spectrum in this system but the magnitude of photoconduction action spectrum in solution grown crystals is larger than that in sublimation grown crystals. The enhanced photocurrent in solution grown crystals is attributed to higher steady state carrier concentrations. The observation of the same power law for dependence of photocurrent on light intensity in both types of crystals is explained by changes in the extent of carrier loss occurring at recombination centres which are of

lower density in solution grown crystals. The photoconduction action spectrum resembles the charge transfer absorption spectrum for this complex.

Studies of the photoconductivity of mixed complexes have led to the conclusion that there are three conditions which must be satisfied in order for the action spectra of mixed complexes to correspond to the appropriately weighted sum of the action spectra of the parent complexes:

Firstly, the density and distribution of defects in the mixed and parent complexes should be similar. In some cases (e.g. dibenzothiophen/dibenzofuran/TCNQ defects alter the shape of the photoconduction action spectrum, producing an enhanced response on the low energy edge of the first charge transfer absorption band. The carrier generation mechanism proposed for this region involves interaction of $D^{+}A^{-}$ excited states with defects. One of the charges is trapped at the defect with a corresponding increase in the probability of the other charge separating to yield a charge carrier. In other cases (e.g. anthracene/PMDA) defects alter the magnitude of conduction but not its spectral response. In either case, the photoconduction action spectrum of a mixed complex cannot be predicted from knowledge of the action spectra of the parent complexes if defect concentrations and distributions are not approximately the same for crystals of all the materials. Thus the design of mixed complexes having predetermined action spectra is not possible because defect density and distribution is difficult to control and characterise in practice.

Secondly, donor-donor and acceptor-acceptor interstack π orbital overlap should be similar in parent and mixed complexes. If not, the efficiency of carrier generation from charge transfer excited states will alter. For mixed complexes which are either isostructural with the parent

complexes or have donors of similar size and shape, this condition is satisfied. Such cases have been identified from the x-ray diffraction studies in this work. In principle, this condition could be exploited to produce enhanced photoconduction in a complex where such interstack overlap was poor, by preparing mixed complexes with a larger donor. Efforts to enhance photoconduction by anthracene/TCNQ in this way, by preparing anthracene/chrysene/TCNQ mixed complexes, have failed. The small extent of incorporation of anthracene into the mixed complex together with the very large difference in efficiency of carrier generation from charge transfer excited states in the two parent complexes probably obscures any such enhancement in this system.

Thirdly, the orientations of the two donors with respect to the acceptor should be the same in the mixed complexes as in the parent complexes. If not, the relative intensities of the two first charge transfer bands will be different in the parent and mixed complexes. This will in turn alter the relative number of charge transfer excited states of the two components of the mixed complex and hence alter the resulting photoconduction action spectrum. This effect has been observed for pyrene$_x$/perylene$_{1-x}$/TCNQ with $x \simeq 0.5$. The absence of photoconduction in this material in the region expected for pyrene/TCNQ photoconduction is consistent with the conclusions from the structural and spectroscopic work reported in this thesis.

The above conclusions from structural, spectroscopic and conductivity studies show that the properties of mixed molecular complexes cannot be completely predicted from knowledge of their composition and of the relevant properties of the parent complexes. Changes in crystal structure or the intensity of charge transfer transitions or the concentration and distribution of physical defects nearly always occur when mixed complexes are formed. These changes can be detected by experiments of the type reported in this thesis. To some extent they can be

rationalised in terms of properties of the molecules involved, as discussed in earlier chapters of the thesis. However, complete prediction of all these changes which may be associated with composition changes for any new mixed complex system remains impossible. This severely limits the possibility of designing new mixed complexes with predetermined structural, spectroscopic or electrical properties. A further limitation revealed by the present work is the difficulty in preparing mixed complexes of certain systems by the method of crystal growth from solution. Even given sufficient data to permit the design of mixed complexes of predetermined properties, this limitation will often prevent isolation of materials with ideal properties.

The following suggestions serve as a guideline for future work aimed at providing a more complete understanding of the properties of mixed molecular complexes:

1) Use of different preparation techniques (e.g. sublimation or melt growth of crystals) to avoid constraints imposed by solubility or formation constant of the complexes in solution.
2) Characterisation of defect concentrations and distributions in several mixed complexes.
3) Determination of the crystal structure of mixed complexes, particularly that of the new phase formed by pyrene/perylene/TCNQ.

* * * * * *

Appendix I

X-Ray Crystallography

A.1.1 Dibenzothiophen/TCNQ Structure Determination

Crystal Data: Dibenzothiophen/TCNQ

$C_{24}H_{12}N_4S$, $\underline{M}$ = 388.4 , triclinic, cell dimensions:

$\underline{a}$ = 16.316(4) , $\underline{b}$ = 8.910(2) , $\underline{c}$ = 6.839(3) Å ,

$\underline{\alpha}$ = 98.35(3) , $\underline{\beta}$ = 98.66(4) , $\underline{\gamma}$ = 100.13(2)° ,

$\underline{U}$ = 952.4 Å^3 , $\underline{D_m}$ = 1.357g.cm^{-3} (by flotation) ,

$\underline{Z}$ = 2 , $\underline{D_c}$ = 1.355 g.cm^{-3} ,

space group $P\bar{1}$.

Crystal Data: Dibenzofuran/TCNQ

$C_{24}H_{12}N_4O$, M = 372.3 , triclinic, cell dimensions:

$\underline{a}$ = 8.010(2) , $\underline{b}$ = 8.997(2) , $\underline{c}$ = 6.780(1) Å ,

α = 97.75(2) , $\underline{\beta}$ = 100.68(2) , γ = 99.58(3)° ,

U = 466.5 Å^3 , Z = 1 .

The problems of structure solution were similar to those for the acenaphthene/TCNQ complex (Tickle & Prout, 1973) which also has a triclinic unit cell containing two molecules of a complex between a non-centrosymmetric donor and a centrosymmetric acceptor. Abnormal distribution of normalised structure factor values in such cases leads to difficulty in structure solution by direct methods. The structure was therefore solved by Patterson and Fourier methods. From a three-dimensional sharpened Patterson synthesis, the plane and orientation of the TCNQ molecule was readily deduced by examination of the extensive

isometric array of peaks with 1.4 Å spacing around the origin. The co-ordinates of the centroid of the TCNQ molecule were deduced from the large 16-fold vector at (0.520 , -0.011 , 0.048) included in the intermolecular vectors between two TCNQ molecules related by the centre of symmetry. An F_o synthesis with phases calculated from the TCNQ atomic co-ordinates revealed the dibenzothiophen molecule. Structure factors calculated from this model, with the overall scale and isotropic temperature factors calculated from a Wilson plot produced an initial R of 0.341. Full matrix refinement of co-ordinates and individual isotropic temperature factors, using unit weights for all observed reflections, gave a converged set of parameters with R=0.161. A difference Fourier synthesis revealed peaks in the positions expected for hydrogen atoms, and showed evidence of anisotropic motion of C , N and S atoms. Hydrogen atoms were therefore placed geometrically, with C-H 1.00 A , to lie in the relevant molecular plane along the bisector of the appropriate C-C-C angle, and assigned isotropic temperature factors of 0.05 Å . Further refinement was by least squares using a large block approximation to the normal matrix, with five blocks as follows:

1) Scale and dummy overall temperature factors
2) TCNQ co-ordinates
3) Dibenzothiophen co-ordinates
4) TCNQ temperature factors
5) Dibenzothiophen temperature factors.

Refinement of all C , N and S co-ordinates and anisotropic temperature factors, with unit weights, converged with R 0.090. An agreement analysis by ranges of F_o showed that the two most intense reflections were notably

inaccurate, with F_o less than F_c. These reflections were considered to be suffering from secondary extinction and were given zero weight. The same analysis showed a trend for increasing inaccuracy with increasing intensity for reflections with $F_o > 250$, and the 70 reflections in this range were given weights $w = 250/F_o$. Refinement of all positional and thermal parameters (C,N,S anisotropic, H isotropic) converged with R 0.080, but several of the hydrogen positions resulting corresponded to C-H bond lengths as short as 0.7 Å with C-H directions well removed from the bisectors of the relevant C-C-C angles. Hydrogen atoms were therefore once more positioned geometrically as before, with isotropic temperature factors equal to those of the carbon atoms to which they were attached. Final refinement of co-ordinates and anisotropic temperature factors of C, N, and S atoms converged with R 0.082. The average and maximum parameter shifts in the final cycle of refinement were 0.03 and 0.60 e.s.d. respectively. All calculations used the Oxford Crystals programs (Carruthers, 1975) on the University of London CDC 7600 computer, with scattering factors for neutral atoms from International Tables for X-ray Crystallography (1974).

TABLE A.1.1 & A.1.2 FINAL ATOMIC CO-ORDINATES AND THERMAL PARAMETERS

ATOM	X/A	Y/B	Z/C	U(ISO)
C(1)	0.3230(3)	0.6327(6)	0.0822(8)	
C(2)	0.3431(3)	0.4805(6)	0.0570(9)	
C(3)	0.2801(4)	0.3510(6)	0.0067(9)	
C(4)	0.1933(4)	0.3659(6)	-0.0206(8)	
C(5)	0.1736(4)	0.5180(7)	0.0057(9)	
C(6)	0.2354(4)	0.6453(6)	0.0545(9)	
C(7)	0.3867(4)	0.7608(6)	0.1349(9)	
C(8)	0.1288(4)	0.2347(7)	-0.0738(9)	
C(9)	0.3706(4)	0.9160(7)	0.1623(10)	
C(10)	0.4750(4)	0.7523(7)	0.1619(10)	
C(11)	0.1464(4)	0.0823(7)	-0.1046(10)	
C(12)	0.0417(4)	0.2457(7)	-0.1005(9)	
N(1)	0.3609(4)	1.0415(6)	0.1884(11)	
N(2)	0.5447(4)	0.7476(6)	0.1863(10)	
N(3)	0.1598(4)	-0.0377(6)	-0.1316(10)	
N(4)	-0.0279(4)	0.2546(7)	-0.1199(10)	
C(13)	0.4024(5)	0.8267(8)	0.6548(11)	
C(14)	0.3184(5)	0.8218(7)	0.6243(10)	
C(15)	0.2640(4)	0.6750(7)	0.5714(9)	
C(16)	0.2963(4)	0.5395(7)	0.5532(9)	
C(17)	0.3838(4)	0.5484(8)	0.5857(9)	
C(18)	0.4363(4)	0.6950(9)	0.6375(11)	
C(19)	0.0659(5)	0.1719(11)	0.3883(11)	
C(20)	0.0758(4)	0.3205(10)	0.4182(11)	
C(21)	0.1498(4)	0.4366(8)	0.4754(9)	
C(22)	0.2300(4)	0.3999(7)	0.4964(9)	
C(23)	0.2381(4)	0.2475(7)	0.4655(10)	
C(24)	0.1648(5)	0.1324(9)	0.4098(11)	
S(1)	0.1538(1)	0.6370(2)	0.5241(3)	
H(1)	0.4034	0.4688	0.0755	0.0348
H(2)	0.2947	0.2463	-0.0105	0.0392
H(3)	0.1133	0.5291	-0.0125	0.0396
H(4)	0.2207	0.7488	0.0740	0.0399
H(5)	0.4416	0.9289	0.6910	0.0602
H(6)	0.2962	0.9187	0.6396	0.0618
H(7)	0.4083	0.4539	0.5713	0.0504
H(8)	0.4988	0.7049	0.6640	0.0592
H(9)	0.0346	0.0883	0.3499	0.0743
H(10)	0.0184	0.3457	0.3996	0.0636
H(11)	0.2947	0.2190	0.4830	0.0545
H(12)	0.1691	0.0217	0.3850	0.0698

TABLE A.1.1 FINAL ATOMIC CO-ORDINATES AND THERMAL PARAMETERS$^{\neq}$ WITH STANDARD DEVIATIONS IN PARENTHESES

ATOM	U(11)	U(22)	U(33)	U(23)	U(13)	U(12)
C(1)	0.0383(34)	0.0308(31)	0.0495(35)	0.0065(26)	0.0076(27)	0.0098(26)
C(2)	0.0382(33)	0.0363(33)	0.0517(36)	0.0080(27)	0.0083(27)	0.0145(28)
C(3)	0.0418(35)	0.0399(34)	0.0498(36)	0.0060(28)	0.0116(28)	0.0163(29)
C(4)	0.0401(34)	0.0401(35)	0.0417(33)	0.0061(27)	0.0067(26)	0.0116(28)
C(5)	0.0393(34)	0.0445(36)	0.0519(37)	0.0062(29)	0.0081(28)	0.0176(29)
C(6)	0.0452(37)	0.0312(32)	0.0536(37)	0.0019(27)	0.0085(29)	0.0161(28)
C(7)	0.0422(37)	0.0364(35)	0.0606(40)	0.0078(29)	0.0103(29)	0.0177(29)
C(8)	0.0417(36)	0.0395(35)	0.0510(37)	0.0043(28)	0.0049(28)	0.0098(29)
C(9)	0.0410(37)	0.0449(40)	0.0687(44)	0.0072(32)	0.0069(31)	0.0059(30)
C(10)	0.0522(42)	0.0361(34)	0.0659(43)	0.0032(30)	0.0112(33)	0.0141(31)
C(11)	0.0456(38)	0.0363(36)	0.0651(43)	-0.0021(31)	0.0089(31)	0.0038(30)
C(12)	0.0494(42)	0.0502(39)	0.0540(40)	0.0001(31)	0.0033(32)	0.0092(32)
N(1)	0.0683(41)	0.0365(32)	0.1234(56)	0.0031(33)	0.0057(37)	0.0162(29)
N(2)	0.0490(35)	0.0557(36)	0.1070(50)	0.0058(33)	0.0121(33)	0.0178(29)
N(3)	0.0726(42)	0.0425(34)	0.1085(52)	0.0009(34)	0.0107(37)	0.0081(31)
N(4)	0.0480(37)	0.0853(46)	0.0985(50)	0.0202(38)	0.0053(34)	0.0136(33)
C(13)	0.0721(51)	0.0537(44)	0.0642(46)	-0.0022(35)	0.0167(38)	-0.0032(38)
C(14)	0.0908(58)	0.0419(40)	0.0637(46)	0.0028(33)	0.0149(40)	0.0208(39)
C(15)	0.0462(37)	0.0608(42)	0.0395(34)	0.0075(30)	0.0062(28)	0.0217(33)
C(16)	0.0402(37)	0.0482(37)	0.0467(36)	0.0120(29)	0.0043(28)	0.0076(29)
C(17)	0.0456(39)	0.0633(44)	0.0501(39)	0.0083(32)	0.0062(30)	0.0136(33)
C(18)	0.0459(40)	0.0760(52)	0.0696(48)	0.0099(39)	0.0088(35)	-0.0002(38)
C(19)	0.0669(53)	0.1031(66)	0.0594(49)	-0.0041(46)	0.0036(40)	-0.0276(49)
C(20)	0.0474(44)	0.1107(66)	0.0535(44)	-0.0075(43)	0.0027(34)	0.0035(45)
C(21)	0.0467(40)	0.0748(47)	0.0394(35)	-0.0004(32)	0.0071(29)	0.0157(35)
C(22)	0.0457(38)	0.0531(40)	0.0438(36)	0.0050(30)	0.0065(29)	0.0107(31)
C(23)	0.0710(47)	0.0516(42)	0.0521(41)	0.0038(32)	0.0121(34)	0.0113(36)
C(24)	0.0831(57)	0.0683(49)	0.0575(46)	0.0019(37)	0.0062(41)	-0.0108(44)
S(1)	0.0557(11)	0.0823(13)	0.0629(11)	0.0048(9)	0.0055(8)	0.0372(9)

TABLE A.1.2 THERMAL PARAMETERS≠ WITH STANDARD DEVIATIONS IN PARENTHESES

≠Anisotropic temperature factors are of the form $\exp[-2\pi^2(U_{11}h^2a^{*2}+U_{22}k^2b^{*2}+U_{33}\ell^2c^{*2}+2U_{12}hka^*b^*+2U_{13}h\ell a^*c^*+2U_{23}k\ell b b^*c^*)]$

TABLE A.1.3 OBSERVED STRUCTURE AMPLITUDES (FO) AND CALCULATED STRUCTURE FACTORS (FC) FOR DIBENZOTHIOPHEN/TCNQ

H	/FO/	/FC/	PHI
** K= 0 L= 0 **			
1	93	71	0
2	587	569	180
3	268	267	180
4	521	468	180
5	167	167	0
6	331	306	0
7	238	222	0
8	65	51	0
9	261	239	180
10	273	279	180
11	44	32	180
12	21	22	0
13	190	192	0
14	11	7	0
15	51	58	180
16	71	67	180
** K= 1 L= 0 **			
-15	15	10	180
-14	59	64	180
-13	150	155	180
-12	20	23	0
-11	54	49	0
-10	14	7	180
-9	69	58	180
-8	134	124	180
-7	145	146	180
-6	39	34	180
-5	237	230	0
-4	95	80	180
-3	35	37	0
-2	1212	1060	0
-1	138	139	180
0	23	53	180
1	63	53	0
2	253	220	180
3	122	121	0
4	258	225	180
5	148	144	180
6	32	32	0
7	55	49	180
8	277	255	0
9	71	69	0
10	32	34	0
11	55	56	0
12	110	103	180
13	64	54	0
14	43	50	0
15	37	29	0
** K= 2 L= 0 **			
-15	13	28	180
-14	188	179	0
-13	44	41	0
-12	22	16	180
-11	101	102	180
-10	39	32	0
-9	79	77	0
-8	178	175	0
-7	33	33	0
-6	142	132	0
-5	98	96	180
-4	721	609	180
-3	77	79	0
-2	177	152	180
-1	200	196	0
0	434	399	180
1	251	241	180

H	/FO/	/FC/	PHI
2	781	710	180
3	59	51	180
4	412	347	180
5	302	268	0
6	514	444	0
7	94	94	180
8	55	42	180
9	206	193	180
10	22	24	180
11	179	177	0
12	92	88	0
13	23	20	180
14	12	6	180
15	43	51	180
** K= 3 L= 0 **			
-16	18	11	180
-15	48	53	0
-14	20	18	0
-13	90	87	0
-12	111	107	0
-11	80	83	0
-10	188	190	180
-9	80	86	0
-8	168	144	0
-7	55	44	0
-6	143	130	0
-5	244	243	180
-4	270	252	180
-3	45	48	0
-2	229	216	0
-1	212	201	0
0	123	107	180
1	223	170	180
2	276	234	0
3	11	11	0
4	104	94	180
5	35	44	0
6	27	25	0
7	124	132	180
8	22	14	180
9	22	21	180
** K= 4 L= 0 **			
-16	31	46	0
-15	21	23	180
-14	136	130	180
-13	103	102	180
-12	143	146	180
-11	200	210	0
-10	55	51	180
-9	73	77	180
-8	41	32	0
-7	91	96	180
-6	34	35	0
-5	42	28	180
-4	218	212	0
-3	211	206	0
-2	163	147	0
-1	223	206	180
0	91	78	0
1	110	105	180
2	511	485	0
3	87	88	0
4	82	64	180
5	52	41	0
6	54	51	180
7	44	44	180
8	101	99	0

H	/FO/	/FC/	PHI
10	32	31	0
11	72	70	180
12	60	57	180
13	35	36	180
** K= 5 L= 0 **			
-15	43	41	0
-14	51	55	0
-13	120	111	180
-12	155	167	180
-11	256	220	0
-10	224	220	0
-9	96	83	180
-8	71	82	180
-7	42	37	180
-6	39	38	180
-5	51	48	180
-4	204	177	0
-3	33	26	0
-2	77	82	180
-1	63	60	180
0	15	9	0
1	45	49	0
2	39	52	0
3	16	9	180
4	36	41	0
5	76	83	180
6	92	101	180
7	49	43	0
8	43	49	0
** K= 6 L= 0 **			
-15	58	52	180
-14	22	28	180
-13	132	128	180
-12	350	312	0
-11	222	213	0
-10	20	15	180
-9	101	102	180
-8	133	133	180
-7	43	43	180
-6	36	36	0
-5	92	80	0
-4	30	27	0
-3	30	30	0
-2	286	270	180
-1	31	29	180
0	46	42	0
1	46	42	180
2	52	59	0
3	60	53	180
4	140	141	180
5	42	45	180
6	63	63	0
7	65	70	180
8	60	65	0
** K= 7 L= 0 **			
-13	31	31	180
-12	15	17	180
-11	24	30	0
-10	36	29	0
-9	95	92	0
-8	95	95	180
-7	46	43	180
-6	31	36	180
-5	67	78	180
-4	133	147	0
-3	105	108	0

H	/FO/	/FC/	PHI
-2	44	48	0
-1	123	129	180
0	201	200	180
1	73	73	0
2	167	167	0
3	41	46	180
4	34	33	180
5	39	43	0
6	98	100	180
8	46	45	0

** K= 8 L= 0 **

H	/FO/	/FC/	PHI
-11	42	40	180
-10	99	95	180
-9	42	43	0
-8	27	27	180
-7	38	39	180
-6	117	124	0
-4	30	24	0
-3	84	97	180
-2	45	50	180
-1	76	73	0
0	102	109	0
2	18	24	0
3	37	34	180
4	50	47	0
5	13	5	0

** K= 9 L= 0 **

H	/FO/	/FC/	PHI
-5	24	29	0
-4	72	70	0
-2	75	69	180
0	20	8	180
1	13	24	0

** K= -9 L= 1 **

H	/FO/	/FC/	PHI
-2	21	28	180
0	36	30	180
1	29	30	0
2	18	26	180
3	15	15	0
5	30	34	180
9	66	65	0

** K= -8 L= 1 **

H	/FO/	/FC/	PHI
-6	40	38	180
-5	19	21	180
-4	57	46	180
-3	23	24	0
-2	27	20	0
-1	56	56	0
0	195	193	0
1	164	163	180
2	22	23	180
3	93	94	0
4	37	36	180
5	44	46	0
6	72	82	0
7	70	64	180
8	91	96	180
9	14	10	180
10	43	40	0

** K= -7 L= 1 **

H	/FO/	/FC/	PHI
-9	24	22	180
-8	53	57	0
-7	55	57	0
-6	59	55	180
-5	52	55	180
-4	97	93	180
-3	58	62	0
-2	369	383	0
-1	125	135	180
0	57	61	0
1	51	58	0
2	180	184	180
3	35	39	180
4	36	46	0
5	57	58	0
6	134	132	0
7	42	35	180
8	80	78	180
9	37	48	180
10	70	64	180
11	65	67	0
13	87	88	0

** K= -6 L= 1 **

H	/FO/	/FC/	PHI
-10	51	52	0
-9	15	13	0
-8	70	77	180
-7	74	73	180
-6	47	14	180
-5	117	123	0
-4	149	149	0
-3	32	46	180
-2	214	216	180
-1	49	53	180
0	127	114	180
1	50	49	0
2	62	59	180
3	41	39	0
4	62	50	180
5	74	85	180
6	27	25	0
7	39	45	180
8	160	155	0
9	91	101	0
10	102	111	180
11	31	37	0
12	52	48	0
14	33	34	0

** K= -5 L= 1 **

H	/FO/	/FC/	PHI
-9	42	44	0
-8	69	60	0
-6	72	75	180
-4	141	135	180
-2	38	6	0
-1	56	52	0
0	221	212	180
1	144	125	180
2	264	256	180
3	208	191	0
4	296	275	0
5	44	23	180
6	12	12	0
7	102	99	180
8	225	223	180
9	23	19	180
10	199	192	0
11	112	108	0
13	102	109	180
14	25	20	180
15	66	63	180

** K= -4 L= 1 **

H	/FO/	/FC/	PHI
-14	28	23	180
-13	27	17	0
-11	94	102	0
-10	144	139	180
-9	73	72	180
-8	28	20	180
-7	45	48	0
-6	284	281	0
-5	15	17	0
-3	195	187	180
-2	49	43	180
-1	122	121	0
0	306	290	0
1	274	272	0
2	517	468	0
3	357	334	180
4	375	357	180
5	146	133	0
6	40	41	0
7	165	166	0
8	129	98	0
9	37	36	180
10	260	259	180
11	94	100	180
12	97	101	0
13	25	23	180
14	49	48	0
15	33	30	180
16	75	78	180

** K= -3 L= 1 **

H	/FO/	/FC/	PHI
-15	42	50	180
-14	81	79	180
-12	139	133	180
-10	205	201	0
-9	49	50	180
-8	92	91	180
-7	12	24	180
-6	69	65	0
-4	200	185	0
-3	169	162	0
-2	66	68	180
-1	153	160	180
0	447	408	0
1	144	143	180
2	149	152	0
3	162	175	0
5	19	22	180
6	21	17	180
8	97	95	0
9	26	38	0
12	150	149	180
13	15	19	0
14	57	62	180
15	81	84	0
16	45	45	0

** K= -2 L= 1 **

H	/FO/	/FC/	PHI
-14	29	33	180
-13	109	107	180
-12	365	370	0
-10	172	171	180
-9	96	86	0
-7	26	21	180
-6	58	59	180
-5	151	151	180
-4	295	313	180
-3	57	51	0
-2	375	376	180
-1	220	229	0

H	/FO/	/FC/	PHI
0	74	78	0
1	235	249	180
2	229	233	180
3	150	159	120
4	51	43	0
5	182	192	0
6	229	224	0
7	248	235	180
8	348	318	180
9	46	21	0
10	142	128	0
11	133	144	0
12	86	77	0
13	79	81	0
15	26	28	120
16	21	27	180

** K= -1 L= 1 **

H	/FO/	/FC/	PHI
-16	53	60	180
-15	70	76	180
-14	239	250	0
-13	179	189	0
-12	65	70	0
-11	18	22	0
-10	142	141	180
-9	139	148	180
-8	188	188	180
-7	72	31	0
-6	330	314	0
-5	163	181	0
-4	191	197	180
-3	122	148	180
-2	359	350	180
-1	36	34	0
0	187	206	0
1	208	239	0
2	34	27	180
3	199	203	180
4	490	498	180
5	222	211	180
6	564	509	180
7	444	418	0
8	428	389	0
9	202	196	180
10	28	34	180
11	136	124	180
12	68	72	0
13	88	95	0
14	63	60	0
15	44	27	180
16	20	27	0

** K= 0 L= 1 **

H	/FO/	/FC/	PHI
-15	81	83	0
-14	86	80	180
-13	139	142	180
-12	120	119	180
-11	107	104	0
-10	48	41	180
-9	173	176	0
-8	224	198	180
-7	257	259	180
-6	635	603	0
-5	26	24	0
-4	361	361	0
-3	219	233	0
-2	82	86	0
-1	121	123	180
0	66	66	180
1	73	81	180
2	219	226	0
3	196	211	0
4	218	211	180
5	169	154	0
6	79	81	180
7	93	106	180
8	181	177	0
9	85	45	0
10	113	108	0
11	12	5	0
12	140	146	180
13	207	222	180
14	102	104	180
16	46	51	0

** K= 1 L= 1 **

H	/FO/	/FC/	PHI
-16	19	17	180
-12	72	62	180
-11	57	62	180
-10	332	315	180
-9	61	62	180
-8	572	522	0
-7	182	189	0
-6	73	61	180
-5	141	158	180
-4	174	181	180
-3	57	71	180
-2	36	43	0
-1	177	206	0
0	269	278	0
1	107	105	180
2	448	427	0
3	332	316	180
4	14	23	0
5	266	249	0
6	280	260	0
7	115	107	0
8	27	24	0
9	141	145	180
10	42	41	180
11	105	108	180
12	239	247	180
13	245	253	0
14	61	66	0
15	16	18	180

** K= 2 L= 1 **

H	/FO/	/FC/	PHI
-16	22	26	180
-15	94	101	180
-14	29	39	0
-13	33	37	180
-12	166	162	0
-11	60	74	0
-10	166	144	0
-9	31	36	180
-8	356	343	180
-7	96	89	180
-6	59	64	0
-5	158	168	0
-4	28	9	0
-3	115	126	180
-2	505	528	180
-1	6	148	180
0	44	30	180
1	134	148	0
2	190	188	0
3	162	159	180
4	277	262	180
5	132	101	180
6	66	63	180
8	233	229	0
9	26	28	180
10	302	307	180
11	129	127	0
12	124	128	0
13	23	21	0
14	96	92	0

** K= 3 L= 1 **

H	/FO/	/FC/	PHI
-16	102	113	0
-15	41	39	0
-14	23	23	0
-13	24	20	180
-12	83	85	180
-11	75	72	0
-10	187	185	0
-9	73	79	0
-8	47	39	180
-7	141	153	180
-6	27	30	180
-5	124	126	180
-4	279	265	0
-3	233	245	0
-2	533	604	180
-1	14	18	180
0	230	219	180
1	141	150	180
2	25	13	180
3	209	190	0
4	87	83	180
5	26	21	180
6	189	188	180
8	50	57	180
9	55	57	0
10	172	175	0
11	96	106	180
12	44	40	0
13	14	0	0
14	12	16	0

** K= 4 L= 1 **

H	/FO/	/FC/	PHI
-16	89	82	180
-15	73	78	0
-14	37	39	180
-13	116	128	0
-12	55	55	0
-11	132	136	180
-10	201	205	180
-8	161	156	0
-7	59	71	0
-6	209	202	0
-5	53	30	0
-4	475	427	180
-3	183	191	180
-2	251	239	0
-1	188	185	0
0	321	307	0
1	109	94	0
2	16	19	0
3	35	48	180
4	82	88	180
5	51	53	0
6	146	144	0
7	59	70	0
8	16	8	180
9	122	128	180

** K= 5 L= 1 **

H	/FO/	/FC/	PHI
-16	17	21	0

H	/FO/	/FC/	PHI
-15	17	13	180
-14	84	94	180
-13	89	90	180
-12	61	70	180
-11	90	86	0
-10	186	185	0
-9	72	74	180
-8	238	244	180
-6	149	136	180
-5	58	70	0
-4	311	299	0
-3	41	36	0
-2	73	76	0
-1	145	150	180
0	55	51	0
1	76	83	0
2	255	261	0
3	69	58	180
4	63	52	180
5	102	108	180
6	36	42	180
7	64	61	0
8	70	66	0
10	32	32	180
11	18	22	0

** K= 6 L= 1 **

H	/FO/	/FC/	PHI
-15	59	49	0
-14	28	20	180
-13	84	91	180
-12	55	58	0
-11	102	105	180
-10	27	27	0
-9	116	123	0
-8	69	66	0
-7	27	29	0
-6	165	165	180
-5	83	85	180
-4	37	38	0
-3	52	55	0
-2	142	133	0
-1	47	38	180
0	77	78	180
1	44	36	180
2	353	365	180
3	17	30	180
4	148	148	0
5	84	83	0
6	25	22	0
7	85	88	180
8	49	56	180
9	44	43	0

** K= 7 L= 1 **

H	/FO/	/FC/	PHI
-13	34	34	0
-12	62	60	0
-10	12	14	0
-8	26	23	180
-7	21	16	0
-6	22	31	180
-5	28	21	0
-4	103	108	0
-3	124	132	180
-2	45	52	180
-1	142	143	0
0	345	360	180
1	30	32	0
2	101	110	0
3	27	23	0
4	53	43	0
5	34	37	180
6	16	22	180
7	22	26	0

** K= 8 L= 1 **

H	/FO/	/FC/	PHI
-11	40	50	0
-10	90	86	0
-8	122	125	180
-7	45	34	180
-6	20	27	0
-5	12	9	180
-4	74	74	0
-3	72	71	0
-2	88	76	180
-1	52	50	180
0	36	34	0
2	98	96	0
3	37	48	0
4	68	67	0

** K= 9 L= 1 **

H	/FO/	/FC/	PHI
-6	76	73	180
-5	56	51	180
-4	69	64	0
-3	20	22	0
-2	57	55	0

** K= -9 L= 2 **

H	/FO/	/FC/	PHI
-2	17	8	180
1	40	34	180
2	34	35	180
3	26	25	0
7	45	38	0

** K= -8 L= 2 **

H	/FO/	/FC/	PHI
-6	38	39	0
-2	109	113	180
0	171	174	0
1	76	82	0
2	88	90	180
3	64	74	180
4	110	116	180
5	88	96	0
6	59	59	0
8	55	54	0
9	74	68	180
10	46	43	180

** K= -7 L= 2 **

H	/FO/	/FC/	PHI
-9	16	10	0
-8	76	81	0
-7	65	65	180
-6	53	50	0
-5	67	73	0
-4	53	58	180
-3	15	20	180
-2	150	157	0
0	27	24	180
1	39	42	180
2	83	79	0
3	55	57	0
5	14	13	180
7	37	36	180
8	56	51	0
9	34	32	0
10	17	19	180
11	81	73	180
12	107	100	180

** K= -6 L= 2 **

H	/FO/	/FC/	PHI
-10	78	80	0
-9	34	14	180
-7	67	66	0
-6	29	31	180
-5	73	76	180
-4	30	24	180
-3	31	20	180
-2	30	29	0
-1	44	47	0
0	103	110	0
1	140	156	180
2	44	41	180
3	58	50	180
5	120	127	0
6	149	151	0
7	18	18	180
8	78	74	180
9	228	230	180
10	144	143	180
11	359	360	0
12	82	79	0

** K= -5 L= 2 **

H	/FO/	/FC/	PHI
-12	106	100	0
-11	49	50	0
-10	69	73	180
-9	56	58	180
-8	24	26	180
-7	15	17	0
-6	32	34	0
-3	60	69	180
-2	267	273	180
-1	56	13	180
0	23	22	0
1	120	129	0
2	86	82	180
3	90	89	180
4	107	118	180
5	27	39	180
7	35	36	180
9	240	238	0
10	21	14	0
11	177	184	180
12	68	71	0
13	57	55	0
14	92	83	0

** K= -4 L= 2 **

H	/FO/	/FC/	PHI
-14	46	42	180
-13	20	22	0
-12	29	17	180
-11	36	32	180
-10	91	97	0
-9	32	32	0
-7	62	63	180
-6	74	68	0
-5	64	61	180
-4	180	169	180
-3	260	263	0
-2	20	15	0
-1	9	4	0
0	146	154	180
1	43	53	180
2	76	78	0
3	163	172	0
4	77	75	180

H	/FO/	/FC/	PHI
5	39	39	0
6	121	128	180
7	46	50	180
8	17	23	0
9	76	80	180
10	173	170	0
11	20	17	180
12	46	51	180
13	103	99	180
14	69	64	180
15	70	69	180

** K= -3 L= 2 **

H	/FO/	/FC/	PHI
-15	27	27	0
-12	24	17	180
-11	88	87	180
-10	17	16	180
-9	90	77	0
-8	21	26	0
-7	12	3	180
-6	223	213	180
-5	47	45	0
-4	289	277	0
-3	96	104	180
-2	257	257	0
-1	142	160	0
0	317	334	0
1	23	16	180
2	20	23	180
3	48	61	180
4	199	197	0
5	17	21	0
6	9	3	180
7	77	83	0
8	30	33	180
9	128	133	180
10	106	103	180
11	37	40	0
12	19	18	0
14	57	57	180

** K= -2 L= 2 **

H	/FO/	/FC/	PHI
-15	18	19	180
-14	82	85	180
-13	76	77	180
-12	135	131	0
-11	85	85	0
-10	49	47	180
-9	80	76	180
-8	333	366	180
-7	23	29	180
-6	224	239	0
-5	144	171	0
-4	300	334	0
-3	116	135	180
-2	95	110	180
-1	236	287	180
0	110	117	0
1	39	30	180
2	183	135	0
3	84	90	180
4	180	192	180
5	143	160	180
6	53	54	180
7	137	147	0
8	159	168	0
9	118	119	0
11	61	70	180
12	84	89	180
13	136	154	0

H	/FO/	/FC/	PHI
14	58	63	0
15	34	28	0

** K= -1 L= 2 **

H	/FO/	/FC/	PHI
-16	43	34	0
-15	14	11	0
-14	40	44	0
-13	132	131	180
-12	13	16	0
-11	37	35	0
-10	116	123	0
-9	157	164	0
-8	82	83	180
-7	81	66	180
-6	55	65	180
-5	84	109	180
-4	194	228	0
-3	62	81	0
-2	10	2	180
-1	380	415	180
0	1524	1958	180
1	339	358	0
2	390	402	0
3	8	3	0
4	147	156	0
5	64	59	180
6	143	150	180
7	100	103	180
8	24	30	0
9	83	90	0
10	161	160	0
11	64	58	0
12	25	24	180
13	107	111	180
14	22	18	180
15	40	40	0

** K= 0 L= 2 **

H	/FO/	/FC/	PHI
-16	66	59	180
-15	53	56	180
-14	61	59	0
-13	134	127	0
-12	103	107	0
-11	17	13	0
-9	88	103	180
-8	9	10	0
-7	106	117	0
-6	283	295	0
-5	25	25	180
-4	83	82	0
-3	298	328	180
-2	1400	1712	180
-1	686	768	0
0	859	969	0
1	180	188	0
2	239	242	0
3	225	246	180
4	121	126	180
5	8	16	0
7	208	217	0
9	140	154	180
10	110	113	180
11	159	162	180
12	71	73	0
13	28	36	0
14	19	19	0

** K= 1 L= 2 **

H	/FO/	/FC/	PHI
-15	11	19	0

H	/FO/	/FC/	PHI
-14	178	186	180
-13	45	48	180
-12	29	21	0
-11	97	104	0
-10	13	10	0
-9	36	39	180
-8	203	209	180
-7	136	153	180
-6	16	25	0
-5	123	156	0
-4	241	271	0
-3	71	79	0
-2	377	329	0
-1	164	182	180
0	329	339	0
1	176	184	0
2	576	584	0
3	48	52	0
4	27	25	180
5	238	241	180
6	337	324	180
7	142	137	0
8	109	113	0
9	105	107	0
10	14	18	0
11	155	157	180
12	81	87	180
13	42	49	0

** K= 2 L= 2 **

H	/FO/	/FC/	PHI
-16	41	54	180
-14	32	39	0
-13	35	28	180
-12	98	99	180
-11	70	80	180
-10	55	56	0
-9	68	72	0
-8	61	65	180
-7	8	8	0
-6	136	83	0
-5	157	167	180
-4	125	87	180
-3	55	79	0
-2	198	220	0
-1	20	15	180
0	18	16	180
1	240	256	180
2	95	89	0
3	181	179	180
4	252	236	180
5	161	157	0
6	125	121	0
7	53	48	0
8	42	43	180
9	73	77	180
10	74	76	0
11	70	71	0
12	29	29	0
13	29	37	0

** K= 3 L= 2 **

H	/FO/	/FC/	PHI
-14	85	92	0
-13	73	72	0
-12	182	186	0
-11	103	109	180
-10	16	13	0
-9	48	52	180
-8	90	50	180
-7	91	115	0
-6	37	48	180

H	/FO/	/FC/	PHI
-5	120	126	0
-4	121	130	180
-3	201	223	180
-2	237	247	180
-1	73	73	0
0	46	42	180
1	129	138	0
2	377	375	180
3	41	43	180
4	68	59	0
5	81	81	180
6	37	35	0
7	60	61	0
8	58	66	0
9	84	83	180
11	31	26	0

** K= 4 L= 2 **

H	/FO/	/FC/	PHI
-16	62	62	0
-14	36	27	180
-13	124	134	180
-12	94	95	0
-11	183	201	0
-10	126	133	180
-9	37	40	180
-7	39	52	180
-6	50	47	180
-4	131	137	0
-3	184	187	0
-1	95	103	180
0	212	218	180
1	116	112	0
2	147	149	0
3	27	41	0
4	24	28	0
5	23	25	180
6	87	94	180
7	46	47	180
9	115	119	0
10	59	61	0
11	64	60	180

** K= 5 L= 2 **

H	/FO/	/FC/	PHI
-15	44	45	0
-14	52	52	0
-13	135	137	0
-12	410	412	180
-11	202	203	180
-10	113	109	0
-9	122	125	0
-8	167	167	0
-7	31	35	0
-6	101	97	180
-5	83	87	180
-4	36	34	0
-3	44	50	180
-2	239	258	0
-1	66	67	0
0	21	25	0
1	64	65	180
3	17	26	180
4	87	86	0
5	102	105	0
8	41	41	0
9	63	66	180
10	53	63	180

** K= 6 L= 2 **

H	/FO/	/FC/	PHI
-14	107	107	180
-13	25	20	180
-12	113	102	0
-11	63	59	0
-10	37	44	0
-9	71	70	180
-8	24	25	180
-5	52	54	0
-4	17	18	0
-3	96	88	180
-2	33	39	180
-1	35	33	0
0	68	68	0
1	85	88	180
2	29	25	180
3	93	97	0
5	87	96	180
6	82	74	0
7	19	28	180
8	61	60	180

** K= 7 L= 2 **

H	/FO/	/FC/	PHI
-10	151	150	0
-7	14	8	180
-6	185	201	180
-4	33	28	0
-3	154	167	0
-2	66	70	0
-1	149	153	180
0	178	185	180
1	57	57	0
2	22	13	0
4	24	22	0
5	33	29	180

** K= 8 L= 2 **

H	/FO/	/FC/	PHI
-9	45	51	0
-8	24	32	180
-7	17	6	0
-4	32	33	180
-3	27	27	180
-2	41	32	0
-1	28	26	0
1	16	6	0
2	78	73	180

** K= -9 L= 3 **

H	/FO/	/FC/	PHI
0	33	28	180
1	65	63	0
3	32	29	180

** K= -8 L= 3 **

H	/FO/	/FC/	PHI
-4	15	8	180
-3	55	58	180
-2	180	182	180
-1	183	180	0
0	16	19	180
1	66	68	180
2	87	87	0
3	17	15	180
4	49	58	180
5	34	30	0

** K= -7 L= 3 **

H	/FO/	/FC/	PHI
-8	77	75	0
-7	49	45	0
-6	76	17	0
-5	99	97	180
-4	162	163	180
-3	142	146	0
-2	101	101	0
-1	22	7	0
0	139	144	0
1	23	18	180
2	29	37	180
3	46	49	180
4	35	34	180
5	91	91	0
6	51	50	0
8	55	56	180
9	93	97	180
10	15	17	0
11	54	56	180

** K= -6 L= 3 **

H	/FO/	/FC/	PHI
-10	34	34	0
-8	75	55	180
-7	48	49	180
-6	17	13	0
-5	51	57	0
-4	163	163	0
-3	35	36	180
-2	20	14	180
-1	65	67	180
0	100	101	0
1	31	33	0
2	94	104	0
3	76	64	180
4	113	109	180
5	19	16	0
6	70	65	180
7	61	51	0
8	147	156	0
9	16	18	180
10	104	107	180
11	16	11	180
12	17	13	180

** K= -5 L= 3 **

H	/FO/	/FC/	PHI
-11	45	46	180
-10	67	49	0
-9	49	43	0
-8	26	25	0
-7	52	58	180
-6	88	95	180
-4	19	20	180
-3	41	43	0
-2	39	40	0
-1	95	58	180
0	112	113	180
1	223	237	180
2	177	186	180
3	195	201	0
4	128	138	0
5	43	24	180
6	37	35	0
7	101	102	180
8	119	113	180
9	46	47	0
10	155	157	0
11	97	98	0
12	35	42	180
13	37	29	0

** K= -4 L= 3 **

H	/FO/	/FC/	PHI
-13	36	37	180
-12	126	114	0

H	/FO/	/FC/	PHI
-11	15	9	180
-10	78	74	180
-8	69	69	180
-7	52	56	0
-6	40	30	0
-5	64	68	0
-4	95	93	180
-3	112	122	180
-2	101	103	180
-1	23	22	0
0	181	181	180
1	278	292	0
2	67	64	0
3	201	211	180
4	70	71	180
5	39	44	180
6	29	26	0
7	92	102	0
8	71	75	0
9	68	67	180
10	109	113	180
12	55	56	0
13	22	14	0
14	61	63	0

** K= -3 L= 3 **

H	/FO/	/FC/	PHI
-14	14	8	0
-13	28	23	180
-12	234	228	180
-11	110	110	0
-10	142	141	0
-9	65	60	180
-8	49	44	180
-7	18	18	180
-5	110	86	0
-4	249	253	0
-3	56	69	0
-2	26	30	180
-1	50	54	180
0	25	22	180
1	128	126	0
2	184	192	0
3	92	105	0
4	44	42	180
5	88	96	180
6	130	136	180
7	111	108	0
8	106	109	0
9	16	3	0
11	117	133	180

** K= -2 L= 3 **

H	/FO/	/FC/	PHI
-15	33	30	0
-14	279	270	180
-13	24	22	180
-12	75	80	0
-11	37	41	180
-10	72	62	0
-9	71	84	0
-8	51	53	0
-7	75	12	180
-6	91	93	180
-5	106	126	180
-4	186	210	0
-3	64	68	180
-2	107	118	0
-1	43	54	0
0	32	33	180
1	78	90	180
2	19	5	0
3	28	25	0
4	166	180	0
5	199	217	0
6	190	192	0
7	253	254	180
8	207	216	180
9	72	66	0
10	25	29	0
11	69	64	0
14	32	27	180

** K= -1 L= 3 **

H	/FO/	/FC/	PHI
-16	88	85	180
-15	65	69	180
-14	105	103	0
-13	106	109	0
-12	121	124	0
-11	13	7	180
-10	26	25	0
-9	126	137	180
-8	88	92	180
-7	32	41	0
-6	112	119	180
-5	68	83	0
-4	62	90	180
-3	171	196	180
-2	195	216	180
-1	43	44	180
0	44	58	0
1	118	130	0
2	80	77	0
3	110	125	180
4	100	91	0
5	337	341	180
6	96	88	180
7	223	232	0
9	35	18	0
10	84	84	180
11	27	31	180
12	91	90	0
13	150	144	0
14	35	29	0

** K= 0 L= 3 **

H	/FO/	/FC/	PHI
-16	74	59	0
-15	62	66	0
-13	84	86	180
-12	50	51	0
-11	27	13	0
-10	233	235	0
-9	23	32	0
-8	424	429	180
-7	19	27	180
-6	16	16	180
-5	80	91	0
-4	168	178	0
-3	128	142	0
-2	38	41	180
-1	96	109	180
0	263	276	180
1	12	8	0
2	12	7	180
3	126	139	0
5	144	148	180
6	227	237	180
7	71	54	180
8	27	26	0
9	103	122	0
10	131	143	0
11	82	91	0
12	27	26	0
13	191	199	180

** K= 1 L= 3 **

H	/FO/	/FC/	PHI
-15	47	40	0
-13	35	20	0
-12	45	40	180
-11	96	97	180
-10	221	231	180
-9	65	68	0
-8	231	288	0
-7	76	83	0
-6	12	15	0
-5	82	97	180
-4	25	26	0
-3	46	44	0
-2	219	243	0
-1	143	145	0
0	132	133	180
1	105	91	0
2	59	58	180
3	17	18	180
4	78	76	0
5	82	87	0
6	50	53	0
7	52	57	0
8	97	102	180
9	44	48	0
10	157	162	0
11	240	248	180
12	68	73	180
13	12	18	0

** K= 2 L= 3 **

H	/FO/	/FC/	PHI
-16	97	95	180
-15	35	26	180
-14	80	76	180
-13	21	17	0
-12	27	29	0
-10	26	19	0
-9	55	62	180
-8	73	76	180
-7	29	8	0
-6	42	40	0
-5	99	105	0
-4	113	72	0
-3	81	104	180
-2	147	140	0
-1	143	145	180
0	67	78	0
1	153	162	0
2	131	129	0
3	86	71	180
4	28	29	0
5	35	45	180
6	18	22	180
7	56	63	0
8	147	154	0
9	103	105	180
10	138	146	180
11	57	55	0
12	52	54	180

** K= 3 L= 3 **

H	/FO/	/FC/	PHI
-16	87	77	0
-15	15	20	180
-14	55	61	0
-13	110	112	180
-12	76	72	180

H	/FO/	/FC/	PHI
-11	95	97	0
-10	145	144	0
-9	55	61	0
-8	78	85	180
-7	55	63	180
-6	231	237	180
-5	13	10	180
-4	373	379	0
-3	15	29	0
-2	127	131	180
-1	135	133	180
0	241	244	180
1	146	139	180
2	57	57	0
3	67	68	0
4	115	121	0
5	99	103	180
6	112	112	180
7	55	62	180
8	24	32	180
9	150	155	0
10	19	17	0

** K= 4 L= 3 **

H	/FO/	/FC/	PHI
-14	91	81	0
-13	122	124	0
-12	42	51	0
-11	129	137	180
-10	148	137	180
-9	57	53	0
-8	133	136	0
-7	55	65	0
-6	179	175	0
-5	74	75	180
-4	331	334	180
-3	57	60	180
-2	47	60	180
-1	130	136	0
1	20	19	180
2	107	103	180
3	24	13	0
4	37	50	180
5	60	61	0
6	60	65	0
8	38	35	180
9	24	31	180

** K= 5 L= 3 **

H	/FO/	/FC/	PHI
-14	22	13	180
-13	19	14	180
-12	103	83	180
-11	123	121	0
-10	74	73	0
-9	106	109	180
-8	24	30	180
-7	55	57	180
-5	70	68	0
-4	18	10	0
-3	45	43	0
-2	52	50	180
-1	36	17	180
1	145	148	0
2	193	202	0
4	88	83	180
5	81	85	180
6	21	17	180
7	60	58	0
8	31	31	0

** K= 6 L= 3 **

H	/FO/	/FC/	PHI
-12	93	78	180
-11	49	51	180
-10	13	13	180
-9	49	47	0
-8	106	109	0
-6	78	75	180
-5	76	68	180
-4	63	56	180
-3	137	134	0
-2	112	119	0
-1	41	39	180
0	252	270	0
1	141	138	180
2	170	175	180
3	18	20	180
4	32	30	0
5	76	78	0

** K= 7 L= 3 **

H	/FO/	/FC/	PHI
-10	41	35	180
-9	13	22	0
-8	89	84	0
-7	47	11	0
-6	49	52	180
-5	51	54	0
-4	68	57	180
-3	96	93	180
-2	191	176	0
-1	26	32	180
0	107	108	180
1	20	16	180
2	83	80	180

** K= -8 L= 4 **

H	/FO/	/FC/	PHI
-4	55	48	0
-3	43	39	180
-2	136	137	180
-1	17	12	0
0	84	77	0
1	34	38	0
2	15	12	180
3	90	84	180
4	33	31	180
5	15	18	0

** K= -7 L= 4 **

H	/FO/	/FC/	PHI
-7	48	46	180
-6	57	53	0
-5	40	39	0
-4	27	41	180
-3	34	30	0
0	63	61	180
1	64	62	0
2	42	39	0
3	27	26	0
4	19	18	180
5	49	49	180
6	70	68	180
7	19	13	0
8	68	65	0
9	100	95	0

** K= -6 L= 4 **

H	/FO/	/FC/	PHI
-8	39	25	0
-7	16	16	0
-3	16	20	0
-2	70	67	0
-1	60	68	0
1	39	43	180
2	13	17	0
3	22	21	180
5	66	68	0
6	49	44	0
7	74	74	0
8	40	31	180
9	262	259	180
10	108	21	0

** K= -5 L= 4 **

H	/FO/	/FC/	PHI
-11	30	27	0
-10	50	48	180
-9	29	28	180
-7	22	20	0
-5	46	48	0
-4	89	85	0
-3	131	148	180
-2	46	45	180
-1	65	55	180
0	84	93	0
1	43	45	0
3	73	70	180
4	13	11	180
5	20	18	180
6	37	40	0
7	32	36	180
8	59	31	0
9	114	115	0
10	118	112	180

** K= -4 L= 4 **

H	/FO/	/FC/	PHI
-12	42	26	180
-11	35	31	0
-10	33	31	0
-8	31	28	180
-7	17	13	0
-6	54	51	0
-5	125	128	180
-4	56	58	180
-3	78	81	0
-2	54	54	180
-1	78	79	180
0	153	161	180
1	27	34	180
2	65	67	0
3	16	21	0
6	57	61	180
7	24	22	180
8	29	25	180
9	93	89	0
10	88	85	0

** K= -3 L= 4 **

H	/FO/	/FC/	PHI
-14	51	38	0
-13	34	28	0
-12	80	72	180
-11	70	62	180
-10	58	47	0
-9	63	60	0
-8	184	175	0
-7	51	47	180
-6	187	182	180
-4	115	114	180
-3	57	60	0
-2	51	49	0
-1	152	163	0
1	12	10	0
2	145	153	180

H	/FO/	/FC/	PHI
3	65	70	0
4	88	93	0
5	22	21	0
6	42	42	0
7	25	27	180
8	60	65	180
9	96	96	180
11	23	32	0
12	46	42	0

** K= -2 L= 4 **

H	/FO/	/FC/	PHI
-14	93	86	180
-13	37	27	0
-12	23	21	0
-11	17	16	0
-10	32	33	0
-9	89	93	180
-8	75	76	180
-7	53	23	180
-5	115	128	0
-4	51	54	0
-3	35	42	0
-1	124	123	0
0	321	355	0
1	93	84	180
2	22	16	0
3	48	46	0
4	54	61	180
5	69	74	180
6	23	18	180
7	38	39	0
8	32	33	0
9	12	16	0
10	43	46	180
11	100	99	180

** K= -1 L= 4 **

H	/FO/	/FC/	PHI
-15	66	61	0
-14	60	52	180
-13	89	84	180
-12	77	83	180
-10	106	114	0
-9	79	63	0
-8	26	30	180
-7	71	78	180
-6	181	195	180
-4	84	92	0
-3	263	284	0
-2	680	718	0
-1	637	663	180
0	562	516	180
1	15	22	180
2	33	29	180
3	153	159	0
4	127	132	0
5	22	17	180
6	76	81	180
7	121	129	180
8	26	21	180
9	127	125	0
10	114	108	0
11	111	109	0
12	54	51	180

** K= 0 L= 4 **

H	/FO/	/FC/	PHI
-15	27	26	180
-14	90	83	0
-13	42	37	0
-12	28	35	0
-11	38	23	180
-10	26	26	180
-8	45	38	0
-7	100	102	0
-6	21	20	180
-5	17	11	0
-4	140	141	0
-3	367	367	180
-2	557	381	180
-1	125	135	0
0	93	88	180
1	33	30	0
2	131	139	180
3	40	48	180
4	27	31	0
5	20	21	0
6	121	123	0
7	49	13	0
8	18	24	180
10	50	50	180
11	35	32	0
12	28	30	0

** K= 1 L= 4 **

H	/FO/	/FC/	PHI
-15	34	24	180
-14	64	61	180
-13	23	20	180
-12	64	61	0
-11	56	60	0
-10	52	47	0
-9	24	23	180
-8	28	29	180
-7	87	91	180
-6	86	87	180
-5	133	145	0
-4	29	30	0
-3	59	56	0
-2	133	141	180
-1	31	32	180
0	80	71	180
1	196	193	0
2	102	96	0
3	194	192	0
4	98	89	0
5	225	210	180
6	119	116	180
7	21	23	180
8	68	66	0
9	91	92	0
10	41	34	180
11	102	99	180

** K= 2 L= 4 **

H	/FO/	/FC/	PHI
-15	21	9	0
-14	19	24	180
-13	45	35	180
-12	132	129	180
-11	16	14	0
-10	32	34	0
-9	49	46	0
-8	13	6	180
-7	11	9	180
-6	65	21	0
-5	102	109	180
-4	45	48	0
-3	138	148	0
-2	163	164	0
-1	34	38	0
0	37	35	180
1	20	18	180
2	164	164	0
3	72	64	180
4	28	30	180
5	50	51	0
7	22	19	180
8	69	73	180
9	19	20	0
10	14	13	0

** K= 3 L= 4 **

H	/FO/	/FC/	PHI
-14	15	6	0
-13	128	122	0
-12	38	35	180
-11	50	52	180
-10	32	32	0
-9	53	54	180
-8	39	27	0
-7	27	30	0
-6	82	75	0
-5	52	26	0
-4	84	82	180
-3	169	167	180
-2	10	10	0
-1	15	11	0
0	188	190	0
1	152	86	180
2	126	121	180
4	36	38	180
6	54	53	0
7	66	66	0
8	23	20	180
9	69	66	180

** K= 4 L= 4 **

H	/FO/	/FC/	PHI
-14	63	56	180
-13	78	78	180
-12	278	275	0
-11	69	68	0
-10	84	82	180
-9	34	38	180
-8	60	67	180
-7	29	28	180
-6	17	19	180
-4	18	12	0
-3	66	69	0
-2	78	85	180
-1	87	98	180
0	69	70	180
1	41	43	0
2	18	17	0
3	20	23	0
5	54	48	180
6	24	30	180
7	58	59	180

** K= 5 L= 4 **

H	/FO/	/FC/	PHI
-12	14	181	180
-11	94	97	180
-10	43	41	180
-9	79	71	0
-8	110	97	0
-7	33	31	0
-6	33	37	180
-5	45	39	180
-4	95	100	180
-3	100	66	0
-2	69	72	0
-1	42	52	0
2	65	70	180

H	/FO/	/FC/	PHI
3	59	61	180
4	46	35	0
5	64	70	0
** K= 6 L= 4 **			
-10	88	77	180
-8	16	10	0
-7	20	16	0
-6	114	108	0
-5	65	22	0
-4	44	27	180
-3	109	108	180
-1	135	128	0
0	83	78	0
1	86	81	180
3	38	39	0
** K= 7 L= 4 **			
-6	55	52	180
-5	53	57	180
-4	24	22	0
-3	92	88	0
** K= -7 L= 5 **			
-5	95	91	180
-4	84	82	180
-3	49	48	0
-2	18	21	180
-1	57	45	0
2	23	26	180
3	21	17	180
4	17	13	0
5	21	10	0
** K= -6 L= 5 **			
-8	33	20	180
-5	43	37	0
-4	37	37	0
-2	43	39	180
-1	24	18	0
0	35	32	0
1	124	113	0
2	64	64	0
3	91	85	180
4	28	26	180
5	32	20	180
6	54	53	180
7	73	63	0
8	81	77	0
** K= -5 L= 5 **			
-10	34	22	0
-9	34	31	0
-8	49	46	0
-7	53	52	180
-6	28	20	180
-5	34	34	180
-4	42	37	0
-3	63	65	0
-2	65	67	0
-1	23	27	0
0	15	21	0
1	194	198	180
2	30	28	180
3	120	119	0
4	35	33	0
5	36	40	0
7	80	81	180
8	81	73	180
9	44	38	0
** K= -4 L= 5 **			
-11	83	70	180
-10	30	27	180
-6	20	19	0
-5	26	20	180
-4	88	84	180
-3	48	51	180
-2	41	39	0
-1	71	74	180
1	31	32	0
2	58	56	180
3	47	46	180
6	44	36	0
7	15	16	0
9	17	22	180
10	36	30	180
** K= -3 L= 5 **			
-12	85	80	180
-11	67	64	0
-9	29	23	180
-8	26	21	180
-7	32	23	180
-6	30	31	180
-5	65	52	0
-4	13	11	180
-3	67	65	0
-2	51	55	180
-1	72	66	180
0	39	35	180
1	45	41	0
2	63	53	0
3	26	29	0
4	65	39	180
5	133	129	180
6	66	66	180
7	111	103	0
8	68	69	0
9	17	24	0
** K= -2 L= 5 **			
-13	42	30	180
-12	76	58	180
-11	15	15	180
-10	18	16	0
-9	71	80	0
-8	77	71	0
-7	12	1	0
-6	59	58	180
-5	11	8	180
-4	23	33	0
-3	91	88	0
-2	118	119	0
-1	30	39	0
0	46	52	180
1	72	67	180
2	87	63	180
3	29	29	0
4	31	20	0
5	217	225	0
6	43	45	0
7	164	167	180
8	35	34	180
9	23	19	180
10	42	43	0
** K= -1 L= 5 **			
-13	68	62	0
-11	23	24	0
-10	66	64	180
-8	138	140	0
-7	35	38	180
-6	25	30	0
-4	35	34	180
-3	81	84	180
-2	22	20	180
0	85	93	0
1	42	44	0
2	26	27	180
3	33	30	0
5	41	45	180
6	90	90	0
7	24	32	0
9	63	50	180
10	106	100	180
** K= 0 L= 5 **			
-14	17	12	180
-13	13	16	180
-12	21	22	180
-11	88	78	0
-10	207	194	0
-9	83	79	180
-8	155	146	180
-7	65	59	180
-6	67	60	180
-5	26	21	0
-4	35	34	0
-3	22	21	0
-2	77	30	180
-1	98	97	180
0	15	6	180
1	87	85	180
2	47	46	0
3	78	76	0
4	28	23	0
5	73	69	180
6	76	78	180
7	63	65	180
** K= 1 L= 5 **			
-14	69	48	0
-12	14	20	0
-11	76	75	180
-10	98	89	180
-9	60	54	0
-8	80	70	0
-7	42	39	0
-6	39	41	180
-5	72	66	180
-4	89	89	180
-3	40	45	0
-2	70	68	0
-1	53	52	0
0	34	42	180
1	70	61	180
2	90	84	180
3	16	3	0
5	32	32	0
6	51	51	0
7	55	61	180
8	105	94	180
9	149	146	0
** K= 2 L= 5 **			

H	/FO/	/FC/	PHI
-13	56	51	0
-12	28	22	0
-11	27	28	180
-10	45	39	180
-9	39	41	180
-8	15	18	0
-7	17	24	0
-6	103	87	0
-5	22	26	0
-4	134	129	180
-3	59	49	0
-2	24	22	0
-1	23	19	0
0	91	87	0
1	95	92	0
2	33	29	180
3	24	14	180
4	40	32	180
5	29	26	0
6	12	9	0
7	67	69	0
8	45	45	0

** K= 3 L= 5 **

H	/FO/	/FC/	PHI
-13	106	93	180
-12	38	32	180
-11	83	79	0
-10	81	79	0
-8	32	17	180
-7	81	74	180
-6	173	157	180
-5	83	77	0
-4	205	207	0
-3	49	43	0
-2	52	52	0
-1	73	72	180
0	66	59	180
1	38	29	180
2	20	16	0
3	61	60	0
4	67	67	0
5	45	44	180
6	54	53	180

** K= 4 L= 5 **

H	/FO/	/FC/	PHI
-11	120	109	180
-10	93	76	180
-9	58	52	0
-7	89	83	0
-6	100	91	0
-5	77	68	180
-4	72	60	180
-3	78	80	180
-2	29	27	0
-1	48	29	0
1	111	101	180
2	69	62	180
3	21	33	180
4	23	14	0

** K= 5 L= 5 **

H	/FO/	/FC/	PHI
-9	46	40	180
-8	63	61	180
-6	57	48	0
-5	37	29	0
-4	20	11	0
-3	82	64	180
-1	35	38	180
0	105	109	180
1	139	127	0

** K= -6 L= 6 **

H	/FO/	/FC/	PHI
-4	31	22	180
-3	58	43	0
-1	33	37	0
0	37	37	180
1	15	7	180

** K= -5 L= 6 **

H	/FO/	/FC/	PHI
-7	12	11	180
-5	101	87	0
-3	44	30	180
-2	13	13	180
-1	23	19	0
0	60	57	0
1	32	27	0
2	24	22	180
4	23	16	180

** K= -4 L= 6 **

H	/FO/	/FC/	PHI
-9	28	23	180
-8	56	47	180
-7	59	57	0
-6	46	46	0
-5	50	53	180
-4	49	40	0
-1	77	67	180
0	41	39	180
2	56	53	0
3	22	26	180
6	29	26	180

** K= -3 L= 6 **

H	/FO/	/FC/	PHI
-10	39	31	180
-9	92	69	0
-8	100	80	0
-7	25	16	180
-6	17	15	180
-5	92	72	180
-4	62	52	180
-3	37	35	180
-2	32	19	0
0	26	23	180
1	21	23	180
2	63	57	180
4	28	25	0
5	56	50	0
6	32	30	0

** K= -2 L= 6 **

H	/FO/	/FC/	PHI
-11	16	15	0
-10	35	29	180
-9	36	26	180
-6	54	48	0
-4	39	38	180
-3	107	108	180
-2	172	170	180
-1	263	277	0
0	122	127	0
1	23	17	180
2	21	16	0
3	31	31	180
4	45	41	180
5	12	9	180
6	23	24	0
7	37	37	0

** K= -1 L= 6 **

H	/FO/	/FC/	PHI
-11	12	1	0
-10	48	43	0
-9	35	31	0
-8	17	17	0
-7	63	57	180
-6	51	44	180
-5	66	65	180
-4	88	91	180
-3	345	359	0
-2	192	206	0
-1	140	144	180
0	35	37	180
1	69	64	180
3	60	56	0
4	39	31	0
5	18	18	0
6	62	60	180
7	74	69	180

** K= 0 L= 6 **

H	/FO/	/FC/	PHI
-11	33	25	180
-10	51	32	180
-8	47	38	0
-7	54	45	0
-5	17	19	0
-4	38	37	0
-3	115	110	180
-2	49	41	0
0	32	25	0
1	77	75	180
2	78	75	180
3	62	69	180
4	21	20	180
5	102	90	0
6	60	56	0

** K= 1 L= 6 **

H	/FO/	/FC/	PHI
-11	19	12	0
-7	61	57	180
-6	52	11	180
-5	47	45	0
-3	53	55	180
-2	75	66	180
-1	72	69	180
2	16	16	180
3	115	110	0
4	12	17	0
5	62	48	180

** K= 2 L= 6 **

H	/FO/	/FC/	PHI
-10	15	15	0
-9	40	29	0
-6	67	55	180
-5	38	38	180
-4	32	24	0
-3	83	86	0
-2	36	27	0
0	107	94	180
1	64	68	0
2	51	49	0
4	33	25	0

** K= 3 L= 6 **

H	/FO/	/FC/	PHI
-9	18	9	180
-7	38	25	0
-6	65	55	0

H	/FO/	/FC/	PHI	H	/FO/	/FC/	PHI	H	/FO/	/FC/	PHI
-5	26	31	0								
-4	54	41	180								
-3	54	44	180								
-1	103	82	0								
0	81	64	0								
1	42	29	180								
** K= 4 L= 6 **											
-6	12	14	0								
-5	18.	8	0								
-4	72	65	0								
-3	53	21	180								
-2	45	40	180								
** K= -3 L= 7 **											
-5	17	18	180								
-3	22	15	180								
-2	49	40	180								
-1	34	28	180								
1	29	21	0								
** K= -2 L= 7 **											
-6	34	30	180								
-5	33	21	180								
-3	54	43	0								
-2	46	38	0								
-1	11	11	0								
0	43	27	180								
1	44	32	180								
2	16	8	180								
** K= -1 L= 7 **											
-7	23	17	0								
-6	40	30	0								
-4	25	18	180								
-3	24	18	180								
-2	15	9	180								
-1	41	34	0								
0	34	27	0								
1	23	23	0								
** K= 0 L= 7 **											
-5	29	22	0								
-4	43	36	0								
-2	39	36	180								
0	15	3	180								
** K= 1 L= 7 **											
-5	42	33	180								
-3	19	21	180								
-2	29	25	0								

APPENDIX II

BASIC Program

```
FILE 'ZPROG2'
10    REM  KUBELKA MUNK PROGRAM
20    FILE *1: "GPD1"
30    FILE *2: "GPD2"
40    FILE *3: "GPD3"
50    REM FILES FOR OUTPUT OF DATA TO GRAPH PLOTTER
60    FILE *4: "LP"
70    FILE *5: "GPCOMM"
80    FILE *11: "DU*P"
90    REM FILES TO LINEPRINTER,GRAPH PLOTTER COMMAND FILE
100   REM AND A FILE TO HOLD A COPY OF THE DATA AS A BACK-UP
110   DIM A(100),B(100),C(100),D(100),E(100),F(100),G(100),H(100)
120   DIM J(100),K(100),L(100),M(100),Y(200)
130   DEF FNA(I) = ((1-C(I))^2)/(2*C(I))
140   DEF FNB(I) = ((1-B(I))^2)/(2*B(I))
150   INPUT W1,W2,S
160   REM W1 AND W2 ARE THE MINIMUM AND MAXIMUM VALUES OF THE
170   REM WAVELENGTH AND S IS THE INTERVAL BETWEEN POINTS
180   PRINT "                R4  VALUES FIRST"
190   LET C = 1
200   FOR I = W1 TO W2 STEP S
210    INPUT Y(I/10)
220   NEXT I
230   PRINT "      NOW THE R1 VALUES"
240   PRINT "        RUN 1 ..."
250   GOSUB 1350
260   FOR I = 1 TO C
270    GOSUB 1310
280    LET F(I) = D(I)-E(I)
290   NEXT I
300   PRINT "        RUN 2 ..."
310   LET C = 1
320   GOSUB 1350
330   FOR I = 1 TO C
340    GOSUB 1310
350    LET G(I) = D(I)-E(I)
360   NEXT I
370   PRINT "        RUN 3 ..."
375   LET C = 1
390   GOSUB 1350
400   FOR I = 1 TO C
410    GOSUB 1310
420    LET H(I) = D(I)-E(I)
430   NEXT I
440   PRINT "UNSCALED VALUES"
450   PRINT "WAVELENGTH","FIRST RUN","SECOND RUN","THIRD RUN"
460   FOR I = 1 TO C
470    PRINT W(I),F(I),G(I),H(I)
480   NEXT I
490   PRINT *4: "WAVELENGTH","FIRST RUN","SECOND RUN","THIRD RUN"
500   PRINT *4:
510   FOR I = 1 TO C
520    PRINT *4: W(I),F(I),G(I),H(I)
530   NEXT I
540   FOR I = 1 TO 5
550    PRINT *4:
560   NEXT I
570   PRINT "INPUT THE WAVELENGTH AT WHICH YOU WANT THE SCALING"
580   INPUT W4
590   FOR I = 1 TO C
600    IF W(I) = W4 THEN 630
610   NEXT I
620   GOTO 840
630   LET N4 = I
640   GOTO 610
650   LET M1 = F(N4)
660   LET M2 = G(N4)
670   LET M3 = H(N4)
680   LET M2 = M1/M2
690   LET M3 = M1/M3
700   LET M1 = 1
710   FOR I = 1 TO C
720    LET G(I) = G(I)*M2
730    LET H(I) = H(I)*M3
740   NEXT I
750   PRINT "FINAL VALUES"
760   PRINT "WAVELENGTH","FIRST RUN","SECOND RUN","THIRD RUN"
770   PRINT "     nm","(UNCHANGED)","(SCALED)","(SCALED)"
780   FOR I = 1 TO C
790    PRINT W(I),F(I),G(I),H(I)
800   NEXT I
```

Appendix II (Cont'd.)

BASIC Program

```
410     PRINT #4: "WAVELENGTH","FIRST RUN","SECOND RUN","THIRD RUN"
420     PRINT #4: "      NM","(UNCHANGED)","(SCALED)","(SCALED)"
430     FOR I = 1 TO C
440       PRINT #4: W(I),F(I),G(I),H(I)
450     NEXT I
460     LET R1 = 0
470     REM  DATA FILES FOR GRAPH PLOTTER
480     FOR I = 1 TO C
490       PRINT #1: W(I),F(I)
500       IF F(I) <= R1 THEN 920
510       LET R1 = F(I)
920       PRINT #2: W(I),G(I)
930       IF G(I) <= R1 THEN 950
940       LET R1 = G(I)
950       PRINT #3: W(I),H(I)
960       IF H(I) <= R1 THEN 980
970       LET R1 = H(I)
980     NEXT I
990     PRINT #1: "ENDS"
1000    PRINT #2: "ENDS"
1010    PRINT #3: "ENDS"
1020    PRINT
1030    PRINT "PLOTTER FILES WRITTEN"
1040    PRINT #5: "TERMIN   ENDS"
1050    PRINT #5: "FORMAT   FREE"
1060    PRINT #5: "SIZE     15 15"
1070    PRINT #5: "XHEAD    WAVELENGTH *LNM*U"
1080    PRINT #5: "YHEAD    KUBELKA-MUNK FUNCTION"
1090    PRINT #5: "YRANGE   -0.1";.1+(.1*INT(R1*10))
1100    PRINT #5: "SYMBOL   1"
1110    PRINT #5: "FILE     1"
1120    PRINT #5: "KEY      FIRST RUN"
1130    PRINT #5: "PARCURVE"
1140    PRINT #5: "FRAME    SAME"
1150    PRINT #5: "AXES     OFF"
1160    PRINT #5: "CHAIN"
1170    PRINT #5: "SYMBOL   5"
1180    PRINT #5: "FILE     2"
1190    PRINT #5: "KEY      SECOND RUN"
1200    PRINT #5: "PARCURVE"
1210    PRINT #5: "DASH"
1220    PRINT #5: "SYMBOL   9"
1230    PRINT #5: "KEY      THIRD RUN"
1240    PRINT #5: "FILE     3"
1250    PRINT #5: "PARCURVE"
1260    PRINT #5: "STOP"
1270    REM COMMANDS FILE FOR GRAPH PLOTTER
1280    PRINT "  PLOTTER COMMANDS FILE WRITTEN"
1290    PRINT
1300    STOP
1310    LET C(I) = A(I)+B(I)
1320    LET D(I) = FNA(I)
1330    LET E(I) = FNE(I)
1340    RETURN
1350    FOR I = W1 TO W2 STEP S
1360      INPUT X
1370      IF X = 0 THEN 1430
1380      PRINT #11: X;",";Y(I/10)
1390      LET A(C) = X
1400      LET B(C) = Y(I/10)
1410      LET W(C) = I
1420      LET C = C+1
1430    NEXT I
1440    LET C = C-1
1450    RETURN
```

References

Chapter 1

Akamatu, H. & Kuroda, H. (1963) *J.Chem.Phys.* 39, 3364

Brackmann, W. (1949) *Rec.Trav.Chim.* 68, 147

Briegleb, G. (1961) *Electronen-Donator-Acceptor-Komplexe* (Springer-Verlag, Berlin, Göttingen - Heidelberg

Eley, D. D., Inokuchi, H. & Willis, M. R. (1959) *Discussions Faraday Soc.* 28, 54

Foster, R. (1969) *Organic Charge Transfer Complexes,* London, Academic Press

Foster, R. (1973) *Molecular Complexes, Vol.1,* Elek Science, London

Fritzsche, J. (1858) *J.Prakt.Chem.* 73, 282

Herbstein, F. H. (1971) *Perspectives in Structural Chemistry Vol.IV,* Ed. Dunitz, J. D. & Ibers, J. A. (Wiley, N.Y.), 166

Hurditch, R. J., Vincent, V. M. & Wright, J. D. (1972) *J.C.S. Faraday I,* 68, 465

Karl, N. & Ziegler, J. (1975) *Chem.Phys.Lett.* 32(3), 438

Koizumi, S. & Matsunaga, Y. (1974) *Bull.Chem.Soc.Jap.*, 47(1), 9

Kuroda, H., Kobayashi, M., Kinoshita, M. & Takemoto, S. (1962) *J.Chem.Phys.* 36, 457

Kuroda, H., Kunii, T., Hiroma, S. & Akamatu, H. (1967) *J.Mol.Spec.* 22, 60

Lower, S. K. (1969) *Mol.Cryst.Liq.Cryst.* 5, 363

Mayoh, B. & Prout, C. K. (1972) *J.Chem.Soc., Faraday Trans.II*, 68, 1072

Mulliken, R. S. (1950) *J.A.C.S.*, 72, 600

Mulliken, R. S. & Person, W. B. (1969) *Molecular Complexes*, John Wiley & Sons, Inc.

Munnoch, P. J. & Wright, J. D. (1976) *J.C.S. Faraday Trans I*, 72, 1981

Ohta, T., Kuroda, H. & Kunii, T. L. (1970) *Theoret.Chim.Acta.*, 19, 167

Pethig, R. & Soni, V. (1975) *J.C.S. Faraday I*, 71, 1534

Prout, C. K. & Kamenar, B. (1973) *Molecular Complexes*, Vol.1, Ed. by Foster, R., Elek Science, London, 151

Prout, C. K., Williams, R. J. P. & Wright, J. D. (1966) *J.Chem.Soc. (A)*, 747

Prout, C. K. & Wright, J. D. (1968) *Ange.Chem.Internat.Ed.*, 7, 659

Vincent, V. M. & Wright, J. D. (1974) *J.C.S. Faraday Trans. I*, 70, 58

Weiss, J. (1942) *J.C.S.*, 245

Wright, J. D. (1963) *Chemistry Part II Thesis* Oxford University

Wright, J. D., Ohta, T. & Kuroda, H. (1976) *Bull.Chem.Soc.Jap.*, 49(11), 2961

Chapter 2

Badger, G. M., Pearce, R. S. & Pettit, R. (1951) *J.C.S.* 3199

Birkofer, L. (1952) *Chem.Ber.* 85, 1023

Colton, R. H. & Henn, D. E. (1970) *J.Chem.Soc.B.*, 1532

Goldberg, I. & Shmueli, U. (1973) *Acta.Cryst.* B29, 440

Hazlett, F. P., Hannan Jr., R. B. & Wells, J. H. (1950) *Anal.Chem.* 22, 1132

Hurditch, R. J., Vincent, V. M. & Wright, J. D. (1972) *J.C.S.Faraday I*, 68, 465

Ishii, K. (1980) *Abstracts from Organic and Biological Semiconductors Symposium*, Univ. of Nottingham, 31

Kobayashi, H. (1973) *Bull.Chem.Soc.Jap.*, 46, 2675

Kobayashi, H. (1973) *Bull.Chem.Soc.Jap.*, 46, 2945

Koizumi, S. & Matsunaga, Y. (1974) *Bull.Chem.Soc.Jap.*, 47(1), 9

MacKenzie, J. C. J., Rodgman, A. & Wright, G. F. (1952) *J.Org.Chem.*, 17, 1666

Martynoff, M. (1957) *Compt.Rend.*, 244, 205

Miller, J. S. & Epstein, A. J. (1978) *J.A.C.S.*, 100, 1639

Mulliken, R. S. & Person, W. B. (1969) *Molecular Complexes*, John Wiley & Sons, Inc., Chapter 7

Munnoch, P. J. (1974) *Ph.D Thesis*, University of Kent

Munnoch, P. J. & Wright, J. D. (1974) *J.C.S. Perkin II*, 1397

Pichat, L., Pesteil, P. & Clement, J. (1953) *J.Chim.Phys.*, 50, 26

Prout, C. K., Tickle, I. J. & Wright, J. D. (1973) *J.C.S. Perkin II*, 528

Prout, C. K., Williams, R. J. P. & Wright, J. D. (1966) *J.Chem.Soc. (A)*, 747

Sawicki, E. & Ray, F. E. (1952) *J.A.C.S.*, 74, 4120

Schnurmann, R., Maddams, W. F. & Barlow, M. C. (1953) *Anal.Chem.*, 25, 1010

Tickle, I. J. & Prout, C. K. (1973) *J.C.S. Perkin II*, 720

Tsuchiya, H., Marumo, F. & Saito, Y. (1972) *Acta Cryst.*, B28, 1935

Vincent, V. M. (1972) *Ph.D thesis*, Univ. of Kent

Werner, E. G. G. (1949) *Rec.Trav.Chim.*, 68, 509

Williams, R. M. & Wallwork, S. C. (1968) *Acta Cryst.*, B24, 168

Wright, J. D., Ohta, T. & Kuroda, H. (1976) *Bull.Chem.Soc.Jap.*, 49(11), 2961

Zander, M. & Franke, W. (1961) *Chem.Ber.*, 94, 446

Chapter 3

Colton, R. H. & Henn, D. E. (1970) *J.Chem.Soc.B.*, 1532

Dewar, M. J. S. & Thompson, Jr., C. C. (1966) *Tetrahedron Suppl.* 7, 97

Fyfe, C. A. (1973) *Molecular Complexes, Vol.1*, Ed. Foster, R., pp.209

Gaultier, J., Hauw, C. & Breton-Lacombe, M. (1969) *Acta Cryst.*, B25 231

Goldberg, I. (1975) *Theoret.Chim.Acta* (Berl.), 40, 271

Goldberg, I. & Shmueli, U. (1973a) *Acta.Cryst.*, B29, 421

Goldberg, I. & Shmueli, U. (1973b) *Acta.Cryst.*, B29, 432

Goldberg, I. & Shmueli, U. (1973c) *Acta.Cryst.*, B29, 440

Goldberg, I. & Shmueli, U. (1977) *Acta.Cryst.*, B33, 2189

Goldstein, P., Seff, K. & Trueblood, K. N. (1968) *Acta.Cryst.*, B24, 778

Herbstein, F. H. (1971) *Perspectives in Structural Chemistry,Vol.IV*, pp.166, Wiley, N.Y.

Johnson, C. K. (1965) *Ortep.* Report ORNL-3794. Oak Ridge National Laboratory, Tennessee

Keesom, W. H. (1912) *Proc.K.Akad.Wetens.Amsterdam*, 15, 256,417,642

Kobayashi, H. (1973a) *Bull.Chem.Soc.Jap.*, 46, 2945

Kobayashi, H. (1973b) *Bull.Chem.Soc.Jap.*, 46, 2675

Kuroda, H., Amano, T., Ikemoto, I. & Akamatu, H. (1967) *J.A.C.S.*, 89:24, 6056

Lennard-Jones, J. E. (1931) *Proc.Phys.Soc.*(London), 43, 461

Lippert, J. L., Hanna, M. W. & Trotter, P. J. (1969) *J.A.C.S.*, 91:15, 4035

London, F. (1937) *Trans.Faraday Soc.*, 33, 8

Long, R. E., Sparks, R. A. & Trueblood, K. N. (1965) *Acta.Cryst.*, 18, 932

Lowitz, D. A. (1967) *J.Chem.Phys.*, 46, 4698

Mayoh, B. & Prout, C. K. (1972) *J.Chem.Soc., Faraday Trans.II*, 68, 1072

Mukherjee, T. K. (1969) *J.Phys.Chem.*, 73, 3442

Mulliken, R. S. (1952) *J.A.C.S.* 74, 811

Mulliken, R. S. (1956) *Rec.Trav.Chim.Pays-Bas.* 75, 845

Munnoch, P. J. & Wright, J. D. (1974) *J.C.S. Perkin Trans.II*, 1397

Prout, C. K., Tickle, I. J. & Wright, J. D. (1973) *J.C.S. Perkin II*, 528

Prout, C. K. & Wallwork, S. C. (1966) *Acta.Cryst.*, 21, 449

Prout, C. K. & Wright, J. D. (1968) *Angew,Chemie*, 80, 688

Schaffrin, R. M. & Trotter, J. (1970) *J.Chem.Soc.(A)*, 1561

Sundareson, T. & Wallwork, S. C. (1972) *Acta.Cryst.*, B28, 1163

Tickle, I. J. & Prout, C. K. (1973a) *J.C.S. Perkin II*, 724

Tickle, I. J. & Prout, C. K. (1973b) *J.C.S. Perkin II*, 727

Williams, R. M. & Wallwork, S. C. (1968) *Acta.Cryst.*, B24, 168

Williams, R. M. & Wallwork, S. C. (1967) *Acta.Cryst.*, 23, 448

Wright, J. D., Ohta, T. & Kuroda, H. (1976) *Bull.Chem.Soc.Jap.*, 49(11), 2961

Chapter 4

Amano, T., Kuroda, H. & Akamatu, H. (1969) *Bull.Chem.Soc.Jap.*, 42, 671

Benesi, H. A., Hildebrand, J. H. (1948) *J.A.C.S.* 70, 2382

Benesi, H. A., Hildebrand, J. H. (1949) *J.A.C.S.* 71, 2703

Coulson, C. A. & Streitwieser, A. (1965) *Supplemental Tables of Calculations with a Dictionary of* π *Electrons*, Oxford Pergamon

Foster, R. (1969) *Organic Charge Transfer Complexes*, London, Academic Press

Körtum, G. F. A. (1969) *Reflectance Spectroscopy; Principles, Methods, Applications* Berlin-Springer

Mulliken, R. S. (1950) *J.A.C.S.* 72, 600

Mulliken, R. S. (1952) *J.A.C.S.* 74, 811

Mulliken, R. S. & Person, W. B. (1969) *Molecular Complexes*, John Wiley & Sons, Inc.

Nakamoto, K. (1952) *J.A.C.S.* 74, 390,392,1739

Ohta, T., Kuroda, H. & Kunii, T. L. (1970) *Theoret.Chim.Acta.*, 19, 167

Vincent, V. M. (1972) *Ph.D Thesis*, University of Kent

Wright, J. D. (1965) *D.Phil. Thesis*, Oxford University

Wright, J. D., Ohta, T. & Kuroda, H. (1976) *Bull.Chem.Soc.Jap.*, 49(11), 2961

Zsom, R. L. J., Schroff, L. G., Bakker, C. J., Verhoeven, J. W., De Boer, TH. J., Wright, J. D. & Kuroda, H. (1978) *Tetrahedron*, 34, 3225

Chapter 5

Bardeen, J. & Schockley, W. (1950) *Phys.Rev.*, 80, 72

Bounds, P. J. & Munn, R. W. (1980) *Abstracts of Ninth Molecular Crystal Symposium*, Mittelberg Kleinwalsertal, 38

Chojnacki, H. (1966) *Acta Physica Polonica*, 30, 715

Dexter, D. H. & Seitz, F. (1952) *Phys.Rev.*, 86, 964

Epstein, A. J. & Miller, J. S. (1978) *J.A.C.S.*, 100, 1639

Farragher, A. L. & Page, F. M. (1967) *Trans.Farad.Soc.*, 63, 2369

Gutman, F. & Lyons, L. E. (1967) *Organic Semiconductors*, Wiley Interscience

Ioffe, A. F. (1959) *Solid States Physics USSR*, 1, 1

Kepler, R. G. (1960) *Phys.Rev.*, 119, 1226

Kokado, H., Hasegawa, K. & Schneider, W. G. (1964) *Canad.J.Chem.*, 42, 1084

Kolninov, O. V. (1969) *Doklady Akad.Nauk S.S.S.R.*, 189, 353

Kronick, P. L. & Labes, M. M. (1963) *J.Chem.Phys.*, 38, 776

Kurematsu, K., Kaneko, N. & Matsumoto, S. (1971) *Bull.Chem.Soc.Jap.*, 44, 2845

Le Blanc Jr., O. H. (1959) *J.Chem.Phys.*, 30, 1443

Meier, H. (1974) *Organic Semiconductors*, Verlag Chemie, 49

Meier, H. (1974) *Organic Semiconductors*, Verlag Chemie, 278

Meier, H. (1974) *Organic Semiconductors*, Verlag Chemie, 56

Mohwald, H., Haarer, D. & Castro, G. (1975) *Chem.Phys.Lett.*, 32(3), 433

Munnoch, P. J. (1974) *Ph.D. Thesis*, University of Kent

Munnoch, P. J. & Wright, J. D. (1976) *J.S.C. Faraday Trans.I*, 72, 1981

Organic Semiconductors (1970). Progress Report No.11, Allen Clark Research Centre, Plessey Ltd.

Pearson, G. L. & Bardeen, J. (1949) *J.Phys.Rev.*, 75, 865

Roberts, G. G., Apsley, N. & Munn, R. W. (1980) *Physics Report*, 60, 127

Roberts, G. G., Apsley, N. & Munn, R. W. (1980) *Physics Report*, 60, 144

Sandman, D. J. (1979) *Mol.Cryst.Liq.Cryst.*, 50, 235

Schein, L. B. (1977) *Chem.Phys.Lett.*, 48(3), 571

Schein, L. B. (1977) *Phys.Rev.B.*, 15(2), 1024

Schein, L. B., Duke, C. B. & McGhie, A. R. (1978) *Phys.Rev.Lett.*, 40(3), 197

Seki, K., Sato, N. & Inokuchi, H. (1980) *Abstracts from Organic and Biological Semiconductors Symposium*, Univ. of Nottingham, 13

Sumi, H. (1979) *J.Chem.Phys.*, 70(8), 3775

Van Ewyk, R. L., Chadwick, A. V. & Wright, J. D. (1980) *J.C.S. Faraday I*, 76, 2194

Vincent, V. M. & Wright, J. D. (1974) *J.C.S. Faraday I*, 70, 58

Wheland, R. C. (1976) *J.A.C.S.*, 98(13), 3926

Zallen, R. & Slade, M. (1974) *Phys.Rev.B.*, 9, 1627

Chapter 6

Akamatu, H. & Kuroda, H. (1963) *J.Chem.Phys.* 39, 3364

Bauser, H. & Ruf, H. H. (1969) *Physica Status Solidi*, 32, 135

Boeyens, J. C. A. & Herbstein, F. H. (1965) *J.Phys.Chem.*, 69, 2153

Borsenberger, P. M., Chowdry, A., Hoesterey, D. C. & Mey, W. (1978) *J.Appl.Phys.*, 49(11), 5555

Dulmage, W. J., Light, W. A., Marino, S. J., Salzberg, C. D., Smith, D. L. & Staudenmayer, W. J. (1978) *J.Appl.Phys.* 49(11), 5548

Karl, N. & Ziegler, J. (1975) *Chem.Phys.Lett.*, 32(3), 438

Koizumi, S. & Matsunaga, Y. (1973) *Bull.Chem.Soc.Jap.*, 46, 1875

Koizumi, S. & Matsunaga, Y. (1974) *Bull.Chem.Soc.Jap.*, 47(1), 9

Mayoh, B. & Prout, C. K. (1972) *J.Chem.Soc., Faraday Trans.II*, 68, 1072

Mukherjee, T. K. (1970) *J.Phys.Chem.*, 74, 3006

Munnoch, P. J. (1974) *Ph.D. Thesis*, University of Kent

Robertson, B. E. & Stezowski, J. J. (1978) *Acta.Cryst.*, B34, 3005

Vincent, V. M. (1972) *Ph.D Thesis*, University of Kent

Vincent, V. M. & Wright, J. D. (1974) *J.C.S. Faraday Trans.I*, 70, 58

Wright, J. D., Ohta, T. & Kuroda, H. (1976) *Bull.Chem.Soc.Jap.*, 49(11), 2961

Appendix I

Carruthers, J. R. (1975) Crystals User Manual, Oxford University Computing Laboratory

International Tables for X-Ray Crystallography (1974) Vol.IV, Birmingham: Kynoch Press

Tickle, I. J. & Prout, C. K. (1973) *J.C.S. Perkin II*, 727

* * * * * *